The Energetics of Self-excited Oscillations in Collapsible Channel Flows

Danyang Wang

Submitted in fulfilment of the requirements for the
Degree of Doctor of Philosophy

School of Mathematics and Statistics
College of Science and Engineering
University of Glasgow

December 2018

Abstract

In this thesis, we study the energetics of two-dimensional flow through a flexible-walled channel, where we mainly consider two models.

The first model we consider is a fluid-membrane model in a long domain where the upper wall is replaced by elastic membrane under external pressure. The normal viscous stress, wall damping, wall inertia and membrane tension are all included in the membrane equation. We establish the corresponding eigenvalue problem of this model and trace the neutrally stable curves of this system across the parameter space. In agreement with previous work, we identify three different modes of instability (*i.e.* Tollmien-Schlichting waves (TS), traveling-wave flutter (TWF) and static divergence (SD) waves). We classify these instabilities into two classes (*i.e.* class A and class B form Benjamin [3]) using wall damping. Class A waves are destabilised by wall damping while class B waves are stabilised by wall damping. Furthermore, we consider the energy budget of the fully nonlinear system as well as that of the linearised system in order to determine whether the energy budget can be used to distinguish these different classes of instability. We found that the concept of 'activation energy' that connects with instability mode classification (Landahl [45], Cairns [17]) is not easily identified with terms in our energy budget. In particular, this wave energy is not equal to the work done by the fluid on the wall in our energy budget, as has previously been attributed to TWF.

The second model we consider is a finite length fluid-beam model formed from a two dimensional channel, where one segment of the upper wall is replaced by a plane strained elastic beam subject to an external pressure. A parabolic inlet flow with constant flux is driven through the channel. We apply the finite element method with adaptive meshing to solve the fully nonlinear system numerically. We demonstrate the stability of the system after small stimulation, where the system exhibit large amplitude self-excited oscillations. In addition, large amplitude vorticity waves are found in the downstream segment of the flexible wall. The energy budget of this fully nonlinear system is calculated; the energy budget of the system balances the kinetic energy, the rate of working of external pressure and the dissipation energy over one oscillation. Moreover, we form the corresponding eigenvalue problem of the fluid-beam model by linearising the system about the corresponding static state to second order. A finite element method (similar to that of the fully nonlinear system) is employed to solve for the linear eigenfunctions.

The observation of stability calculated from the eigenvalue problem are consistent with that calculated from the fully nonlinear problem. We identify the stability of the system and establish the neutral stability curve in the parameter space spanned by the beam extensional stiffness and Reynolds number. Two modes of instabilities are identified (*i.e.* mode-2 and mode-3, here the system is mode-*i* when the oscillation to the elastic beam contains *i* half wavelengths). Finally, we derive the energy budget of the linearised system at second order. The energy budget of the linearised system exhibits a balance between the averaged second order dissipation energy, the work done by non-linear Reynolds stresses and the rate of working of perturbation fluid stress on the elastic wall. We anticipate that the precise balance of energy might serve as a robust method to distinguish the different modes of oscillation, although this has yet to be confirmed.

Contents

List of Tables

List of Figures

Acknowledgements

I would like to express my gratitude and respect to my supervisor's Prof. Xiaoyu Luo and Dr. Peter Stewart for their instructive suggestions and valuable guidance over this project. I would also like to express my appreciation to them for their encouragement and support during my Ph.D. study.

I would like to thank my fellow doctoral students for their useful discussions and suggestions.

Special thanks to my beloved families for their unconditional supports.

Declaration

I, Danyang Wang, declare that this thesis titled, 'The Energetics of Self-excited Oscillations in Collapsible Channel Flows' and the work presented in it are my own. I confirm that:

- This work was done wholly or mainly while in candidature for a research degree at this University.
- Where any part of this thesis has previously been submitted for a degree or any other qualification at this University or any other institution, this has been clearly stated.
- Where I have consulted the published work of others, this is always clearly attributed.
- Where I have quoted from the work of others, the source is always given. With the exception of such quotations, this thesis is entirely my own work.
- I have acknowledged all main sources of help.
- Where the thesis is based on work done by myself jointly with others, I have made clear exactly what was done by others and what I have contributed myself.

Signed: _____

Date: _____

Chapter 1

Introduction

There are many examples of collapsible tubes in the human body. When a fluid flow is driven through these tubes, a variety of interesting physiological phenomena can arise. In the arteries, the internal blood pressure is normally greater than the external pressure in the surrounding tissue, so these arteries are usually subject to a positive transmural pressure (internal minus external pressure). However, there are many cases when other blood vessels are subjected to a negative transmural pressure which leads them to collapse. For example, in veins above the heart, the transmural pressure is subatmospheric due to the hydrostatic pressure decrease with height so spontaneous collapse can occur in these vessels (Wild [75]).

These collapsible vessels are very sensitive to changes in internal fluid pressure. This leads to interaction between the fluid and the solid wall of the vessel, which can promote many physiological phenomena, such as flow limitation and self-excited oscillations. One application of self-excited oscillation is so-called 'Korotkoff sound' generation during blood pressure measurement. In this method the brachial artery is compressed by a large external pressure through an inflated cuff tied around the upper arm; as the external pressure decreases, self-excited oscillations occur and generates a noise known as the 'Korotkoff sound' (Ur and Gordon [72], Bertram *et al*. [11]). This noise initialise when the external pressure is equal to the systolic pressure. As the external pressure continues to drop, the Korotkoff sounds persist. At the point that the external pressure equals to the diastolic pressure, the Korotkoff sound stops. This is a useful method to detect the pressure range of the heart and is used widely by clinicians.

Self-excited oscillations are frequently observed in experiments involving Starling resistors (*e.g*. Bertram *et al*. [13], Bertram and Tscherry [15]), and the problem of understanding their origins has grasped researchers' attention over the last 30 years. Studies of such systems have progressed from lumped parameter models (e.g. Katz & Chen [43]), one-dimensional models (*e.g*. Shaprio [64], Jensen [39]), two-dimensional models (*e.g*. Pedley [56]; Luo and Pedley [49]; Luo *et al*. [48]; Stewart *et al*. [69], and three-dimensional models (*e.g*. Heil [31], Marzo *et al*. [53], Zhang *et al*. [78]). In particular, Luo *et al*. [48] carried out a stability analysis of a fluid-beam

system in a flow through a rigid channel where one segment of the channel is replaced by an elastic beam. Their results revealed a cascade structure in the flow-driven system that included different modes of oscillations where the profiles of the oscillations have different numbers of extreme (*i.e*. mode-2, mode-3 and mode-4). Hao *et al*. [25] developed a more efficient numerical method based on a similar two-dimensional model as Luo *et al*. [48].

In this thesis, we analyse the energy budget of a two-dimensional channel fluid-structure interaction system. Calculating the energy budget of the system could be a useful way to analyse the stability mechanism in collapsible channel flow system. Jensen & Heil [42] showed that self-excited oscillation can grow by extracting kinetic energy from the mean flow and two-third of the kinetic energy flux is dissipated by the oscillation for pressure-driven problem. Stewart *et al* [68] showed that energy budget behaviors differently between different modes of oscillation.

This chapter is arranged as follows. We give an introduction to some pertinent laboratory experiments of the fluid-conveying elastic tube in *Sec*. 1.1. The theoretical models used to analyse the self-excited oscillation are summarized in *Sec*. 1.2. Then we review local instability in unbounded channel flows (*Sec*. 1.3). Finally, we outline the structure of this thesis in *Sec*. 1.4.

1.1 Experiments

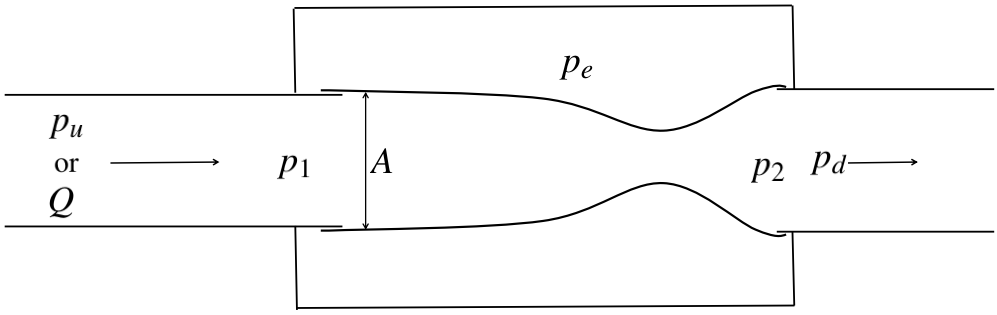

Figure 1.1: Sketch of the experimental setup, which is known as Starling resistor. Here p_1, p_2 represent the upstream and downstream pressure of the elastic tube, respectively. The total pressure and flow rate on the far upstream are denoted as p_u and Q, respectively. While the pressure on the far downstream is denoted as p_d. The cross-section area of the inlet tube is indicated as A and the external pressure subjected to the tube in the chamber is indicated as p_e (Bertram [5]).

Many experimental works on flow driven through collapsible tubes have observed a variety of flow-induced oscillations using a standard laboratory experiment setup called the 'Starling resistor', sketched in figure 1.1. A segment of collapsible tube is mounted between two ends of rigid tubes. The elastic segment is contained in a pressure chamber, with external pressure p_e

applied to this segment. We denote p_u and p_d as the pressure on the far upstream and downstream (shown in figure 1.1), respectively. Also p_1 and p_2 are the pressure on the upstream and downstream elastic segment, respectively. The upstream and downstream pressures, p_1 and p_2, can be measured and controlled by resistance in the upstream and downstream rigid tubes. We denote the cross-sectional area of the inlet tube as A, and Q is the flow rate at the inlet boundary of the rigid tube. Fluid is driven through the tube, and can be controlled either by fixing the pressure drop between the far upstream and downstream rigid tubes $\Delta p_{ud} = p_u - p_d$ or by fixing the flow rate Q.

When the external pressure p_e is sufficiently large, the tube will collapse. A buckled tube is highly compliant, so that even a small variation in external pressure can lead to extensive changes in cross-section area. Some early experiments of flow driven through collapsible tube have been reviewed by Bertram [6]. Experimentalists exhibit the relationship between the pressure drop along the elastic tube $\Delta p_{12} = p_1 - p_2$ and the flow rate Q under different control conditions. When the pressure difference between the outlet pressure and the external pressure, $\Delta p_{e2} = p_e - p_2$ is held fixed, the pressure drop Δp_{12} is constant for large enough flux Q, thus Δp_{12} is independent of flux Q (see figure 1.2(a), Bertram *et al*. [12]). This is known as the 'pressure-drop limitation'. Conversely, when the pressure difference between the inlet pressure and the external pressure, $\Delta p_{e1} = p_e - p_1$ is held fixed, the flow rate reaches a maximum value as Δp_{12} initially increases and then decreases (shown in figure 1.2(b)). The flow rate is essentially independent of Δp_{12} where the curves are close to vertical, and this is known as 'flow limitation' (Bertram and Castles [7]).

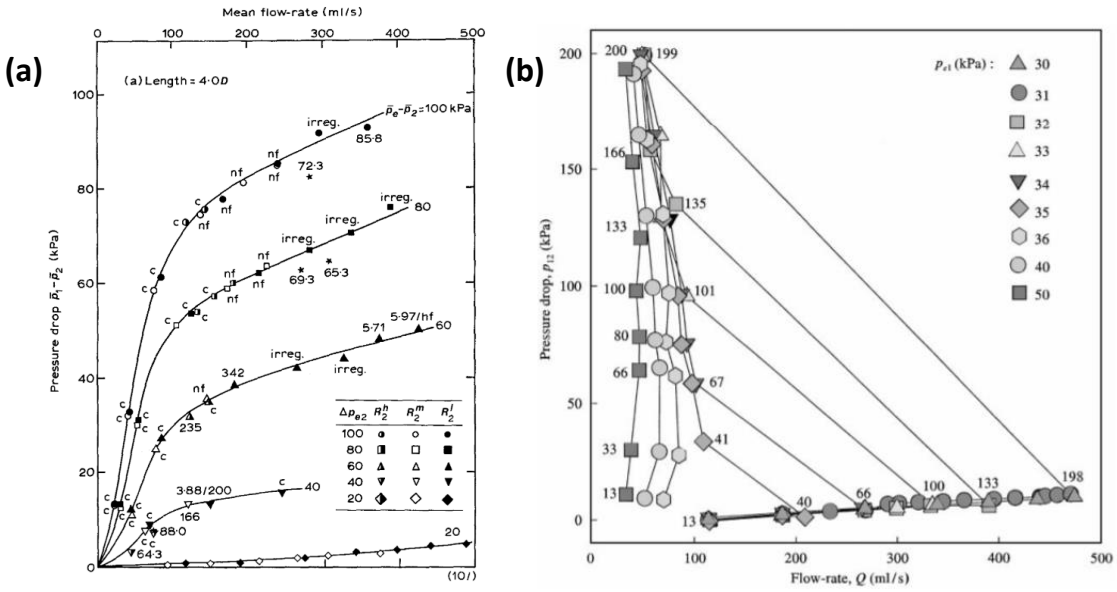

Figure 1.2: The pressure drop Δp_{12} against flow rate Q for (a) constant pressure difference Δp_{e2} (from Bertram *et al*. 1990); (b) constant pressure difference Δp_{e1} (from Bertram *et al*. 1999).

For ranges of parameters with Reynolds number not less than 200, large-amplitude flow-induced

oscillations have been observed whereas steady flow could not be obtained. A systematic series of experiments on these self-excited oscillations with thick-walled silicone rubber tubes has been made by Bertram and his coworkers (Bertram [4], [5], Bertram *et al*. [12], [13]). They showed that self-excited oscillations appear in four frequency bands for minimal downstream resistance under different parameter settings [5]. They then investigated the oscillations for four different tube lengths using the same apparatus as in [5], and divided the self-excited oscillations into 3 well-separated bands, *i.e*. low, intermediate and high frequency. Tube length did not influence the frequency of self-excited oscillation strongly, whereas their predominant effect was predisposed a particular mode of oscillation for the system, *i.e*. intermediate frequencies could not be achieved in the shortest tubes while they replace high frequencies in the longest tubes [12]. Bertram's [13] paper gives examples that demonstrate the evolution of the downstream pressure p_2 against time t for different tube lengths: this system exhibits a variety of qualitatively different types of self-excited oscillation (shown in figure 1.3).

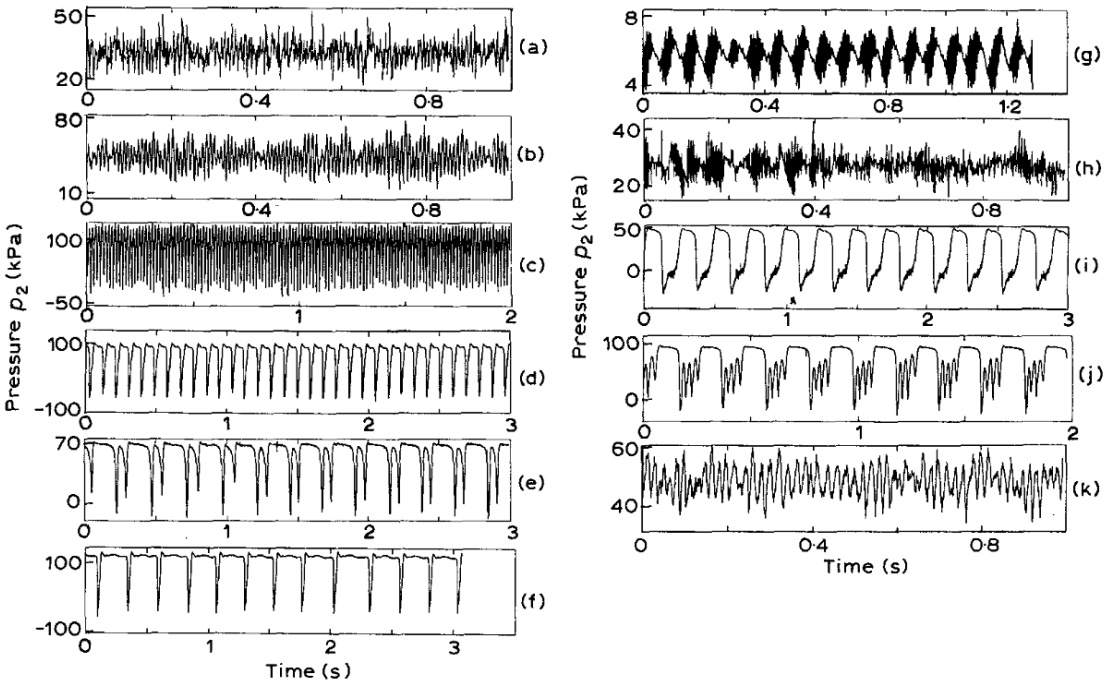

Figure 1.3: Self-excited oscillation : pressure on downstream elastic tube p_2 against time t under different controlled condition (from Bertram *et al*. 1991).

Later experiments used a laser Doppler anemometry to measure the velocity of flow just downstream of the collapsible segment during self-excited oscillations, and flow features have been studied for a variety of Reynolds numbers in the range $300-550$ (laminar flow, Bertram *et al*. [14]) to Reynolds number about 10000 (turbulent flow, Bertram *et al*. [8], Bertram and Nugent [9]).

1.2 Theoretical models

Theoretical models of flow in a collapsible channel (or tube) have been developed to understand the vast dynamical features observed from experiments using the Starling resistor. Earlier studies of this fluid-structure interaction problem began with lumped parameter models (Conrad [21], [43], Bertram & Pedley [10]). For these models, the system was described by variables which are averaged in cross-sectional area and length, *i.e*. the variables used in these models are only time-dependent variables. Bertram & Pedley [10] showed that the energy loss due to flow-separation at the downstream flexible segment of the tube is important for the generation of self-excited oscillation. Although approximate, the results of these mathematical models agreed qualitatively with some experimental observations. However, the weakness of the lumped parameter models lies in its failure to capture some of the mechanical properties of the tube.
In this section, we discuss the spatially one-dimensional models (*Sec*.1.2.1), two-dimensional models (*Sec*.1.2.2) and three-dimensional models (*Sec*.1.2.3) used to analyse flexible-walled channels (tubes) conveying flow.

1.2.1 One-dimensional models

One-dimensional models are useful ways to understand a variety of collapsible tubes or channels conveying flow. The variables considered in these models are usually evaluated as a cross-sectionally averaged. The system is governed by equations of conservation of mass and momentum, coupled with elastic properties described by a tube law, *i.e*. a relationship between transmural pressure (internal minus external) and the corresponding cross-sectional area.
Shapiro [64] developed a general one-dimensional theory in a thin-walled flexible tube, which employed a long-wavelength approximation. He described the flow as choked when the flow speed became comparable to the wave speed. At this state, the steady flow is unable to be sustained and unsteady behavior appears; flow limitation is usually produced as a result.
Cancelli & Pedley [18] developed a one-dimensional model to describe flow in collapsible tubes. Two significant characteristics of this model were the inclusion of longitudinal wall tension and energy loss due to flow separation downstream of the collapsible segment. They also described a choking mechanism for a tube whose collapsible segment is long enough. Solving the system numerically using a finite-difference scheme, they showed self-excited oscillation can be found when the flow became supercritical (*i.e*. the flow speed exceeds the wave speed), also the generation of these oscillations is a result of the coupling of the pressure wave and the position of the flow separation point.
Jensen & Pedley [41] methodically investigated steady solutions using the same model as Cancelli & Pedley [18]. For fully attached flow (*i.e*. neglecting energy dissipation), they divided a parameter space into four areas and identified a region with no existence of the steady solution, as well as a region with multiple steady solutions. These results are similar to those of Reyn [59],

but the elasticity relationship of the tube they applied is much simpler. Jensen and Pedley also showed that there always exists a steady solution of the model when the energy loss due to flow separation downstream of the flexible segment is included.

Jensen [39] further investigated the linear stability of the steady flows identified in Jensen & Pedley [41], by introducing small time-dependent perturbation to these steady solutions. He was able to show that these steady solutions could be unstable to mode-2, mode-3 and mode-4 (or even mode-5) oscillations. Here mode-j represents the oscillatory mode whose perturbation over the whole tube contains j half-wavelengths. These different modes of oscillation fall into distinct frequency bands. Jensen [40] later investigated nonlinear mode interactions giving rise to quasiperiodic oscillatory behavior that agreed with experimental observations.

Other numerical researches of one-dimensional models (*e.g.* Hayashi *et al.* [26] and Ikeda *et al.* [37], [68] *etc.*) all revealed a rich variety of self-excited oscillations.

Another family of one-dimensional models which include energy losses due to viscous dissipation but not due to flow separation were proposed by Jensen and coworkers. In particular, Stewart *et al.* [68] introduced energy budget analysis of instability in a pressure driven system and conclude $2/3$ of the energy extracted from the mean flow is lost to viscous dissipation, which agreed with Jensen & Heil's [42] prediction of a two-dimensional system (see discussion below). Using a similar model, Xu *et al.* ([76], [77]) identified low-frequency self-excited oscillations and a 'sawtooth' oscillation when the downstream rigid channel is sufficiently long.

More recently, Stewart [65] considered a flux-driven problem with high Reynolds number and large uniform external pressure using a similar fluid-membrane model as mentioned above ([68], [77]). He predicted multiple static solutions of the system at large Reynolds number and identified these static states were unstable to distinct families of oscillation modes. A mechanism of energy transfer to maintain the self-excited oscillations was also given: the oscillation increases the mean minimal channel width over a period of oscillation compared with corresponding static state, which reduces the overall dissipation in the system, and this excess energy sustains the oscillation.

1.2.2 Two-dimensional models

Despite the fact that one-dimensional models have been a successful tool in understanding complex dynamical behavior of collapsed tubes conveying flow, their disadvantage in using $ad-hoc$ assumptions pushed researchers to develop rational two-dimensional theory. We consider a finite-length channel with one segment of the upper wall replaced by an elastic material.

Pedley [56] considered a symmetric two-dimensional channel, with one segment of both of the upper and lower wall replaced by elastic membranes which were held under longitudinal tension. Pedley analysed the system using lubrication theory, which assumed small membrane slope, low Reynolds number, and that wall inertia was negligible. He concluded that the steady solution would break down if the membrane longitudinal tension reaches zero. Later development of the

collapsible channel model conveying fluid using lubrication theory has been made by Matsuzaki & Fujimura [54], who also included bending stiffness in the membrane equilibrium equation. They conclude that steady solutions exist when longitudinal tension is small or even zero.

Lowe & Pedley [47] considered a Stokes flow (fluid at zero Reynolds number) in a two-dimensional channel, in which one segment of the upper wall was replaced by an elastic membrane under longitudinal tension. They adopted an iterative method to solve the system numerically. The fluid and membrane wall were discretized independently and an iteration scheme was used to obtain a coupled solution between fluid and solid. Their prediction of the steady solution at high wall tension agreed with the results obtained using lubrication theory (Pedley 1992). However, the breakdown at low wall tension was believed to be a consequence of numerical iteration rather than the mechanism analysed by lubrication theory (Pedley [40]).

Following a similar iteration method, Luo & Pedley [49] studied steady flow in a fluid-membrane coupled system. The finite element method was used to solve the Navier-Stokes equations for a given membrane shape. They predicted a range of steady solutions and illustrated the change of wall shape when varying the longitudinal tension. They showed that when the tension falls below a critical value, the upstream end of the membrane begins to bulge out while the downstream of the membrane remains collapsed, a beam shape which can also be observed in our two-dimensional fluid-beam model in chapter 3. However, at sufficient small tension, they failed to obtain converged solutions.

Rast [58] considered a similar fluid-membrane system as Luo & Pedley [49], at finite Reynolds number $(1 - 600)$. He computed the system using a fully-coupled finite element method, where the fluid and membrane are solved simultaneously. The fluid field is discretized using an adaptive spines mesh (Ruschak [60]) and displayed a range of complex steady solutions. In particular, a series of downstream recirculation eddies developed when increasing Reynolds number.

Luo & Pedley [50] extended the numerical method used by Rast (1994) and developed a time-dependent simulation with variable time increments for a fluid-membrane problem, to obtain the unsteady behavior of the coupled system. They assumed a vertical movement of the elastic surface for simplicity of tracking material points on the wall. They found that for sufficiently large Reynolds numbesr, the steady solution broke down as tension decreased below a critical value. As tension continues to decrease, self-excited oscillation appears and a series of period-doubling bifurcations are observed, which agreed with experimental observations [12]. Furthermore, during each cycle of oscillation, a series of large-amplitude vorticity waves downstream of the elastic segment were captured. This prediction is similar to what was observed experimentally (Pedley & Stephanoff [57]), as well as in our two-dimensional fluid-beam model in later chapter 3.

Luo & Pedley [51] continued above approach to investigate the effect of wall inertia on the self-excited oscillations in a collapsed channel. They found a flutter-type self-excited oscillation with relatively high frequency superposed on original large-amplitude, low-frequency oscilla-

tion when including wall inertia into the system. In addition, a different phase between the wall pressure and wall displacement enabled the fluid to do work on the wall. Thus they concluded that this flutter-type high-frequency oscillation is caused by the energy transfer from the fluid to the wall. A possible mechanics for the generation of these vorticity waves through spatially localised growth was presented by Stewart *et al*. [67].

Luo & Pedley [52] used their approach described above ([50], [51]) to investigate the steady and unsteady behavior of collapsible two-dimensional channel with flow limitation. They illustrate both steady and unsteady solutions when the flow is limited and conclude that there is no direct correlation between the onset of self-excited oscillation and flow limitation. Moreover, the instability of steady solutions was found to be deeply affected by the unsteady boundary conditions (*e.g*. varying Reynolds number while keeping upstream and downstream transmural pressure fixed).

Jensen & Heil [42] considered a fluid-membrane model with finite length channel for high Reynolds number. They studied the unsteady behavior of a pressure-driven system using two approaches: an asymptotic approach at large membrane tensions and a fully coupled finite element method to solve the Navier-Stokes equations at lower membrane tensions. They concluded that oscillations can grow when extracting kinetic energy from the mean flow is faster than the energy lost to viscous dissipation, two-thirds of the net flux kinetic energy is lost to dissipation energy and the remainder modifies the mean flow. They identified axial sloshing motions driven by the oscillations upstream and downstream of the membrane.

Cai & Luo [16] employed a more general and realistic model compared with the fluid-membrane model, *i.e*. a fluid-beam model where the membrane was replaced by a plane strained elastic beam with large deflection. Both extensional and bending stiffness of the elastic beam were taken into consideration. They analysed the system using both asymptotic and numerical methods. The latter was a finite element method with rotating spines. They illustrate that if the stretch-induced tension is small compared with the initial tension, the steady behavior of the fluid-beam model is similar to the fluid-membrane case. However, different behaviors were obtained when varying the wall stiffness.

Considering a similar model ([16]), Luo *et al*. [48] discussed the unsteady behavior and linear stability of the fluid-beam collapsible channel. The initial membrane tension was chosen to be zero to ensure a stress-free initial configuration and finite Reynolds number (200-600) was considered. Two approaches were used: unsteady finite element stimulation with rotating spines; and linearized eigenvalue stimulation solving the Orr-Sommerfeld equation directly. Different modes of self-excited oscillations were identified (mode-2, mode-3, and mode-4). They discovered a cascade of instabilities in parameter space spanned by Reynolds number and wall stiffness for a flow-driven problem (*i.e*. keeping the upstream flux fixed). The system first lost stability to mode-2 oscillations when reducing wall stiffness; as the wall stiffness reduced further the system re-stabilized through a ‘tongue shape’ region and then became unstable to mode-3 oscillation.

Mode-4 self-excited oscillations were observed for sufficiently small wall stiffness. Following a similar idea, we develop our two-dimensional fluid-beam model but with a modified beam law (discussed in later chapter 3).

Liu *et al*. [46] analysed the stability and energy budget of the similar fluid-beam model ([16], [48]) with the pressure-driven problem (*i.e*. keeping the upstream pressure fixed). Unlike flow-driven problem, they did not find a cascade instability structure for a pressure-driven problem. Also, the dominating unsteady mode is mode-1 instead of mode-2 in a flow-driven problem. They concluded that for particular mode-1 oscillations, the generation of self-excited oscillation was by extracting kinetic energy from the mean flow and two-thirds of the net kinetic energy flux was consumed by viscous dissipation, as already shown by Jensen & Heil [42]. However, this mechanism failed to explain mode-1 oscillations with large wall deformation as well as mode-2 oscillations.

Stewart *et al*. [66] studied the instability of a fluid-membrane model, with high Reynolds number flow driven through a finite-length channel. One segment of the upper channel wall was replaced by a massless membrane under longitudinal tension. A pressure-driven problem was considered. The system exhibited a high-frequency sloshing oscillation at high tension and performed a slamming oscillation at low membrane tension. They analysed the energy budget for the system and illustrated that the growth of the oscillations was affected by the transfer of kinetic energy to a viscous dissipation energy.

1.2.3 Three-dimensional models

Two-dimensional models discussed above proved to be a useful analog of flow driven through a collapsed three-dimensional tube. However, these two-dimensional models ignore many three-dimensional effects. Therefore, three-dimensional theories of collapsible tube conveying flow have been developed. In this section, we give introductions of the development of these three-dimensional models.

Earlier theories of steady three-dimensional flow driven through three-dimensional compliant tubes have been developed by Heil & Pedley ([28], [29]) and Heil [30]. They represent the wall using geometrically nonlinear Kirchoff-Love shell theory coupled to the fluid that was described using lubrication theory. A finite element method was used to analyse this fluid-solid system. A mechanism involved in the axisymmetric deformation of the tube has been made by examining a range of boundary conditions corresponding to various experimental setups ([28]). Linear stability of this cylindrical shell conveying flow has been conducted and demonstrated how the stability and buckling deformation of the tube can be affected by the variations in the upstream pressure and the axial pre-stretch ([30]). An analysis of the post-buckling deformations of the system ([29]) demonstrated that a violent collapse of the tube after the buckling emerged if the volume flux was fixed, while this collapse can be prevented by the fluid-solid coupling if the pressure drop was fixed.

Heil [31] studied Stokes flow through the similar three-dimensional tube as mentioned above. He investigated the behavior of the fluid-solid system for different boundary conditions corresponding to experiments and showed good agreement between numerical and experimental results. He also noted that lubrication theory predictions were consistent with the predictions of this full Stokes system.

Hazel & Heil [27] investigated the steady Navier-Stokes equations using a similar model as mentioned above. They showed the tube can buckle non-axisymmetrically under sufficiently small transmural pressure. The fluid inertia (absent in the lubrication theory) can promote tube buckling in a phenomenon known as the Bernoulli effect.

As many experiments are conducted using a thick-walled elastic tubes, Marzo *et al*. [53] studied a three-dimensional thick-walled tube conveying steady flow. The system of elastic wall coupled with steady Navier-Stokes equations was solved using FIDAP finite-element software. The numerical predictions of this system showed good agreements with Hazel and Heil (2003) when a small thickness tube was specified, as well as with the results of the experiments.

Heil & Waters [32] considered unsteady flows with small-amplitude, high-frequency oscillations in thin-walled elastic tubes. Numerical and asymptotic methods have been employed to analyse this coupled system. They showed that wall-motion induced unsteady flow is independent of the steady flow for sufficiently small amplitudes and transverse flow in the tube cross-sections is the dominant flow during oscillation.

Heil & Waters [33] extended above simulation of unsteady flows in a three-dimensional tube to analyse the overall energy budget. Whittaker ([74], [73]) studied the energetics of prescribed small-amplitude oscillations of a three-dimensional tube, as well as their applications to flow conveying through an axially non-uniform tube. These studies established a critical Reynolds number at which the wall extracts kinetic energy from the mean flow, and thus oscillation becomes favorable. This is similar to the sloshing mechanism proposed by Jensen & Heil [42] for two-dimensional models.

Zhang *et al*. [78] established a numerical method for three-dimensional flow conveying through a hyperelastic collapsible tube. The Arbitrary Lagrangian-Eulerian (ALE) method and the method of rotating spines were used to solve the system numerically.

1.3 Local instability in unbounded channel

A variety of studies have investigated the stability of small-amplitude perturbations to flow in an unbounded channel, *i.e*. no upstream and downstream boundary conditions, and discovered many local instabilities. For a detailed review of these studies see Carpenter [19]. In this section, we give an introduction of three most common modes of local instabilities in a coupled fluid-flexible wall system: Tollmien-Schlichting (TS), traveling-wave flutter (TWF) and static-divergence (SD). A classification scheme is summarized as well.

A well-known classification was introduced by Benjamin ([2], [3]) and Landahl [45] to distinguish different modes of instabilities: they divided these instabilities into three categories class A, class B and class C. Class A waves are destabilised by wall damping and irreversible energy transfer from the fluid to the wall while class B is stabilised by wall damping and irreversible energy transfer from the fluid to the wall [2]. Another way to distinguish these classes is by introducing a concept of 'activation energy', which is defined to be the energy required to generate the mode ([45], [3]). The activation energy of class A waves is negative, class B waves have positive activation energy, and class C waves have zero activation energy and not influenced by wall damping (Cairns [17]).

TS waves are hydrodynamic modes of instability in fluid boundary layers first identified in rigid channels by Tollmien [71] and Schlichting [61]. This TS mode is only slightly modified by wall compliance but is destabilized by wall damping (Carpenter *et al*. [20]). TS waves are class A waves that can be stabilised by energy transfer from the fluid to the wall.

Traveling-wave flutter (TWF) instability is a class B instability that is stabilized by wall damping. The energy transfer from the flow to the wall destabilise these waves. Viscous effects confined to critical layers is shown to led to TWF (Davies and Carpenter [22], Huang [35]). Stewart *et al*. [69] discussed local instabilities of an infinitely long channel consisting of a massless elastic membrane and a rigid wall conveying a Poiseuille flow with constant flow rate. A Chebyshev spectral method was used to solve the eigenvalue problem based on the Orr-Sommerfeld equation. Different modes of instability were identified, *e.g*. Tollmien-Schlichting (TS) waves and traveling-wave flutter (TWF). They proposed a new asymptotic mechanism for TWF based on a weak critical layer at the center of the channel.

Static-divergence (SD) instability is either a class A or C instability depending on the context, *i.e*. the activation energy of SD is revealed to be negative or zero (Davies & Carpenter [22]). Stewart *et al*. [69] showed SD to be class A in an asymmetric long channel.

1.4 Thesis structure

In this section, we illustrate the structure of this thesis. We mainly study two models. In chapter 2, we study an infinitely long fluid-membrane two-dimensional model where the upper wall is replaced by an elastic membrane subject to an external pressure gradient. We include the effect of longitudinal tension wall, inertia and damping. We consider the eigenvalue problem of the fluid-membrane model to discuss linear stability and energetics of this system in chapter 2. The eigenvalue problem based on the Orr-Sommerfeld equation is considered to discuss the local instability of the system, three modes of instabilities (TS, TWF, and SD) are found in parameter space. The stability of these modes of instability is discussed for different parameters. We derive the energetics for the fully non-linear system as well as for the linearised system. Finally, the second order energy budget is calculated at several neutrally stable points.

In Chapter 3 we study a two-dimensional finite length fluid-beam model where one segment of the upper wall is replaced by an elastic beam under constant external pressure.
Chapter 3 considers a finite fluid-beam channel based on the model developed by Luo *et al*. [48] with modified beam equations. A finite element method with rotating spines is employed to consider the instability of this system. The corresponding fully non-linear energy budget is derived and calculated numerically.
Chapter 4 studies the linear stability of the fluid-beam model and the corresponding energy budget is derived. Similar to the fully non-linear system, a finite element method with rotating spines is used to solve the eigenvalue problem numerically. The growth rate and frequency of the oscillation are considered. A neutrally stable curve is calculated in the parameter space spanned in wall stiffness and Reynolds number. A flow chart of the structure of the energy budget for the fluid-beam model is shown in figure 1.4.

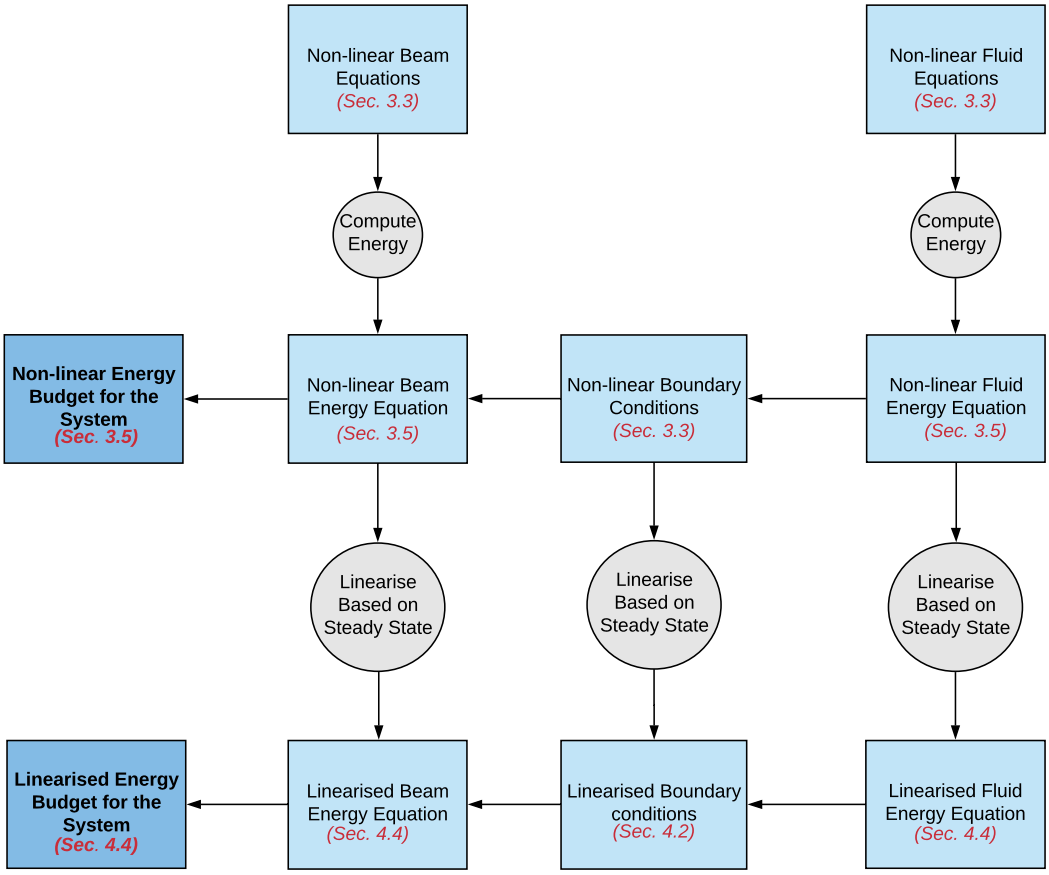

Figure 1.4: Flow chart of system energy budget calculations

Chapter 2

Fluid-membrane model

In this chapter, we analyse the energetics of flow through an infinitely long flexible-walled channel where one wall of the channel is rigid and the other is an elastic wall subject to an external pressure. We first summarize the model in *Sec*. 2.1, then we establish the governing equations for the coupled system (*Sec*. 2.2). In *Sec*. 2.3, we derive the energy budget for the fully nonlinear membrane-fluid system. We then linearize all the variables in *Sec*. 2.2 and retain terms up to second order to introduce the perturbation governing equations (*Sec*. 2.4). Our next step is substituting the linearized variables into fluid energy equation to obtain the second order energy budgets (*Sec*. 2.5). By assuming a wavelike form for all the first order variables, we obtain the eigenvalue problems in *Sec*. 2.6. We solve the eigenvalue problem in *Sec*. 2.6 using a Chebyshev spectral method, we give neutrally stable curves for four different cases and the corresponding second order energy budgets over one period of time and wavelength (*Sec*. 2.7).

2.1 The model

We consider the flow setup shown in Figure 2.1 in a channel of baseline width a. The channel carries parabolic flow of flux Q, while ρ and μ are the density of the membrane and viscosity of the fluid, respectively. We establish Cartesian coordinates along the rigid wall denoted x and y, while $\mathbf{g}_1$, $\mathbf{g}_2$ are the unit vectors in horizontal and vertical directions of the coordinate. Let $\mathbf{u} = u(x,y,t)\mathbf{g}_1 + v(x,y,t)\mathbf{g}_2$ and p be the velocity and pressure of the fluid, respectively.
We consider a simplified membrane model which we ignore the axial motion, when the membrane is under large axial prestress. We note that certain modes of instability are not possible in this model [44], [63]. The membrane is located at $y = h(x,t)$ at time t, and the membrane subjected to an external pressure p_e. We denote T_0, d_0 and m as the longitudinal tension, damping and the mass of the membrane, respectively. Here the damping that due to membrane itself will contribute to an irreversible energy transfer from fluid to the flexible wall, and will be used for

instability classification in later section 2.7.4.

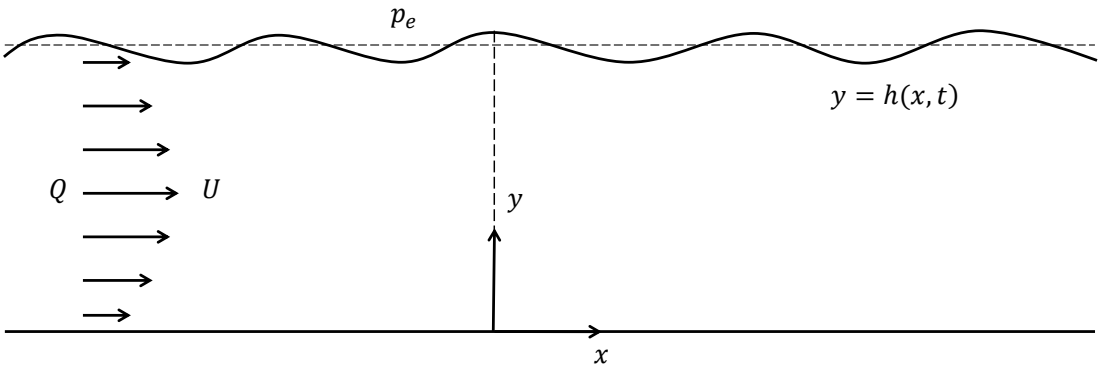

Figure 2.1: The fluid-membrane model, the channel carries steady Poiseuille flow of dimensional flux Q.

2.2 Governing Equation for Fluid and Membrane

We introduce the dimensionless variables (marked with tilde) using the following scalings,

$$\tilde{\mathbf{u}} = \frac{\mathbf{u}a}{Q}, \quad \tilde{p} = \frac{pa^2}{\rho Q^2}, \quad \tilde{t} = \frac{tQ}{a^2}, \quad \tilde{x} = \frac{x}{a}. \tag{2.2.1}$$

Using the same scaling, we obtain the dimensionless parameters (marked with tilde) as,

$$\tilde{R} = \frac{Q\rho}{\mu}, \quad \tilde{T} = \frac{aT_0}{\rho Q^2}, \quad \tilde{d} = \frac{ad_0}{\rho Q}, \quad \tilde{m} = \frac{m}{\rho a}, \tag{2.2.2}$$

where $\tilde{R}$ is the Reynolds number of the flow, $\tilde{T}$ is the dimensionless membrane tension, $\tilde{d}$ is the dimensionless wall damping and $\tilde{m}$ is the dimensionless wall mass. We henceforth drop the tildes for convenience.
The fluid flow is governed by the incompressible Navier-Stokes equations in 2D,

$$u_x + v_y = 0, \tag{2.2.3}$$
$$u_t + uu_x + vu_y = -p_x + R^{-1}(u_{xx} + u_{yy}), \tag{2.2.4}$$
$$v_t + uv_x + vv_y = -p_y + R^{-1}(v_{xx} + v_{yy}). \tag{2.2.5}$$

We apply the no-slip and no-penetration boundary conditions on the rigid wall, in the form

$$u = 0, \quad v = 0, \qquad (y = 0). \tag{2.2.6}$$

while on the flexible membrane, the boundary conditions of no-slip and the kinematic conditions on the elastic membrane take the form

$$\mathbf{u}\cdot\mathbf{t}=0,\quad \mathbf{u}\cdot\mathbf{n}=\frac{h_t}{\sqrt{1+h_x^2}},\qquad (y=h),\quad (2.2.7)$$

which become

$$u=-\frac{h_t h_x}{1+h_x^2},\quad v=\frac{h_t}{1+h_x^2},\qquad (y=h),\quad (2.2.8)$$

where $\mathbf{t}=(1,h_x)/\sqrt{1+h_x^2}$ and $\mathbf{n}=(-h_x,1)/\sqrt{1+h_x^2}$ are the tangent and normal unit vectors for each point on the membrane.
The motion of the membrane is governed by a normal stress balance,

$$p-p_e=-\frac{T}{Ra}+m\mathbf{a}\cdot\mathbf{n}+R^{-1}\left[\left(\nabla\mathbf{u}+\nabla\mathbf{u}^{\mathrm{T}}\right)\mathbf{n}\right]\cdot\mathbf{n}+d\mathbf{v}\cdot\mathbf{n},\qquad (2.2.9)$$

where $R_a=\left(1+h_x^2\right)^{3/2}/h_{xx}$ is the dimensionless radius of membrane curvature. While $\mathbf{v}=(0,h_t)$ and $\mathbf{a}=(0,h_{tt})$ are the membrane velocity and acceleration, respectively. For simplicity, we ignore axial motion of the membrane by assuming the membrane is under large axial pre-stress here, although this is permitted in the model considered in chapter 3 and chapter 4. Here the transmural pressure (*i.e.* $p-p_e$) is balanced by the wall tension, the wall inertia, the viscous stress and wall damping in normal direction.
Expressing R_a, $\mathbf{a}$ and $\mathbf{v}$ in terms of channel width $h(x,t)$, the membrane governing equation (2.2.9) becomes

$$\begin{aligned}p-p_e=&-\frac{Th_{xx}}{(1+h_x^2)^{\frac{3}{2}}}+\frac{mh_{tt}}{(1+h_x^2)^{\frac{1}{2}}}+\frac{2}{R(1+h_x^2)}\left[v_y-h_x(u_y+v_x)+h_x^2u_x\right]\\&+\frac{dh_t}{(1+h_x^2)^{\frac{1}{2}}}\qquad (y=h).\quad (2.2.10)\end{aligned}$$

2.3 Energy Budget of the System

We want to analyse the energy budget of the modes of instability which occur in this collapsible channel system. We obtain this budget by taking the scalar product of the momentum equations (2.2.4), (2.2.5) with the fluid velocity $\mathbf{u}$ in the form,

$$\begin{aligned}&(uu_t+vv_t)+u(uu_x+vv_x)+v(uu_y+vv_y)+\frac{1}{2}(u^2+v^2)(u_x+v_y)\\&=-up_x-vp_y+R^{-1}(u\nabla^2u+v\nabla^2v)-p(u_x+v_y),\end{aligned}\qquad (2.3.1)$$

where ∇^2 denotes the 2D Laplacian operator in Cartesian coordinates.
Since the fluid is incompressible, we can rearrange (2.3.1) into the following form,

$$\frac{1}{2}(u^2+v^2)_t + \left[\frac{1}{2}u(u^2+v^2)\right]_x + \left[\frac{1}{2}v(u^2+v^2)\right]_y + (up)_x + (vp)_y - R^{-1}(u\nabla^2 u + v\nabla^2 v) = 0. \tag{2.3.2}$$

Now we integrate equation (2.3.2) across the channel width $(0 \le y \le h)$ to obtain the energy equation,

$$\underbrace{\int_0^h \frac{1}{2}(u^2+v^2)_t \,\mathrm{d}y}_{I} + \underbrace{\int_0^h \left[\frac{1}{2}u(u^2+v^2)\right]_x \mathrm{d}y}_{II} + \underbrace{\int_0^h \left[\frac{1}{2}v(u^2+v^2)\right]_y \mathrm{d}y}_{III}$$
$$+ \underbrace{\int_0^h \left[(up)_x + (vp)_y\right] \mathrm{d}y}_{IV} - \underbrace{R^{-1}\int_0^h (u\nabla^2 u + v\nabla^2 v)\,\mathrm{d}y}_{V} = 0. \tag{2.3.3}$$

We label the above terms $I, II, ..., V$ as the label of underbraces and consider each term in turn.
We take the time derivative outside the integral for term I in the form,

$$I = \underbrace{\left[\frac{1}{2}\int_0^h (u^2+v^2)\mathrm{d}y\right]_t}_{K} - \frac{1}{2}h_t\left(u^2+v^2\right)\Big|^{y=h}. \tag{2.3.4}$$

We denote the first term K, the rate of change of kinetic energy.
Using the Leibniz's rule and the no-slip condition (2.2.6), the term II can be written in the form,

$$II = \underbrace{\left[\frac{1}{2}\int_0^h u(u^2+v^2)\mathrm{d}y\right]_x}_{F} - \frac{1}{2}h_x u(u^2+v^2)\Big|^{y=h}. \tag{2.3.5}$$

We denote the first term F, the kinetic energy flux into the system.
Using the no-slip condition(2.2.6), the term III can be written in the form,

$$III = \frac{1}{2}v\left(u^2+v^2\right)\Big|^{y=h}. \tag{2.3.6}$$

We group the last terms in both I, II and term III, then apply boundary condition (2.2.8) we have

$$\left[\frac{1}{2}\left(h_t + h_x u - v\right)\left(u^2+v^2\right)\right]^{y=h} = \left[\frac{1}{2}(h_t - h_x^2 v - v)(u^2+v^2)\right]^{y=h} = 0. \tag{2.3.7}$$

For IV, we take the derivative with respect to x outside the integral for the first part and apply boundary condition (2.2.6) for second part, we have

$$IV = -p\left(uh_x - v\right)\Big|^{y=h} + \underbrace{\left[\int_0^h (up)\,\mathrm{d}y\right]_x}_{P}. \tag{2.3.8}$$

We denote the second term as P, the rate of working of pressure forces axially.
We add extra zero term $R^{-1}\left(\nabla\cdot(\nabla\mathbf{u})^{\mathrm{T}}\right)\cdot\mathbf{u} = 0$ to term V to facilitate manipulation of the energy budget into its required form,

$$V = R^{-1}\int_0^h \left[u\nabla^2 u + v\nabla^2 v + \left(\nabla\cdot(\nabla\mathbf{u})^{\mathrm{T}}\right)\cdot\mathbf{u}\right]\,\mathrm{d}y.$$

Rearranging we obtain,

$$\begin{aligned} V =& R^{-1}\int_0^h \left[(uu_x + vv_x)_x - u_x^2 - v_x^2 - u_y^2 - v_y^2\right]\,\mathrm{d}y + R^{-1}\left[uu_y + vv_y\right]_{y=0}^{y=h} \\ &+ R^{-1}\int_0^h \left[(uu_x + vu_y)_x - u_x^2 - v_y^2 - 2u_y v_x\right]\,\mathrm{d}y + R^{-1}\left[uv_x + vv_y\right]_{y=0}^{y=h}. \end{aligned}$$

Using the membrane equation (2.2.10) and the boundary condition on the wall (2.2.6, 2.2.8) we obtain

$$\begin{aligned} V =& h_t\left(p - p_e + \frac{Th_{xx}}{(1+h_x^2)^{\frac{3}{2}}} - \frac{mh_{tt}}{(1+h_x^2)^{\frac{1}{2}}} - \frac{dh_t}{(1+h_x^2)^{\frac{1}{2}}}\right)^{y=h} \\ &\underbrace{- R^{-1}\left(\int_0^h \left[2u_x^2 + 2v_y^2 + (u_y + v_x)^2\right]\,\mathrm{d}y - \left[\int_0^h (2uu_x + vv_x + vu_y)\,\mathrm{d}y\right]_x\right)}_{D}. \end{aligned} \tag{2.3.9}$$

We denote the second term as D, the rate of energy loss due to fluid viscosity in the bulk. Note that the viscous term vanish in the first term after applying the elastic membrane equation (2.2.10).
Gathering the first terms in both IV and V, and denoting this as E, the rate of working of fluid stress on the membrane, we have

$$E = \left[p(uh_x - v) + h_t\left(p - p_e + \frac{Th_{xx}}{(1+h_x^2)^{\frac{3}{2}}} - \frac{mh_{tt}}{(1+h_x^2)^{\frac{1}{2}}} - \frac{dh_t}{(1+h_x^2)^{\frac{1}{2}}}\right)\right]^{y=h}. \tag{2.3.10}$$

Applying the boundary conditions (2.2.8) on the elastic wall, we have

$$E = \left[-h_t p_e + \frac{Th_t h_{xx}}{(1+h_x^2)^{\frac{3}{2}}} - \frac{mh_{tt}}{(1+h_x^2)^{\frac{1}{2}}} - \frac{dh_t}{(1+h_x^2)^{\frac{1}{2}}}\right]^{y=h}. \tag{2.3.11}$$

In conclusion, the energy budget (2.3.3) can be written as,

$$K+F+P-E+D=0, \tag{2.3.12}$$

where

$$K=\left[\frac{1}{2}\int_0^h (u^2+v^2)\,\mathrm{d}y\right]_t, \tag{2.3.13}$$

$$F=\left[\frac{1}{2}\int_0^h u(u^2+v^2)\,\mathrm{d}y\right]_x, \tag{2.3.14}$$

$$P=\left[\int_0^h (up)\,\mathrm{d}y\right]_x, \tag{2.3.15}$$

$$E=\left[-h_t p_e+\frac{Th_t h_{xx}}{(1+h_x^2)^{\frac{3}{2}}}-\frac{mh_{tt}}{(1+h_x^2)^{\frac{1}{2}}}-\frac{dh_t}{(1+h_x^2)^{\frac{1}{2}}}\right]^{y=h}, \tag{2.3.16}$$

$$D=R^{-1}\left(\int_0^h \left[2u_x^2+2v_y^2+(u_y+v_x)^2\right]\,\mathrm{d}y-\left[\int_0^h (2uu_x+vv_x+vu_y)\,\mathrm{d}y\right]_x\right). \tag{2.3.17}$$

where K is the rate of change of kinetic energy, F is the kinetic energy flux into the system, P is the rate of working of pressure axially, E is the rate of working of fluid stress at the membrane and D is the rate of energy loss due to fluid viscosity in the bulk.

2.4 Linear Stability Analysis

We assume the velocity and pressure of the steady flow when the membrane is flat to be of the form,

$$(u,v)=(U(y),0)=(6y(1-y),0),\quad p=P(x)=C-\left(\frac{12}{R}\right)x,\quad p_e=P(x),\quad h=1. \tag{2.4.1}$$

where C is a constant. This is a solution to equation (2.2.3-2.2.8). We note that the external pressure is not constant in this case, we are instead applying an external pressure gradient to maintain a flat base state.

We add a small perturbation to this steady flow in the form,

$$(u,v,p,h)=(U(y),0,P(x),1)+\varepsilon(\hat{\phi}_y,-\hat{\phi}_x,\hat{p},\hat{\eta})+\varepsilon^2(\breve{\phi}_y,-\breve{\phi}_x,\breve{p},\breve{\eta})+O(\varepsilon^3), \tag{2.4.2}$$

where $\varepsilon \ll 1$, $\hat{\phi}$ and $\breve{\phi}$ are the perturbation streamfunctions at $O(\varepsilon)$ and $O(\varepsilon^2)$. Note that (2.2.3) is satisfied automatically as we have expressed the perturbation velocity in terms of the streamfunctions $\hat{\phi}$ and $\breve{\phi}$.

We substitute the linearised variables into the Navier-Stokes equations (2.2.4-2.2.5), the bound-

ary condition (2.2.6, 2.2.8) and the membrane equations (2.2.10). At $O(1)$ these equations are satisfied automatically as the assumption we made for the velocity and pressure for the steady flow (2.4.1). At $O(\varepsilon)$, the governing equations of the system becomes,

$$\hat{\phi}_{yt} + U\hat{\phi}_{xy} - \hat{\phi}_x U_y + \hat{p}_x - R^{-1}(\hat{\phi}_{xxy} + \hat{\phi}_{yyy}) = 0, \tag{2.4.3}$$

$$\hat{\phi}_{xt} + U\hat{\phi}_{xx} - \hat{p}_y - R^{-1}(\hat{\phi}_{xxx} + \hat{\phi}_{xyy}) = 0, \tag{2.4.4}$$

$$\hat{\phi}_y = 0, \quad \hat{\phi}_x = 0, \qquad (y=0), \tag{2.4.5}$$

$$\hat{\phi}_y = 6\hat{\eta}, \quad \hat{\phi}_x = -\hat{\eta}_t \qquad (y=1), \tag{2.4.6}$$

$$\hat{p} = -T\hat{\eta}_{xx} + m\hat{\eta}_{tt} + \frac{2}{R}\left(6\hat{\eta}_x - \hat{\phi}_{xy}\right) + d\hat{\eta}_t, \qquad (y=1). \tag{2.4.7}$$

At $O(\varepsilon^2)$ the governing equations of the system becomes,

$$\breve{\phi}_{yt} + U\breve{\phi}_{xy} - U_y\breve{\phi}_x + \breve{p}_x - R^{-1}(\breve{\phi}_{xxy} + \breve{\phi}_{yyy}) = \hat{\phi}_x\hat{\phi}_{yy} - \hat{\phi}_y\hat{\phi}_{xy}, \tag{2.4.8}$$

$$\breve{\phi}_{xt} + U\breve{\phi}_{xx} - \breve{p}_y - R^{-1}(\breve{\phi}_{xxx} + \breve{\phi}_{xyy}) = \hat{\phi}_x\hat{\phi}_{xy} - \hat{\phi}_y\hat{\phi}_{xx}, \tag{2.4.9}$$

$$\breve{\phi}_x = 0, \quad \breve{\phi}_y = 0, \qquad (y=0), \tag{2.4.10}$$

$$\breve{\phi}_y - 6\breve{\eta} + \hat{\eta}\hat{\phi}_{yy} - 6\hat{\eta}^2 + \hat{\eta}_x\hat{\eta}_t = 0, \quad \breve{\phi}_x + \hat{\eta}\hat{\phi}_{xy} + \breve{\eta}_t = 0, \qquad (y=1), \tag{2.4.11}$$

$$\breve{p} + T\breve{\eta}_{xx} - m\breve{\eta}_{tt} + \frac{2}{R}\left(\breve{\phi}_{xy} - 6\breve{\eta}_x\right) - d\breve{\eta}_t = \frac{2}{R}\left[-\hat{\eta}\hat{\phi}_{xyy} + 12\hat{\eta}\hat{\eta}_x - \hat{\eta}_x\left(\hat{\phi}_{yy} - \hat{\phi}_{xx}\right)\right] - \hat{\eta}\hat{p}_y,$$
$$(y=1). \tag{2.4.12}$$

2.5 Perturbation Energy Budget

In this section we obtain the corresponding energy budget at $O(\varepsilon)$ and $O(\varepsilon^2)$ by substituting the expansion (2.4.2) into the energy equation (2.3.1). At the first order (*i.e.* $O(\varepsilon)$) the energy equation becomes,

$$U\hat{\phi}_{yt} + U^2\hat{\phi}_{xy} - UU_y\hat{\phi}_x = U\left[-\hat{p}_x + R^{-1}(\hat{\phi}_{xxy} + \hat{\phi}_{yyy})\right] + (-P_x + U_{yy}R^{-1})\hat{\phi}_y, \tag{2.5.1}$$

which can be simplified into,

$$\hat{\phi}_{yt} + U\hat{\phi}_{xy} - U_y\hat{\phi}_x = -\hat{p}_x + R^{-1}(\hat{\phi}_{xxy} + \hat{\phi}_{yyy}). \tag{2.5.2}$$

Equation (2.5.2) is the same as (2.4.3), so no new information is provided. Only at higher orders does the energy budget provide some useful information.
Therefore we analyse the energy equation (2.3.1) at the second order (*i.e.* $O(\varepsilon^2)$) we have,

$$(U\breve{\phi}_{yt} + U^2\breve{\phi}_{xy} - UU_y\breve{\phi}_x) + (\hat{\phi}_x\hat{\phi}_{xt} + \hat{\phi}_y\hat{\phi}_{yt} + U\hat{\phi}_x\hat{\phi}_{xx} + 2U\hat{\phi}_y\hat{\phi}_{xy} - U_y\hat{\phi}_x\hat{\phi}_y + U\hat{\phi}_x\hat{\phi}_{yy}),$$

$$= \left[-U\breve{p}_x - P_x\breve{\phi}_y + R^{-1}(U\breve{\phi}_{yxx} + U\breve{\phi}_{yyy} + U_{yy}\breve{\phi}_y)\right]$$
$$+ \left[-\hat{p}_x\hat{\phi}_y + \hat{p}_y\hat{\phi}_x + R^{-1}(\hat{\phi}_y\hat{\phi}_{yxx} + \hat{\phi}_y\hat{\phi}_{yyy} + \hat{\phi}_x\hat{\phi}_{xxx} + \hat{\phi}_x\hat{\phi}_{xyy})\right]; \tag{2.5.3}$$

rearranging we obtain,

$$\frac{1}{2}(\hat{\phi}_x^2 + \hat{\phi}_y^2)_t + \frac{1}{2}U(3\hat{\phi}_y^2 + \hat{\phi}_x^2)_x - (U\hat{\phi}_x\hat{\phi}_y)_y + (\hat{\phi}_y\hat{p})_x - (\hat{\phi}_x\hat{p})_y - R^{-1}[\hat{\phi}_x(\bigtriangledown^2\hat{\phi})_x + \hat{\phi}_y(\bigtriangledown^2\hat{\phi})_y]$$
$$+ U\breve{\phi}_{yt} + U^2\breve{\phi}_{xy} - UU_y\breve{\phi}_x + U\breve{p}_x + P_x\breve{\phi}_y - R^{-1}(U\breve{\phi}_{yxx} + U\breve{\phi}_{yyy} + U_{yy}\breve{\phi}_y) = 0. \tag{2.5.4}$$

Gathering the terms consisting of breved variables and denoting as $\breve{\varepsilon}$, we obtain

$$\breve{\varepsilon} = U\breve{\phi}_{yt} + U^2\breve{\phi}_{xy} - UU_y\breve{\phi}_x + U\breve{p}_x + P_x\breve{\phi}_y - R^{-1}(U\breve{\phi}_{yxx} + U\breve{\phi}_{yyy} + U_{yy}\breve{\phi}_y). \tag{2.5.5}$$

These terms can then be manipulated to obtain,

$$\breve{\varepsilon} = U\left[\breve{\phi}_{yt} + U\breve{\phi}_{xy} - U_y\breve{\phi}_x + \breve{p}_x - R^{-1}(\breve{\phi}_{xxy} + \breve{\phi}_{yyy})\right] + P_x\breve{\phi}_y - R^{-1}U_{yy}\breve{\phi}_y. \tag{2.5.6}$$

We substitute equation (2.4.8) for the term in square brackets and with $P_x = -12/R$ to obtain,

$$\breve{\varepsilon} = U(-\hat{\phi}_y\hat{\phi}_{xy} + \hat{\phi}_x\hat{\phi}_{yy}) + \left(-\frac{12}{R}\breve{\phi}_y\right) - \left(-\frac{12}{R}\breve{\phi}_y\right) = U(-\hat{\phi}_y\hat{\phi}_{xy} + \hat{\phi}_x\hat{\phi}_{yy}). \tag{2.5.7}$$

We substitute $\breve{\varepsilon}$ back into the energy equation at $O(\varepsilon^2)$ (2.5.4), to obtain the perturbation energy equation in terms of hatted (first order) terms only,

$$U(-\hat{\phi}_y\hat{\phi}_{xy} + \hat{\phi}_x\hat{\phi}_{yy}) + \frac{1}{2}(\hat{\phi}_x^2 + \hat{\phi}_y^2)_t + \frac{1}{2}U(3\hat{\phi}_y^2 + \hat{\phi}_x^2)_x - (U\hat{\phi}_x\hat{\phi}_y)_y + (\hat{\phi}_y\hat{p})_x - (\hat{\phi}_x\hat{p})_y$$
$$- R^{-1}\left[\hat{\phi}_x(\nabla^2\hat{\phi})_x + \hat{\phi}_y(\nabla^2\hat{\phi})_y\right] = 0. \tag{2.5.8}$$

This can be rearranged to the well known Reynolds-Orr equation (Schmid and Henningson [62]),

$$U_y\hat{\phi}_x\hat{\phi}_y - R^{-1}\left(\hat{\phi}_{xx}^2 + \hat{\phi}_{yy}^2 + 2\hat{\phi}_{xy}^2\right) + \left[-\frac{1}{2}U(\hat{\phi}_x^2 + \hat{\phi}_y^2) - \hat{p}\hat{\phi}_y + R^{-1}\left(\hat{\phi}_{xy}\hat{\phi}_y + \hat{\phi}_{xx}\hat{\phi}_x\right)\right]_x$$
$$+ \left[\hat{p}\hat{\phi}_x + R^{-1}\left(\hat{\phi}_{yy}\hat{\phi}_y + \hat{\phi}_{xy}\hat{\phi}_x\right)\right]_y = \hat{\phi}_x\hat{\phi}_{xt} + \hat{\phi}_y\hat{\phi}_{yt}. \tag{2.5.9}$$

To obtain the corresponding perturbation energy budget, we integrate (2.5.8) across the channel ($0 \le y \le 1$) to obtain,

$$\underbrace{\int_0^1 \frac{1}{2}(\hat{\phi}_x^2 + \hat{\phi}_y^2)_t \,\mathrm{d}y}_{I} + \underbrace{\int_0^1 \frac{1}{2}U(3\hat{\phi}_y^2 + \hat{\phi}_x^2)_x \,\mathrm{d}y}_{II} - \underbrace{\int_0^1 (U\hat{\phi}_x\hat{\phi}_y)_y \,\mathrm{d}y}_{III} + \underbrace{\int_0^1 (\hat{\phi}_y\hat{p})_x - (\hat{\phi}_x\hat{p})_y \,\mathrm{d}y}_{IV}$$

$$\underbrace{-R^{-1}\int_0^1 \left[\hat{\phi}_x(\nabla^2\hat{\phi})_x+\hat{\phi}_y(\nabla^2\hat{\phi})_y\right]\,\mathrm{d}y}_{V}+\underbrace{\int_0^1 U(-\hat{\phi}_y\hat{\phi}_{xy}+\hat{\phi}_x\hat{\phi}_{yy})\,\mathrm{d}y}_{\hat{S}}=0. \tag{2.5.10}$$

We label above terms in $I, II, ..., V$ and consider each term in turn. We label the last term as $\hat{S}$, the rate of work of nonlinear Reynolds stresses, which occurs due to the second order terms in the perturbation expansion.
For I, we take the time derivative outside the integral to obtain,

$$I=\underbrace{\left[\frac{1}{2}\int_0^1 \left(\hat{\phi}_x^2+\hat{\phi}_y^2\right)\,\mathrm{d}y\right]_t}_{\hat{K}}. \tag{2.5.11}$$

We denote I as $\hat{K}$, the rate of change of kinetic energy.
As U is only dependent on y, we take the derivative in respect of x outside the integral for term II to obtain,

$$II=\underbrace{\left[\int_0^1 \frac{1}{2}U(3\hat{\phi}_y^2+\hat{\phi}_x^2)\,\mathrm{d}y\right]_x}_{\hat{F}}. \tag{2.5.12}$$

We denote II as $\hat{F}$, the net kinetic energy flux extracted from the mean flow.
We apply the no-slip boundary conditions for III, as $U(0)=U(1)=0$, we have,

$$III=U(1)\left(\hat{\phi}_x\hat{\phi}_y\right)\Big|^{y=1}-U(0)\left(\hat{\phi}_x\hat{\phi}_y\right)\Big|_{y=0}=0. \tag{2.5.13}$$

We apply boundary conditions to IV to obtain,

$$IV=\left[\int_0^1(\hat{\phi}_y\hat{p})\,\mathrm{d}y\right]_x-(\hat{\phi}_x\hat{p})\Big|_{y=0}^{y=1}=\underbrace{\left[\int_0^1(\hat{\phi}_y\hat{p})\,\mathrm{d}y\right]_x}_{\hat{P}}-(\hat{\phi}_x\hat{p})\Big|^{y=1}. \tag{2.5.14}$$

We denote the first term as $\hat{P}$, the rate of working of pressure forces axially.
We add zero term $R^{-1}\hat{\phi}_y\left[(\hat{\phi}_y)_{xx}-(\hat{\phi}_x)_{xy}\right]-R^{-1}\hat{\phi}_x\left[(\hat{\phi}_y)_{xy}-(\hat{\phi}_x)_{yy}\right]=0$ to V. After rearrangement and applying integration by parts we have,

$$\begin{aligned}V=&R^{-1}\int_0^1\left[(\hat{\phi}_x\hat{\phi}_{xx}+\hat{\phi}_y\hat{\phi}_{xy})_x+(\hat{\phi}_x\hat{\phi}_{xy}+\hat{\phi}_y\hat{\phi}_{yy})_y-(\hat{\phi}_{xx})^2-(\hat{\phi}_{xy})^2-(\hat{\phi}_{xy})^2-(\hat{\phi}_{yy})^2\right]\,\mathrm{d}y\\&+R^{-1}\int_0^1\left[(\hat{\phi}_y\hat{\phi}_{xy}-\hat{\phi}_x\hat{\phi}_{yy})_x+(\hat{\phi}_x\hat{\phi}_{xy}-\hat{\phi}_y\hat{\phi}_{xx})_y-(\hat{\phi}_{xy})^2-(\hat{\phi}_{xy})^2+2\hat{\phi}_{xx}\hat{\phi}_{yy}\right]\,\mathrm{d}y;\end{aligned}$$

we then apply the boundary conditions $\hat{\phi}_x=\hat{\phi}_y=0$ at $y=0$ to obtain,

$$V = -\underbrace{R^{-1}\left(\int_0^1 \left[4\hat{\phi}_{xy}^2 + (\hat{\phi}_{yy} - \hat{\phi}_{xx})^2\right] \mathrm{d}y - \left[\int_0^1 \left(2\hat{\phi}_y\hat{\phi}_{xy} + \hat{\phi}_x\hat{\phi}_{xx} - \hat{\phi}_x\hat{\phi}_{yy}\right) \mathrm{d}y\right]_x\right)}_{\hat{D}}$$
$$+ R^{-1}\left(2\hat{\phi}_x\hat{\phi}_{xy} + \hat{\phi}_y\hat{\phi}_{yy} - \hat{\phi}_y\hat{\phi}_{xx}\right)\Big|^{y=1}. \tag{2.5.15}$$

We denote the first term as $\hat{D}$, the energy loss due to viscous dissipation.
Gathering the leftover terms from IV and V and denote it as $\hat{E}$, the rate of working of fluid stress on the membrane. We have

$$\hat{E} = \left[\hat{\phi}_x\hat{p} + R^{-1}\left(2\hat{\phi}_x\hat{\phi}_{xy} + \hat{\phi}_y\hat{\phi}_{yy} - \hat{\phi}_y\hat{\phi}_{xx}\right)\right]^{y=1}. \tag{2.5.16}$$

Therefore, energy equation at $O(\varepsilon^2)$ (2.5.10) becomes,

$$\hat{K} + \hat{F} + \hat{P} - \hat{E} + \hat{D} + \hat{S} = 0, \tag{2.5.17}$$

where,

$$\hat{K} = \left[\int_0^1 \frac{1}{2}(\hat{\phi}_x^2 + \hat{\phi}_y^2)\,\mathrm{d}y\right]_t, \tag{2.5.18}$$
$$\hat{F} = \left[\int_0^1 \frac{1}{2}U(3\hat{\phi}_y^2 + \hat{\phi}_x^2)\,\mathrm{d}y\right]_x, \tag{2.5.19}$$
$$\hat{P} = \left[\int_0^1 (\hat{\phi}_y\hat{p})\,\mathrm{d}y\right]_x, \tag{2.5.20}$$
$$\hat{E} = \left[\hat{\phi}_x\hat{p} + R^{-1}\left(2\hat{\phi}_x\hat{\phi}_{xy} + \hat{\phi}_y\hat{\phi}_{yy} - \hat{\phi}_y\hat{\phi}_{xx}\right)\right]^{y=1}, \tag{2.5.21}$$
$$\hat{D} = R^{-1}\left(\int_0^1 \left[4\hat{\phi}_{xy}^2 + (\hat{\phi}_{yy} - \hat{\phi}_{xx})^2\right] \mathrm{d}y - \left[\int_0^1 \left(2\hat{\phi}_y\hat{\phi}_{xy} + \hat{\phi}_x\hat{\phi}_{xx} - \hat{\phi}_x\hat{\phi}_{yy}\right) \mathrm{d}y\right]_x\right), \tag{2.5.22}$$
$$\hat{S} = \int_0^1 U(-\hat{\phi}_y\hat{\phi}_{xy} + \hat{\phi}_x\hat{\phi}_{yy})\,\mathrm{d}y. \tag{2.5.23}$$

Here $\hat{K}$ is the rate of change of kinetic energy, $\hat{F}$ is the net kinetic energy flux extracted from the mean flow, $\hat{P}$ is the rate of working of pressure force axially, $\hat{E}$ is the rate of working of fluid stress at the membrane, $\hat{D}$ is the energy loss due to viscous dissipation and $\hat{S}$ is the work of nonlinear Reynolds stresses. Note that the second term in $\hat{D}$ will disappear over one wavelength, the form of the first term suggests that the value of $\hat{D}$ is not less than zero over one wavelength (all terms appear as quadratics).
In this derivation, we eliminate the breved variables in $\breve{\varepsilon}$ (2.5.5) in favor of first order variables and then integrate it across the static channel $(0 \le y \le 1)$ to obtain the term $\hat{S}$. However, we can

also manipulate $\breve{\varepsilon}$ directly into terms including breved variables. Rearranging $\breve{\varepsilon}$ we have,

$$\begin{aligned}\breve{\varepsilon} = &\left(U\breve{\phi}_y\right)_t + \left(\frac{3}{2}\breve{\phi}_y U^2\right)_x - \left(\frac{1}{2}\breve{\phi}_x U^2\right)_y + (U\breve{p})_x + \breve{\phi}_y P_x \\ &- R^{-1}\left[U\left(\breve{\phi}_{yyy} + \breve{\phi}_{xxy}\right) + U_{yy}\breve{\phi}_y\right].\end{aligned} \tag{2.5.24}$$

Integrating (2.5.24) across the static channel ($0 \le y \le 1$) we obtain,

$$\begin{aligned}\hat{S} = &\underbrace{\int_0^1 \left(U\breve{\phi}_y\right)_t \,\mathrm{d}y}_{I} + \underbrace{\int_0^1 \left[\left(\frac{3}{2}\breve{\phi}_y U^2\right)_x - \left(\frac{1}{2}\breve{\phi}_x U^2\right)_y\right]\mathrm{d}y}_{II} + \underbrace{\int_0^1 \left[(U\breve{p})_x + \breve{\phi}_y P_x\right]\mathrm{d}y}_{III} \\ &\underbrace{- R^{-1}\int_0^1 \left[U\left(\breve{\phi}_{yyy} + \breve{\phi}_{xxy}\right) + U_{yy}\breve{\phi}_y\right]\mathrm{d}y}_{IV},\end{aligned} \tag{2.5.25}$$

we label above terms in $I, II, ..., IV$ and consider each term in turn.
For I, we take the time derivative outside the integral to obtain,

$$I = \underbrace{\left[\int_0^1 U\breve{\phi}_y \mathrm{d}y\right]_t}_{\breve{K}}. \tag{2.5.26}$$

We denote I as $\breve{K}$, the rate of working of kinetic energy that contains second order variables.
For II, taking the derivatives with respect to x and y outside the integrals we have,

$$II = \left[\int_0^1 \left(\frac{3}{2}\breve{\phi}_y U^2\right)\mathrm{d}y\right]_x - \left[\frac{1}{2}\breve{\phi}_x U^2\right]_{y=0}^{y=1} = \underbrace{\left[\int_0^1 \left(\frac{3}{2}\breve{\phi}_y U^2\right)\mathrm{d}y\right]_x}_{\breve{F}}. \tag{2.5.27}$$

We denote II as $\breve{F}$, the contribution to the kinetic energy flux that contains second order variables. We also apply $U(0) = U(1) = 0$ here.
Similarly, for III taking the derivatives outside the integrals we obtain,

$$III = \underbrace{\left[\int_0^1 (U\breve{p})\,\mathrm{d}y\right]_x + \left[P\breve{\phi}_y\right]^{y=1}}_{\breve{P}}. \tag{2.5.28}$$

We denote the first term as $\breve{P}$, the work done by the pressure force that contains the second order variables. Here we apply the boundary condition (2.4.10), $\breve{\phi}_x = 0$ at $y = 0$ for the second term, while the remainder of this term will contribute below.
For IV, similar to the derivation of $\hat{D}$ (2.5.15), we add zero term $R^{-1}\left[U\left((\breve{\phi}_y)_{xx} - (\breve{\phi}_x)_{xy}\right) - U_{xy}\breve{\phi}_x\right] =$

0 to obtain,

$$\begin{aligned} IV =& R^{-1}\int_0^1 \left[\left(U\breve{\phi}_{yy}\right)_y - U_y\breve{\phi}_{yy} + \left(U\breve{\phi}_{xy}\right)_x + \left(U_y\breve{\phi}_y\right)_y - U_y\breve{\phi}_{yy} \right] \mathrm{d}y \\ &+ R^{-1}\int_0^1 \left[\left(U\breve{\phi}_{xy}\right)_x - \left(U\breve{\phi}_{xx}\right)_y + U_y\breve{\phi}_{xx} - \left(U_y\breve{\phi}_x\right)_x + U_y\breve{\phi}_{xx} \right] \mathrm{d}y, \end{aligned}$$

taking the derivatives outside the integrals and applying boundary conditions $\breve{\phi}_y = 0$ at $y = 0$ we obtain,

$$\begin{aligned} IV =& R^{-1}\left[U\breve{\phi}_{yy} + U_y\breve{\phi}_y - U\breve{\phi}_{xx} \right]_{y=0}^{y=1} + R^{-1}\left[\int_0^1 \left(2U\breve{\phi}_{xy} - U_y\breve{\phi}_x\right) \mathrm{d}y \right]_x \\ &- R^{-1}\int_0^1 2U_y\left(\breve{\phi}_{yy} - \breve{\phi}_{xx}\right) \mathrm{d}y, \\ =& \underbrace{R^{-1}\left[U_y\breve{\phi}_y \right]^{y=1}}_{\breve{E}} \underbrace{- R^{-1}\int_0^1 2U_y\left(\breve{\phi}_{yy} - \breve{\phi}_{xx}\right) \mathrm{d}y - R^{-1}\left[\int_0^1 \left(2U\breve{\phi}_{xy} - U_y\breve{\phi}_x\right) \mathrm{d}y \right]_x}_{\breve{D}}. \end{aligned} \tag{2.5.29}$$

We denote the first term as $\breve{E}$, the work done by the fluid stress at the membrane that contains second order varibales. We denote the second term as $\breve{D}$, the work done by dissipation that contains second order variables.
Therefore, equation (2.5.25) becomes,

$$\hat{S} = \breve{K} + \breve{F} + \breve{P} - \breve{E} + \breve{D}, \tag{2.5.30}$$

where,

$$\breve{K} = \left[\int_0^1 \left(U\breve{\phi}_y\right) \mathrm{d}y \right]_t, \tag{2.5.31}$$

$$\breve{F} = \left[\int_0^1 \left(\frac{3}{2}\breve{\phi}_y U^2 \right) \mathrm{d}y \right]_x, \tag{2.5.32}$$

$$\breve{P} = \left[\int_0^1 \left(U\breve{p}\right) \mathrm{d}y \right]_x + \left[P\breve{\phi}_y \right]^{y=1}, \tag{2.5.33}$$

$$\breve{E} = R^{-1}\left[U_y\breve{\phi}_y \right]^{y=1}, \tag{2.5.34}$$

$$\breve{D} = R^{-1}\int_0^1 2U_y\left(\breve{\phi}_{yy} - \breve{\phi}_{xx}\right) \mathrm{d}y - R^{-1}\left[\int_0^1 \left(2U\breve{\phi}_{xy} - U_y\breve{\phi}_x\right) \mathrm{d}y \right]_x. \tag{2.5.35}$$

Here $\breve{K}$ is the rate of working of kinetic energy that contains second order variables, $\breve{F}$ is the net kinetic energy flux extracted from the mean flow that contains second order variables, $\breve{P}$ is the work done by the pressure force that contains the second order variables, $\breve{E}$ is the work done

by the fluid stress at the membrane that contains second order variables, $\breve{D}$ is the work done by dissipation that contains second order variables.
In total, the linearized energy budget at $O(\varepsilon^2)$ can also be expressed as,

$$\left(\hat{K}+\breve{K}\right)+\left(\hat{F}+\breve{F}\right)+\left(\hat{P}+\breve{P}\right)-\left(\hat{E}+\breve{E}\right)+\left(\hat{D}+\breve{D}\right)=0. \tag{2.5.36}$$

Here $\hat{E}+\breve{E}$ is total energy exchange between the fluid and membrane at $O(\varepsilon^2)$.

2.6 Eigenvalue problems

To solve equations (2.4.3-2.4.7), we assume all the hatted variables and breved variables are in the wave-like forms

$$\hat{f}(x,y,t)=f(y)e^{i(kx-\omega t)}+\left(f(y)(e^{i(kx-\omega t)}\right)^*, \tag{2.6.1}$$

$$\breve{g}(x,y,t)=g_1(y)e^{2i(kx-\omega t)}+g_0(y)+\left(g_1(y)e^{2i(kx-\omega t)}\right)^*, \tag{2.6.2}$$

where k is wavenumber and ω is frequency, while $*$ denotes complex conjugation. We use $\hat{f}$ and $\breve{g}$ to represent all the hatted variables ($\hat{\phi}$, $\hat{p}$ and $\hat{\eta}$) and breved variables ($\breve{\phi}$, $\breve{p}$ and $\breve{\eta}$), respectively.
Substituting (2.6.1) into the system governing equations at $O(\varepsilon)$ (2.4.3-2.4.7), we have

$$\left(U-\frac{\omega}{k}\right)\phi_y-\phi U_y=-p+(ikR)^{-1}\left(-k^2\phi_y+\phi_{yyy}\right), \tag{2.6.3}$$

$$k^2\left(U-\frac{\omega}{k}\right)\phi=-p_y+(ikR)^{-1}\left(-k^4\phi+k^2\phi_{yy}\right), \tag{2.6.4}$$

$$\phi=0,\quad \phi_y=0, \qquad (y=0), \tag{2.6.5}$$

$$\phi_y=6\eta,\quad \phi=\frac{\omega}{k}\eta,\quad p=Tk^2\eta-m\omega^2\eta+\frac{2}{R}ik(6\eta-\phi_y)-di\omega\eta, \qquad (y=1). \tag{2.6.6}$$

Combining (2.6.3) and (2.6.4) by eliminating p, we obtain the classical Orr-Sommerfeld equation (Schmid and Heinningson [62]),

$$\left(U-\frac{\omega}{k}\right)\left(\phi_{yy}-k^2\phi\right)-U_{yy}\phi=(ikR)^{-1}\left(\phi_{yyyy}-2k^2\phi_{yy}+k^4\phi\right). \tag{2.6.7}$$

We solve this eigenvalue problem for ϕ using a Chebyshev spectral method. We fix the wavenumber $k\in\mathbb{R}$ and compute the corresponding frequency $\omega=\omega_r+i\omega_i\in\mathbb{C}$. Details of the numerical scheme are given in Stewart *et al*. [66]. This scheme has been substantially modified to include the influence of wall mass.
Substituting (2.6.1) and (2.6.2) into the second order Navier-Stokes equation (2.4.8) and boundary conditions (2.4.10,2.4.11), we consider steady streaming terms which are independent of both x and t (here we drop the time dependent terms as these terms will make no contribution to

the steady system after one period of time) to obtain ODEs in the form,

$$\phi_{0yyy} = R\left[(ik\phi_y)\phi_y^* + (ik\phi_y)^*\phi_y - (ik\phi)^*\phi_{yy} - (ik\phi)\phi_{yy}^*\right], \tag{2.6.8}$$

$$\phi_{0y} = 0, \qquad (y=0), \tag{2.6.9}$$

$$\phi_{0y} = -\eta^*\phi_{yy} - \eta\phi_{yy}^* + 12\eta\eta^* - 2k\omega\eta\eta^*, \qquad (y=1). \tag{2.6.10}$$

We find that the additional boundary condition (kinematic boundary condition) is identically zero. Here we assume $\eta_0 = 0$ at $y = 1$ to ensure the mass of fluid stays fixed. By integrating (2.6.8) and applying boundary conditions (2.6.9, 2.6.10) we have,

$$\phi_{0y} = \int_0^y \int_0^{y'} R\left[(ik\phi_\varsigma)\phi_\varsigma^* + (ik\phi_\varsigma)^*\phi_\varsigma - (ik\phi)^*\phi_{\varsigma\varsigma} - (ik\phi)\phi_{\varsigma\varsigma}^*\right] \mathrm{d}\varsigma\,\mathrm{d}y' + C_1 y, \tag{2.6.11}$$

$$\phi_{0yy} = \int_0^y R\left[(ik\phi_\varsigma)\phi_\varsigma^* + (ik\phi_\varsigma)^*\phi_\varsigma - (ik\phi)^*\phi_{\varsigma\varsigma} - (ik\phi)\phi_{\varsigma\varsigma}^*\right] \mathrm{d}\varsigma + C_1, \tag{2.6.12}$$

where the constant C_1 is,

$$\begin{aligned} C_1 = &-\int_0^1 \int_0^y R\left[(ik\phi_\varsigma)\phi_\varsigma^* + (ik\phi_\varsigma)^*\phi_\varsigma - (ik\phi)^*\phi_{\varsigma\varsigma} - (ik\phi)\phi_{\varsigma\varsigma}^*\right] \mathrm{d}\varsigma\,\mathrm{d}y \\ &+ \left[12\eta\eta^* - \eta^*\phi_{yy} - \eta\phi_{yy}^* - (ik\eta)^*(-i\omega\eta) - (ik\eta)(-i\omega\eta)^*\right]^{y=1}. \end{aligned} \tag{2.6.13}$$

Using the predictions of eigenfunctions from (2.6.7) and substituting into the above equations (2.6.11) and (2.6.12), we can obtain the numerical predictions of the time and space averaged breved variables. Therefore, we can compute the breved energy budgets (*e.g.* $\breve{P}$, $\breve{E}$, $\breve{D}$, *etc.*) as well as the hatted terms ($\hat{S}$, $\hat{D}$, $\hat{P}$, *etc.*) directly. This is a significant step forward from the work of Stewart *et al*. [69] who only compute the hatted energy budget.

2.7 Numerical Results

For fixed Reynolds number R and wavenumber k, solving the eigenvalue problem (2.6.7) using Chebyshev spectral method, we obtain the corresponding eigenvalues ω (frequency) and eigenfunctions $\hat{\phi}$. The system is unstable when the imaginary part of frequency $\omega_i > 0$ and stable when $\omega_i < 0$. For a given R, wavenumber k that separates stable from unstable is called neutrally stable point (*i.e.* $\omega_i = 0$).

In this section, we search for neutrally stable curves in the parameter space spanned by R and k using a bisection method. In particular, we consider four different slices through the parameter space (figures 2.2 - 2.5). We also calculate the system's corresponding average energy budgets over one period and wavelength for several points on the neutrally stable curves, listed in the tables 2.1 and 2.2.

2.7.1 Case with no wall mass or damping

As a baseline case, we show the neutrally stable curves in the parameter space spanned by Reynolds number R and wavenumber k for tension $T = 10$, mass $m = 0$, and damping $d = 0$, shown in figure 2.2 (a). These parameter values were previously considered by Stewart *et al*. [69].

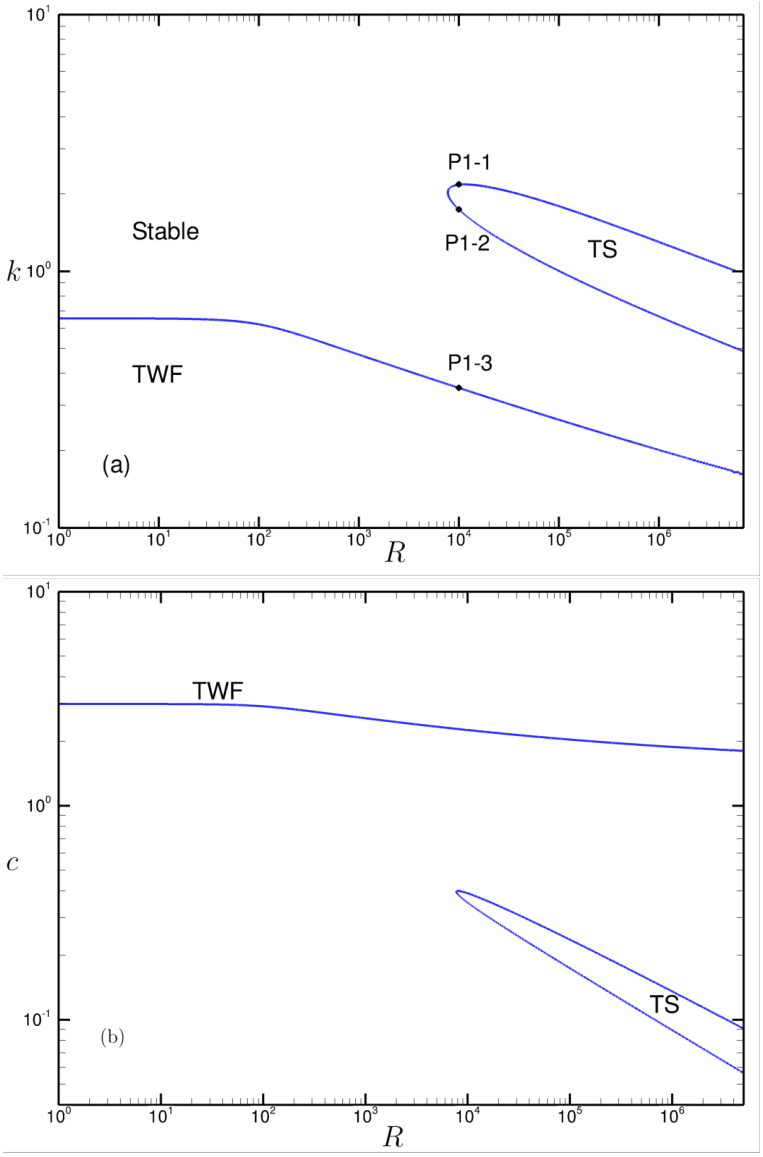

Figure 2.2: (a) Neutrally stable curves (*i.e.* $\omega_i = 0$) in wavenumber k against Reynolds number R, for $m = 0, T = 10$, and $d = 0$. For low wavenumber k, the system is unstable to TWF, for large R the system is unstable to TS in a tongue-shape region; (b) Corresponding neutrally stable curves in wave speed c against Reynolds number R, for $m = 0, T = 10$ and $d = 0$.

We identify three neutral points P1-1, P1-2, P1-3 in this figure. For low wavenumber k, the system is unstable to traveling-wave flutter (TWF), see Davies and Carpenter [22] and Stewart

et al [66] for more details. For large R the system is unstable to Tollmien-Schlichting wave (TS) in a tongue-shape region (Stewart *et al* [66]).

The corresponding wave speed of the neutrally stable perturbations $c = \omega/k$ against Reynolds number is plotted in figure 2.2 (b). The wave speed of TWF wave is much faster than the wave speed of TS wave, and it tends to a finite value $(3/2)$ as $R \to \infty$ (Stewart *et al*. [69]).

2.7.2 Case including wall mass

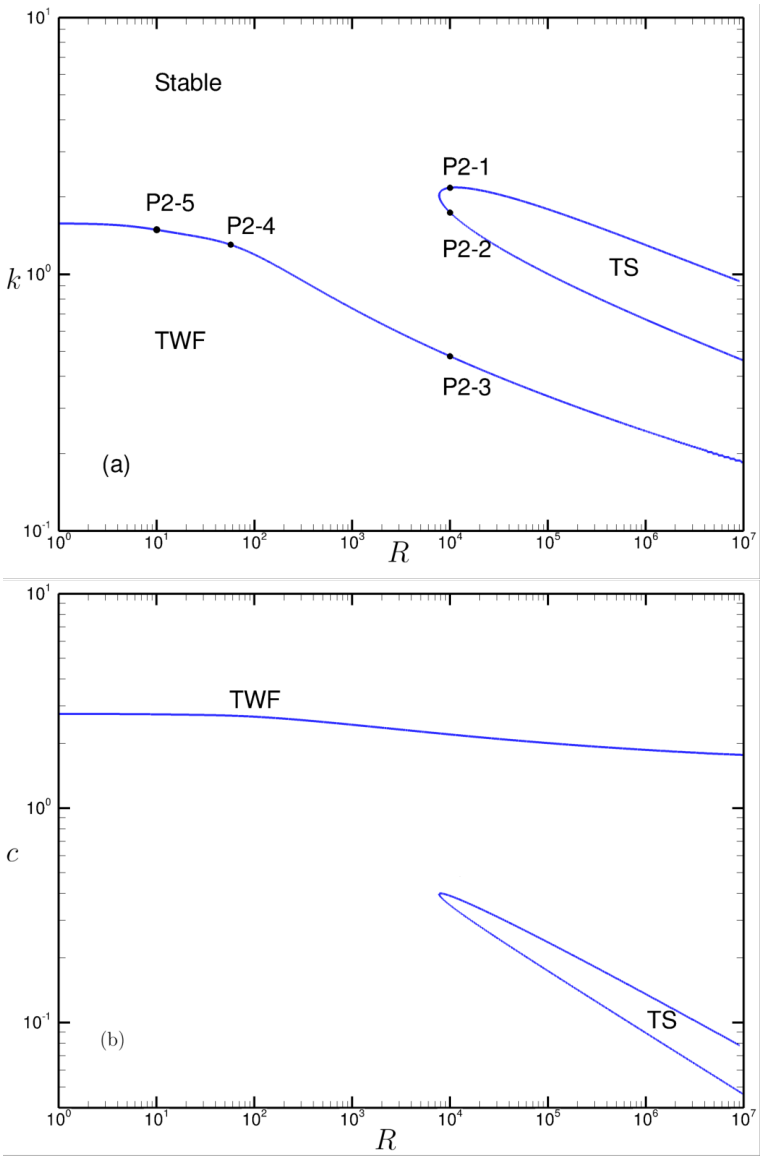

Figure 2.3: (a) Neutrally stable curves (*i.e.* $\omega_i = 0$), wavenumber k against Reynolds number R for mass $m = 1$, tension $T = 10$, and damping $d = 0$, the system is unstable to TS in the tongue-shaped region, and unstable to TWF for lower k. (b) Corresponding neutrally stable curves in wavespeed c against Reynolds number R, for $m = 1, T = 10$ and $d = 0$.

To assess the change to the neutral curve including wall mass, figure 2.3(a) gives the neutrally stable curve in parameter space R against wavenumber k for small wall mass $m = 1$, tension $T = 10$ and damping $d = 0$. Similar to figure 2.2, the system is unstable to TS in the tongue-shape region for large Reynolds number R, and unstable to TWF for low wavenumber k. However, the unstable region of TWF is significantly enlarged compared to the baseline case. We identify five neutrally stable points P2-1, P2-2, P2-3, P2-4 and P2-5, and give the numerical results of frequency and second order energy budgets over one period of time and wavelength in table 2.1,2.2 below.

Figure 2.3(b) plot the corresponding wave speed against R when $m = 1$, $T = 10$ and $d = 0$. Similar to the case with no wall mass and damping, the wave speed of TWF is much higher than the wave speed of TS wave and it tends to $3/2$ when $R \to \infty$.

Figure 2.4 shows the neutrally stable curve in parameter space wall mass m against wavenumber k for fixed Reynolds number $R = 100$, tension $T = 10$ without considering damping, *i.e.* $d = 0$, shown in Figure 2.3. The system is unstable to TWF for low wavenumber and stable for high wavenumber. We observe that the system eventually becomes short wavelength unstable as $m \to \infty$, as well as that the critical wavenumber $k_c \sim m$ but we do not explore this scaling further here.

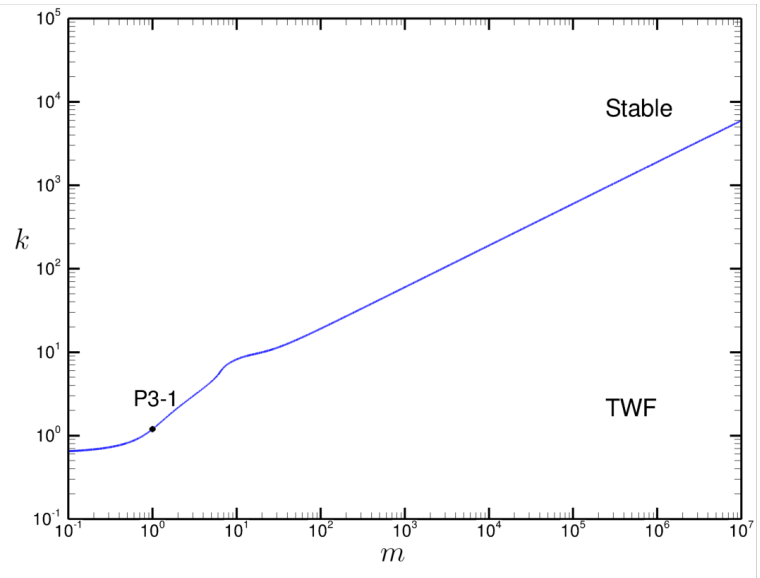

Figure 2.4: Neutrally stable curves (*i.e.* $\omega_i = 0$), in parameter space wavenumber k against wall mass m for fixed $R = 100, T = 10$, and $d = 0$. The system is unstable to TWF for low wavenumber, and stable to higher wavenumber.

2.7.3 Case including wall mass and damping

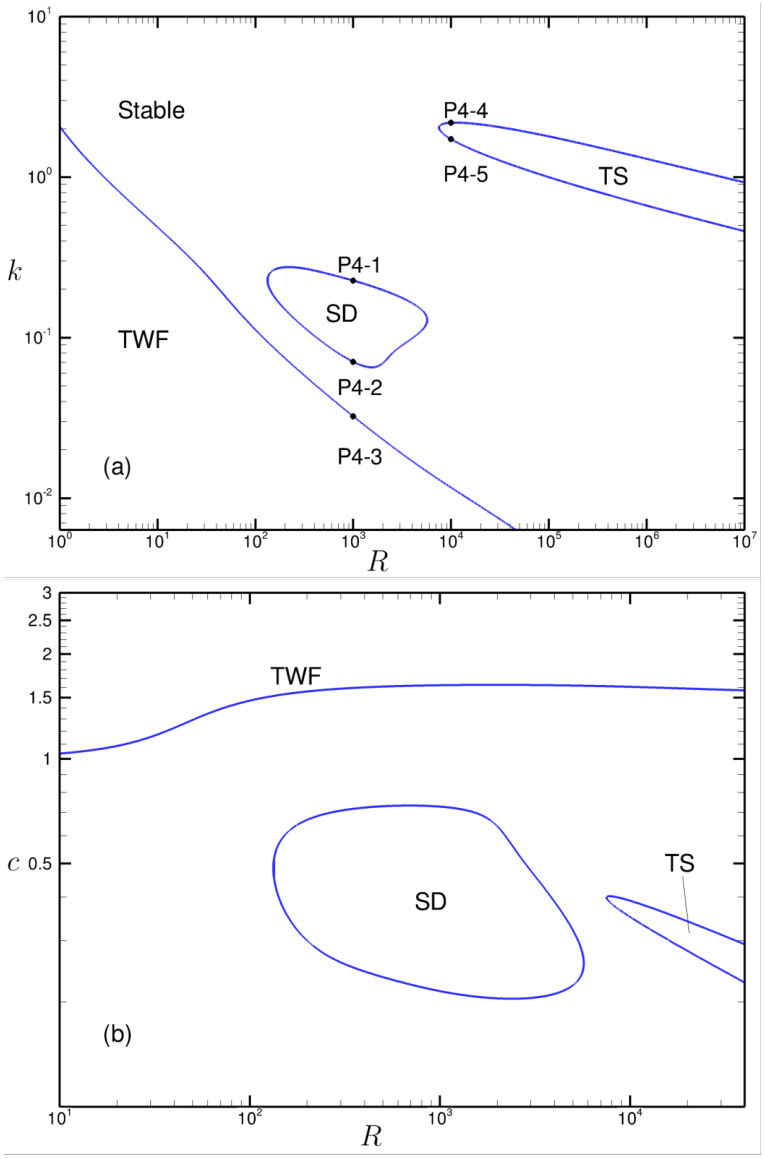

Figure 2.5: (a) Neutrally stable curves (*i.e.* $\omega_i = 0$), wavenumber k against Reynolds number R for mass $m = 10$, tension $T = 10$, and damping $d = 10$, the system is unstable to TS in the tongue-shaped region, unstable to TWF for lower k, and unstable to SD in loop-shape region; (b) Corresponding neutrally stable curves in wavespeed c against Reynolds number R for $m = 10, T = 10$ and $d = 10$.

Figure 2.5(a) shows the neutrally stable curve in parameter space R against k for wall mass $m = 10$, tension $T = 10$ and damping $d = 10$. Similar to the previous two figures (figures 2.2 and 2.3), the system is unstable to TWF for low wavenumber k and unstable to TS in the tongue-shape region for large Reynolds number. However, we also found an additional loop-shaped neutrally stable curve inside which the system is unstable to Static Divergence (SD). This SD is destabilized by wall damping consistent with a class A instability. We track the frequency and

linearized energy budgets over one period of time and wavelength for five neutrally stable points labels as P4-1, P4-2, P4-3 P4-4 and P4-5 in tables 2.1 and 2.2 below. The corresponding wave speed against R is plotted in figure 2.5(b). The wave speed of TWF wave is faster than that of SD wave, as well as the wave speed of TS wave.

2.7.4 Stability of TS, TWF and SD wave

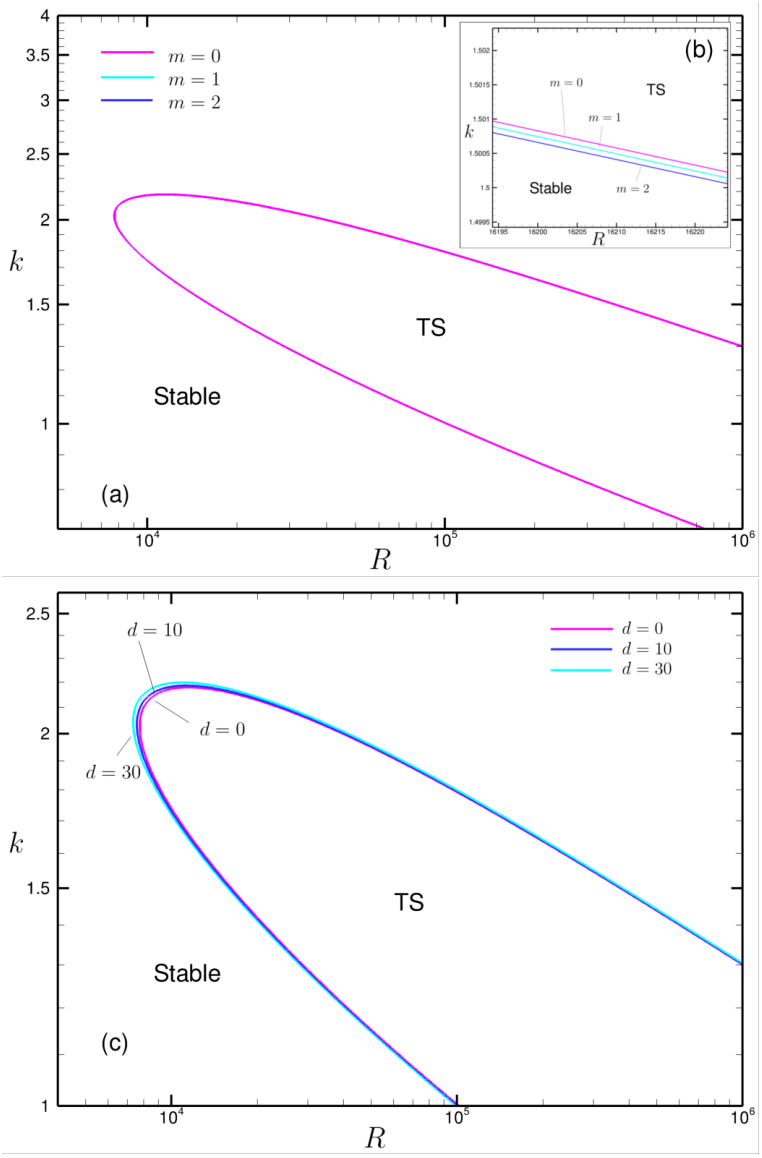

Figure 2.6: (a) TS neutrally stable curves (*i.e.* $\omega_i = 0$), in wavenumber k against R for $T = 10, d = 0$ and $m = 0, 1, 2$; (b) zoom in of (a); (c) TS neutrally stable curves in wavenumber k against R for $m = 1, T = 10$ and $d = 0, 10, 30$.

In this section, we discuss the stability of TS, TWF and SD wave, respectively. We plot the neutrally stable curve in parameter space (k, R) for different modes of instability where we

control the the value of wall mass and damping.

Figure 2.6 considers the neutrally stable curve of the TS wave. Figure 2.6(a) and 2.6(c) show the neutrally stable curve while we change the wall mass as $m = 0, 1, 2$ and the wall damping as $d = 0, 10, 30$, respectively. Figure 2.6(b) gives the zoom in figure of lower branch of TS neutrally stable curve of figure 2.6(a). The TS wave is slightly destabilised by wall damping (shown in figure 2.6(c)), which agrees with the observation by Davies & Carpenter [22]. This behavior indicates a class A instability (Benjamin [2], Landahl [45] and Benjamin [3]). Figure 2.6(a), (b) show that the TS wave is also mildly destabilized by the wall mass as well.

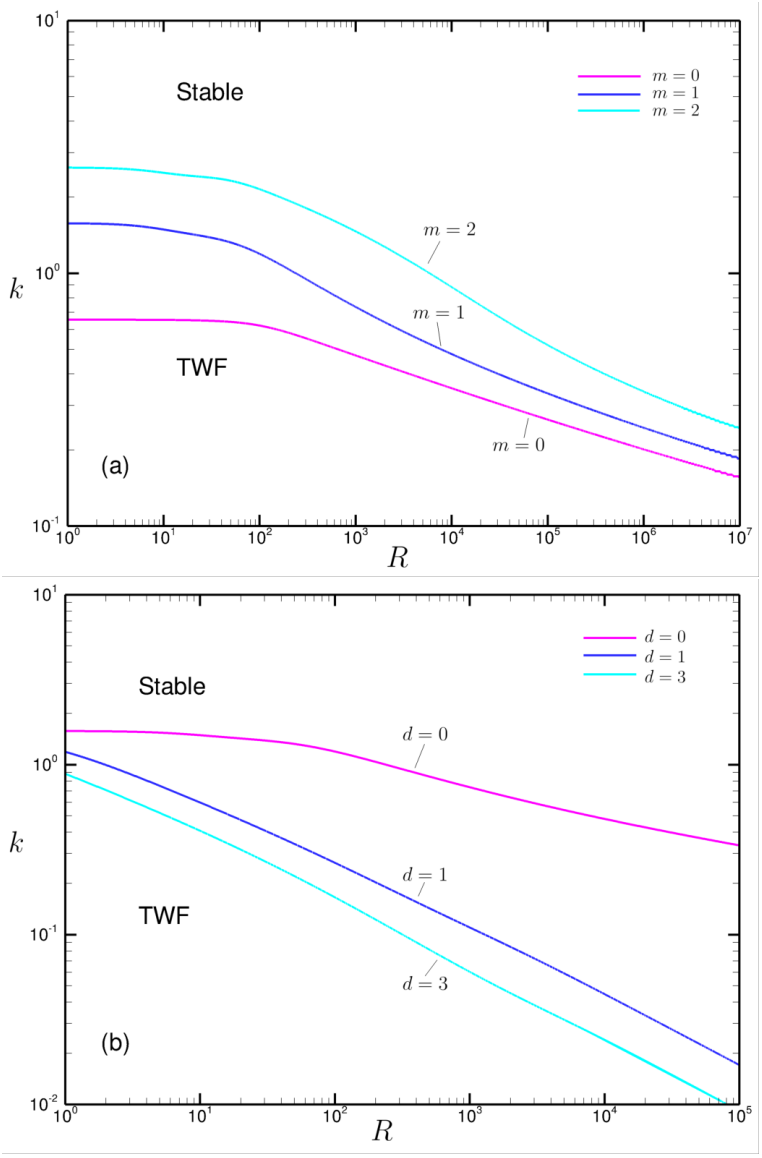

Figure 2.7: (a) TWF neutrally stable curves (*i.e.* $\omega_i = 0$) in wavenumber k against Reynolds number R for $T = 10, d = 0$ and $m = 0, 1, 2$; (b) TWF neutrally stable curves in wavenumber k against R for $m = 1, T = 10$ and $d = 0, 1, 3$.

Figure 2.7 considers the neutral stability curve of TWF mode. Figure 2.7(a) and 2.7(b) plot the

neutrally stable curve in parameter space (k,R) for wall mass $m = 0,1,2$ and damping $d = 0,1,3$, respectively. The TWF mode is slightly stabilized by wall damping (shown in figure 2.7(b)), which implies a class B instability (Benjamin [2], Landahl [45] and Benjamin [3]). Similar to the TS wave, the TWF mode can be destabilised by wall mass (shown in figure 2.7(a)).

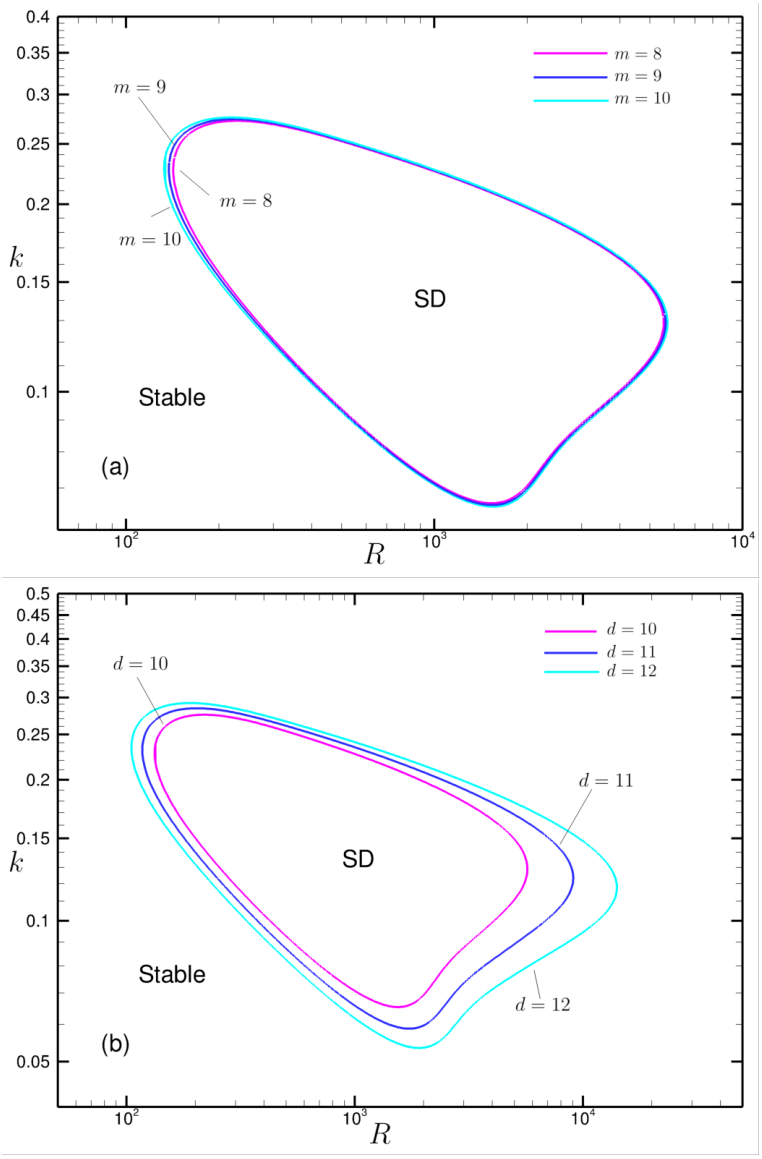

Figure 2.8: (a) SD neutrally stable curves (*i.e.* $\omega_i = 0$) in wavenumber k against R for $T = 10, d = 10$ and $m = 8,9,10$; (b) SD neutrally stable curves in wavenumber k against R for $m = 10, T = 10$ and $d = 10,11,12$.

Figure 2.8 plots the neutrally stable curves of the SD mode when we vary the wall mass as $m = 8,9,10$ (shown in figure 2.8(a)) and damping as $d = 10,11,12$ (shown in figure 2.8(b)). Figure 2.8(b) shows that the SD mode can be destabilised by damping, hence a class A instability (Benjamin [2], Landahl [45] and Benjamin [3]). Larger wall mass can weakly destabilize the SD mode (see figure 2.8(a)).

2.7.5 Energy budgets on neutrally stable points

In this section, we evaluate the second order energy budget of the system over one period of time and wavelength, and compute at several of the neutrally stable points in figure 2.2-2.5.
First, we simplify the linearized energy budget. For $\hat{S}$ in (2.5.23), we rewrite the second term using integration by parts as,

$$\begin{aligned}\hat{S} &= \int_0^1 U\left[-\hat{\phi}_y\hat{\phi}_{xy} + \left(\hat{\phi}_x\hat{\phi}_y\right)_y - \hat{\phi}_y\hat{\phi}_{xy}\right] \mathrm{d}y, \\ &= \left[U\hat{\phi}_x\hat{\phi}_y\right]_{y=0}^{y=1} - \int_0^1 \left(U_y\hat{\phi}_x\hat{\phi}_y\right) \mathrm{d}y - \int_0^1 U\left(\hat{\phi}_y^2\right)_x \mathrm{d}y,\end{aligned}$$

as U is independent of x. Applying the boundary condition at $U(0) = U(1) = 0$ we have,

$$\hat{S} = -\int_0^1 \left(U_y\hat{\phi}_x\hat{\phi}_y\right) \mathrm{d}y - \left[\int_0^1 \left(U\hat{\phi}_y^2\right) \mathrm{d}y\right]_x. \tag{2.7.1}$$

The second term will disappear when averaged over one wavelength.
For $\hat{E}$ in (2.5.21), we apply the boundary conditions (2.4.6, 2.4.7) to obtain

$$\begin{aligned}\hat{E} &= \left[T\hat{\eta}_t\hat{\eta}_{xx} - m\hat{\eta}_t\hat{\eta}_{tt} - d\hat{\eta}_t^2 + \frac{2}{R}(6\hat{\eta}_x - \hat{\phi}_{xy})\hat{\phi}_x + R^{-1}\left(2\hat{\phi}_x\hat{\phi}_{xy} + \hat{\phi}_y\hat{\phi}_{yy} - \hat{\phi}_y\hat{\phi}_{xx}\right)\right]^{(y=1)}, \\ &= \left[R^{-1}\left(\hat{\phi}_y\hat{\phi}_{yy} - 3\hat{\phi}_y\hat{\phi}_{xx}\right) - d\hat{\eta}_t^2\right]^{(y=1)} + \left[T\hat{\eta}_t\hat{\eta}_x - \frac{2}{R}\left(6\hat{\eta}\hat{\phi}_x - 2\hat{\phi}_y\hat{\phi}_x\right)\right]_x^{(y=1)} \\ &\quad - \left(\frac{T}{2}\hat{\eta}_x^2 + \frac{m}{2}\hat{\eta}_t^2\right)_t^{y=1}.\end{aligned} \tag{2.7.2}$$

The last two terms will disappear over one period of time and wavelength.
Substituting the wave-like form (2.6.1) for the hatted variables, and taking an average over both a period of time and wavelength, the energy budget (2.5.17-2.5.23) reduces to,

$$\bar{\hat{S}} + \bar{\hat{D}} - \bar{\hat{E}} = 0, \tag{2.7.3}$$

where,

$$\bar{\hat{S}} = \int_0^1 U\left[(ik\phi)^*\phi_{yy} + (ik\phi)\phi_{yy}^*\right] \mathrm{d}y, \tag{2.7.4}$$

$$\bar{\hat{D}} = R^{-1}\int_0^1 \left(8k^2\phi_y\phi_y^* + 2k^4\phi\phi^* + 2\phi_{yy}\phi_{yy}^* + 2k^2\phi^*\phi_{yy} + 2k^2\phi\phi_{yy}^*\right) \mathrm{d}y, \tag{2.7.5}$$

$$\bar{\hat{E}} = \left[R^{-1}\left(\phi_y^*\phi_{yy} + \phi_y\phi_{yy}^* + 3k^2\phi_y^*\phi + 3k^2\phi_y\phi^*\right) + 2d\omega^2\eta\eta^*\right]^{y=1}. \tag{2.7.6}$$

The energy of the perturbed system is extracted from the mean flow by $\bar{\hat{S}}$, $\bar{\hat{E}}$ (work done by nonlinear Reynolds stresses and rate of working of fluid stress at the membrane) and consumed

by $\bar{\tilde{D}}$ (energy loss due to dissipation).
Taking an average over one period of both time and wavelength, then substituting wavelike form (2.6.2) for all the breve variables, the energy budget (2.5.30-2.5.35) becomes,

$$\bar{\tilde{S}} = \bar{\breve{P}} - \bar{\breve{E}} + \bar{\breve{D}}, \tag{2.7.7}$$

where

$$\bar{\breve{P}} = -\int_0^1 \frac{12}{R}\breve{\phi}_y \,\mathrm{d}y = -\frac{12}{R}\breve{\phi}(1), \tag{2.7.8}$$

$$\bar{\breve{E}} = -\left(\frac{6}{R}\breve{\phi}_y\right)^{y=1}, \tag{2.7.9}$$

$$\bar{\breve{D}} = \int_0^1 \frac{12}{R}(1-2y)\breve{\phi}_{yy}\,\mathrm{d}y. \tag{2.7.10}$$

In other words, the system's energy budget at $O(\varepsilon^2)$ can also be expressed as,

$$\bar{\breve{P}} - (\bar{\tilde{E}} + \bar{\breve{E}}) + (\bar{\tilde{D}} + \bar{\breve{D}}) = 0. \tag{2.7.11}$$

Using the numerical results computed from the above eigenvalue problems, we can calculate the terms in the perturbation energy budgets in equation (2.7.11). In figure 2.9, we display the Reynolds number R against the second order energy exchange from fluid to membrane $\bar{E} = \bar{\tilde{E}} + \bar{\breve{E}}$ on several neutral points (including P2-1, P2-2, P2-3, P2-4 and P2-5) in figure 2.3 ($m = 1$, $T = 10$, $d = 0$). Figure 2.11 shows the Reynolds number against the energy exchange $\bar{E}$ on points (including P3-1 - P3-5) picked from figure 2.4 ($m = 10$, $T = 10$, $d = 10$). Figure 2.10 and 2.12 show the zoom in plots of figure 2.9 and 2.11, respectively.
The blue line in figure 2.9 shows the energy exchange $\bar{E}$ on neutrally stable points that separate TWF unstable points from stable points in parameter spanned by space (R,k), shown in figure 2.3. At low Reynolds number, $\bar{E}$ (net energy exchange to the membrane) is positive (see point P2-5). As Reynolds number increases, $\bar{E}$ decreases rapidly. For point P2-4 (Reynolds number $R = 57.34$), there is almost no energy exchange between fluid and membrane ($i.e. \bar{E} = 0$). For neutral points whose Reynolds number is larger than $R = 57.34$, $\bar{E}$ is negative (see point P2-3). As we continue increasing Reynolds number, $\bar{E}$ eventually increases but approaches zero for large R. Hence, this wave is class B by its response to wall damping (figure 2.7(b)), yet the work done by the fluid on the wall changes sign as the Reynolds number increases.

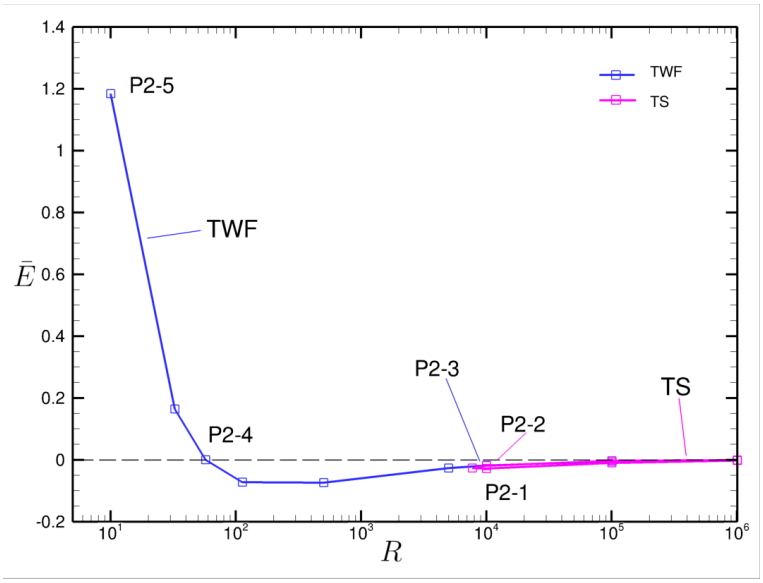

Figure 2.9: Energy exchange between fluid and membrane $\bar{E}$ against Reynolds number R on neutrally stable points in figure 2.3 for $m = 1, T = 10$, $d = 0$. Points P2-1 to P2-5 are the neutrally stable points labeled in figure 2.3.

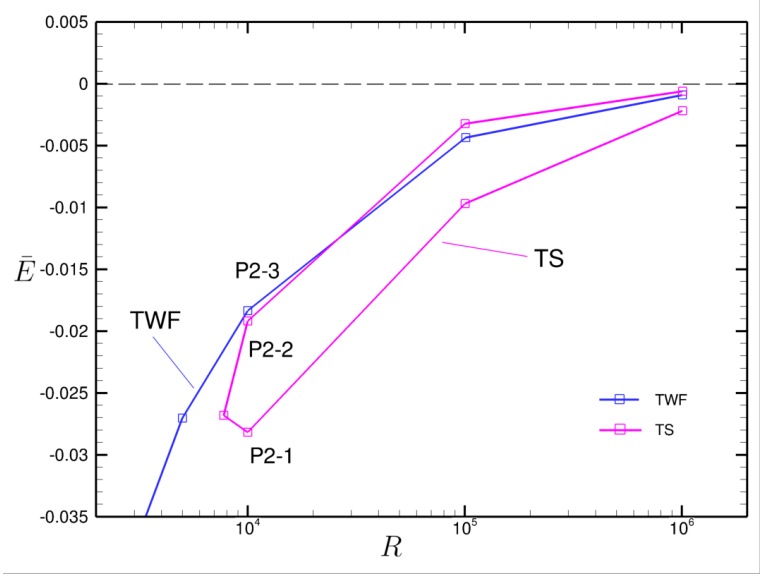

Figure 2.10: Zoom in plot of figure 2.9.

The magenta tongue shape line in figure 2.10 shows $\bar{E}$ evaluated on neutrally stable points that separate TS unstable points from stable points shown in figure 2.3. For all these neutral points, $\bar{E}$ are negative (see points P2-1 and P2-2), which also tend to zero for large Reynolds number.

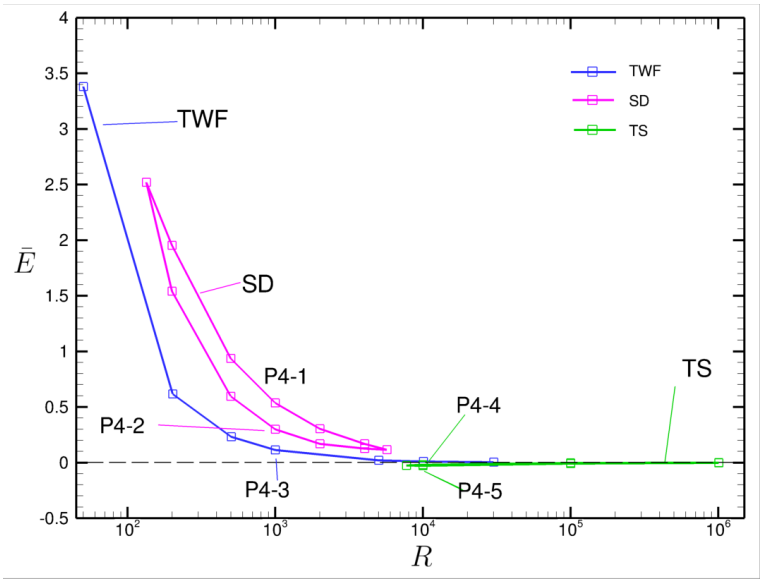

Figure 2.11: Energy exchange $\bar{E}$ against Reynolds number R on neutrally stable points in figure 2.4 for $m = 10, T = 10$, $d = 10$. Points P3-1 till P3-5 are the neutrally stable points labeled in figure 2.4.

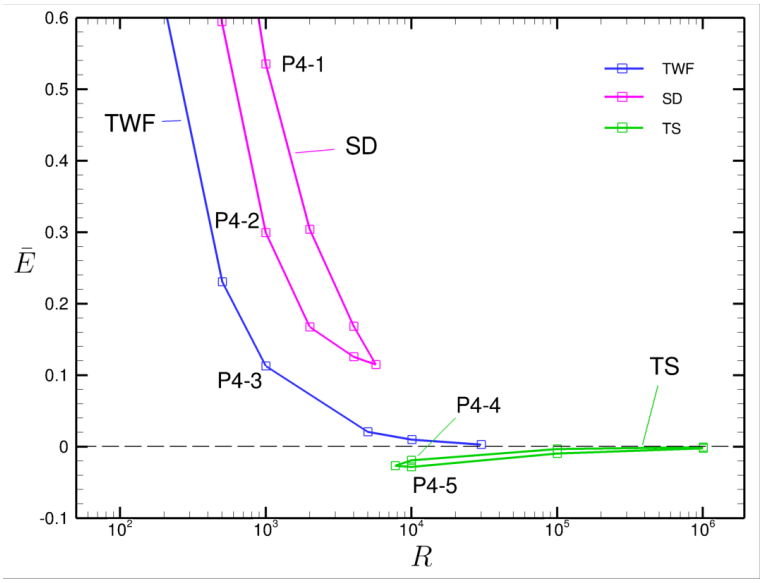

Figure 2.12: Zoom in plot of figure 2.11.

The blue line in figure 2.11 shows $\bar{E}$ calculated on neutrally stable points that separate TWF instability from stable points shown in figure 2.4. The green loop line demonstrates the value of $\bar{E}$ on neutrally stable points which separate SD unstable points from stable points shown in figure 2.4. For all these neutral points, $\bar{E}$ are all greater than zero (see points P3-1, P3-2 and P3-3), and decrease significantly when increasing the Reynolds number.

Similar to figure 2.10, the magenta tongue shape line in figure 2.12 gives the values of $\bar{E}$ com-

puted on neutrally stable points which separate the TS instability from stable points shown in figure 2.4. $\bar{E}$ are less than zero on all these neutral points (see points P3-4, P3-5), and tend to zero for large Reynolds number. The table 2.1, 2.2 list the numerical results of perturbed energy budgets for points labeled in Figure 2.2, 2.3, 2.4 and 2.5. As shown in the table 2.1, the perturbation energy budget $\bar{\hat{T}} = \bar{\hat{S}} + \bar{\hat{D}} - \bar{\hat{E}} = \bar{\bar{P}} - \bar{E} + (\bar{\hat{D}} + \bar{\bar{D}}) = 0$ on neutrally stable points listed (*i.e.* $Im(\omega) = 0$), as expected. The perturbation dissipation energy budget $\bar{\hat{D}}$ on all the neutrally stable points are always positive as expected. Table 2.2 lists the value of all the breve energy budgets, $\bar{E}$ and $\bar{D} = \bar{\hat{D}} + \bar{\bar{D}}$ are the total energy exchanged between the fluid and membrane and the total energy loss due to dissipation at $O(\varepsilon^2)$ over one period of time and wavelength, respectively. This table gives the values of $\bar{E}$ on three neutrally stable points P2-3, P2-4 and P2-5 labeled in figure 2.3, for neutral point at low Reynolds number P2-5, the energy exchange from fluid to membrane $\bar{E}$ is positive, while for neutral point at high Reynolds number P2-3, the energy exchange from fluid to membrane is negative. In between, we found one neutrally stable point P2-4 that the energy exchange between fluid and membrane is zero.

Point	m	d	R	T	k	$Re(\omega)$	$Im(\omega)$	$\bar{\hat{S}}$	$\bar{\hat{D}}$	$\bar{\hat{E}}$	$\bar{\hat{T}}$	Instability
P1-1	0	0	10000	10	2.173	0.8477	9.263e-08	-7.815e-01	7.676e-01	-1.391e-02	-1.170e-05	TS
P1-2	0	0	10000	10	1.741	0.6138	3.300e-06	-4.291e-01	4.195e-01	-9.495e-03	-9.718e-05	TS
P1-3	0	0	10000	10	0.3514	0.7935	-3.418e-07	-2.362e-02	9.249e-03	-1.438e-02	3.838e-06	TWF
P2-1	1	0	10000	10	2.173	0.8477	4.427e-08	-7.794e-01	7.653e-01	-1.408e-02	-4.994e-06	TS
P2-2	1	0	10000	10	1.740	0.6138	-2.969e-08	-4.280e-01	4.185e-01	-9.587e-03	-2.977e-07	TS
P2-3	1	0	10000	10	0.4796	1.057	-3.324e-08	-1.264e-02	4.722e-03	-7.919e-03	2.441e-07	TWF
P2-4	1	0	57.34	10	1.303	3.518	-4.442e-08	-1.783e-01	3.362e-01	1.578e-01	2.444e-07	TWF
P2-5	1	0	10	10	1.490	4.082	7.421e-07	-1.525e-01	1.627	1.475	-3.787e-06	TWF
P3-1	1	0	100	10	1.195	3.190	-8.713e-08	-1.486e-01	2.082e-01	5.958e-02	4.771e-07	TWF
P4-1	10	10	1000	10	0.2272	0.0488	8.822e-08	9.024e-03	2.686e-01	2.776e-01	-6.568e-07	SD
P4-2	10	10	1000	10	0.0708	0.0516	3.107e-08	-8.121e-03	1.655e-01	1.574e-01	-2.325e-07	SD
P4-3	10	10	1000	10	0.0324	0.0528	5.144e-08	-2.025e-03	6.285e-02	6.083e-02	-3.289e-07	TWF
P4-4	10	10	10000	10	2.183	0.853	-3.026e-07	-8.134e-01	7.742e-01	-3.920e-02	6.475e-06	TWF
P4-5	10	10	10000	10	1.727	0.606	-5.656e-08	-4.321e-01	4.103e-01	-2.181e-02	5.158e-07	TWF

Table 2.1: Neutral points labeled on Figure 2.2-2.5, and the corresponding second order energy budget. The perturbation energy budget $\overline{\hat{S}}+\overline{\hat{D}}-\overline{\hat{E}}=0$ when $Im(\omega)=0$, as expected.

Point	m	d	R	T	k	$Re(\omega)$	$Im(\omega)$	$\bar{\bar{P}}$	$\bar{\bar{E}}$	$\bar{\bar{D}}$	$\bar{E}$	$\bar{D}$	Instability
P1-1	0	0	10000	10	2.173	0.8477	9.263e-08	7.676e-01	-1.393e-02	-1.563	-2.784e-02	-7.954e-01	TS
P1-2	0	0	10000	10	1.741	0.6138	3.300e-06	4.196e-01	-9.514e-03	-8.583e-01	-1.900e-02	-4.387e-01	TS
P1-3	0	0	10000	10	0.3514	0.7935	-3.418e-07	4.531e-03	-1.909e-02	-4.726e-02	-3.348e-02	-3.801e-02	TWF
P2-1	1	0	10000	10	2.173	0.8477	4.431e-08	7.653e-01	-1.410e-02	-1.558	-2.818e-02	-7.935e-01	TS
P2-2	1	0	10000	10	1.740	0.6138	-2.966e-08	4.184e-01	-9.606e-03	-8.561e-01	-1.919e-02	-4.376e-01	TS
P2-3	1	0	10000	10	0.4796	1.057	-3.324 e-08	2.207e-03	-1.043e-02	-2.528e-02	-1.835e-02	-2.056e-02	TWF
P2-4	1	0	57.34	10	1.303	3.518	-4.442e-08	2.050e-02	-1.578e-01	-3.567e-01	3.425e-07	-2.050e-02	TWF
P2-5	1	0	10	10	1.490	4.082	7.421e-07	-1.388e-01	-2.914e-01	-3.051e-01	1.183	1.322	TWF
P3-1	1	0	100	10	1.195	3.190	-8.698e-08	2.405e-02	-1.246e-01	-2.973e-01	-6.502e-02	-8.908e-02	TWF
P4-1	10	10	1000	10	0.2272	0.0488	8.822e-08	2.484e-01	2.574e-01	1.804e-02	5.351e-01	2.867e-01	SD
P4-2	10	10	1000	10	0.0708	0.0516	3.107e-08	1.499e-01	1.418e-01	-1.624e-02	2.992e-01	1.493e-01	SD
P4-3	10	10	1000	10	0.0324	0.0528	9.583e-08	5.413e-02	5.210e-02	-4.050e-03	1.129e-01	5.880e-02	TWF
P4-4	10	10	10000	10	2.183	0.853	-3.026e-07	8.007e-01	-1.266e-02	-1.626	-5.187e-02	-8.526e-01	TWF
P4-5	10	10	10000	10	1.727	0.606	-5.656e-08	4.240e-01	-8.085e-03	-8.643e-01	-2.989e-02	-4.539e-01	TWF

Table 2.2: Breve energy budgets calculated on neutral points labeled on Figure 2.2-2.5. $\bar{E}$ is the system's second order energy exchange between fluid and membrane. $\bar{D}$ is the system's second order energy loss due to dissipation.

2.8 Discussion

In this chapter, we considered the stability and energetics of a two-dimensional fluid-membrane model. We considered a simple membrane model, similar to the membrane model considered by Stewart *et al*. [69] and Luo & Pedley [51], in which the membrane slopes are assuming to be sufficiently small and its wall shear stress is considered to be small comparing to the initial tension. We included the normal viscous stress, the mass and damping of the membrane (2.2.10) and derived the corresponding fully non-linear energy budgets for this system (2.3.12). One significant difference with the previous energy derivation (Stewart *et al*. [69]) is that we divided the work done by viscous forces into two parts: one part is the work done by viscous stresses on the membrane (E in equation (2.3.16)); the remaining term is denoted as D (in equation (2.3.17)) which is the dissipation due to the viscosity of the bulk flow, which is always positive (*i.e*. energy is always consumed in the bulk).

We obtained the energy budget of the system by perturbing all variables to second order. Here the system's average second order energy budget consists of hatted terms $\bar{\hat{E}}$, $\bar{\hat{D}}$ and $\bar{\hat{S}}$ which involve productions of first order variables and the breved terms $\breve{\breve{P}}$, $\breve{\breve{E}}$ and $\breve{\breve{D}}$ which involve second order variables only. We solved the (first order) eigenvalue problem numerically. We then substituted the numerical results for first order variables into the second order governing equations, and after applying the corresponding boundary conditions (equation 2.4.8 -2.4.12), we were able to obtain breved variables (second order variables) explicitly. These enabled us to calculate numerical values for all the terms in the energy budgets over one period of time and wavelength. This is a improvement over existing work (*e.g*. Stewart *et al*. [69]), who only computed the hatted terms and grouped all the breved terms together into the work done by nonlinear Reynolds stresses.

We first elucidated the neutrally stable curves in parameter space spanned by wavenumber and Reynolds number (as well as plotting wavespeed and Reynolds number). Similar to previous work (Davies & Carpenter [22]) we observed three modes of instabilities (TS, TWF and SD).

One important motivation of this work is to determine if the energy budget can be used to distinguish different classification of instability (*i.e*. class A,B and C from Benjamin [3]). Our computational results suggest that even though TWF mode is classified as class B, the work done by the fluid on the wall over one period of time and wavelength $\bar{E}$ for TWF changes sign along the neutral curves: $\bar{E}$ is positive for low Reynolds number and then becomes negative as Reynolds number increases, eventually tending to zero as Reynolds number becomes infinite. Moreover, this mechanism of TWF differs slightly to that identified by Davies & Carpenter [22], who state that TWF is sustained by an irreversible energy transfer from the fluid to the wall. In addition, for TS, $\bar{E}$ is always negative on neutrally stable points, while for SD, $\bar{E}$ is always positive on neutrally stable points. However, both TS and SD are termed class A. Hence, the concept of 'activation energy' which is linked to the instability mode classification (Benjamin [3], Landahl [45], Cairns [17]) is not equivalent to the work done by the fluid on the wall.

Deducing the equivalence between the energy budget and the ‘activation energy’ is an on-going area of future work.

Chapter 3

Instability of a finite-length fluid-beam model

In this chapter we consider the energetics of fluid flow through a finite-length rigid channel, where one segment of the upper wall is replaced by a plane strained elastic beam subject to a uniform external pressure. We first give a general description of the model (*Sec*. 3.1) and summarise the channel geometry (*Sec*. 3.2). Then the full governing equations for the fluid and the elastic beam are derived in *Sec*. 3.3. We isolate static configurations of the system in *Sec*. 3.4. We then take the dot product between the governing equations and the velocity to obtain the energy budget of the system in *Sec*. 3.5. We further obtain the steady energy budget for the system in *Sec*. 3.6. The numerical method used to solve for the fully nonlinear system is introduced in *Sec*. 3.7, and the numerical results are given in *Sec*. 3.8.

3.1 The model

We consider fluid-filled channel of finite length $L_u + L_0 + L_d$ and constant width D. The channel is rigid along most of its length, but one segment of length L_0 of the upper wall is replaced by an elasticated beam. The length of the upstream and downstream rigid segments are L_u and L_d, respectively. We use Ω, $\partial\Omega_u$, $\partial\Omega_d$ and $\partial\Omega_b$ to denote the entire domain, the upstream channel inlet, the downstream channel outlet, and the deformed elastic beam, respectively. This model is similar to the system introduced by Pedley [56] and analysed extensively by Cai & Luo [16] and Luo *et al*. [48].

We consider a parabolic inlet flow to the channel with flux Q (per unit width on the out-of-plane direction) and average velocity $U = Q/D$. Conversely, at the downstream end of the channel we set the outlet fluid pressure, which is chosen to be zero without loss of generality. The fluid is assumed to be Newtonian and incompressible with constant density ρ and viscosity μ.

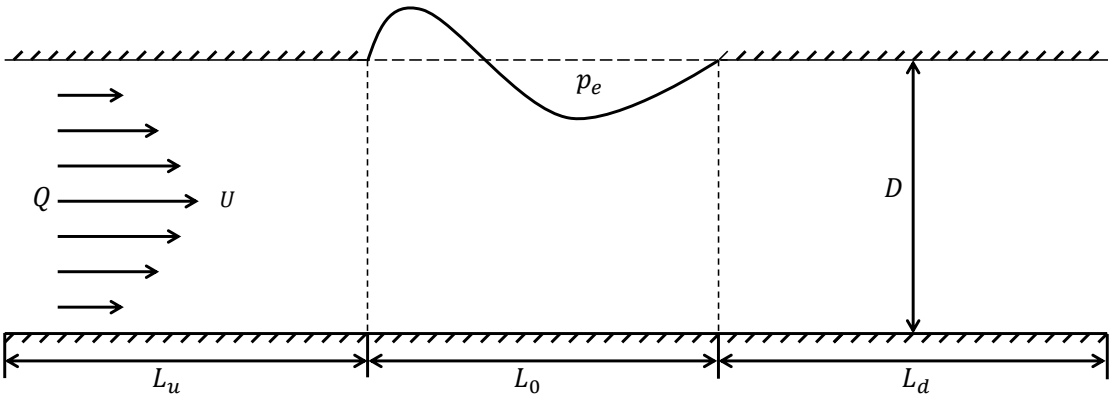

Figure 3.1: The fluid-beam model, the channel carries steady Poiseuille flow of flux Q. The average velocity, density and viscosity of the fluid are U, ρ and μ respectively. The beam is subjected to an external pressure p_e, the extensional and bending stiffness of the beam is EA and EJ,where E is the Young's modulus. ρ_m is the density of the beam.

The elastic beam is modeled using the Kirchhoff law [16] of elastic plates and is subjected to a uniformed external pressure p_e. We denote ρ_m as the beam density and T as the pre-tensional axial force in the beam. Further, we denote EA and EJ as the extensional and bending stiffness of the beam, respectively. We denote the beam thickness as h.

3.2 Geometry of the channel

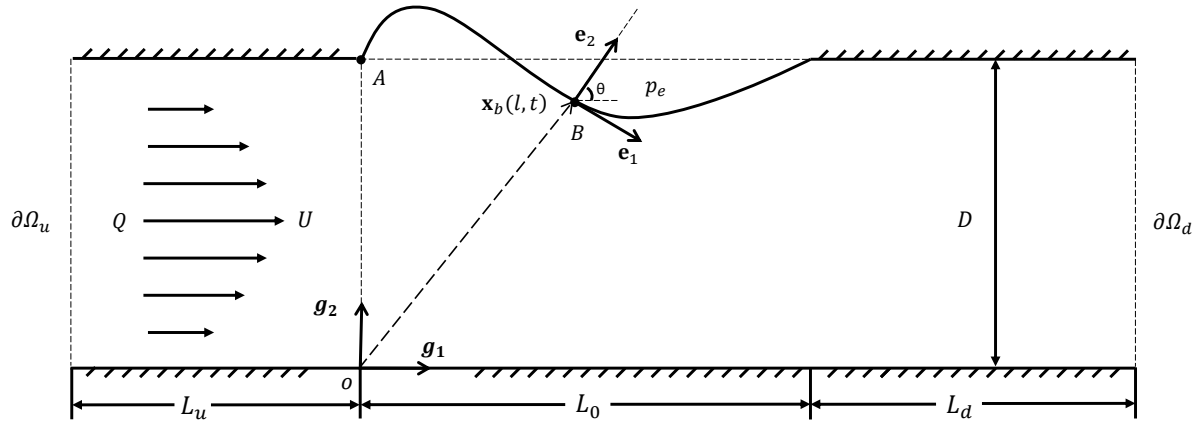

Figure 3.2: Sketch of the fluid-beam model in dimensional variables

We establish two coordinate systems (both shown in Figure 3.2). Firstly, $\mathbf{g}_1,\ \mathbf{g}_2,\ \mathbf{g}_3$ are the unit vectors of the Cartesian coordinate system with $\mathbf{g}_1$ aligned along the bottom wall of the channel, $\mathbf{g}_2$ parallel to the channel inlet and $\mathbf{g}_3$ is normal to the plane of the channel. Hence, a general point in the channel can be described using the coordinates $\mathbf{x} = x\mathbf{g}_1 + y\mathbf{g}_2 + z\mathbf{g}_3$, where $x,\ y,\ ,z$

measure displacement along the unit vectors $\mathbf{g}_1,\ \mathbf{g}_2,\ \mathbf{g}_3$, respectively, from the point on the lower wall where the upstream rigid section joins to the flexible section.
Conversely, $\mathbf{e}_1,\ \mathbf{e}_2,\ \mathbf{e}_3$ are unit vectors of the current coordinates for the deformed beam, where $\mathbf{e}_1$ is the local tangent to the beam, $\mathbf{e}_2$ is the local normal to the beam and $\mathbf{e}_3$ is normal to the plane of the channel ($\mathbf{g}_3 = \mathbf{e}_3$). In what follows, we ignore deflections in the out-of-plane direction and so consider all vectors as purely two-dimensional. In the absence of fluid loading, we assume the beam is flat and parallel to the channel wall.
In the beam reference description, we denote an arbitrary point B on the flat beam in the Cartesian coordinate as $\mathbf{x}_r(l) = l\mathbf{g}_1 + D\mathbf{g}_2$ where $0 < l < L_0$. After deformation we assume point B moves to,

$$\mathbf{x}_b(l,t) = x_b(l,t)\mathbf{g}_1 + y_b(l,t)\mathbf{g}_2. \tag{3.2.1}$$

So the displacement of the beam described with respect to the reference coordinates is,

$$\mathbf{x}_b(l,t) - \mathbf{x}_r(l) = (x_b(l,t) - l)\mathbf{g}_1 + (y_b(l,t) - D)\mathbf{g}_2. \tag{3.2.2}$$

We then can calculate relationship between the coordinate systems in the form,

$$\mathbf{e}_1 = \frac{1}{\lambda}\frac{\partial \mathbf{x}_b}{\partial l} = \frac{1}{\lambda}\left(\frac{\partial x_b}{\partial l}\mathbf{g}_1 + \frac{\partial y_b}{\partial l}\mathbf{g}_2\right), \quad \mathbf{e}_2 = \mathbf{e}_3 \times \mathbf{e}_1 = \frac{1}{\lambda}\left(-\frac{\partial y_b}{\partial l}\mathbf{g}_1 + \frac{\partial x_b}{\partial l}\mathbf{g}_2\right), \tag{3.2.3}$$

where the principal stretch of the beam $\lambda(l,t)$ is calculated as,

$$\lambda = \left(\left(\frac{\partial x_b}{\partial l}\right)^2 + \left(\frac{\partial y_b}{\partial l}\right)^2\right)^{\frac{1}{2}}. \tag{3.2.4}$$

Rearranging (3.2.3) we can express the channel unit vectors in terms of the current coordinate system of the beam, in the form

$$\mathbf{g}_1 = \frac{1}{\lambda}\left(\frac{\partial x_b}{\partial l}\mathbf{e}_1 - \frac{\partial y_b}{\partial l}\mathbf{e}_2\right), \quad \mathbf{g}_2 = \frac{1}{\lambda}\left(\frac{\partial y_b}{\partial l}\mathbf{e}_1 + \frac{\partial x_b}{\partial l}\mathbf{e}_2\right), \quad \mathbf{g}_3 = \mathbf{e}_3. \tag{3.2.5}$$

Therefore, the deflection of the beam $\mathbf{x}_b(l,t)$ can also be expressed with respect to the unit vectors of the deformed beam configuration as,

$$\mathbf{x}_b = \frac{1}{\lambda}\left(x_b\frac{\partial x_b}{\partial l} + y_b\frac{\partial y_b}{\partial l}\right)\mathbf{e}_1 + \frac{1}{\lambda}\left(\frac{\partial x_b}{\partial l}y_b - \frac{\partial y_b}{\partial l}x_b\right)\mathbf{e}_2. \tag{3.2.6}$$

The beam velocity can be expressed as the material time derivative of the beam deflection $\mathbf{x}_b$. In this case we take time derivatives for the beam with respect to the reference description *i.e.*

holding l fixed, so we have

$$\mathbf{u}_b(l,t) = \left.\frac{\partial \mathbf{x}_b(l,t)}{\partial t}\right|_l = \left.\frac{\partial x_b(l,t)}{\partial t}\right|_l \mathbf{g}_1 + \left.\frac{\partial y_b(l,t)}{\partial t}\right|_l \mathbf{g}_2. \tag{3.2.7}$$

In this chapter, all time derivatives for beam variables are taken holding l fixed unless otherwise specified.

Substituting (3.2.5) into (3.2.7), after rearrangement we can obtain the expression $\mathbf{u}_b$ in terms of the unit vectors of the current (spatial) description,

$$\mathbf{u}_b = u_{b1}\mathbf{e}_1 + u_{b2}\mathbf{e}_2 = \lambda^{-1}\left(\frac{\partial x_b}{\partial l}\frac{\partial x_b}{\partial t} + \frac{\partial y_b}{\partial l}\frac{\partial y_b}{\partial t}\right)\mathbf{e}_1 + \lambda^{-1}\left(\frac{\partial x_b}{\partial l}\frac{\partial y_b}{\partial t} - \frac{\partial y_b}{\partial l}\frac{\partial x_b}{\partial t}\right)\mathbf{e}_2. \tag{3.2.8}$$

We denote s to be the arclength along the deformed beam between the fixed point A (Figure 3.2) and any point on the deformed beam in the current configuration, where

$$s = \int_0^l \lambda(l',t)\,\mathrm{d}l', \quad \frac{\partial s}{\partial l} = \lambda, \tag{3.2.9}$$

for a differential element of the deformed beam. Therefore, we can express the unit vectors of the reference coordinates (3.2.5) in the current (spatial) description as,

$$\mathbf{g}_1 = \frac{\partial x_b^{(c)}(s,t)}{\partial s}\mathbf{e}_1 - \frac{\partial y_b^{(c)}(s,t)}{\partial s}\mathbf{e}_2, \quad \mathbf{g}_2 = \frac{\partial y_b^{(c)}(s,t)}{\partial s}\mathbf{e}_1 + \frac{\partial x_b^{(c)}(s,t)}{\partial s}\mathbf{e}_2, \tag{3.2.10}$$

here we use the superscript (c) represent variables expressed with respect to the current (spatial) description.

The deformed beam position $\mathbf{x}_b$ and its velocity $\mathbf{u}_b$ can also be expressed in current (spatial) description as,

$$\mathbf{x}_b{}^{(c)}(s,t) = \left(x_b^{(c)}\frac{\partial x_b^{(c)}}{\partial s} + y_b^{(c)}\frac{\partial y_b^{(c)}}{\partial s}\right)\mathbf{e}_1 + \left(y_b^{(c)}\frac{\partial x_b^{(c)}}{\partial s} - x_b^{(c)}\frac{\partial y_b^{(c)}}{\partial s}\right)\mathbf{e}_2, \tag{3.2.11}$$

$$\begin{aligned}\mathbf{u}_b{}^{(c)}(s,t) &= u_{b1}^{(c)}(s,t)\mathbf{e}_1 + u_{b2}^{(c)}(s,t)\mathbf{e}_2, \\ &= \left(\frac{\partial x_b^{(c)}}{\partial s}\frac{\partial x_b^{(c)}}{\partial t} + \frac{\partial y_b^{(c)}}{\partial s}\frac{\partial y_b^{(c)}}{\partial t}\right)\mathbf{e}_1 + \left(\frac{\partial x_b^{(c)}}{\partial s}\frac{\partial y_b^{(c)}}{\partial t} - \frac{\partial y_b^{(c)}}{\partial s}\frac{\partial x_b^{(c)}}{\partial t}\right)\mathbf{e}_2.\end{aligned} \tag{3.2.12}$$

Here the variables with superscript (c) are the push-forward of the corresponding variables described in reference (material) description (Holzapfel [34]), *i.e.* $\mathbf{x}_b^{(c)}$ and $\mathbf{u}_b^{(c)}$ are the push-forward of $\mathbf{x}_b$ and $\mathbf{u}_b$, respectively. Therefore, identities $\mathbf{x}_b{}^{(c)}(s,t) = \mathbf{x}_b(l,t)$, $\mathbf{u}_b{}^{(c)}(s,t) = \mathbf{u}_b(l,t)$ hold true. Note that time derivatives in equation (3.2.12) are material time derivatives, *i.e.* holding l fixed [48].

At points in the following derivations the current (spatial) description will prove useful, but all final results for the beam will be presented in the material description justifying our choice of time derivative.

3.3 Governing equations for coupled system

We discuss the governing equations and non-dimensionalisation for the coupled system in this section.

3.3.1 Governing equations for the fluid

We consider the incompressible Navier-Stokes equations for the fluid and apply no-slip and no-penetration boundary conditions on the rigid channel walls. So the governing equations for the fluid are,

$$\nabla \cdot \mathbf{u} = 0, \qquad (\mathbf{x} \in \Omega), \tag{3.3.1}$$

$$\rho\left(\frac{\partial \mathbf{u}}{\partial t} + (\mathbf{u}\cdot\nabla)\,\mathbf{u}\right) = \nabla \cdot \left(-p\mathbf{I} + \mu\left(\nabla\mathbf{u} + \nabla\mathbf{u}^{\mathrm{T}}\right)\right), \qquad (\mathbf{x} \in \Omega), \tag{3.3.2}$$

$$\mathbf{u} = \mathbf{0}, \qquad (y = 0;\ \ y = 1, -L_u < x < 0,\ L_0 < x < L_0 + L_d), \tag{3.3.3}$$

$$\mathbf{u} = \mathbf{u}_b, \qquad (\mathbf{x} \in \partial\Omega_b), \tag{3.3.4}$$

where $\mathbf{u} = u_1\mathbf{g}_1 + u_2\mathbf{g}_2$ is the velocity (expressed with respect to the Cartesian coordinate system) of the fluid, p is the fluid's pressure and $\boldsymbol{\sigma} = -p\mathbf{I} + \mu\left(\nabla\mathbf{u} + \nabla\mathbf{u}^{\mathrm{T}}\right)$ is the Newtonian fluid stress tensor. Here $\mathbf{I}$ is the identity matrix and the superscript T represents matrix transpose. In the fluid, time derivatives are taken with respect to the current (Eulerian) configuration for the fluid.

3.3.2 Governing equations for the beam

In this section we focus on deriving the governing equations for the beam by first establishing conservation of momentum (both linear and angular) and then simplifying using the geometry relationships of the beam (*Sec*. 3.2).

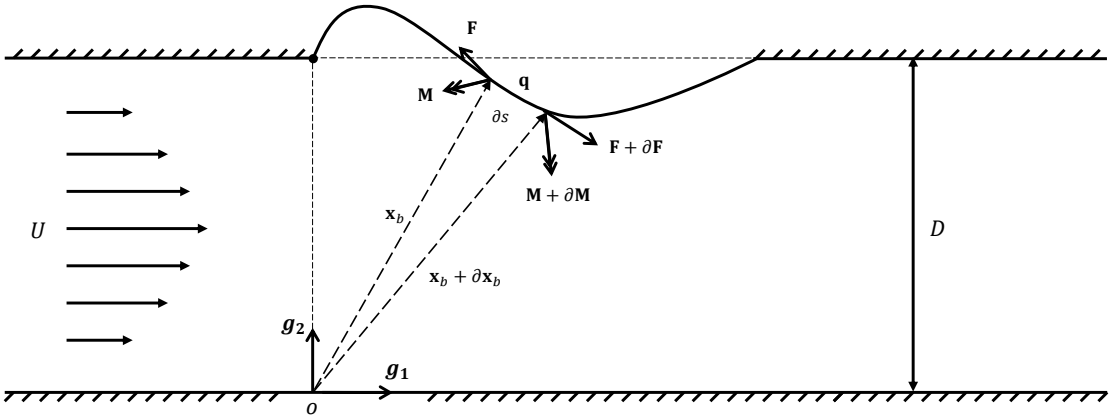

Figure 3.3: Sketch of a small displacement along the beam

We consider an elastic beam as shown in Figure 3.3. We consider a virtual displacement and establish the equations of conservation of momentum for a differential element of the beam first in the form (Cai & Luo [16]),

$$\frac{\partial}{\partial t}\left(\rho_m \frac{\partial \mathbf{x}_b}{\partial t}\partial l\right) = \partial \mathbf{F} + \mathbf{q}\partial s, \tag{3.3.5}$$

$$\frac{\partial}{\partial t}\left(\rho_m \mathbf{x}_b \times \frac{\partial \mathbf{x}_b}{\partial t}\partial l\right) = \partial \mathbf{M} + \mathbf{x}_b \times \mathbf{q}\partial s + (\mathbf{x}_b + \partial \mathbf{x}_b) \times (\mathbf{F} + \partial \mathbf{F}) - \mathbf{x}_b \times \mathbf{F}, \tag{3.3.6}$$

where ∂l, ∂s and $\partial \mathbf{x}_b$ are the length, arc-length and the displacement of a differential element of the beam respectively. In the beam momentum equations (3.3.5, 3.3.6), $\mathbf{F}$, $\mathbf{F}+\partial\mathbf{F}$ and $\mathbf{M}$, $\mathbf{M}+\partial\mathbf{M}$ are the force and moment acting on the differential element, $\mathbf{q}$ is the force applied to the beam by the fluid.

In the derivations in the following sections we integrate over the shape of the deformed beam, parameterized by the arc length s ($s \in \partial\Omega_b$). However, since we assume all time derivatives are taken holding l fixed, it is convenient to eventually transform back to the reference (material) description. In this case, we express the beam equations using reference (material) description and neglect the higher order (*i.e.* the product of two or more than two incremental terms) to obtain (detailed derivation in appendix A.1),

$$\frac{\rho_m}{\lambda}\left(\frac{\partial x_b}{\partial l}\frac{\partial^2 x_b}{\partial t^2} + \frac{\partial y_b}{\partial l}\frac{\partial^2 y_b}{\partial t^2}\right) = \frac{\partial F_1}{\partial l} - \lambda\kappa F_2 + \lambda q_1, \qquad (0 \le l \le L_0), \tag{3.3.7}$$

$$\frac{\rho_m}{\lambda}\left(\frac{\partial x_b}{\partial l}\frac{\partial^2 y_b}{\partial t^2} - \frac{\partial y_b}{\partial l}\frac{\partial^2 x_b}{\partial t^2}\right) = \frac{\partial F_2}{\partial l} + \lambda\kappa F_1 + \lambda q_2, \qquad (0 \le l \le L_0), \tag{3.3.8}$$

$$\frac{\partial M}{\partial l} + \lambda F_2 = 0, \qquad (0 \le l \le L_0), \tag{3.3.9}$$

where $\mathbf{F} = F_1\mathbf{e}_1 + F_2\mathbf{e}_2$, $\mathbf{M} = M\mathbf{e}_3$ and $\mathbf{q} = q_1\mathbf{e}_1 + q_2\mathbf{e}_2$, and the beam curvature κ is determined

by,

$$\kappa = \frac{1}{\lambda^3}\left(\frac{\partial x_b}{\partial l}\frac{\partial^2 y_b}{\partial l^2} - \frac{\partial y_b}{\partial l}\frac{\partial^2 x_b}{\partial l^2}\right). \tag{3.3.10}$$

The first two equations (3.3.7) and (3.3.8) follow from linear momentum conservation for a differential element, while equation (3.3.9) follows from conservation of angular momentum.
For later use, we also introduce the polar angle θ which measures the angle between the tangent vector to the beam $\mathbf{e}_1$ and the unit vector along the channel wall $\mathbf{g}_1$, $\theta = \arccos(\mathbf{e}_1 \cdot \mathbf{g}_1)$. Here the time derivatives are material time derivatives, *i.e.* holding l fixed.
The distributive force here is the fluid stress on the beam, which we denote as $\mathbf{q} = \sigma_1 \mathbf{e}_1 + (\sigma_2 - p_e)\mathbf{e}_2$, where σ_1 and σ_2 are the components of the (Newtonian) fluid stress tensor in the tangent and normal directions, so

$$\sigma_1 = (-\boldsymbol{\sigma}\mathbf{e}_2)\cdot\mathbf{e}_1, \quad \sigma_2 = (-\boldsymbol{\sigma}\mathbf{e}_2)\cdot\mathbf{e}_2. \tag{3.3.11}$$

According to the Kirchhoff law for elastic plates we can write,

$$F_1 = T + EA(\lambda - 1), \quad M = EJ(\lambda\kappa - \kappa_0), \tag{3.3.12}$$

where T is the pre-tensional axial force in the beam and κ_0 is the initial curvature of the beam. In our case, we only consider $\kappa_0 = 0$. This constitutive law is very similar to the one used by Luo *et al* [48], the only difference is the principal stretch λ we introduced in the expression of angular momentum, which is used to ensure the bending stiffness related beam energy budget term can be written as a complete time derivative (see *Sec*. 3.5 below).
We then choose F_2 to conserve angular momentum (3.3.9). Substituting the distributive force and (3.3.12) into (3.3.7), (3.3.8) and (3.3.9), the governing equations of the beam become (detailed derivation see appendix A.1),

$$\frac{\rho_m}{\lambda}\left(\frac{\partial x_b}{\partial l}\frac{\partial^2 x_b}{\partial t^2} + \frac{\partial y_b}{\partial l}\frac{\partial^2 y_b}{\partial t^2}\right) = EJ\kappa\frac{\partial(\lambda\kappa)}{\partial l} + EA\frac{\partial\lambda}{\partial l} + \lambda\sigma_1, \qquad (0 \le l \le L_0), \tag{3.3.13}$$

$$\frac{\rho_m}{\lambda}\left(\frac{\partial x_b}{\partial l}\frac{\partial^2 y_b}{\partial t^2} - \frac{\partial y_b}{\partial l}\frac{\partial^2 x_b}{\partial t^2}\right) = -EJ\frac{\partial}{\partial l}\left(\frac{1}{\lambda}\frac{\partial(\lambda\kappa)}{\partial l}\right) + EA\lambda\kappa(\lambda - 1) + \lambda\kappa T + \lambda\sigma_2 - \lambda p_e, \qquad (0 \le l \le L_0). \tag{3.3.14}$$

Equation (3.3.13) is the momentum balance in the tangent direction to the beam and (3.3.14) is the momentum in the normal direction to the beam.

3.3.3 Dimensionless governing equations for the coupled system

We introduce dimensionless variables (marked with tilde) using the following scalings based on the channel width, the steady inlet flow and the inertial pressure scale (where the outlet pressure has been set to zero),

$$\tilde{p} = \frac{pD^2}{\rho Q^2}, \quad \tilde{\mathbf{x}} = \frac{\mathbf{x}}{D}, \quad \tilde{\mathbf{u}} = \frac{\mathbf{u}D}{Q}, \quad \tilde{\boldsymbol{\sigma}} = \frac{\boldsymbol{\sigma}D^2}{\rho Q^2}, \quad \tilde{t} = \frac{tQ}{D^2}, \quad \tilde{l} = \frac{l}{D}, \quad \tilde{\mathbf{x}}_b = \frac{\mathbf{x}_b}{D},$$
$$\tilde{\mathbf{u}}_b = \frac{\mathbf{u}_b D}{Q}, \quad \tilde{\kappa} = \kappa D. \tag{3.3.15}$$

Using these scalings, we also obtain the dimensionless parameters (marked with tilde),

$$\tilde{R} = \frac{Q\rho}{\mu}, \quad \tilde{L}_u = \frac{L_u}{D}, \quad \tilde{L}_d = \frac{L_d}{D}, \quad \tilde{L}_0 = \frac{L_0}{D}, \quad \tilde{T} = \frac{TD}{\rho Q^2}, \quad \tilde{\rho}_m = \frac{\rho_m}{D\rho},$$
$$\tilde{c}_\lambda = \frac{(EA)D}{\rho Q^2}, \quad \tilde{c}_\kappa = \frac{EJ}{\rho Q^2 D}, \tag{3.3.16}$$

where $\tilde{R}$ is the Reynolds number, $\tilde{L}_u$, $\tilde{L}_d$ and $\tilde{L}_0$ are the dimensionless lenghts of upstream, downstream and collapsible segments of the channel, $\tilde{T}$ is the dimensionless wall tension, $\tilde{\rho}_m$ is the dimensionless beam density, $\tilde{c}_\lambda$ is the dimensionless extensional stiffness, $\tilde{c}_\kappa$ is the dimensionless bending stiffness.

Therefore, we can write out the dimensionless governing equations for the coupled system in the form (dropping tildes),

$$\nabla \cdot \mathbf{u} = 0, \qquad (\mathbf{x} \in \Omega), \tag{3.3.17}$$
$$\frac{\partial \mathbf{u}}{\partial t} + (\mathbf{u} \cdot \nabla)\,\mathbf{u} = \nabla \cdot \boldsymbol{\sigma} = \nabla \cdot \left(-p\mathbf{I} + R^{-1}\left(\nabla \mathbf{u} + \nabla \mathbf{u}^{\mathrm{T}}\right)\right), \qquad (\mathbf{x} \in \Omega), \tag{3.3.18}$$
$$\mathbf{u} = \mathbf{0}, \qquad (y = 0;\ y = 1, -L_u < x < 0,\ L_0 < x < L_0 + L_d), \tag{3.3.19}$$
$$\mathbf{u} = \mathbf{u}_b{}^{(c)}. \qquad (\mathbf{x} \in \partial\Omega_b), \tag{3.3.20}$$
$$\int_0^L u_1 \,\mathrm{d}y = 1, \qquad (\mathbf{u} \in \partial\Omega_u), \tag{3.3.21}$$
$$\boldsymbol{\sigma}\mathbf{n} = \mathbf{0}, \qquad (\mathbf{x} \in \partial\Omega_d), \tag{3.3.22}$$
$$\frac{\partial x_b}{\partial l} = \lambda \cos(\theta), \qquad (0 \le l \le L_0), \tag{3.3.23}$$
$$\frac{\partial y_b}{\partial l} = \lambda \sin(\theta), \qquad (0 \le l \le L_0), \tag{3.3.24}$$
$$\frac{\partial \theta}{\partial l} = \lambda \kappa, \qquad (0 \le l \le L_0), \tag{3.3.25}$$
$$\frac{\rho_m}{\lambda}\left(\frac{\partial x_b}{\partial l}\frac{\partial^2 x_b}{\partial t^2} + \frac{\partial y_b}{\partial l}\frac{\partial^2 y_b}{\partial t^2}\right) = c_\kappa \kappa \frac{\partial(\lambda\kappa)}{\partial l} + c_\lambda \frac{\partial \lambda}{\partial l} + \lambda \sigma_1, \qquad (0 \le l \le L_0), \tag{3.3.26}$$

$$\frac{\rho_m}{\lambda}\left(\frac{\partial x_b}{\partial l}\frac{\partial^2 y_b}{\partial t^2}-\frac{\partial y_b}{\partial l}\frac{\partial^2 x_b}{\partial t^2}\right)=-c_\kappa\frac{\partial}{\partial l}\left(\frac{1}{\lambda}\frac{\partial(\lambda\kappa)}{\partial l}\right)+c_\lambda\lambda\kappa(\lambda-1)+\lambda\kappa T,$$

$$+\lambda\sigma_2-\lambda p_e, \qquad (0\le l\le L_0), \quad (3.3.27)$$

$$\mathbf{u}_b=0, \qquad (l=0,L_0), \quad (3.3.28)$$

$$\frac{\partial\theta}{\partial t}=0, \qquad (l=0,L_0). \quad (3.3.29)$$

Detailed derivation of equations (3.3.23-3.3.25) are in appendix A.2.
In order to use the energy exchange between the beam and the fluid in later section, we write the beam governing equations into the current (spatial) description in the form,

$$\frac{\rho_m}{\lambda^{(c)}}\left(\frac{\partial x_b^{(c)}}{\partial s}\frac{\partial^2 x_b^{(c)}}{\partial t^2}+\frac{\partial y_b^{(c)}}{\partial s}\frac{\partial^2 y_b^{(c)}}{\partial t^2}\right)=c_\kappa\kappa^{(c)}\frac{\partial\left(\lambda^{(c)}\kappa^{(c)}\right)}{\partial s}+c_\lambda\frac{\partial\lambda^{(c)}}{\partial s}+\sigma_1,$$

$$(s\in\partial\Omega_b), \quad (3.3.30)$$

$$\frac{\rho_m}{\lambda^{(c)}}\left(\frac{\partial x_b^{(c)}}{\partial s}\frac{\partial^2 y_b^{(c)}}{\partial t^2}-\frac{\partial y_b^{(c)}}{\partial s}\frac{\partial^2 x_b^{(c)}}{\partial t^2}\right)=-c_\kappa\frac{\partial^2(\lambda^{(c)}\kappa^{(c)})}{\partial s^2}+c_\lambda\kappa^{(c)}(\lambda^{(c)}-1)$$

$$+\kappa^{(c)}T+\sigma_2-p_e, \qquad (s\in\partial\Omega_b). \quad (3.3.31)$$

For later use, we also rewrite the beam equations (3.3.30, 3.3.31) in vector form and dot with the beam velocity to obtain the beam energy equation,

$$\begin{aligned}(\boldsymbol{\sigma}\mathbf{n})\cdot\mathbf{u}_b=&-(\sigma_1\mathbf{e}_1+\sigma_2\mathbf{e}_2)\cdot\left(u_{b1}^{(c)}\mathbf{e}_1+u_{b2}^{(c)}\mathbf{e}_2\right),\\
=&-\frac{\rho_m}{\lambda^{(c)}}\left(\frac{\partial x_b^{(c)}}{\partial s}\frac{\partial^2 x_b^{(c)}}{\partial t^2}+\frac{\partial y_b^{(c)}}{\partial s}\frac{\partial^2 y_b^{(c)}}{\partial t^2}\right)u_{b1}^{(c)}\\
&-\frac{\rho_m}{\lambda^{(c)}}\left(\frac{\partial x_b^{(c)}}{\partial s}\frac{\partial^2 y_b^{(c)}}{\partial t^2}-\frac{\partial y_b^{(c)}}{\partial s}\frac{\partial^2 x_b^{(c)}}{\partial t^2}\right)u_{b2}^{(c)}\\
&+c_\kappa\left[\kappa^{(c)}\frac{\partial\left(\lambda^{(c)}\kappa^{(c)}\right)}{\partial s}u_{b1}^{(c)}-\frac{\partial^2(\lambda^{(c)}\kappa^{(c)})}{\partial s^2}u_{b2}^{(c)}\right]+\left(\kappa^{(c)}T-p_e\right)u_{b2}^{(c)}\\
&+c_\lambda\left[\frac{\partial\lambda^{(c)}}{\partial s}u_{b1}^{(c)}+\kappa^{(c)}(\lambda^{(c)}-1)u_{b2}^{(c)}\right], \qquad (\mathbf{x}_b{}^{(c)}\in\partial\Omega_b). \quad (3.3.32)\end{aligned}$$

This final system is very similar to that derived by Luo *et. al.* [48], the only difference is due to the different Kirchhoff constitutive law (3.3.12) employed here.

3.4 Steady governing equations for the system

For some parameter values, this coupled fluid-beam system admits a steady solution (see for example Luo & Pedley [49], Luo *et. al.* [48]). We denote the steady flow through the channel with velocity $\mathbf{U} = U_1\mathbf{g}_1 + U_2\mathbf{g}_2$ with corresponding pressure P and steady Newtonian stress tensor $\mathbf{\Sigma} = -P\mathbf{I} + R^{-1}\left(\nabla\mathbf{U} + \nabla\mathbf{U}^{\mathrm{T}}\right)$. The curvature and stretch of the steady beam are denoted K and Λ, respectively and the tangent and normal unit vectors to the steady beam are denoted $\mathbf{N}$ and $\mathbf{T}$, respectively. We say $\partial\bar{\Omega}_b$ represents the deformed beam in the static state, while $\bar{\Omega}$ denotes the whole domain in the static state. In the steady state, the governing equations for the system take the form,

$$\nabla\cdot\mathbf{U} = 0, \qquad (\mathbf{x}\in\bar{\Omega}), \quad (3.4.1)$$

$$(\mathbf{U}\cdot\nabla)\mathbf{U} = \nabla\cdot\left(-P\mathbf{I} + R^{-1}\left(\nabla\mathbf{U} + \nabla\mathbf{U}^{\mathrm{T}}\right)\right), \qquad (\mathbf{x}\in\bar{\Omega}), \quad (3.4.2)$$

$$\mathbf{U} = \mathbf{0}, \qquad (y = 0;\ \ y = 1, -L_u < x < 0,\ L_0 < x < L_0 + L_d), \quad (3.4.3)$$

$$\mathbf{U} = \mathbf{0}, \qquad (\mathbf{x}\in\partial\bar{\Omega}_b), \quad (3.4.4)$$

$$c_\kappa K\frac{\partial(\Lambda K)}{\partial l} + c_\lambda\frac{\partial\Lambda}{\partial l} + \Lambda(\mathbf{\Sigma}\mathbf{N})\cdot\mathbf{T} = 0, \qquad (0\le l\le L_0), \quad (3.4.5)$$

$$-c_\kappa\frac{\partial}{\partial l}\left(\frac{1}{\Lambda}\frac{\partial(\Lambda K)}{\partial l}\right) + c_\lambda\Lambda K(\Lambda-1) + \Lambda KT + \Lambda(\mathbf{\Sigma}\mathbf{N})\cdot\mathbf{N} - \Lambda p_e = 0,$$

$$(0\le l\le L_0), \quad (3.4.6)$$

$$\frac{\partial\Theta}{\partial t} = 0, \qquad (l = 0, L_0). \quad (3.4.7)$$

here all the variables are independent of time, i.e. $\mathbf{U} = \mathbf{U}(x,y), P = P(x,y), \Lambda = \Lambda(l), K = K(l)$.

3.5 Fully non-linear energy budgets

In previous studies of collapsible channel flow, it was found that energy budget of the system is a useful method to quantify the mechanisms of self-excited oscillations (*e.g.* Jensen & Heil [42], Stewart *et al* [68]). To consider the energy budget, we consider the dot product of the fluid velocity with the momentum equations of the fluid (3.3.18) to obtain the energy equation in the form (Schmid & Henningson [62]),

$$\frac{\partial\mathbf{u}}{\partial t}\cdot\mathbf{u} + ((\mathbf{u}\cdot\nabla)\mathbf{u})\cdot\mathbf{u} = (\nabla\cdot\boldsymbol{\sigma})\cdot\mathbf{u} = \left[\nabla\cdot\left(-p\mathbf{I} + R^{-1}\left(\nabla\mathbf{u} + \nabla\mathbf{u}^{\mathrm{T}}\right)\right)\right]\cdot\mathbf{u}, (\mathbf{x}\in\Omega). \quad (3.5.1)$$

As the fluid is incompressible, we can rearrange the above fluid energy equation to obtain the simplified form (detailed derivation see *Sec.* *A*.3),

$$\frac{1}{2}\frac{\partial(\mathbf{u}\cdot\mathbf{u})}{\partial t}+\frac{1}{2}\nabla\cdot((\mathbf{u}\cdot\mathbf{u})\mathbf{u}) = -\nabla\cdot(p\mathbf{u})+R^{-1}\left[\nabla\cdot\left((\nabla\mathbf{u}+\nabla\mathbf{u}^{\mathrm{T}})\mathbf{u}\right)\right] - R^{-1}\left[\mathrm{Tr}\left((\nabla\mathbf{u}+\nabla\mathbf{u}^{\mathrm{T}})\nabla\mathbf{u}\right)\right], \qquad (\mathbf{x}\in\Omega). \tag{3.5.2}$$

We integrate (3.5.2) over the domain Ω to get the energy budget of the system,

$$\underbrace{\int_\Omega \frac{1}{2}\frac{\partial(\mathbf{u}\cdot\mathbf{u})}{\partial t}\,\mathrm{d}A}_{I}+\underbrace{\int_\Omega\left[\frac{1}{2}\nabla\cdot((\mathbf{u}\cdot\mathbf{u})\mathbf{u})\right]\mathrm{d}A}_{II} = \underbrace{\int_\Omega\left[-\nabla\cdot(p\mathbf{u})\right]\mathrm{d}A}_{III}+\underbrace{\int_\Omega R^{-1}\left[\nabla\cdot\left((\nabla\mathbf{u}+\nabla\mathbf{u}^{\mathrm{T}})\mathbf{u}\right)-\mathrm{Tr}\left((\nabla\mathbf{u}+\nabla\mathbf{u}^{\mathrm{T}})\nabla\mathbf{u}\right)\right]\mathrm{d}A}_{IV}. \tag{3.5.3}$$

We label these four terms $I-IV$ as above and consider each in turn.
By the Reynolds transport theorem, term I becomes,

$$\begin{aligned} I &= \frac{1}{2}\frac{\partial}{\partial t}\int_\Omega(\mathbf{u}\cdot\mathbf{u})\,\mathrm{d}A-\frac{1}{2}\int_{\partial\Omega}(\mathbf{u}\cdot\mathbf{u})(\mathbf{v}\cdot\mathbf{n})\,\mathrm{d}s \\ &= \underbrace{\frac{\partial}{\partial t}\int_\Omega\left(\frac{1}{2}\mathbf{u}\cdot\mathbf{u}\right)\mathrm{d}A}_{K_f}-\int_{\partial\Omega_b}\frac{1}{2}(\mathbf{u}\cdot\mathbf{u})(\mathbf{u}\cdot\mathbf{n})\,\mathrm{d}s, \end{aligned} \tag{3.5.4}$$

where $\mathbf{v}$ and $\mathbf{n}$ are the velocity and the normal unit vector of the boundary $\partial\Omega$, respectively. On the inlet and outlet boundary, $\mathbf{v}=\mathbf{0}$, while on the elastic beam $\mathbf{v}=\mathbf{u}_b^{(c)}=\mathbf{u}$ (3.3.20). We denote the first term as K_f, the rate of working of kinetic energy, while the second term cancels below. Using the divergence theorem, we can write term II in the form,

$$II=\frac{1}{2}\int_{\partial\Omega}(\mathbf{u}\cdot\mathbf{u})\,(\mathbf{u}\cdot\mathbf{n})\,\mathrm{d}s=\underbrace{\left[\int_0^1\frac{1}{2}(\mathbf{u}\cdot\mathbf{u})\,(\mathbf{u}\cdot\mathbf{n})\,\mathrm{d}y\right]_{x=-L_u}^{x=L_0+L_d}}_{F_f}+\frac{1}{2}\int_{\partial\Omega_b}(\mathbf{u}\cdot\mathbf{u})\,(\mathbf{u}\cdot\mathbf{n})\,\mathrm{d}s. \tag{3.5.5}$$

We denote the first term as F_f, the net kinetic energy flux extracted between the channel ends. Note that the second term on the right hand side of equation (3.5.5) cancels identically with equation (3.5.4) when we compute the sum of $I+II$.
By the divergence theorem, term III can be written,

$$III=\int_{\partial\Omega}\Big(-p\mathbf{u}\cdot\mathbf{n}\Big)\,\mathrm{d}s=\underbrace{\left[\int_0^1(-p\mathbf{u}\cdot\mathbf{n})\,\mathrm{d}y\right]_{x=-L_u}^{x=L_0+L_d}}_{P_f}+\int_{\partial\Omega_b}\Big(-p\mathbf{u}\cdot\mathbf{n}\Big)\,\mathrm{d}s. \tag{3.5.6}$$

We denote the first term as P_f, the rate of working of pressure force at the channel ends. Again using the divergence theorem, term IV can be written as,

$$IV = R^{-1}\int_{\partial\Omega_b}\left[\Big(\left(\nabla\mathbf{u}+\nabla\mathbf{u}^{\mathrm{T}}\right)\mathbf{u}\Big)\cdot\mathbf{n}\right]\mathrm{d}s - \underbrace{R^{-1}\int_{\Omega}\mathrm{Tr}\Big(\left(\nabla\mathbf{u}+\nabla\mathbf{u}^{\mathrm{T}}\right)\nabla\mathbf{u}\Big)\,\mathrm{d}A}_{D_f}, \tag{3.5.7}$$

assuming that the inlet and outlet flows are parallel to the rigid wall (parallel flow assumption). We denote the second term as D_f, the energy loss in the bulk due to fluid viscosity.
We gather the remaining terms (from (3.5.6) and (3.5.7)) evolved on the beam and define E_f as the work done by fluid stresses on the beam in the form,

$$E_f = \int_{\partial\Omega_b}\Big(-p\mathbf{u}\cdot\mathbf{n}\Big)\,\mathrm{d}s + R^{-1}\int_{\partial\Omega_b}\Big(\left(\nabla\mathbf{u}+\nabla\mathbf{u}^{\mathrm{T}}\right)\mathbf{u}\cdot\mathbf{n}\Big)\,\mathrm{d}s = \int_{\partial\Omega_b}\left[(\boldsymbol{\sigma}\mathbf{u})\cdot\mathbf{n}\right]\mathrm{d}s. \tag{3.5.8}$$

It follows that we can reverse the position of $\mathbf{u}$ and $\mathbf{n}$ in (3.5.8) since $\boldsymbol{\sigma}$ is symmetric in the form,

$$E_f = \int_{\partial\Omega_b}\left[(\boldsymbol{\sigma}\mathbf{n})\cdot\mathbf{u}\right]\mathrm{d}s. \tag{3.5.9}$$

Gathering all the terms from (3.5.3) together, the total energy budget of the system can be written as,

$$K_f + F_f - E_f - P_f + D_f = 0, \tag{3.5.10}$$

where,

$$K_f = \frac{\partial}{\partial t}\int_{\Omega}\left(\frac{1}{2}\mathbf{u}\cdot\mathbf{u}\right)\mathrm{d}A, \tag{3.5.11}$$

$$F_f = \left[\int_0^1 \frac{1}{2}(\mathbf{u}\cdot\mathbf{u})\,(\mathbf{u}\cdot\mathbf{n})\,\mathrm{d}y\right]_{x=-L_u}^{x=L_0+L_d}, \tag{3.5.12}$$

$$E_f = \int_{\partial\Omega_b}\left[(\boldsymbol{\sigma}\mathbf{n})\cdot\mathbf{u}\right]\mathrm{d}s, \tag{3.5.13}$$

$$P_f = \left[\int_0^1 (-p\mathbf{u}\cdot\mathbf{n})\,\mathrm{d}y\right]_{x=-L_u}^{x=L_0+L_d}, \tag{3.5.14}$$

$$D_f = R^{-1}\int_{\Omega}\mathrm{Tr}\Big(\left(\nabla\mathbf{u}+\nabla\mathbf{u}^{\mathrm{T}}\right)\nabla\mathbf{u}\Big)\,\mathrm{d}A. \tag{3.5.15}$$

Here, K_f is the rate of working of kinetic energy, F_f is the net kinetic energy flux extracted between the channel ends, E_f is the rate of working of fluid stress on the beam, P_f is the rate of working of pressure force at the channel ends and D_f is the energy loss due to viscosity. This

dissipation energy is non-negative, since D_f can be expressed as

$$D_f = R^{-1}\int_\Omega \left[2\left(\frac{\partial u_1}{\partial x}\right)^2 + 2\left(\frac{\partial u_2}{\partial y}\right)^2 + \left(\frac{\partial u_1}{\partial y}+\frac{\partial u_2}{\partial x}\right)^2\right] \mathrm{d}A. \tag{3.5.16}$$

This formulation represents an improvement on the energy budget presented by Stewart *et. al.* [66], where the dissipation term they derived included part of the work done by viscous forces on the wall and so could take either sign depending on the parameters.
To fully evaluate E_f we substitute the beam energy equation (3.3.32) and boundary condition (3.3.20) to obtain,

$$\begin{aligned}
E_f &= \int_{\partial\Omega_b} [(\boldsymbol{\sigma}\mathbf{n})\cdot\mathbf{u}]\,\mathrm{d}s = \int_{\partial\Omega_b}\left[(\boldsymbol{\sigma}\mathbf{n})\cdot\mathbf{u}_b^{(c)}\right]\mathrm{d}s,\\
&= \underbrace{-\int_{\partial\Omega_b}\frac{\rho_m}{\lambda^{(c)}}\left(\frac{\partial x_b^{(c)}}{\partial s}\frac{\partial^2 x_b^{(c)}}{\partial t^2}+\frac{\partial y_b^{(c)}}{\partial s}\frac{\partial^2 y_b^{(c)}}{\partial t^2}\right)u_{b1}^{(c)}\,\mathrm{d}s}_{I}\\
&\quad \underbrace{-\int_{\partial\Omega_b}\frac{\rho_m}{\lambda^{(c)}}\left(\frac{\partial x_b^{(c)}}{\partial s}\frac{\partial^2 y_b^{(c)}}{\partial t^2}-\frac{\partial y_b^{(c)}}{\partial s}\frac{\partial^2 x_b^{(c)}}{\partial t^2}\right)u_{b2}^{(c)}\,\mathrm{d}s}_{I}\\
&\quad \underbrace{+\int_{\partial\Omega_b} c_\kappa\left(\kappa^{(c)}\frac{\partial\left(\lambda^{(c)}\kappa^{(c)}\right)}{\partial s}u_{b1}^{(c)}-\frac{\partial^2(\lambda^{(c)}\kappa^{(c)})}{\partial s^2}u_{b2}^{(c)}\right)\mathrm{d}s}_{II}\\
&\quad \underbrace{+\int_{\partial\Omega_b}\left[c_\lambda\left(\frac{\partial\lambda^{(c)}}{\partial s}u_{b1}^{(c)}+\kappa^{(c)}(\lambda^{(c)}-1)u_{b2}^{(c)}\right)+\kappa^{(c)}Tu_{b2}^{(c)}\right]\mathrm{d}s}_{III} \underbrace{-\int_{\partial\Omega_b}\left(p_e u_{b2}^{(c)}\right)\mathrm{d}s.}_{IV}
\end{aligned} \tag{3.5.17}$$

We label the above four terms $I-IV$ and consider them in turn.
For I, by rewriting the terms in vector form we obtain,

$$\begin{aligned}
I &= \int_{\partial\Omega_b}\frac{\rho_m}{\lambda^{(c)}}\left(\frac{\partial x_b^{(c)}}{\partial s}\frac{\partial^2 x_b^{(c)}}{\partial t^2}+\frac{\partial y_b^{(c)}}{\partial s}\frac{\partial^2 y_b^{(c)}}{\partial t^2}\right)\left(\mathbf{e}_1\cdot\mathbf{u}_b^{(c)}\right)\mathrm{d}s\\
&\quad +\int_{\partial\Omega_b}\frac{\rho_m}{\lambda^{(c)}}\left(\frac{\partial x_b^{(c)}}{\partial s}\frac{\partial^2 y_b^{(c)}}{\partial t^2}-\frac{\partial y_b^{(c)}}{\partial s}\frac{\partial^2 x_b^{(c)}}{\partial t^2}\right)\left(\mathbf{e}_2\cdot\mathbf{u}_b^{(c)}\right)\mathrm{d}s\\
&= \int_{\partial\Omega_b}\frac{\rho_m}{\lambda^{(c)}}\left[\frac{\partial^2 x_b^{(c)}}{\partial t^2}\left(\frac{\partial x_b^{(c)}}{\partial s}\mathbf{e}_1-\frac{\partial y_b^{(c)}}{\partial s}\mathbf{e}_2\right)+\frac{\partial^2 y_b^{(c)}}{\partial t^2}\left(\frac{\partial y_b^{(c)}}{\partial s}\mathbf{e}_1+\frac{\partial x_b^{(c)}}{\partial s}\mathbf{e}_2\right)\right]\cdot\mathbf{u}_b^{(c)}\,\mathrm{d}s.
\end{aligned} \tag{3.5.18}$$

We then change the variables back to reference (material) description since all time derivatives are taken holding l fixed. By applying $\mathbf{x}_b^{(c)} = \mathbf{x}_b$, $\mathbf{u}_b^{(c)} = \mathbf{u}_b$ and substituting the two equations in (3.2.10) for the unit vectors $\mathbf{e}_1$ and $\mathbf{e}_2$, we obtain,

$$\begin{aligned} I &= \int_0^L \left[\rho_m \left(\frac{\partial^2 x_b}{\partial t^2}\mathbf{g}_1 + \frac{\partial^2 x_b}{\partial t^2}\mathbf{g}_2 \right) \cdot \mathbf{u}_b \right] \mathrm{d}l = \int_0^L \left(\rho_m \frac{\partial \mathbf{u}_b}{\partial t} \cdot \mathbf{u}_b \right) \mathrm{d}l, \\ &= \underbrace{\frac{\partial}{\partial t} \int_0^L \left(\frac{\rho_m}{2} \mathbf{u}_b \cdot \mathbf{u}_b \right) \mathrm{d}l}_{K_b}. \end{aligned} \tag{3.5.19}$$

We denote the final form of I as K_b, the rate of working of kinetic energy in the beam.
For terms II, III we need to use the following identities. In appendix $A.4$ we derive the time rate of change of the principal stretch λ and the angle θ in the spatial (current) description in the form,

$$\frac{\partial \lambda^{(c)}}{\partial t} = \lambda^{(c)} \frac{\partial u_{b1}^{(c)}}{\partial s} - \lambda^{(c)} \kappa^{(c)} u_{b2}^{(c)}, \qquad (s \in \partial\Omega_b), \tag{3.5.20}$$

$$\frac{\partial \theta^{(c)}}{\partial t} = \frac{\partial u_{b2}^{(c)}}{\partial s} + \kappa^{(c)} u_{b1}^{(c)}, \qquad (s \in \partial\Omega_b). \tag{3.5.21}$$

In appendix $A.2$ we relate the gradient of the angle θ to the beam curvature in the material (reference) description in the form,

$$\frac{\partial \theta}{\partial l} = \lambda \kappa, \qquad (0 \le l \le L_0). \tag{3.5.22}$$

To manipulate II, we use integration by parts for the second term to obtain,

$$\begin{aligned} II = &\int_{\partial\Omega_b} \left(c_\kappa \kappa^{(c)} \frac{\partial (\lambda^{(c)} \kappa^{(c)})}{\partial s} u_{b1}^{(c)} \right) \mathrm{d}s - \left[c_\kappa \frac{\partial (\lambda^{(c)} \kappa^{(c)})}{\partial s} u_{b2}^{(c)} \right]_0^{S_0} \\ &+ \int_{\partial\Omega_b} \left(c_\kappa \frac{\partial (\lambda^{(c)} \kappa^{(c)})}{\partial s} \frac{\partial u_{b2}^{(c)}}{\partial s} \right) \mathrm{d}s, \end{aligned} \tag{3.5.23}$$

where S_0 is the total arc-length of the deformed beam. The second term cancels due to the boundary conditions (3.3.28). Hence, using (3.5.21) we obtain,

$$\begin{aligned} II &= \int_{\partial\Omega_b} \left(c_\kappa \kappa^{(c)} \frac{\partial (\lambda^{(c)} \kappa^{(c)})}{\partial s} u_{b1}^{(c)} \right) \mathrm{d}s + \int_{\partial\Omega_b} \left[c_\kappa \frac{\partial (\lambda^{(c)} \kappa^{(c)})}{\partial s} \left(\frac{\partial \theta^{(c)}}{\partial t} - \kappa u_{b1}^{(c)} \right) \right] \mathrm{d}s \\ &= \int_{\partial\Omega_b} \left(c_\kappa \frac{\partial (\lambda^{(c)} \kappa^{(c)})}{\partial s} \frac{\partial \theta^{(c)}}{\partial t} \right) \mathrm{d}s; \end{aligned} \tag{3.5.24}$$

integrating by parts again we obtain,

$$II = \left[c_\kappa \lambda^{(c)} \kappa^{(c)} \frac{\partial \theta^{(c)}}{\partial t} \right]_0^{S_0} - \int_{\partial\Omega_b} \left[c_\kappa \lambda^{(c)} \kappa^{(c)} \frac{\partial}{\partial s} \left(\frac{\partial \theta^{(c)}}{\partial t} \right) \right] \mathrm{d}s. \tag{3.5.25}$$

The first term disappears due to the boundary condition (3.3.29). Since time derivatives are measured with l held fixed, we transform the remaining formula to the reference (material) description to write as a complete time derivative,

$$II = -\int_0^{L_0} \left[c_\kappa \lambda \kappa \frac{\partial}{\partial l} \left(\frac{\partial \theta}{\partial t} \right) \right] \mathrm{d}l = -\int_0^{L_0} \left[c_\kappa \lambda \kappa \frac{\partial}{\partial t} \left(\frac{\partial \theta}{\partial l} \right) \right] \mathrm{d}l. \tag{3.5.26}$$

We apply (3.5.22) to the second term to obtain,

$$II = -\int_0^{L_0} \left[c_\kappa \lambda \kappa \frac{\partial}{\partial t} (\lambda \kappa) \right] \mathrm{d}l = -\underbrace{\frac{\partial}{\partial t} \int_0^{L_0} \left[\frac{c_\kappa}{2} (\lambda \kappa)^2 \right] \mathrm{d}l}_{U_\kappa}, \tag{3.5.27}$$

where we denote the final form of II as U_κ, the rate of working of bending stresses.
For III, in the same manner, we integrate by parts to obtain,

$$\begin{aligned} III = &\int_{\partial\Omega_b} \left(c_\lambda \kappa^{(c)} (\lambda^{(c)} - 1) u_{b2}^{(c)} + \kappa^{(c)} T u_{b2}^{(c)} \right) \mathrm{d}s + \left[c_\lambda \lambda^{(c)} u_{b1}^{(c)} \right]_0^{S_0} \\ &- \int_{\partial\Omega_b} \left(c_\lambda \lambda^{(c)} \frac{\partial u_{b1}^{(c)}}{\partial s} \right) \mathrm{d}s, \end{aligned} \tag{3.5.28}$$

where the second term disappears due to the boundary condition (3.3.28), and S_0 is the arc-length of the deformed beam. Using (3.5.20) we can write,

$$\begin{aligned} III &= \int_{\partial\Omega_b} \left(c_\lambda \kappa^{(c)} (\lambda^{(c)} - 1) u_{b2}^{(c)} + \kappa^{(c)} T u_{b2}^{(c)} \right) \mathrm{d}s - \int_{\partial\Omega_b} c_\lambda \lambda^{(c)} \left(\frac{1}{\lambda^{(c)}} \frac{\partial \lambda^{(c)}}{\partial t} + \kappa u_{b2}^{(c)} \right) \mathrm{d}s \\ &= -\int_{\partial\Omega_b} \left(c_\lambda \frac{\partial \lambda^{(c)}}{\partial t} \right) \mathrm{d}s - \int_{\partial\Omega_b} \left((c_\lambda - T) \kappa^{(c)} u_{b2}^{(c)} \right) \mathrm{d}s. \end{aligned} \tag{3.5.29}$$

Using (3.5.20) again for the second term we have,

$$\begin{aligned} III &= \int_{\partial\Omega_b} \left(-c_\lambda \frac{\partial \lambda^{(c)}}{\partial t} \right) \mathrm{d}s + \int_{\partial\Omega_b} \left[-(c_\lambda - T) \left(\frac{\partial u_{b1}^{(c)}}{\partial s} - \left(\lambda^{(c)} \right)^{-1} \frac{\partial \lambda^{(c)}}{\partial t} \right) \right] \mathrm{d}s \\ &= \left[-(c_\lambda - T) u_{b1}^{(c)} \right]_0^{S_0} - \int_{\partial\Omega_b} \left[c_\lambda \left(1 - \left(\lambda^{(c)} \right)^{-1} \right) + T \left(\lambda^{(c)} \right)^{-1} \right] \frac{\partial \lambda^{(c)}}{\partial t} \mathrm{d}s, \end{aligned} \tag{3.5.30}$$

the first term cancels due to the boundary condition (3.3.28) and we transform the second term into the reference (material) description to obtain,

$$\begin{aligned} III &= -\int_0^{L_0} \Big(T + c_\lambda\,(\lambda-1)\Big)\frac{\partial \lambda}{\partial t}\,\mathrm{d}l = -\int_0^{L_0} \Big(T + c_\lambda(\lambda-1)\Big)\frac{\partial(\lambda-1)}{\partial t}\,\mathrm{d}l, \\ &= \underbrace{-\frac{\partial}{\partial t}\int_0^{L_0}\left[T\,(\lambda-1) + c_\lambda\frac{(\lambda-1)^2}{2}\right]\mathrm{d}l}_{U_\lambda}. \end{aligned} \tag{3.5.31}$$

Here, we denote the remaining term in III as U_λ, the rate of working of extensional stresses in the beam.

For IV, we change to the reference (material) description and substitute expression (3.2.8) to obtain,

$$IV = \int_{\partial\Omega_b}\Big(p_e u_{b2}^{(c)}\Big)\,\mathrm{d}s = \int_0^{L_0}(\lambda\, p_e u_{b2})\,\mathrm{d}l = \underbrace{\int_0^{L_0} p_e\Big(\mathbf{u}_b\cdot\mathbf{e}_2\Big)\lambda\,\mathrm{d}l}_{P_e}; \tag{3.5.32}$$

we denote the remaining term in IV as P_e, the rate of working of external pressure on the beam. Hence, the rate of working of fluid stress on the beam E_f can be written as,

$$E_f = -K_b - U_\kappa - U_\lambda - P_e, \tag{3.5.33}$$

where,

$$K_b = \frac{\partial}{\partial t}\int_0^{L_0}\Big(\frac{\rho_m}{2}\mathbf{u}_b\cdot\mathbf{u}_b\Big)\,\mathrm{d}l, \tag{3.5.34}$$

$$U_\kappa = \frac{\partial}{\partial t}\int_0^{L_0}\Big[\frac{c_\kappa}{2}(\lambda\kappa)^2\Big]\,\mathrm{d}l, \tag{3.5.35}$$

$$U_\lambda = \frac{\partial}{\partial t}\int_0^{L_0}\left[T(\lambda-1) + c_\lambda\frac{(\lambda-1)^2}{2}\right]\mathrm{d}l, \tag{3.5.36}$$

$$P_e = \int_0^{L_0} p_e\Big(\mathbf{u}_b\cdot\mathbf{e}_2\Big)\lambda\,\mathrm{d}l. \tag{3.5.37}$$

Here K_b is the rate of working of kinetic energy of beam, U_κ is the rate of working of bending stresses, U_λ is the rate of working of extensional stresses and P_e is the rate of working of external pressure. Substituting (3.5.33) into (3.5.10), we obtain the fully non-linear energy budget,

$$K_f + F_f - P_f + D_f + K_b + U_\kappa + U_\lambda + P_e = 0, \tag{3.5.38}$$

where,

$$K_f = \frac{\partial}{\partial t}\int_\Omega \left(\frac{1}{2}\mathbf{u}\cdot\mathbf{u}\right)\mathrm{d}A, \tag{3.5.39}$$

$$F_f = \left[\int_0^1 \frac{1}{2}(\mathbf{u}\cdot\mathbf{u})(\mathbf{u}\cdot\mathbf{n})\,\mathrm{d}y\right]_{x=-L_u}^{x=L_0+L_d}, \tag{3.5.40}$$

$$P_f = \left[\int_0^1 (-p\mathbf{u}\cdot\mathbf{n})\,\mathrm{d}y\right]_{x=-L_u}^{x=L_0+L_d}, \tag{3.5.41}$$

$$D_f = R^{-1}\int_\Omega \mathrm{Tr}\Big(\left(\nabla\mathbf{u}+\nabla\mathbf{u}^{\mathrm{T}}\right)\nabla\mathbf{u}\Big)\,\mathrm{d}A, \tag{3.5.42}$$

$$K_b = \frac{\partial}{\partial t}\int_0^{L_0}\left(\frac{\rho_m}{2}\mathbf{u}_b\cdot\mathbf{u}_b\right)\mathrm{d}l, \tag{3.5.43}$$

$$U_\kappa = \frac{\partial}{\partial t}\int_0^{L_0}\left[\frac{c_\kappa}{2}(\lambda\kappa)^2\right]\mathrm{d}l, \tag{3.5.44}$$

$$U_\lambda = \frac{\partial}{\partial t}\int_0^{L_0}\left[T(\lambda-1)+c_\lambda\frac{(\lambda-1)^2}{2}\right]\mathrm{d}l, \tag{3.5.45}$$

$$P_e = \int_0^{L_0} p_e\Big(\mathbf{u}_b\cdot\mathbf{e}_2\Big)\lambda\,\mathrm{d}l. \tag{3.5.46}$$

We will compute the terms in (3.5.38) below to distinguish various models of self-excited oscillation.

3.6 Steady energy budgets

For the static state, all variables are independent of time (detailed in *Sec*. 3.4). So the system energy budget K_f, K_b, U_κ and U_λ vanish. As the beam velocity in the static state is zero, we also have $P_e = 0$. Therefore, the energy budget for the steady system can be expressed simply as,

$$F_f^{(s)} - P_f^{(s)} + D_f^{(s)} = 0, \tag{3.6.1}$$

where,

$$F_f^{(s)} = \left[\int_0^1 \left(\frac{1}{2}(\mathbf{U}\cdot\mathbf{U})(\mathbf{U}\cdot\mathbf{N})\right)\mathrm{d}y\right]_{x=-L_u}^{x=L_0+L_d}, \tag{3.6.2}$$

$$P_f^{(s)} = \left[\int_0^1 (-P\mathbf{U}\cdot\mathbf{N})\,\mathrm{d}y\right]_{x=-L_u}^{x=L_0+L_d}, \tag{3.6.3}$$

$$D_f^{(s)} = R^{-1}\int_{\bar\Omega}\mathrm{Tr}\left(\left(\nabla\mathbf{U}+\nabla\mathbf{U}^{\mathrm{T}}\right)\nabla\mathbf{U}\right)\mathrm{d}A. \tag{3.6.4}$$

Here we denote the energy budget with superscript (s) as the energy budget in the static state, *i.e*. $F_f^{(s)}$ is the net kinetic energy flux extracted between the channel ends in the steady state, $P_f^{(s)}$ is the rate of working of the steady pressure force at the channel inlet and $D_f^{(s)}$ is the energy loss

due to viscosity in the steady flow.
In analysing self-excited oscillations, it is useful to consider the excess energy terms due to these oscillations (*i.e.* subtracting the steady component), where we compute as,

$$F_e = F_f - F_f^{(s)},\ P_e = P_f - P_f^{(s)},\ D_e = D_f - D_f^{(s)}. \tag{3.6.5}$$

These excess energies are computed in later *Sec*.3.8.4.

3.7 Numerical method

In this section, we describe the numerical methods used to solve the coupled beam-fluid system using the finite element method. We first describe the adaptive mesh we use for this system and then give a detailed explanation of numerical methods we adopt to solve the fully non-linear system and construct its energy budget.

3.7.1 Mesh

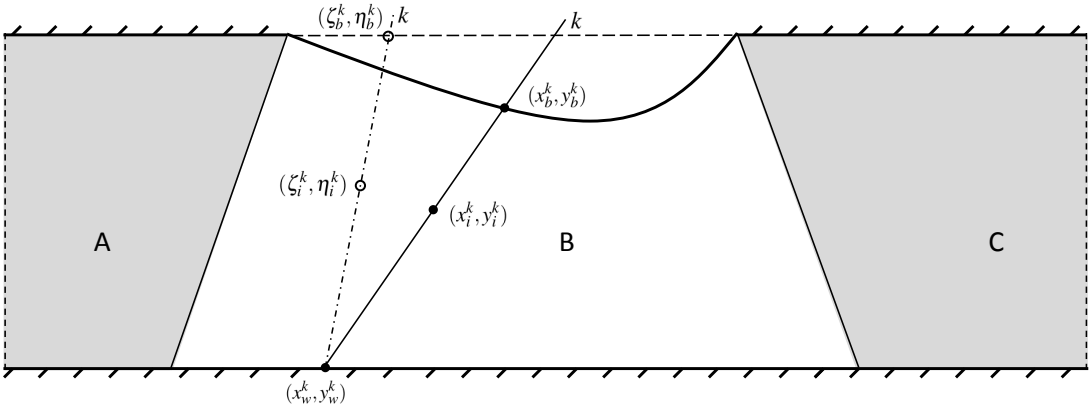

Figure 3.4: Adaptive mesh for beam-fluid system

We divide the fluid domain into three sections, shown in figure 3.4. The sections under rigid wall A, C, and section under elastic beam B, as described by Luo & Pedley [50], Luo *et al*. [48]). We adopt an adaptive mesh in section B since the beam is deformable, while we use fixed mesh for section A and C. For sections A and C, the flow is described using a Eulerian description, whereas the flow is described using an Arbitrary Lagrangian-Eulerian (ALE) method [23] for section B. The element locations in these subdomains are linked to the elements of the boundaries (particularly inlet, outlet and elastic boundaries), so that the elements along the boundaries contain three nodes.
Across the elastic section (section B), we employ numerical spines, as shown in figure 3.4. We seed nodes along the rigid wall and connect these to nodes on the beam by straight lines. These

straight lines are approximately equally spaced initially and cannot cross. Element nodes are then seeded along these spines covering the entirety of region B in a uniform manner. Each spine can rotate around its fixed node on the rigid wall, all the nodes along each spine can move with this spine as the elastic beam is deformed. This allows the mesh to adapt during deformation of the beam.

Taking spine k as an example, in the initial state, spine k is formed by connecting node on the undeformed beam $(\zeta_b^k, \eta_b^k)^{\mathrm{T}}$ with fixed node $\mathbf{x}_w^k = (x_w^k, y_w^k)^{\mathrm{T}}$ on the rigid lower wall (see figure 3.4). Node i on spine k is located in $(\zeta_i^k, \eta_i^k)^{\mathrm{T}}$. After deformation, the node on elastic beam $(\zeta_b^k, \eta_b^k)^{\mathrm{T}}$ moves to $\mathbf{x}_b^k = (x_b^k, y_b^k)^{\mathrm{T}}$, while node i moves to $\mathbf{x}_i^k = (x_i^k, y_i^k)^{\mathrm{T}}$. Since the relative position of each node on spine k remains the same, we can express the position of node i in the deformed state as,

$$x_i^k = x_w^k + \omega_i^k \left(x_b^k - x_w^k\right), \quad y_i^k = y_w^k + \omega_i^k \left(y_b^k - y_w^k\right), \tag{3.7.1}$$

where ω_i^k is a fixed scale factor defined as,

$$\omega_i^k = \frac{\sqrt{\left(\zeta_i^k - x_w^k\right)^2 + \left(\eta_i^k - y_w^k\right)^2}}{\sqrt{\left(\zeta_b^k - x_w^k\right)^2 + \left(\eta_b^k - y_w^k\right)^2}}. \tag{3.7.2}$$

3.7.2 Time derivatives

The time derivatives in the system governing equations (3.3.17-3.3.29) are time derivatives taken holding the node position fixed (*i.e.* Eulerian time derivatives). However, nodes in section B are constrained to move as the elastic beam is moving. Therefore, we apply an ALE method to shift the Eulerian time derivatives in the system governing equations into time derivatives taken following a moving nodes along these spines, in the form

$$\frac{\delta}{\delta t} = \frac{\partial}{\partial t} + \frac{\mathrm{d}\mathbf{x}}{\mathrm{d}t} \cdot \nabla, \tag{3.7.3}$$

here $\delta/\delta t$ denotes the time derivative following a moving node, $\partial/\partial t$ denotes the Eulerian time derivative, $\mathbf{x} = (x, y)^{\mathrm{T}}$ represents the node position. Taking the position of ith node (3.7.1) on spine k as an example, $\mathrm{d}\mathbf{x}_i^k/\mathrm{d}t$ can be written as

$$\frac{\mathrm{d}\mathbf{x}_i^k}{\mathrm{d}t} = \omega_i^k \frac{\mathrm{d}\mathbf{x}_b^k}{\mathrm{d}t}, \tag{3.7.4}$$

Therefore, the time derivative following a moving node evaluated on ith node in the ALE method can be written as

$$\frac{\delta}{\delta t} = \frac{\partial}{\partial t} + \omega_i^k \frac{\mathrm{d}\mathbf{x}_b^k}{\mathrm{d}t} \cdot \nabla. \tag{3.7.5}$$

3.7.3 Numerical methods for fully non-linear governing equations

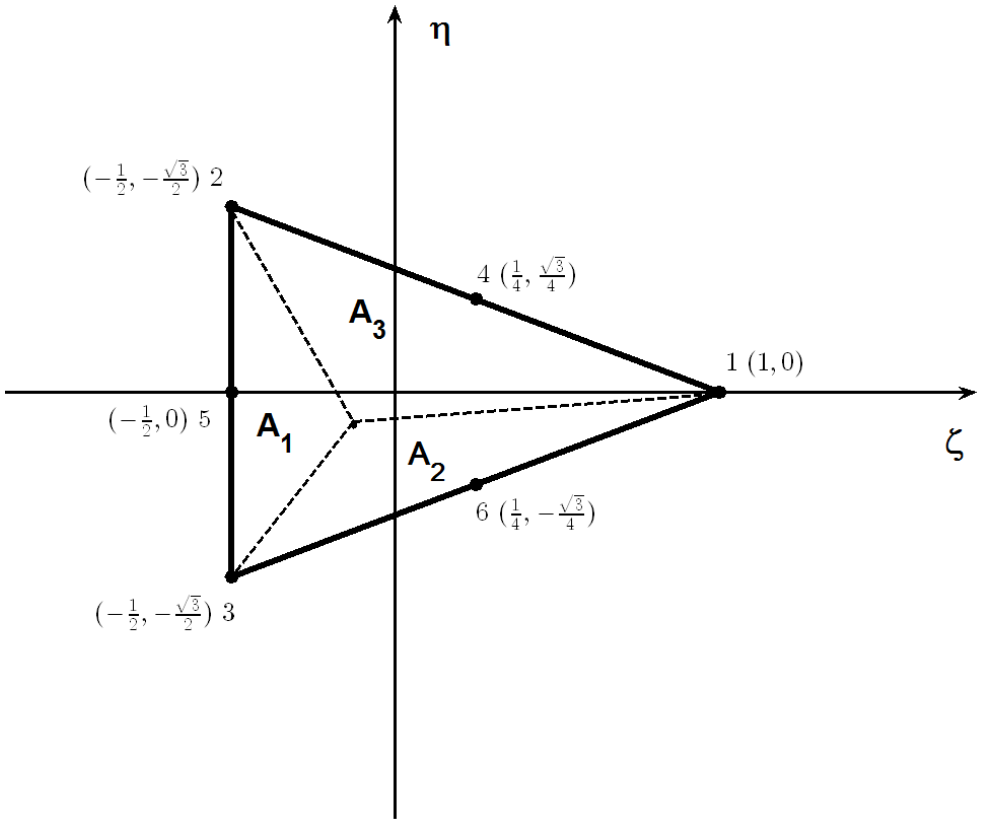

Figure 3.5: Six nodes triangular element in local coordinate (Rast [58]).

The weighted residual method is used to discretize the system governing equations (3.3.17-3.3.29). We use 6-node triangular elements with second order shape functions for components of fluid u_1 and u_2, and linear shape functions for the fluid pressure p. The corresponding shape functions for beam variables $x_b, y_b, \theta, \lambda$ and κ are chosen as second order shape functions evaluated on 3-node beam elements (Huyakorn *et al*. [36]). Each triangular element maps from Cartesian coordinates $(x,y)^{\mathrm{T}}$ to local $(\zeta,\eta)^{\mathrm{T}}$ coordinates in the element, shown in figure 3.5 (Rast [58]). So we have,

$$u_1 = \sum_{i=1}^{i=6} u_{1i} N_i(\zeta,\eta), \quad u_2 = \sum_{i=1}^{i=6} u_{2i} N_i(\zeta,\eta), \quad p = \sum_{i=1}^{i=3} p_i L_i(\zeta,\eta),$$

$$
\begin{aligned}
&x = \sum_{i=1}^{i=6} x_i(x_b) N_i(\zeta,\eta), \;\; y = \sum_{i=1}^{i=6} y_i(y_b) N_i(\zeta,\eta), \\
&x_b = \sum_{i=1}^{i=3} x_{bi} N_i(s), \;\; y_b = \sum_{i=1}^{i=3} y_{bi} N_i(s), \;\; \theta = \sum_{i=1}^{i=3} \theta_i N_i(s), \\
&\lambda = \sum_{i=1}^{i=3} \lambda_i N_i(s), \;\; \kappa = \sum_{i=1}^{i=3} \kappa_i N_i(s),
\end{aligned} \tag{3.7.6}
$$

where s is the deformed coordinate along the beam, N_i is the 6-node quadratic shape function, L_i is the linear shape function, while $N_i(s)$ is the shape function evaluated on 3-node beam element. Therefore, nodal velocities are evaluated at all nodes of each element whereas pressure is evaluated only at 3 nodes of each element. The coordinate position $(x,y)^{\mathrm{T}}$ in section B depends on the moving beam. From equations (3.7.6) the Jacobian matrix $\mathbf{J}$ of the coordinate transformation for elements under the moving beam (section B) take the form,

$$
\mathbf{J} = \frac{\partial(x,y)}{\partial(\zeta,\eta)} = \begin{pmatrix} \partial x/\partial\zeta & \partial y/\partial\zeta \\ \partial x/\partial\eta & \partial y/\partial\eta \end{pmatrix}. \tag{3.7.7}
$$

In addition, the linear shape functions L_i is defined as

$$
L_i = \frac{A_i}{A} \; (i = 1,2,3), \;\; A = A_1 + A_2 + A_3, \tag{3.7.8}
$$

where A_i and A represent the area of triangle in figure 3.5. The second order shape function can be expressed as (details see Zienkiewicz [79]),

$$
\begin{aligned}
&N_1 = L_1(2L_1 - 1), \;\; N_2 = L_2(2L_2 - 1), \;\; N_3 = L_3(2L_3 - 1), \\
&N_4 = 4L_1L_2, \;\; N_5 = 4L_2L_3, \;\; N_6 = 4L_1L_3.
\end{aligned} \tag{3.7.9}
$$

The above shape functions are non-zero only within each element and have the characteristics that at each node i the shape function is

$$
N_j(x_i,y_i) = \delta_{ij}, \;\; L_j(x_i,y_i) = \delta_{ij}, \tag{3.7.10}
$$

here δ_{ij} is Kronecker delta function; at each node in an element

$$
\sum_{i=1}^{i=6} N_i(\zeta,\eta) = 1, \;\; \sum_{i=1}^{i=3} L_i(\zeta,\eta) = 1. \tag{3.7.11}
$$

The weighted residuals method is used to discretize the system to determine the nodal values of variables. Multiplying the system governing equations (3.3.17-3.3.29) with shape functions and

then integrate over the domain, we obtain the discretized matrix equation as (identical to [48]),

$$\mathbf{M}\frac{\mathrm{d}\mathbf{U}'}{\mathrm{d}t}+\mathbf{K}(\mathbf{U}')-\mathbf{F}=\mathbf{R}=\mathbf{0}, \tag{3.7.12}$$

here $\mathbf{M}$ is the mass matrix, $\mathbf{K}(\mathbf{U}')$ is the stiffness matrix, and $\mathbf{F}$ is the external force vector. The vector $\mathbf{U}'=(u_{1i},p_i,u_{2i},x_{bi},y_{bi},\theta_i,\lambda_i,\kappa_i)^{\mathrm{T}}$ is the global vector of unknowns. Finally $\mathbf{R}$ is the residual vector, we have

$$\mathbf{R}=(R_c,R_x,R_y,R_{ex},R_{ey},R_{e\theta},R_{e\lambda},R_{e\kappa})^{\mathrm{T}}; \tag{3.7.13}$$

we denote R_c,R_x,R_y as residuals from the continuity equation (3.3.17) and the x and y components of the fluid momentum equations (3.3.18), respectively. We denote $R_{ex},R_{ey},R_{e\theta},R_{e\lambda}$ and $R_{e\kappa}$ as the residuals to the beam position x_b and y_b (3.3.23) (3.3.24), the beam angle θ related equation (3.3.25), the beam momentum equation (3.3.26) in the tangential direction, the beam momentum equation (3.3.27) in the normal direction, respectively.

We use different weighting functions when discretizing the system governing equations. For fluid residuals R_x and R_y we choose the weighting function N_l, whereas the weighting function L_k is chosen for R_c. The weighting function $\mathrm{d}N_l/\mathrm{d}l$ is chosen for beam residuals $R_{ex},R_{ey},R_{e\theta},R_{e\lambda}$ and the weighting function N_l is chosen for $R_{e\kappa}$.

For each element we can expand the residual R_c choosing L_k as the weighting function,

$$R_c^k=\sum_{i=1}^{i=6}u_{1i}\int\int\frac{\partial N_i}{\partial x}L_k\,\mathrm{d}x\mathrm{d}y+\sum_{i=1}^{i=6}u_{2i}\int\int\frac{\partial N_i}{\partial y}L_k\,\mathrm{d}x\mathrm{d}y=0. \tag{3.7.14}$$

Here $k=1,2,3$, the same number as that of the pressure unknowns. The transformation of derivatives of shape functions with respect to global coordinates x and y to local coordinates ζ and η takes the form,

$$\frac{\partial N_i}{\partial x}=\frac{1}{|\mathbf{J}|}\sum_{j=1}^{j=6}y_jA_{ij},\quad\frac{\partial N_i}{\partial y}=\frac{1}{|\mathbf{J}|}\sum_{j=1}^{j=6}x_jA_{ji}, \tag{3.7.15}$$

here $|\cdot|$ represents the determinant of a matrix and the symbol A_{ij} is defined as

$$A_{ij}=-A_{ji}=\frac{\partial N_i}{\partial\zeta}\frac{\partial N_j}{\partial\eta}-\frac{\partial N_i}{\partial\eta}\frac{\partial N_j}{\partial\zeta}; \tag{3.7.16}$$

The integration transform to the local coordinate as

$$\int\int\mathrm{d}x\mathrm{d}y=\int\int|\mathbf{J}|\mathrm{d}\zeta\mathrm{d}\eta. \tag{3.7.17}$$

For each element we can expand R_x using (3.7.6), the residual using N_l as weighting function to write in the form,

$$\begin{aligned}
R_x^l = &\sum_{i=1}^{i=6} \frac{\delta u_{1i}}{\delta t} \int\int N_i N_l \,\mathrm{d}x\mathrm{d}y - \sum_{k=1}^{k=3}\sum_{i=1}^{i=6}\sum_{j=1}^{j=6} u_{1i}\omega_j^k \frac{\mathrm{d}x_b^k}{\mathrm{d}t} \int\int \frac{\partial N_i}{\partial x} N_j N_l \,\mathrm{d}x\mathrm{d}y \\
&- \sum_{k=1}^{k=3}\sum_{i=1}^{i=6}\sum_{j=1}^{j=6} u_{1i}\omega_j^k \frac{\mathrm{d}y_b^k}{\mathrm{d}t} \int\int \frac{\partial N_i}{\partial y} N_j N_l \,\mathrm{d}x\mathrm{d}y + \sum_{i=1}^{i=6}\sum_{j=1}^{j=6} u_{1i}u_{1j} \int\int \frac{\partial N_i}{\partial x} N_j N_l \,\mathrm{d}x\mathrm{d}y \\
&+ \sum_{i=1}^{i=6}\sum_{j=1}^{j=6} u_{1i}u_{2j} \int\int \frac{\partial N_i}{\partial y} N_j N_l \,\mathrm{d}x\mathrm{d}y + \sum_{i=1}^{i=3} p_i \int L_i N_l \left(-\sin(\theta)\right) \mathrm{d}s \\
&- \sum_{i=1}^{i=3} p_i \int\int L_i \frac{\partial N_l}{\partial x} \,\mathrm{d}x\mathrm{d}y + R^{-1} \sum_{i=1}^{i=6} u_{1i} \int\int \frac{\partial N_i}{\partial x}\frac{\partial N_l}{\partial x} \,\mathrm{d}x\mathrm{d}y \\
&- R^{-1} \sum_{i=1}^{i=6} u_{1i} \int \frac{\partial N_i}{\partial x} N_l(-\sin(\theta)) \,\mathrm{d}s + R^{-1} \sum_{i=1}^{i=6} u_{1i} \int\int \frac{\partial N_i}{\partial y}\frac{\partial N_l}{\partial y} \,\mathrm{d}x\mathrm{d}y \\
&- R^{-1} \sum_{i=1}^{i=6} u_{1i} \int \frac{\partial N_i}{\partial y} N_l \cos(\theta) \,\mathrm{d}s = 0.
\end{aligned} \tag{3.7.18}$$

Here we applied the ALE method (3.7.5) for the time derivative term. The divergence theorem is used to eliminate the derivative of pressure in respect to x since pressure varies linearly between nodes. The divergence theorem is applied for viscous terms to reduce the derivative to first order as well, $\int \mathrm{d}s$ denotes integration on the boundary of the node.
Similar to R_x, for each element we use N_l as a weighting function and the expansion of R_y is,

$$\begin{aligned}
R_y^l = &\sum_{i=1}^{i=6} \frac{\delta u_{2i}}{\delta t} \int\int N_i N_l \,\mathrm{d}x\mathrm{d}y - \sum_{k=1}^{k=3}\sum_{i=1}^{i=6}\sum_{j=1}^{j=6} u_{2i}\omega_j^k \frac{\mathrm{d}x_b^k}{\mathrm{d}t} \int\int \frac{\partial N_i}{\partial x} N_j N_l \,\mathrm{d}x\mathrm{d}y \\
&- \sum_{k=1}^{k=3}\sum_{i=1}^{i=6}\sum_{j=1}^{j=6} u_{2i}\omega_j^k \frac{\mathrm{d}y_b^k}{\mathrm{d}t} \int\int \frac{\partial N_i}{\partial y} N_j N_l \,\mathrm{d}x\mathrm{d}y + \sum_{i=1}^{i=6}\sum_{j=1}^{j=6} u_{2i}u_{1j} \int\int \frac{\partial N_i}{\partial x} N_j N_l \,\mathrm{d}x\mathrm{d}y \\
&+ \sum_{i=1}^{i=6}\sum_{j=1}^{j=6} u_{2i}u_{2j} \int\int \frac{\partial N_i}{\partial y} N_j N_l \,\mathrm{d}x\mathrm{d}y + \sum_{i=1}^{i=3} p_i \int L_i N_l \cos(\theta) \,\mathrm{d}s \\
&- \sum_{i=1}^{i=3} p_i \int\int L_i \frac{\partial N_l}{\partial y} \,\mathrm{d}x\mathrm{d}y + R^{-1} \sum_{i=1}^{i=6} u_{2i} \int\int \frac{\partial N_i}{\partial x}\frac{\partial N_l}{\partial x} \,\mathrm{d}x\mathrm{d}y \\
&- R^{-1} \sum_{i=1}^{i=6} u_{2i} \int \frac{\partial N_i}{\partial x} N_l(-\sin(\theta)) \,\mathrm{d}s + R^{-1} \sum_{i=1}^{i=6} u_{2i} \int\int \frac{\partial N_i}{\partial y}\frac{\partial N_l}{\partial y} \,\mathrm{d}x\mathrm{d}y \\
&- R^{-1} \sum_{i=1}^{i=6} u_{2i} \int \frac{\partial N_i}{\partial y} N_l \cos(\theta) \,\mathrm{d}s = 0.
\end{aligned} \tag{3.7.19}$$

The equation number l of R_x^l and R_y^l equals the number of velocity nodal values.
For each element, we choose $\mathrm{d}N_l/\mathrm{d}l$ as a weighting function for R_{ex} to construct,

$$R_{ex}^l = \sum_{i=1}^{i=3} x_{bi} \int \frac{\mathrm{d}N_i}{\mathrm{d}l}\frac{\mathrm{d}N_l}{\mathrm{d}l}\,\mathrm{d}l - \sum_{i=1}^{i=3} \lambda_i \int N_i \frac{\mathrm{d}N_l}{\mathrm{d}l}\,\mathrm{d}l = 0. \tag{3.7.20}$$

The number of equations evaluated on the elastic boundary $l = 3,5,2$ as the elements are oriented.
Similarly, choosing $\mathrm{d}N_l/\mathrm{d}l$ as a weighting function, the expansion of R_{ey} can be written as,

$$R_{ey}^l = \sum_{i=1}^{i=3} y_{bi} \int \frac{\mathrm{d}N_i}{\mathrm{d}l}\frac{\mathrm{d}N_l}{\mathrm{d}l}\,\mathrm{d}l - \sum_{i=1}^{i=3} \lambda_i \int N_i \frac{\mathrm{d}N_l}{\mathrm{d}l}\,\mathrm{d}l = 0. \tag{3.7.21}$$

For each element, choosing $\mathrm{d}N_l/\mathrm{d}l$ as the weighting function, the expansion of $R_{e\theta}$ is,

$$R_{e\theta}^l = \sum_{i=1}^{i=3} \theta_i \int N_i \frac{\mathrm{d}N_l}{\mathrm{d}l}\,\mathrm{d}l - \sum_{i=1}^{i=3}\sum_{j=1}^{j=3} \lambda_i \kappa_j \int N_i N_j \frac{\mathrm{d}N_l}{\mathrm{d}l}\,\mathrm{d}l = 0. \tag{3.7.22}$$

Finally, using $\mathrm{d}N_l/\mathrm{d}l$ as a weighting function, the expansion of $R_{e\lambda}$ can be written as,

$$\begin{aligned}
R_{e\lambda}^l =& \sum_{i=1}^{i=3}\sum_{j=1}^{j=3} \rho_m \left(x_{bi}\frac{\delta u_{b1j}}{\delta t} + y_{bi}\frac{\delta u_{b2j}}{\delta t}\right) \int \frac{\mathrm{d}N_i}{\mathrm{d}l} N_j \frac{\mathrm{d}N_l}{\mathrm{d}l}\frac{1}{\lambda}\,\mathrm{d}l \\
&- \sum_{i=1}^{i=3}\sum_{j=1}^{j=3}\sum_{k=1}^{k=3} c_\kappa \left(\kappa_i\lambda_j\kappa_k + \kappa_i\kappa_j\lambda_j\right) \int N_i N_j \frac{\mathrm{d}N_k}{\mathrm{d}l}\frac{\mathrm{d}N_l}{\mathrm{d}l}\,\mathrm{d}l - \sum_{i=1}^{i=3} c_\lambda \lambda_i \int \frac{\mathrm{d}N_i}{\mathrm{d}l}\frac{\mathrm{d}N_l}{\mathrm{d}l}\,\mathrm{d}l \\
&+ R^{-1} \sum_{i=1}^{i=6}\sum_{j=1}^{j=6}\sum_{k=1}^{k=3} \left(x_i u_{2j} + y_i u_{1j}\right)\lambda_k \int A_{ij} N_k \frac{\mathrm{d}N_l}{\mathrm{d}l}\sin(2\theta)|\mathbf{J}|^{-1}\,\mathrm{d}l \\
&+ R^{-1} \sum_{i=1}^{i=6}\sum_{j=1}^{j=6}\sum_{k=1}^{k=3} \left(x_i u_{1j} - y_i u_{2j}\right)\lambda_k \int A_{ij} N_k \frac{\mathrm{d}N_l}{\mathrm{d}l}\cos(2\theta)|\mathbf{J}|^{-1}\,\mathrm{d}l = 0,
\end{aligned} \tag{3.7.23}$$

where $\mathbf{J}$ is the Jacobian matrix. The Eulerian time derivative $\partial/\partial t$ in residual $R_{e\lambda}$ is equal to time derivative following a moving node $\delta/\delta t$ on the elastic beam.
For each element, we choose N_l as weighting function for residual $R_{e\kappa}$ and apply integration by parts for the c_κ term, we obtain

$$\begin{aligned}
R_{e\kappa}^l =& \sum_{i=1}^{i=3}\sum_{j=1}^{j=3} \rho_m \left(x_{bi}\frac{\delta u_{b2j}}{\delta t} - y_{bi}\frac{\delta u_{b1j}}{\delta t}\right) \int \frac{\mathrm{d}N_i}{\mathrm{d}l} N_j N_l \frac{1}{\lambda}\,\mathrm{d}l \\
&+ \sum_{i=1}^{i=3} \left[c_\kappa \left(\lambda_i\kappa_2 + \lambda_2\kappa_i\right)\frac{1}{\lambda_2}\frac{\mathrm{d}N_i}{\mathrm{d}l}\right]^{\text{Node 2}} - \sum_{i=1}^{i=3} \left[c_\kappa \left(\lambda_i\kappa_3 + \lambda_3\kappa_i\right)\frac{1}{\lambda_3}\frac{\mathrm{d}N_i}{\mathrm{d}l}\right]_{\text{Node 3}} \\
&- \sum_{i=1}^{i=3}\sum_{j=1}^{j=3} c_\kappa \left(\lambda_i\kappa_j + \lambda_j\kappa_i\right) \int \frac{\mathrm{d}N_i}{\mathrm{d}l} N_j \frac{\mathrm{d}N_l}{\mathrm{d}l}\,\mathrm{d}l
\end{aligned}$$

$$
\begin{aligned}
&-\sum_{i=1}^{i=3}\sum_{j=1}^{j=3}\sum_{k=1}^{k=3} c_\lambda \lambda_i \lambda_j \kappa_k \int N_i N_j N_k N_l \,\mathrm{d}l + \sum_{i=1}^{i=3}\sum_{j=1}^{j=3} (c_\lambda - T)\lambda_i \kappa_j \int N_i N_j N_l \,\mathrm{d}l \\
&+\sum_{i=1}^{i=3} p_e \lambda_i \int N_i N_l \,\mathrm{d}l - \sum_{i=1}^{i=3}\sum_{j=1}^{j=3} \lambda_i p_j \int N_i N_j N_l \,\mathrm{d}l \\
&+R^{-1}\sum_{i=1}^{j=6}\sum_{j=1}^{j=6}\sum_{k=1}^{k=3} \left(x_i u_{b2\,j} + y_i u_{b1\,j}\right)\lambda_k \int A_{ij} N_k N_l \cos(2\theta)|\mathbf{J}|^{-1}\,\mathrm{d}l \\
&-R^{-1}\sum_{i=1}^{j=6}\sum_{j=1}^{j=6}\sum_{k=1}^{k=3} \left(x_i u_{b1\,j} - y_i u_{b2\,j}\right)\lambda_k \int A_{ij} N_k N_l \sin(2\theta)|\mathbf{J}|^{-1}\,\mathrm{d}l = 0.
\end{aligned} \tag{3.7.24}
$$

Here superscript 'Node 2' and subscript 'Node 3' represent the two end point of elastic beam since the three points for each element on elastic beam are numbered as 3, 5, 2.

Time integration

An implicit finite difference scheme is used to obtain the time integration of the discrete nonlinear matrix equation (3.7.12) as

$$
\mathbf{M}(\mathbf{U'}_{n+1})\dot{\mathbf{U}}'_{n+1} + \mathbf{K}(\mathbf{U'}_{n+1})\mathbf{U'}_{n+1} - \mathbf{F}(\mathbf{U'}_{n+1}) = \mathbf{R}(\mathbf{U'}_{n+1}, \mathbf{U'}_n) = \mathbf{0}, \tag{3.7.25}
$$

where the subscript n denotes the time step. For the first four time steps, $\dot{\mathbf{U}}'_{n+1}$ is approximated by a backward-Euler first order scheme with constant time increment ($\mathrm{d}t$), *i.e.* $\dot{\mathbf{U}}'_{n+1} = (\mathbf{U'}_{n+1} - \mathbf{U'}_n)/\mathrm{d}t$. Then a varying time increment second order predictor-corrector scheme is applied to approximate $\dot{\mathbf{U}}'_{n+1}$. A predictor at time step $n+1$ (denote as $\mathbf{U'}^{p}_{n+1}$) is applied by using the second order accurate Adams-Bashforth explicit scheme

$$
\mathbf{U'}^{p}_{n+1} = \mathbf{U'}_n + \frac{\mathrm{d}t_n}{2}\left[\left(2 + \frac{\mathrm{d}t_n}{\mathrm{d}t_{n-1}}\right)\dot{\mathbf{U}}'_n - \frac{\mathrm{d}t_n}{\mathrm{d}t_{n-1}}\dot{\mathbf{U}}'_{n-1}\right], \tag{3.7.26}
$$

which gives the truncation error

$$
\mathbf{U'}^{p}_{n+1} - \mathbf{U'}(n+1) = -\frac{1}{12}\left(2 + 3\frac{\mathrm{d}t_{n-1}}{\mathrm{d}t_n}\right)(\mathrm{d}t_n)^3 \ddot{\mathbf{U}}'_{n+1} + O(\mathrm{d}t_n)^4. \tag{3.7.27}
$$

Here $\mathbf{U'}(n+1)$ is the exact solution at time step $n+1$, this truncation error is later used to estimate the next time increment. Then, a corrector step is applied by solving equation (3.7.25) for $\mathbf{U'}^{c}_{n+1}$ with time derivation approximation

$$
\dot{\mathbf{U}}'^{c}_{n+1} = \frac{2}{\mathrm{d}t_n}\left(\mathbf{U}'_{n+1} - \mathbf{U}'_n\right) - \dot{\mathbf{U}}'_n, \tag{3.7.28}
$$

with a truncation error

$$\mathbf{d}_{n+1} = \mathbf{U}'^{c}_{n+1} - \mathbf{U}'(n+1) = \frac{1}{12}(\mathrm{d}t_n)^3 \ddot{\mathbf{U}}'_{n+1} + O(\mathrm{d}t_n)^4. \tag{3.7.29}$$

Combining equation (3.7.27) with equation (3.7.29) we obtain

$$\mathbf{d}_{n+1} = \mathbf{U}'^{c}_{n+1} - \mathbf{U}'^{p}_{n+1} - \frac{1}{12}\left(2 + 3\frac{\mathrm{d}t_{n-1}}{\mathrm{d}t_n}\right)(\mathrm{d}t_n)^3 \ddot{\mathbf{U}}'_{n+1} + O(\mathrm{d}t_n)^4, \tag{3.7.30}$$

from equation (3.7.29) we have

$$\left(2 + 3\frac{\mathrm{d}t_{n-1}}{\mathrm{d}t_n}\right)\mathbf{d}_{n+1} = \frac{1}{12}(\mathrm{d}t_n)^3 \ddot{\mathbf{U}}'_{n+1}\left(2 + 3\frac{\mathrm{d}t_{n-1}}{\mathrm{d}t_n}\right) + O(\mathrm{d}t_n)^4. \tag{3.7.31}$$

Combining equation (3.7.30) and equation (3.7.31) we obtain the relationship

$$\mathbf{d}_{n+1} = \frac{\mathrm{d}t_n\left(\mathbf{U}'^{c}_{n+1} - \mathbf{U}'^{p}_{n+1}\right)}{3(\mathrm{d}t_n + \mathrm{d}t_{n-1})} + O(\mathrm{d}t_n)^4. \tag{3.7.32}$$

Based on the assumption that the norm of next time step's error should be less than required input error, we setting $\|\mathbf{d}_{n+2}\| = \xi$. Therefore, equation (3.7.32) can be used to estimate the next time increment,

$$\frac{\mathrm{d}t_{n+1}}{\mathrm{d}t_n} = \left(\frac{\xi}{\|\mathbf{d}_{n+1}\|}\right)^{\frac{1}{3}} = SFAC. \tag{3.7.33}$$

The factor *SFAC* is calculated at each step, the next time increment dt_{n+1} is increased when $SFAC > 1$ while dt_{n+1} is decreased when $SFAC < 1$. For a detailed derivation see Luo & Pedley [50].

Newton-Raphson iteration

At each time step, a frontal method (Irons & Bruce [38], Rast [58]) is used to assemble the global matrix equation (3.7.25). A frontal method is based on Gaussian elimination, for which the elimination is implemented after assembling the system matrix equation. While for frontal method the elimination and assembly perform alternatively. Frontal method first scans the element matrices, when one entry's degree of freedom has been assembled completely it is denoted as the pivot, and use the row that contains this pivot to eliminate the rest rows. After the elimination, the row that contains this pivot is stored in external storage. Repeating previous steps till all the elements are scanned, and solve for the global vector, eventually.

A Newton-Raphson iteration scheme is applied to solve the global matrix equation (3.7.25) for

$\mathbf{U}'_{n+1}$ (Luo & Pedley [50]) in the form

$$\frac{\partial \mathbf{R}_{n+1}(\mathbf{U}'^{j}_{n+1}, \mathbf{U}'_{n})}{\partial \mathbf{U}'^{j}_{n+1}} \left(\mathbf{U}'^{j+1}_{n+1} - \mathbf{U}'^{j}_{n+1} \right) \approx -\mathbf{R}_{n+1} \left(\mathbf{U}'^{j}_{n+1}, \mathbf{U}'_{n} \right), \tag{3.7.34}$$

where j is the iteration number. When

$$\max|\mathbf{U}'^{j+1}_{n+1} - \mathbf{U}'^{j}_{n+1}| \leqslant \xi, \quad \max|\mathbf{R}_{n+1}| \leqslant \xi, \tag{3.7.35}$$

we obtain the solution at time step $n+1$, denoted $\mathbf{U}'^{j+1}_{n+1}$.

3.7.4 Numerical method for computing the fully non-linear energy budget

In this section, we use the expansions of variables in the shape functions (3.7.6) to obtain the discretized fully non-linear system energy budget (3.5.38). We consider the massless beam-fluid system, so the energy budget can be written as,

$$K_f + D_f + F_f - P_f + U_\kappa + U_\lambda + P_e = 0. \tag{3.7.36}$$

For the fluid kinetic energy K_f (3.5.39), using the ALE method and the discretization of K_f takes the form,

$$\begin{aligned}
K_f = &\sum_{\Delta_a} \left(\sum_{i=1}^{i=6} \sum_{j=1}^{j=6} \left(u_{1i} \frac{\delta u_{1j}}{\delta t} + u_{2i} \frac{\delta u_{2j}}{\delta t} \right) \int\int N_i N_j \, \mathrm{d}x\mathrm{d}y \right) \\
&- \sum_{\Delta_a} \left(\sum_{m=1}^{m=3} \sum_{l=1}^{l=6} \sum_{i=1}^{i=6} \sum_{j=1}^{j=6} \sum_{k=1}^{k=6} \omega_l^m \frac{\mathrm{d}x_b^m}{\mathrm{d}t} \left(u_{1i} u_{1j} + u_{2i} u_{2j} \right) y_k \int\int N_l N_i A_{jk} |\mathbf{J}|^{-1} \, \mathrm{d}x\mathrm{d}y \right) \\
&+ \sum_{\Delta_a} \left(\sum_{m=1}^{m=3} \sum_{l=1}^{l=6} \sum_{i=1}^{i=6} \sum_{j=1}^{j=6} \sum_{k=1}^{k=6} \omega_l^m \frac{\mathrm{d}y_b^m}{\mathrm{d}t} \left(u_{1i} u_{1j} + u_{2i} u_{2j} \right) x_k \int\int N_l N_i A_{jk} |\mathbf{J}|^{-1} \, \mathrm{d}x\mathrm{d}y \right) \\
&+ \sum_{\Delta_a} \left(\sum_{l=1}^{l=6} \sum_{i=1}^{i=6} \sum_{j=1}^{j=6} \frac{1}{2} \left(u_{1l} u_{1i} u_{2j} + u_{2l} u_{2i} u_{2j} \right) \int N_l N_i N_j \cos(\theta) \, \mathrm{d}s \right) \\
&- \sum_{\Delta_a} \left(\sum_{l=1}^{l=6} \sum_{i=1}^{i=6} \sum_{j=1}^{j=6} \frac{1}{2} \left(u_{1l} u_{1i} u_{1j} + u_{1l} u_{2i} u_{2j} \right) \int N_l N_i N_j \sin(\theta) \, \mathrm{d}s \right).
\end{aligned} \tag{3.7.37}$$

Here the double integration $\int\int \mathrm{d}x\mathrm{d}y$ is taken over each triangular element Δ_a. We then sum these over the entire domain.

The discretized form of dissipation energy D_f (3.5.42) can be written as

$$\begin{aligned} D_f = &\sum_{\Delta_a}\left(R^{-1}\sum_{l=1}^{l=6}\sum_{i=1}^{i=6}\sum_{j=1}^{j=6}\sum_{k=1}^{k=6}(2u_{1l}u_{1i}+u_{2l}u_{2i})\,y_j y_k\int\int A_{lk}A_{ij}|\mathbf{J}|^{-2}\,\mathrm{d}x\mathrm{d}y\right)\\ &+\sum_{\Delta_a}\left(R^{-1}\sum_{l=1}^{l=6}\sum_{i=1}^{i=6}\sum_{j=1}^{j=6}\sum_{k=1}^{k=6}(u_{1l}u_{1i}+2u_{2l}u_{2i})\,x_j x_k\int\int A_{lk}A_{ij}|\mathbf{J}|^{-2}\,\mathrm{d}x\mathrm{d}y\right)\\ &-\sum_{\Delta_a}\left(R^{-1}\sum_{l=1}^{l=6}\sum_{i=1}^{i=6}\sum_{j=1}^{j=6}\sum_{k=1}^{k=6}2u_{1l}u_{2i}y_j x_k\int\int A_{lk}A_{ij}|\mathbf{J}|^{-2}\,\mathrm{d}x\mathrm{d}y\right). \end{aligned} \tag{3.7.38}$$

The expansion of the net kinetic energy flux energy budget F_f (3.5.40) can be written as

$$F_f = \sum_{I_r}\left(\left[\sum_{l=1}^{l=6}\sum_{i=1}^{i=6}\sum_{j=1}^{j=6}\frac{1}{2}\left(u_{1l}u_{1i}u_{1j}+u_{1l}u_{2i}u_{2j}\right)\int N_l N_i N_j\,\mathrm{d}y\right]_{\text{inlet}}^{\text{outlet}}\right), \tag{3.7.39}$$

where the $\int \mathrm{d}y$ is the integration evaluated along each three-node element (I_r) on the inlet and outlet boundaries. The superscript 'outlet' and subscript 'inlet' represent the outlet and inlet boundary of the channel, respectively.

Similarly, the work done by pressure forces at the channel boundaries P_f (3.5.41) is

$$P_f = \sum_{I_r}\left(\left[\sum_{l=1}^{l=6}\sum_{i=1}^{i=3}-u_{1l}p_i\int N_l L_i\,\mathrm{d}y\right]_{\text{inlet}}^{\text{outlet}}\right). \tag{3.7.40}$$

The rate of working of bending stresses U_κ (3.5.44) takes the form

$$U_\kappa = \sum_{I_e}\left(\sum_{l=1}^{l=3}\sum_{i=1}^{i=3}\sum_{j=1}^{j=3}\sum_{k=1}^{k=3}c_\kappa\left(\lambda_l\kappa_i\frac{\delta\lambda_j}{\delta t}\kappa_k+\lambda_l\kappa_i\lambda_j\frac{\delta\kappa_k}{\delta t}\right)\int N_l N_i N_j N_k\,\mathrm{d}l\right), \tag{3.7.41}$$

where $\int \mathrm{d}l$ is the integration evaluated along each three-node element (I_e) on the elastic beam. We then sum these over the entire elastic beam.

The rate of working of extensional stresses U_λ (3.5.45) takes the form

$$U_\lambda = \sum_{I_e}\left(\sum_{l=1}^{l=3}(T-c_\lambda)\frac{\delta\lambda_l}{\delta t}\int N_l\,\mathrm{d}l+\sum_{l=1}^{l=3}\sum_{i=1}^{i=3}c_\lambda\lambda_l\frac{\delta\lambda_i}{\delta t}\int N_l N_i\,\mathrm{d}l\right). \tag{3.7.42}$$

By substituting the normal vector $\mathbf{e}_1 = (-\sin(\theta),\cos(\theta))^{\mathrm{T}}$ into P_e (3.5.46), the rate of working of external pressure P_e can be rearranged as

$$P_e = \int_0^{L_0} p_e\lambda\left[u_2\cos(\theta)-u_1\sin(\theta)\right]\mathrm{d}l, \tag{3.7.43}$$

which takes the form

$$P_e = \sum_{I_e} \left(\sum_{l=1}^{l=3} \sum_{i=1}^{i=6} \left[p_e \lambda_l u_{2i} \int N_l N_i \cos(\theta)\, \mathrm{d}l - p_e \lambda_l u_{1i} \int N_l N_i \sin(\theta)\, \mathrm{d}l \right] \right). \tag{3.7.44}$$

3.8 Numerical results

In this section, we demonstrate numerical results for steady and unsteady cases, as well as the numerical results of energy budgets for the fully-nonlinear system.
The dimensionless parameters are chosen to be $L_u = L_0 = 5$, $L_d = 30$, $T = 0$, $\rho_m = 0$, $p_e = 1.95$, $p_d = 0$ and $c_\kappa / c_\lambda = h^2/12D^2 \approx 10^{-5} (h/D = 0.01)$.

3.8.1 Mesh validation

We verified our code by comparing the pressure on the deformed wall in the static state for different meshes for parameters $R = 211.875, c_\lambda = 1600, p_e = 1.95$. Several meshes: Mesh-1, Mesh-2, Mesh-3 and Mesh-4 are compared, listed below (table 3.1).

Mesh	Number of beam element	Total number of elements
Mesh-1	60	6152
Mesh-2	80	12157
Mesh-3	100	18977
Mesh-4	120	22597

Table 3.1: List of meshes

The mid-point pressure on the static deformed beam from the meshes Mesh-1, Mesh-2 and Mesh-3 is compared to Mesh-4, listed in table 3.2 below.

Mesh	p_{mid}	percentage
Mesh-1	1.66434	0.8%
Mesh-2	1.66844	0.6%
Mesh-3	1.66944	0.5%
Mesh-4	1.67853	

Table 3.2: Mid-point pressure p_{mid} of different meshes.

We compared the pressure distribution along the deformed beam and the corresponding beam shape at the static state for Reynolds number $R = 211.875$, extensional stiffness $c_\lambda = 1600$ and external pressure $p_e = 1.95$ using two different meshes: Mesh-2 and Mesh-4, shown in figure 3.6. The pressure distribution and steady beam shape tested are graphically identical. In this chapter, we use the Mesh-2 of 12157 elements for fully nonlinear system and later eigenvalue simulations in Chapter 4.

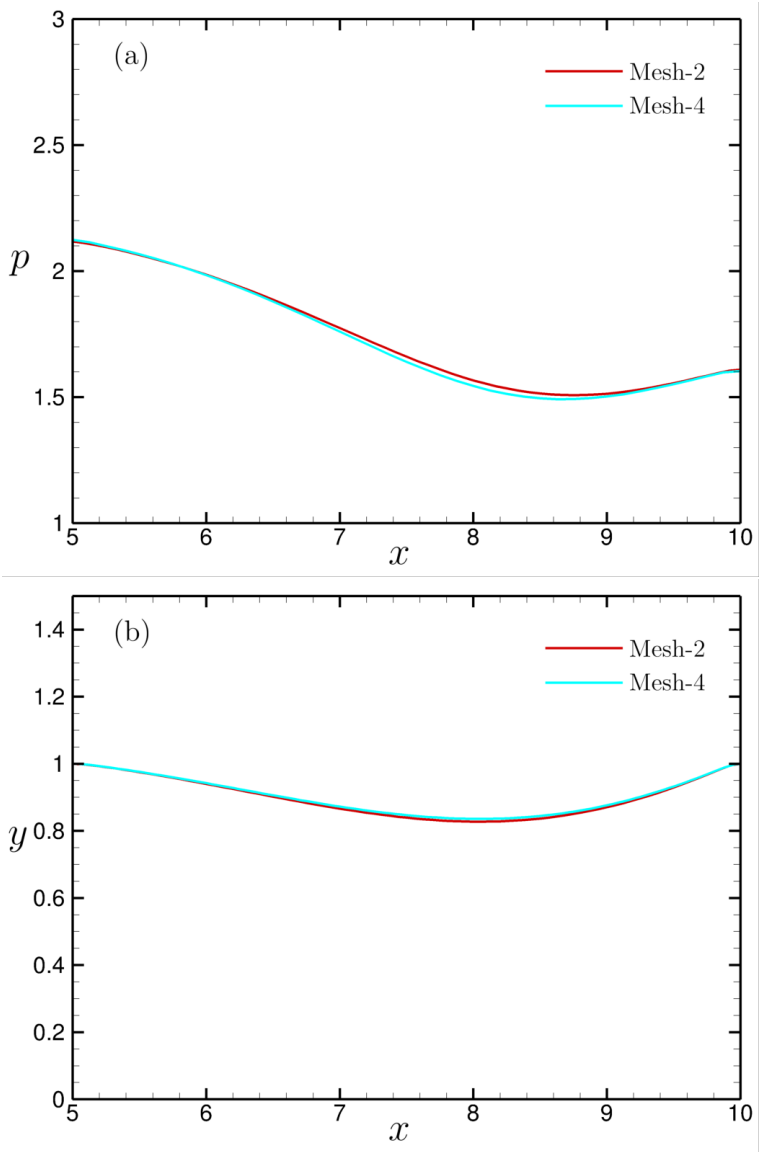

Figure 3.6: Comparison of (a) pressure distribution on static deformed beam; (b) static beam shape for different meshes when $R = 211.875, c_\lambda = 1600, p_e = 1.95$.

3.8.2 Numerical results for steady case

We demonstrate three beam-shapes that can occur in collapsible tube when conveying fluid (shown in figure 3.7), *i.e.* totally bulged out (the blue line in figure 3.7), bulged out near the

upstream of the elastic beam and collapsed near the downstream of elastic beam (the red line in figure 3.7), and entirely collapsed beam-shapes (the cyan line in figure 3.7).

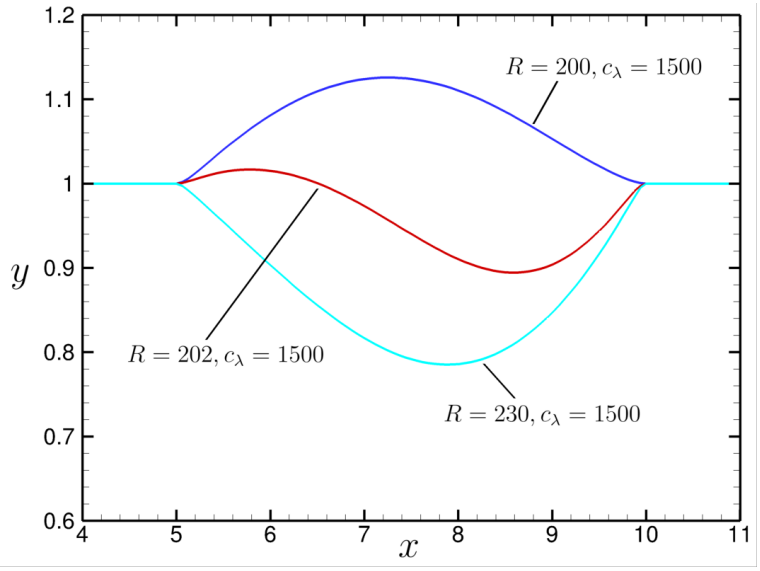

Figure 3.7: The three possible steady beam-shapes for different Reynolds number, $c_\lambda = 1500, p_e = 1.95$.

The steady beam-shapes are computed for different Reynolds number with fixed extensional stiffness $c_\lambda = 1600$ and external pressure $p_e = 1.95$, shown in figure 3.8. As the Reynolds number increases, the wall deformation increases (*i.e.* the channel becomes more constricted) and the location of maximum wall deformation moves towards the central of the collapsible segment. The observation is consistent with the one-dimensional models of Xu *et al*. [76] and Stewart [65], as well as two-dimensional model of Luo *et al*. [48]. The beam is sucked towards the opposite rigid wall through the Bernoulli effect. We hypothesize that the wall deformation would be entirely symmetric in the inviscid limit ($R \to \infty$), which is again consistent with Xu *et al*. [76] and Stewart [65].

The corresponding minimal channel width y_{min} is plotted against Reynolds number is given in figure 3.9 with fixed external pressure $p_e = 1.95$, for three different extensional stiffness $c_\lambda = 1600, 1800$ and $c_\lambda = 2100$, respectively. As Reynolds number increases, y_{min} decreases rapidly first and then gradually approaches a limit value.

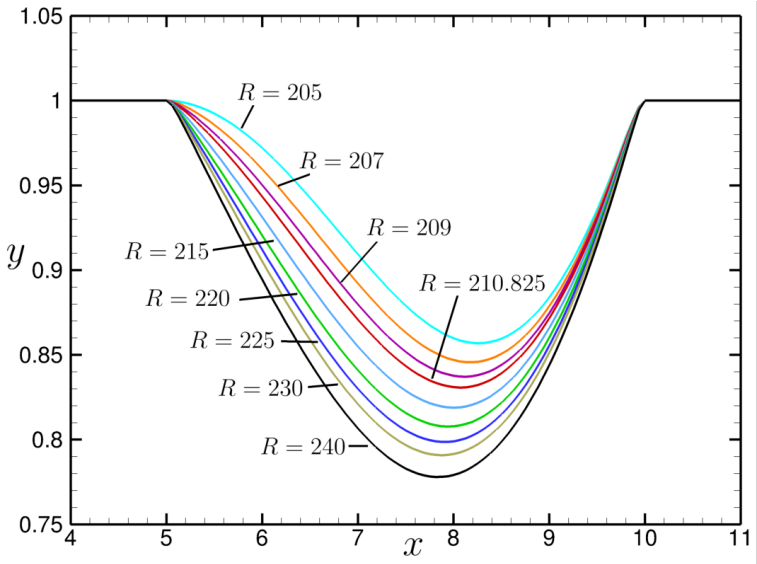

Figure 3.8: The static beam shape for different Reynolds number, $c_\lambda = 1600, p_e = 1.95$.

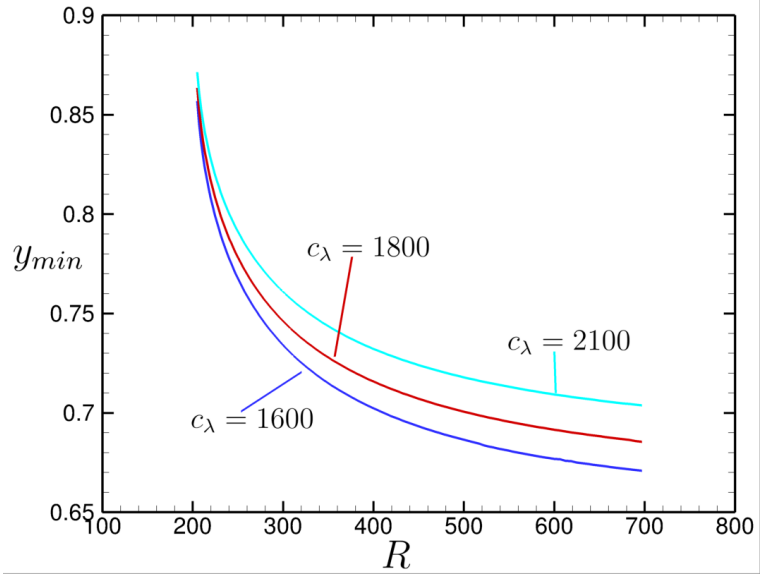

Figure 3.9: The minimal channel width for different Reynolds number with $p_e = 1.95$ and $c_\lambda = 1600, 1800, 2100$.

3.8.3 Numerical results for unsteady case

In order to test the stability of the system, we apply a small perturbation to the steady solution (here we use a slightly different steady solution as the initial guess for the system). We say the system is stable if the solution converges to the corresponding steady solution following perturbation, while the system is unstable if the solution grows oscillates with time. The neutrally stable point is the critical point at which the system becomes unstable.

Figure 3.10 demonstrates the mid-point pressure p_{mid} and minimal channel width y_{min} of a stable

case after we apply small perturbations to the steady solution (here Reynolds number $R = 207$, extensional stiffness $c_\lambda = 1600$ and external pressure $p_e = 1.95$), *i.e.* both p_{mid} and y_{min} tend to its corresponding steady solution as time increases.

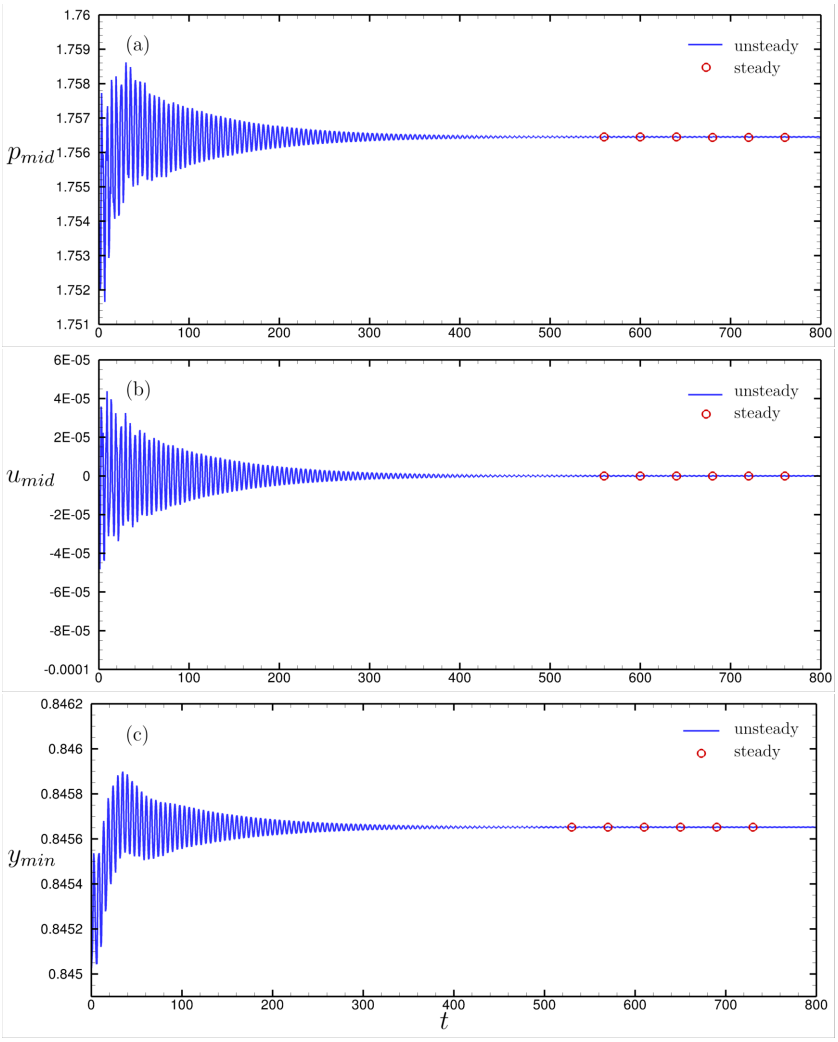

Figure 3.10: (a) The time evolution of mid-point pressure of stable case;(b) The time evolution of mid-point velocity of stable case; (c) The time evolution of minimal channel width of stable case for Reynolds number $R = 207$, $c_\lambda = 1600, p_e = 1.95$.

Figure 3.11 shows the mid-point pressurep_{mid} and minimal channel width y_{min} of an unstable case with Reynolds number $R = 214$, extensional stiffness $c_\lambda = 1600$ and external pressure $p_e = 1.95$. Both p_{mid} and y_{min} grow in an oscillatory manner and eventually stalemate to a fixed amplitude limit cycle.

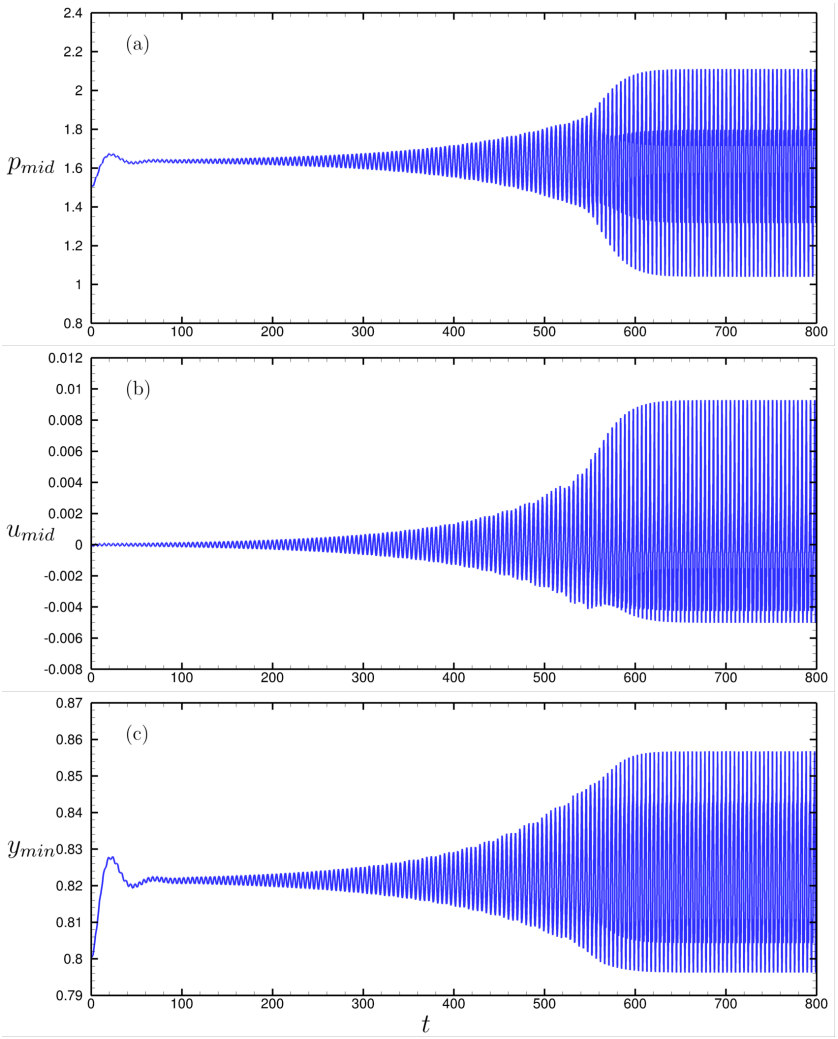

Figure 3.11: (a) The time evolution of mid-point pressure of unstable case;(b) The time evolution of mid-point velocity of unstable case; (c) The time evolution of minimal channel width of unstable case for Reynolds number $R = 214$, $c_\lambda = 1600, p_e = 1.95$.

We plot the maximal and minimal y_{min} over a period of the fully developed oscillation against Reynolds number for fixed $c_\lambda = 1600$, $p_e = 1.95$ (shown in figure 3.12). The system is unstable when R is greater than the critical point $R_c = 210.825$, *i.e.* the neutrally stable point. We compute the average y_{min} over one period of oscillation, denoted as triangle in figure 3.12, and find that the average y_{min} is slightly greater than the y_{min} at the static state, however, the differences between the average y_{min} and static y_{min} are very small and stay nearly the same as Reynolds number increases. This behavior is consistent with that observed by Stewart [65], where he noted that the bifurcation for fully developed oscillations is supercritical , and that the mean channel width is increased over an oscillation.

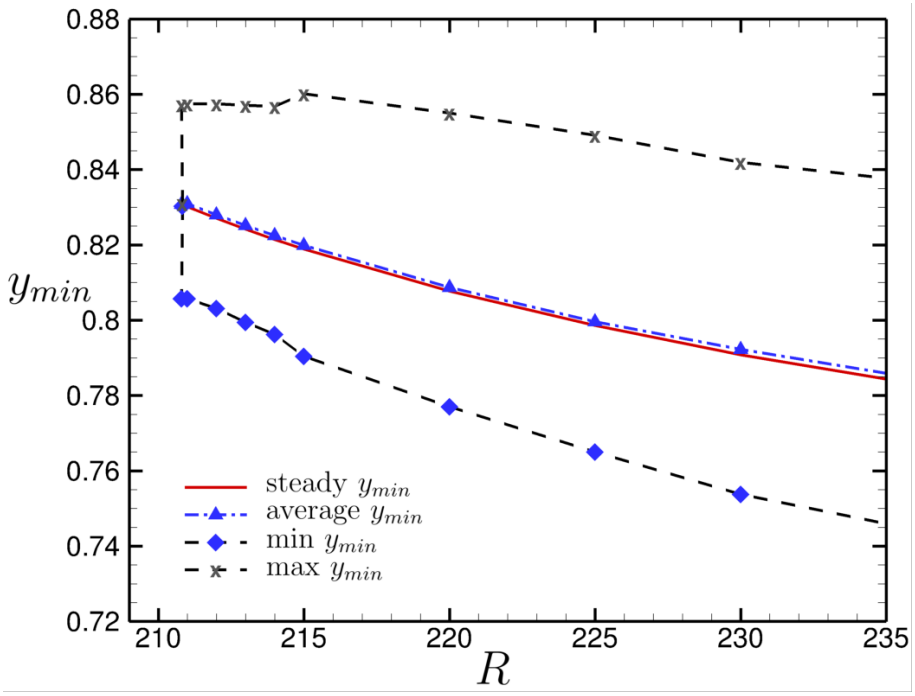

Figure 3.12: The minimal channel width against Reynolds number for $c_\lambda = 1600$, $p_e = 1.95$. Red solid line represents the minimal channel width for steady case; Cross line represents the maximal channel width over one period of oscillation for unsteady case; Diamond line represents the minimal channel width over one period of oscillation for unsteady case; Triangle line represents the average channel width over one period of oscillation for unsteady case.

We demonstrate the streamlines at seven different time instant (as labeled $1-7$ in figure 3.14), as shown in figure 3.13. The generation of vorticity wave downstream has been observed, which is similar to the observations of Luo *et al*. [48].

The time evolution of mid-point velocity, pressure and minimal channel width are illustrated in figure 3.14 in fully developed oscillation at $R = 220$, $c_\lambda = 1600$ and $p_e = 1.95$.

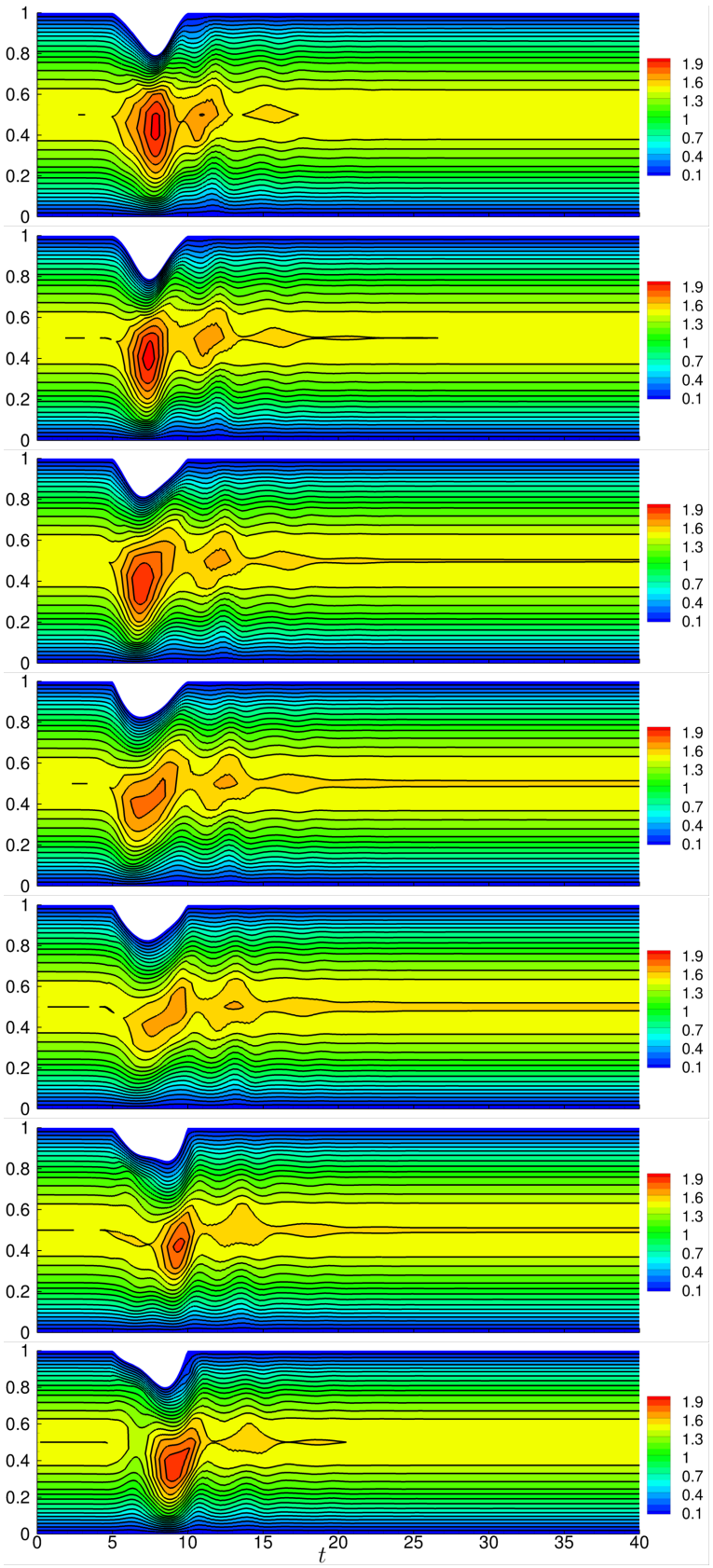

Figure 3.13: The streamlines at seven different times as labeled in figure 3.14 for $R = 220$, $c_\lambda = 1600$ and $p_e = 1.95$.

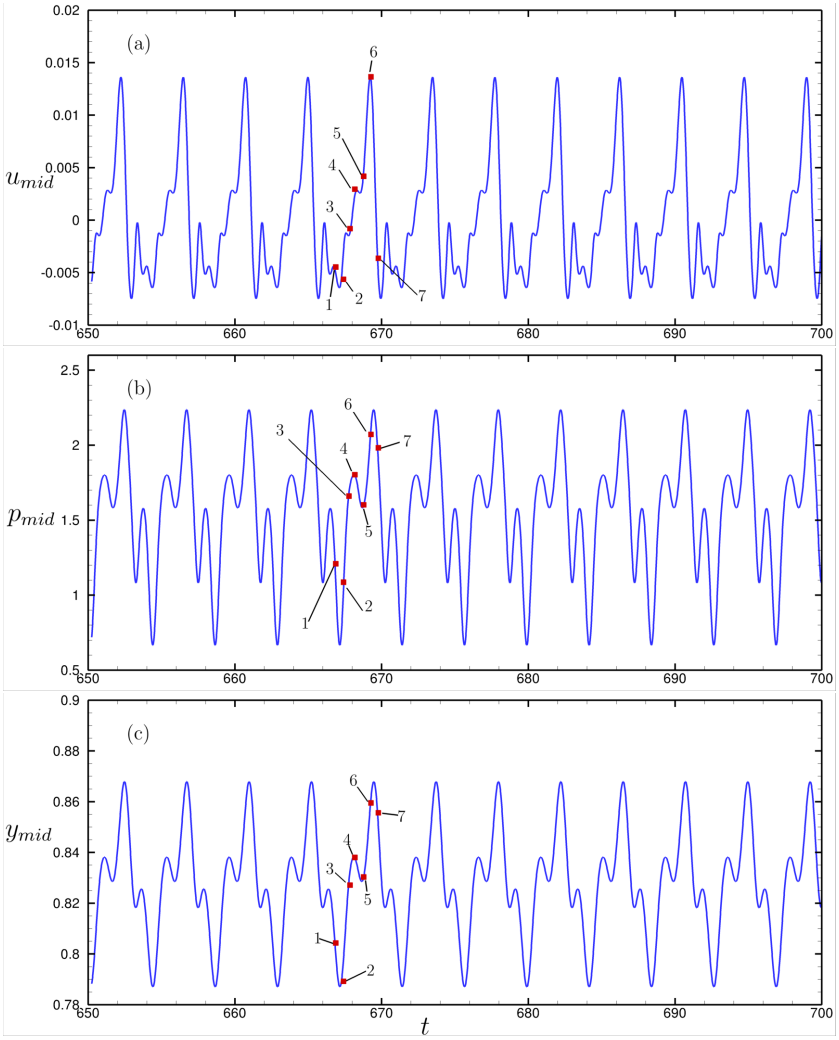

Figure 3.14: (a) The time evolution of mid-point velocity; (b) The time evolution of mid-point pressure; (c) The time evolution of mid-point position for $R = 220$, $c_\lambda = 1600$ and $p_e = 1.95$.

3.8.4 Energy budget of fully nonlinear system

Using the numerical solutions of the fully nonlinear system, we are able to numerically calculate the energy budget of the system. Considering the energy budget of the unsteady system over one fully developed period of oscillation, the average fluid and beam kinetic energy $K_f^{(avg)}$, $K_b^{(avg)}$ and the average of the rate of working of bending and extensional stiffness $U_\kappa^{(avg)}$, $U_\lambda^{(avg)}$, as well as the average of the rate of working of external pressure $P_e^{(avg)}$ should all vanish. Therefore, the energy budget of the system (3.5.38) over one period of oscillation becomes,

$$F_f^{(avg)} - P_f^{(avg)} + D_f^{(avg)} = 0, \tag{3.8.1}$$

where $F_f^{(avg)}$ is the average of the net kinetic energy flux over a period, $P_f^{(avg)}$ denotes the average of the rate of working of pressure force over a period and $D_f^{(avg)}$ denotes the average of the

energy loss due to viscosity over a period.

We calculate the corresponding average energy budget of the unsteady system for several Reynolds numbers with fixed $c_\lambda = 1600$, $p_e = 1.95$, listed in table 3.3, which also gives the steady energy budget $F_f^{(s)}$, $P_f^{(s)}$ and $D_f^{(s)}$ discussed in *Sec*.3.6. The main energy balance is between the rate of working of pressure forces and the viscous dissipation for both the unsteady and steady systems. We also compute the average of the rate of working of fluid stress on the beam $E_f^{(avg)}$, which are all positive (relatively small compared with $P_f^{(avg)}$ and $D_f^{(avg)}$) and increase as Reynolds number increases.

R	$F_f^{(avg)}$	$P_f^{(avg)}$	$D_f^{(avg)}$	$E_f^{(avg)}$	$F_f^{(s)}$	$P_f^{(s)}$	$D_f^{(s)}$
210.825	6.9787E-05	2.4117	2.4114	8.4470E-05	1.5587E-06	2.4042	2.4043
215	9.6508E-05	2.3882	2.3875	2.6678E-04	2.1192E-06	2.3740	2.3741
220	1.5461E-04	2.3573	2.3559	8.7346E-04	2.9367E-06	2.3359	2.3360
225	2.4680E-04	2.3269	2.3252	1.6758E-03	3.9507E-06	2.2972	2.2973
230	3.3566E-04	2.2990	2.2991	4.0555E-03	5.1993E-06	2.2588	2.2589
240	4.5760E-04	2.2413	2.2436	1.7601E-02	8.5615E-06	2.1841	2.1842

Table 3.3: Fully nonlinear energy budget for fluid-beam system, here extensional stiffness $c_\lambda = 1600$, external pressure $p_e = 1.95$.

We then consider the excess energy between the average energy budget over one period of oscillation and its corresponding steady energy budget discussed in *Sec*.3.6,

$$F_e^{(avg)} = F_f^{(avg)} - F_f^{(s)},\ P_e^{(avg)} = P_f^{(avg)} - P_f^{(s)},\ D_e^{(avg)} = D_f^{(avg)} - D_f^{(s)}. \tag{3.8.2}$$

Table 3.4 shows the average excess energy for fixed $c_\lambda = 1600$, $p_e = 1.95$. For $R > R_c$, the system is unstable. The absolute value of excess energy increases as Reynolds number increases. Also we found that $D_e^{(avg)} > 0$ for $R > R_c$, which means the presence of oscillation increases the overall dissipative energy in the system. This is contradictory to the observations of Stewart [65] who found that the oscillation reduced the overall dissipation energy in the system. We do not fully understand the mechanism of this phenomena yet.

R	$F_e^{(avg)}$	$P_e^{(avg)}$	$D_e^{(avg)}$
210.825	6.8228E-05	7.4571E-03	7.0841E-03
215	9.4389E-05	1.4183E-02	1.3449E-02
220	1.5168E-04	2.1440E-02	1.9949E-02
225	2.4285E-04	2.9686E-02	2.7843E-02
230	3.3046E-04	4.0179E-02	4.0213E-02
240	4.4904E-04	5.7162E-02	5.9429E-02

Table 3.4: Excess energy budget for fluid-beam system, here extensional stiffness $c_\lambda = 1600$, external pressure $p_e = 1.95$.

3.9 Discussion

In this chapter we considered flow through a finite length flexible-walled channel and obtained the fully nonlinear governing equations of the fluid and solid by establishing conservation of mass and momentum. In this calculation we employed a new Kirchhoff law for the elastic beam, which distinguishes our model from that of Luo *et al*. 2008. Our new contribution is to obtain the energy budget of the fully non-linear system. Special notice should be paid to the work done by viscous forces, which has been divided into two parts. One part contributes to the rate of working of fluid stresses on the wall (denoted E_f), that is the energy exchange between the fluid and beam which can be either positive or negative. The remainder goes into the viscous dissipation in the bulk fluid which is always positive (*i.e*. viscous effects in the fluid always consume energy). Combining the fluid energy budget with the beam energy budget, we obtained the energy budget for the fully nonlinear coupled fluid-beam system (3.5.38).

We established a numerical method to solve the fully nonlinear system, using an adaptive mesh for the elastic section since the beam is deformable. In particular, we applied an ALE method for this section. A finite element method with six node triangular element was used to discretize the system governing equations and the Newton-Raphson iteration method was applied to solve for the residual vector; at each iteration step a frontal method was used to solve for the global vector of unknowns.

Finally, numerical results were presented in *Sec*.3.8. Several steady beam shapes were computed with different Reynolds numbers (figure 3.8). The constriction of the stable channel increases when increasing the Reynolds number (figure 3.9), consistent with some of the previous results including one-dimensional models (Xu *et al*. [76], Stewart [65]) and two-dimensional models (Luo *et al*. [48]).

Two possible unsteady states were demonstrated. The stable solution converge to this corresponding steady solution after small stimulation (figure 3.10). For the unstable solution, a small perturbation will grow and the amplitude will eventually saturate to a limit cycle (figure 3.11). The bifurcation plot of the time-averaged minimal channel width against Reynolds number of this model (figure 3.12) behaves slightly differently to that of Stewart [65], in that it is not clearly a supercritical bifurcation. The streamlines at seven different time instants were given (figure 3.13), demonstrating the generation of vorticity waves in the downstream rigid section which is also observed in Luo *et al*. [48]. We then calculated the average energy budget of the fully nonlinear system over one oscillation. The viscous dissipation is always positive as we expected. However, the time-averaged dissipation energy of the fully saturated oscillation (*i.e*. the average dissipation energy budget minus the corresponding steady dissipation energy budget) is positive, which is consistent with the observation of Liu *et al*. [46]. This means the driving pressure must work harder during the oscillation compared to the static state (the converse was found by Stewart [65], who shared that oscillations required less work overall in his system). However, the mechanism of the this phenomena, that the average amount of dissipation energy in the unstable state is greater than its stable state, remains unclear to us and is an on-going topic of investigation.

Chapter 4

Linear stability eigensolver for the fluid-beam model

In this chapter, we revisit the model for flow in a collapsible channel of chapter 3. Whereas in this case we form a fully linearised model by perturbing around the steady state identified in *Sec*. 3.4 (*Sec*. 4.1) to introduce the perturbed governing equations (*Sec*. 4.2) and the associated eigen-solver problem (*Sec*. 4.3). We then derive the corresponding linearised energy budget for the system (*Sec*. 4.4). The numerical method and results are in *Sec*. 4.5 and *Sec*. 4.6, respectively.

4.1 Linearised variables

The excess energies constructed in *Sec*. 3.6 are a useful way to quantify the energies of self-excited oscillations. However, the quantities F_e, P_e and D_e are often very small compared to their steady components and so it can be difficult to evaluate these when they are combined with the effects of error in the numerical computations. An alternative method is to construct the excess energies of the system directly using a linear stability eigensolver. Such an eigensolver was presented in this context by Luo *et al*. [48], which we now extend to also consider the perturbation energy budget.

We use the same model as presented in *Sec*. 3.3 and identical notation. All variables are assumed already dimensionless unless stated otherwise.

We add a small perturbation to the steady mean flow and the steady beam with constant amplitude $\varepsilon \ll 1$. For the fluid variables, we express this perturbation in the form,

$$\begin{aligned}&\Big(\mathbf{u}(x,y,t), p(x,y,t), \boldsymbol{\sigma}(x,y,t)\Big)\\ =&\Big(\mathbf{U}(x,y), P(x,y), \boldsymbol{\Sigma}(x,y)\Big) + \varepsilon\Big(\hat{\mathbf{u}}(x,y,t), \hat{p}(x,y,t), \hat{\boldsymbol{\sigma}}(x,y,t)\Big)\end{aligned}$$

$$+\varepsilon^2\Big(\breve{\mathbf{u}}(x,y,t),\breve{p}(x,y,t),\breve{\boldsymbol{\sigma}}(x,y,t)\Big)+O(\varepsilon^3),\qquad(\mathbf{x}\in\bar{\Omega}),\qquad(4.1.1)$$

where $\hat{\mathbf{u}}=\hat{u}_1\mathbf{g}_1+\hat{u}_2\mathbf{g}_2$, and $\breve{\mathbf{u}}=\breve{u}_1\mathbf{g}_1+\breve{u}_2\mathbf{g}_2$ represent first and second order perturbations to the steady state. In what follows, the perturbation fluid problem must be constructed on the domain of the steady configuration. Hence, all boundary conditions on the fluid-beam interface must be projected back to this static configuration (as considered in related problems with free surface such as Kelvin Helmholtz instability (Drazin & Crepeau [24]) or in the wave motion of flagellar sheets (Taylor [70])).

To expand the beam variables we begin in the reference (material) description. This is necessary as all time derivatives are taken holding l fixed, in the form

$$\begin{aligned}&\Big(\mathbf{x}_b(l,t),\boldsymbol{\lambda}(l,t),\boldsymbol{\kappa}(l,t),\theta(l,t),\mathbf{u}_b(l,t)\Big)\\=&\Big(\mathbf{X}_b(l),\Lambda(l),K(l),\Theta(l),\mathbf{0}\Big)+\varepsilon\Big(\hat{\mathbf{x}}_b(l,t),\hat{\boldsymbol{\lambda}}(l,t),\hat{\boldsymbol{\kappa}}(l,t),\hat{\theta}(l,t),\hat{\mathbf{u}}_b(l,t)\Big)\\&+\varepsilon^2\Big(\breve{\mathbf{x}}_b(l,t),\breve{\boldsymbol{\lambda}}(l,t),\breve{\boldsymbol{\kappa}}(l,t),\breve{\theta}(l,t),\breve{\mathbf{u}}_b(l,t)\Big)+O(\varepsilon^3),\qquad(0\le l\le L_0),\end{aligned}\qquad(4.1.2)$$

where the steady variables, first order variables and second order variables of the system are denoted with capital letters, hatted terms and breved terms respectively.

We expand the beam variables in current (spatial) description for the use in deriving the linearised energy budget for the system in a later section. However, the linearised beam-related energy budget must eventually be expressed using the reference (material) description, as the time derivatives are taken holding l fixed. As previously stated, the perturbed beam equations are projected onto the steady beam shape. We parametrize the current (spatial) description of the steady beam using the arc length coordinate S, where

$$S=\int_0^l\Lambda(l')\,\mathrm{d}l',\quad S_0=\int_0^{L_0}\Lambda(l')\,\mathrm{d}l'.\qquad(4.1.3)$$

Hence, we can express each of the perturbed beam variables using the current (spatial) coordinate in the form,

$$\begin{aligned}&\Big(\mathbf{x}_b^{(c)}(s,t),\boldsymbol{\lambda}^{(c)}(s,t),\boldsymbol{\kappa}^{(c)}(s,t),\theta^{(c)}(s,t),\mathbf{u}_b^{(c)}(s,t)\Big),\\=&\Big(\mathbf{X}_b^{(c)}(S),\Lambda^{(c)}(S),K^{(c)}(S),\Theta^{(c)}(S),\mathbf{0}\Big)\\&+\varepsilon\Big(\hat{\mathbf{x}}_b^{(c)}(S,t),\hat{\boldsymbol{\lambda}}^{(c)}(S,t),\hat{\boldsymbol{\kappa}}^{(c)}(S,t),\hat{\theta}^{(c)}(S,t),\hat{\mathbf{u}}_b^{(c)}(S,t)\Big)\\&+\varepsilon^2\Big(\breve{\mathbf{x}}_b^{(c)}(S,t),\breve{\boldsymbol{\lambda}}^{(c)}(S,t),\breve{\boldsymbol{\kappa}}^{(c)}(S,t),\breve{\theta}^{(c)}(S,t),\breve{\mathbf{u}}_b^{(c)}(S,t)\Big)+O(\varepsilon^3),\ (S\in\partial\bar{\Omega}_b),\end{aligned}\qquad(4.1.4)$$

where capital letters represent beam variables in the steady state, while the hatted and breved terms denote the first order and second order beam variables, respectively.

We denote the first and second order beam velocity as $\hat{\mathbf{u}}_b^{(c)}=\hat{u}_{b1}^{(c)}\mathbf{T}+\hat{u}_{b2}^{(c)}\mathbf{N}$ and $\breve{\mathbf{u}}_b^{(c)}=\breve{u}_{b1}^{(c)}\mathbf{T}+$

$\breve{u}_{b2}^{(c)}\mathbf{N}$, respectively. The linearised beam variables in current (spatial) description (denoted with superscript (c)) at each order are the push-forward variables of the corresponding linearised beam variables in reference (material) description (Holzapfel [34]), *i.e.* $F(S)^{(c)}$, $\hat{f}(S,t)^{(c)}$ and $\breve{f}(S,t)^{(c)}$ are the push-forward variables of $F(l)$, $\hat{f}(l,t)$ and $\breve{f}(l,t)$, respectively. It follows that identities $F(S(l))^{(c)} = F(l)$, $\hat{f}(S(l),t)^{(c)} = \hat{f}(l,t)$, $\breve{f}(S(l),t)^{(c)} = \breve{f}(l,t)$ hold true.

4.2 Linearised governing equations

In this section we discuss the perturbed governing equations. In perturbing the beam equation we must formally perturb the vector form since the unit vectors to the beam $\mathbf{e}_1$ and $\mathbf{e}_2$ will be perturbed too. The total beam momentum equation can be written in the form

$$\mathbf{M} = M_1\mathbf{e}_1 + M_2\mathbf{e}_2 = \mathbf{0}, \tag{4.2.1}$$

where M_1 and M_2 represent the components of the beam equations (3.3.26) and (3.3.27), respectively. Expanding, at $O(1)$ we obtain,

$$\overline{M}_1\bar{\mathbf{e}}_1 + \overline{M}_2\bar{\mathbf{e}}_2 = \overline{M}_1\mathbf{T} + \overline{M}_2\mathbf{N} = \mathbf{0}, \tag{4.2.2}$$

where the over-line represents static quantities. The tangent and normal vectors to the static beam $\bar{\mathbf{e}}_1$ and $\bar{\mathbf{e}}_2$ will be denoted as $\mathbf{T}$ and $\mathbf{N}$ in later sections. At $O(\varepsilon)$ we have,

$$\hat{M}_1\bar{\mathbf{e}}_1 + \hat{M}_2\bar{\mathbf{e}}_2 + \overline{M}_1\hat{\mathbf{e}}_1 + \overline{M}_2\hat{\mathbf{e}}_2 = \hat{M}_1\bar{\mathbf{e}}_1 + \hat{M}_2\bar{\mathbf{e}}_2 = \hat{M}_1\mathbf{T} + \hat{M}_2\mathbf{N} = \mathbf{0}, \tag{4.2.3}$$

as $\overline{M}_1$ and $\overline{M}_2$ are identically zero. Here the hatted quantities represent quantities at the first order. Hence, the first order expanded beam equations are simply the normal and tangential components of the beam equations expanded to first order, evaluated with the unit vectors for the static configuration at that point. A similar idea occurs at the second order, where the expanded beam equations are the components of the beam equations expanded to second order evaluated with the unit vectors for the static configuration at that point, since $\overline{M}_1$, $\overline{M}_2$, $\hat{M}_1$ and $\hat{M}_2$ are identically zero, *i.e.*

$$\breve{M}_1\bar{\mathbf{e}}_1 + \breve{M}_2\bar{\mathbf{e}}_2 + \hat{M}_1\hat{\mathbf{e}}_1 + \hat{M}_2\hat{\mathbf{e}}_2 + \overline{M}_1\breve{\mathbf{e}}_1 + \overline{M}_2\breve{\mathbf{e}}_2 = \breve{M}_1\bar{\mathbf{e}}_1 + \breve{M}_2\bar{\mathbf{e}}_2 = \breve{M}_1\mathbf{T} + \breve{M}_2\mathbf{N} = 0. \tag{4.2.4}$$

Here the breved terms denote the quantities at the second order.
Therefore, we can simply perturb the scalar form of the tangential and normal components of the beam equations to obtain the linearised equations for the system. These equations are used to obtain system's eigenvalue problem and perturbed energy in later sections.

Substituting (4.1.1) into equations (3.3.17-3.3.29), at $O(1)$ we obtain,

$$\frac{\partial U_1}{\partial x}+\frac{\partial U_2}{\partial y}=0, \qquad (\mathbf{x}\in\bar{\Omega}), \tag{4.2.5}$$

$$U_1\frac{\partial U_1}{\partial x}+U_2\frac{\partial U_1}{\partial y}=-\frac{\partial P}{\partial x}+R^{-1}\left(\frac{\partial^2 U_1}{\partial x^2}+\frac{\partial^2 U_1}{\partial y^2}\right), \qquad (\mathbf{x}\in\bar{\Omega}), \tag{4.2.6}$$

$$U_1\frac{\partial U_2}{\partial x}+U_2\frac{\partial U_2}{\partial y}=-\frac{\partial P}{\partial y}+R^{-1}\left(\frac{\partial^2 U_2}{\partial x^2}+\frac{\partial^2 U_2}{\partial y^2}\right), \qquad (\mathbf{x}\in\bar{\Omega}), \tag{4.2.7}$$

$$\mathbf{U}=\mathbf{0}, \qquad (y=0;\ \ y=1,-L_u<x<0,\ L_0<x<L_0+L_d), \tag{4.2.8}$$

$$\mathbf{U}=\mathbf{0}, \qquad (\mathbf{x}\in\partial\bar{\Omega}_b), \tag{4.2.9}$$

$$\frac{\partial X_b}{\partial l}=\Lambda\cos(\Theta), \qquad (0\le l\le L_0), \tag{4.2.10}$$

$$\frac{\partial Y_b}{\partial l}=\Lambda\sin(\Theta), \qquad (0\le l\le L_0), \tag{4.2.11}$$

$$\frac{\partial \Theta}{\partial l}=\Lambda K, \qquad (0\le l\le L_0), \tag{4.2.12}$$

$$c_\kappa K\frac{\partial(\Lambda K)}{\partial l}+c_\lambda\frac{\partial\Lambda}{\partial l}+\Lambda(\mathbf{\Sigma N})\cdot\mathbf{T}=0, \qquad (0\le l\le L_0), \tag{4.2.13}$$

$$-c_\kappa\frac{\partial}{\partial l}\left(\frac{1}{\Lambda}\frac{\partial(\Lambda K)}{\partial l}\right)+c_\lambda\Lambda K(\Lambda-1)+\Lambda KT+\Lambda(\mathbf{\Sigma N})\cdot\mathbf{N}-\Lambda p_e=0, \qquad (0\le l\le L_0), \tag{4.2.14}$$

$$\frac{\partial\Theta}{\partial t}=0, \qquad (l=0,L_0). \tag{4.2.15}$$

These are simply the steady governing equations for the system discussed previously in *Sec*. 3.4. At $O(\varepsilon)$, the governing equations for the system (3.3.17-3.3.29) become,

$$\frac{\partial\hat{u}_1}{\partial x}+\frac{\partial\hat{u}_2}{\partial y}=0, \qquad (\mathbf{x}\in\bar{\Omega}), \tag{4.2.16}$$

$$\frac{\partial\hat{u}_1}{\partial t}+U_1\frac{\partial\hat{u}_1}{\partial x}+U_2\frac{\partial\hat{u}_1}{\partial y}+\hat{u}_1\frac{\partial U_1}{\partial x}+\hat{u}_2\frac{\partial U_1}{\partial y}=-\frac{\partial\hat{p}}{\partial x}+R^{-1}\left(\frac{\partial^2\hat{u}_1}{\partial x^2}+\frac{\partial^2\hat{u}_1}{\partial y^2}\right), \qquad (\mathbf{x}\in\bar{\Omega}), \tag{4.2.17}$$

$$\frac{\partial\hat{u}_2}{\partial t}+U_1\frac{\partial\hat{u}_2}{\partial x}+U_2\frac{\partial\hat{u}_2}{\partial y}+\hat{u}_1\frac{\partial U_2}{\partial x}+\hat{u}_2\frac{\partial U_2}{\partial y}=-\frac{\partial\hat{p}}{\partial y}+R^{-1}\left(\frac{\partial^2\hat{u}_2}{\partial x^2}+\frac{\partial^2\hat{u}_2}{\partial y^2}\right), \qquad (\mathbf{x}\in\bar{\Omega}), \tag{4.2.18}$$

$$\hat{\mathbf{u}}=\mathbf{0}, \qquad (y=0;\ \ y=1,-L_u<x<0,\ L_0<x<L_0+L_d), \tag{4.2.19}$$

$$\left[\hat{\mathbf{u}}+\left(\hat{x}_b^{(c)}\frac{\partial\mathbf{U}}{\partial x}+\hat{y}_b^{(c)}\frac{\partial\mathbf{U}}{\partial y}\right)\right]=\hat{\mathbf{u}}_b^{(c)}, \qquad (\mathbf{x}\in\partial\bar{\Omega}_b), \tag{4.2.20}$$

$$\frac{\partial\hat{x}_b}{\partial l}=-\Lambda\hat{\theta}\sin(\Theta)+\hat{\lambda}\cos(\Theta), \qquad (0\le l\le L_0), \tag{4.2.21}$$

$$\frac{\partial\hat{y}_b}{\partial l}=\Lambda\hat{\theta}\cos(\Theta)+\hat{\lambda}\sin(\Theta), \qquad (0\le l\le L_0), \tag{4.2.22}$$

$$\frac{\partial \hat{\theta}}{\partial l} = \Lambda\hat{\kappa} + \hat{\lambda}K, \qquad (0 \le l \le L_0), \quad (4.2.23)$$

$$\frac{\rho_m}{\Lambda}\left(\frac{\partial X_b}{\partial l}\frac{\partial^2 \hat{x}_b}{\partial t^2} + \frac{\partial Y_b}{\partial l}\frac{\partial^2 \hat{y}_b}{\partial t^2}\right) = c_\kappa\left(K\frac{\partial(\Lambda\hat{\kappa}+\hat{\lambda}K)}{\partial l} + \hat{\kappa}\frac{\partial(\Lambda K)}{\partial l}\right) + c_\lambda\frac{\partial\hat{\lambda}}{\partial l}$$
$$+\left[\left(\hat{\boldsymbol{\sigma}} + \hat{x}_b\frac{\partial\boldsymbol{\Sigma}}{\partial x} + \hat{y}_b\frac{\partial\boldsymbol{\Sigma}}{\partial y}\right)\mathbf{N}\right]\cdot\mathbf{T}, \qquad (0 \le l \le L_0), \quad (4.2.24)$$

$$\frac{\rho_m}{\Lambda}\left(\frac{\partial X_b}{\partial S}\frac{\partial^2 \hat{y}_b}{\partial t^2} - \frac{\partial Y_b}{\partial S}\frac{\partial^2 \hat{x}_b}{\partial t^2}\right) = -c_\kappa\frac{\partial}{\partial l}\left[\frac{1}{\Lambda}\left(K\frac{\partial\hat{\lambda}}{\partial l} + \hat{\kappa}\frac{\partial\Lambda}{\partial l}\right) - \frac{\hat{\lambda}}{\Lambda^2}K\frac{\partial\Lambda}{\partial l} + \frac{\partial\hat{\kappa}}{\partial l}\right]$$
$$+c_\lambda\left[\Lambda K\hat{\lambda} + (\Lambda\hat{\kappa}+\hat{\lambda}K)(\Lambda-1)\right] + \left(\Lambda\hat{\kappa}+\hat{\lambda}K\right)T,$$
$$+\left[\left(\hat{\boldsymbol{\sigma}} + \hat{x}_b\frac{\partial\boldsymbol{\Sigma}}{\partial x} + \hat{y}_b\frac{\partial\boldsymbol{\Sigma}}{\partial y}\right)\mathbf{N}\right]\cdot\mathbf{N} - \hat{\lambda}p_e \qquad (0 \le l \le L_0), \quad (4.2.25)$$

$$\hat{\mathbf{u}}_b = \mathbf{0}, \qquad (l = 0, L_0), \quad (4.2.26)$$

$$\frac{\partial\hat{\theta}}{\partial t} = 0, \qquad (l = 0, L_0). \quad (4.2.27)$$

Special notice should be paid to equations (4.2.20), (4.2.24) and (4.2.25), where we need to use Taylor expansions about the steady configuration to account for the fact that perturbation eigenfunctions (hatted quantities) must be evaluated on the steady configuration. Taking the velocity boundary condition (3.3.20) on the elastic beam as an example, applying a Taylor expansions to the linearised fluid velocity on the steady beam in the form,

$$\begin{aligned}
\mathbf{u}\big|_{\left(x_b^{(c)},y_b^{(c)}\right)} &= \left[\mathbf{U}+\varepsilon\hat{\mathbf{u}}+\varepsilon^2\breve{\mathbf{u}}\right]_{\left(x_b^{(c)},y_b^{(c)}\right)},\\
&= \left[\mathbf{U} + \left(x_b^{(c)}-X_b^{(c)}\right)\frac{\partial\mathbf{U}}{\partial x} + \left(y_b^{(c)}-Y_b^{(c)}\right)\frac{\partial\mathbf{U}}{\partial y} + \frac{1}{2}\left(x_b^{(c)}-X_b^{(c)}\right)^2\frac{\partial^2\mathbf{U}}{\partial x^2}\right]_{\left(X_b^{(c)},Y_b^{(c)}\right)}\\
&\quad + \left[\frac{1}{2}\left(y_b^{(c)}-Y_b^{(c)}\right)^2\frac{\partial^2\mathbf{U}}{\partial y^2} + \frac{1}{2}\left(x_b^{(c)}-X_b^{(c)}\right)\left(y_b^{(c)}-Y_b^{(c)}\right)\frac{\partial^2\mathbf{U}}{\partial x\partial y}\right]_{\left(X_b^{(c)},Y_b^{(c)}\right)}\\
&\quad + \varepsilon\left[\hat{\mathbf{u}} + \left(x_b^{(c)}-X_b^{(c)}\right)\frac{\partial\hat{\mathbf{u}}}{\partial x} + \left(y_b^{(c)}-Y_b^{(c)}\right)\frac{\partial\hat{\mathbf{u}}}{\partial y}\right]_{\left(X_b^{(c)},Y_b^{(c)}\right)} + \varepsilon^2\breve{\mathbf{u}}\big|_{\left(X_b^{(c)},Y_b^{(c)}\right)},\\
&= \mathbf{U}\big|_{\left(X_b^{(c)},Y_b^{(c)}\right)} + \varepsilon\left(\hat{\mathbf{u}} + \hat{x}_b^{(c)}\frac{\partial\mathbf{U}}{\partial x} + \hat{y}_b^{(c)}\frac{\partial\mathbf{U}}{\partial y}\right)_{\left(X_b^{(c)},Y_b^{(c)}\right)}\\
&\quad + \varepsilon^2\left[\breve{\mathbf{u}} + \breve{x}_b^{(c)}\frac{\partial\mathbf{U}}{\partial x} + \breve{y}_b^{(c)}\frac{\partial\mathbf{U}}{\partial y} + \frac{\left(\hat{x}_b^{(c)}\right)^2}{2}\frac{\partial^2\mathbf{U}}{\partial x^2} + \frac{\hat{x}_b^{(c)}\hat{y}_b^{(c)}}{2}\frac{\partial^2\mathbf{U}}{\partial x\partial y}\right]_{\left(X_b^{(c)},Y_b^{(c)}\right)}\\
&\quad + \varepsilon^2\left[\frac{\left(\hat{y}_b^{(c)}\right)^2}{2}\frac{\partial^2\mathbf{U}}{\partial y^2} + \hat{x}_b^{(c)}\frac{\partial\hat{\mathbf{u}}}{\partial x} + \hat{y}_b^{(c)}\frac{\partial\hat{\mathbf{u}}}{\partial y}\right]_{\left(X_b^{(c)},Y_b^{(c)}\right)}.
\end{aligned} \quad (4.2.28)$$

Whereas, the linearised beam velocity is,

$$\mathbf{u}_b{}^{(c)} = \varepsilon\hat{\mathbf{u}}_b^{(c)} + \varepsilon^2\breve{\mathbf{u}}_b^{(c)}, \qquad (S \in \partial\bar{\Omega}_b). \quad (4.2.29)$$

as the beam velocity at the static state equals zero.
Applying continuity of the fluid velocity, at $O(1)$ we have,

$$\mathbf{U} = \mathbf{0}. \qquad (\mathbf{x} \in \partial\bar{\Omega}_b). \quad (4.2.30)$$

At $O(\varepsilon)$ we have

$$\hat{\mathbf{u}} + \left(\hat{x}_b^{(c)}\frac{\partial \mathbf{U}}{\partial x} + \hat{y}_b^{(c)}\frac{\partial \mathbf{U}}{\partial y}\right) = \hat{\mathbf{u}}_b^{(c)}, \qquad (\mathbf{x} \in \partial\bar{\Omega}_b). \quad (4.2.31)$$

At $O(\varepsilon^2)$, we have

$$\breve{x}_b^{(c)}\frac{\partial \mathbf{U}}{\partial x} + \breve{y}_b^{(c)}\frac{\partial \mathbf{U}}{\partial y} + \frac{\left(\hat{x}_b^{(c)}\right)^2}{2}\frac{\partial^2 \mathbf{U}}{\partial x^2} + \frac{\hat{x}_b^{(c)}\hat{y}_b^{(c)}}{2}\frac{\partial^2 \mathbf{U}}{\partial x \partial y} + \frac{\left(\hat{y}_b^{(c)}\right)^2}{2}\frac{\partial^2 \mathbf{U}}{\partial y^2} + \hat{x}_b^{(c)}\frac{\partial \hat{\mathbf{u}}}{\partial x} + \hat{y}_b^{(c)}\frac{\partial \hat{\mathbf{u}}}{\partial y}$$
$$+ \breve{\mathbf{u}} = \breve{\mathbf{u}}_b^{(c)}, \qquad (\mathbf{x} \in \partial\bar{\Omega}_b). \quad (4.2.32)$$

Details of the expansion of the fluid stress tensor on the steady beam are given in appendix (A.5). The stress and velocity components are consistent with the formulation in chapter 2, where the membrane can only move parallel to $\mathbf{g}_2$, so $(\hat{x}_b^{(c)}, \hat{y}_b^{(c)})^{\mathrm{T}} = (0, \hat{\eta})^{\mathrm{T}}$. Taking the velocity boundary condition (4.2.20) as an example, since the static and first order fluid velocity in the fluid-membrane model takes the form

$$\mathbf{U} = \big(U(y), 0\big)^{\mathrm{T}} = \big(6y(1-y)), 0\big)^{\mathrm{T}} \quad (4.2.33)$$
$$\hat{\mathbf{u}} = \big(\hat{\phi}_y, -\hat{\phi}_x\big)^{\mathrm{T}}. \quad (4.2.34)$$

Substituting (4.2.33) and (4.2.34) the the velocity boundary condition (4.2.20) at the steady state (*i.e.* undeformed membrane for the fluid-membrane model) take the form

$$\big(\hat{\phi}_y, -\hat{\phi}_x\big)^{\mathrm{T}} + \hat{\eta}\,\big(U_y(1), 0\big)^{\mathrm{T}} = \big(0, \hat{\eta}_t\big)^{\mathrm{T}}. \quad (4.2.35)$$

Thus, we can conclude the appropriate velocity boundary conditions are

$$\hat{\phi}_y - 6\hat{\eta} = 0, \quad -\hat{\phi}_x = \hat{\eta}_t, \quad (4.2.36)$$

these are identical to (2.4.6).
At $O(\varepsilon^2)$ equations (3.3.17-3.3.29) become,

$$\frac{\partial \breve{u}_1}{\partial x}+\frac{\partial \breve{u}_2}{\partial y}=0, \qquad (\mathbf{x}\in\bar{\Omega}), \quad (4.2.37)$$

$$\frac{\partial \breve{u}_1}{\partial t}+U_1\frac{\partial \breve{u}_1}{\partial x}+U_2\frac{\partial \breve{u}_1}{\partial y}+\breve{u}_1\frac{\partial U_1}{\partial x}+\breve{u}_2\frac{\partial U_1}{\partial y}+\frac{\partial \breve{p}}{\partial x}-R^{-1}\left(\frac{\partial^2 \breve{u}_1}{\partial x^2}+\frac{\partial^2 \breve{u}_1}{\partial y^2}\right)$$
$$=-\left(\hat{u}_1\frac{\partial \hat{u}_1}{\partial x}+\hat{u}_2\frac{\partial \hat{u}_1}{\partial y}\right), \qquad (\mathbf{x}\in\bar{\Omega}), \quad (4.2.38)$$

$$\frac{\partial \breve{u}_2}{\partial t}+U_1\frac{\partial \breve{u}_2}{\partial x}+U_2\frac{\partial \breve{u}_2}{\partial y}+\breve{u}_1\frac{\partial U_2}{\partial x}+\breve{u}_2\frac{\partial U_2}{\partial y}+\frac{\partial \breve{p}}{\partial y}-R^{-1}\left(\frac{\partial^2 \breve{u}_2}{\partial x^2}+\frac{\partial^2 \breve{u}_2}{\partial y^2}\right)$$
$$=-\left(\hat{u}_1\frac{\partial \hat{u}_2}{\partial x}+\hat{u}_2\frac{\partial \hat{u}_2}{\partial y}\right), \qquad (\mathbf{x}\in\bar{\Omega}), \quad (4.2.39)$$

$$\breve{\mathbf{u}}=\mathbf{0}, \qquad (y=0;\ y=1,-L_u<x<0,\ L_0<x<L_0+L_d), \quad (4.2.40)$$

$$\left(\breve{x}_b^{(c)}\frac{\partial \mathbf{U}}{\partial x}+\breve{y}_b^{(c)}\frac{\partial \mathbf{U}}{\partial y}+\frac{\left(\hat{x}_b^{(c)}\right)^2}{2}\frac{\partial^2 \mathbf{U}}{\partial x^2}+\frac{\hat{x}_b^{(c)}\hat{y}_b^{(c)}}{2}\frac{\partial^2 \mathbf{U}}{\partial x\partial y}+\frac{\left(\hat{y}_b^{(c)}\right)^2}{2}\frac{\partial^2 \mathbf{U}}{\partial y^2}+\hat{x}_b^{(c)}\frac{\partial \hat{\mathbf{u}}}{\partial x}+\hat{y}_b^{(c)}\frac{\partial \hat{\mathbf{u}}}{\partial y}\right)$$
$$+\breve{\mathbf{u}}=\breve{\mathbf{u}}_b^{(c)}, \qquad (\mathbf{x}\in\partial\bar{\Omega}_b), \quad (4.2.41)$$

$$\frac{\rho_m}{\Lambda}\left(\frac{\partial X_b}{\partial l}\frac{\partial^2 \breve{x}_b}{\partial t^2}+\frac{\partial Y_b}{\partial l}\frac{\partial^2 \breve{y}_b}{\partial t^2}+\frac{\partial \hat{x}_b}{\partial l}\frac{\partial^2 \hat{x}_b}{\partial t^2}+\frac{\partial \hat{y}_b}{\partial l}\frac{\partial^2 \hat{y}_b}{\partial t^2}\right)-\frac{\rho_m\hat{\lambda}}{\Lambda^2}\left(\frac{\partial X_b}{\partial l}\frac{\partial^2 \hat{x}_b}{\partial t^2}+\frac{\partial Y_b}{\partial l}\frac{\partial^2 \hat{y}_b}{\partial t^2}\right)$$
$$=c_\kappa K\frac{\partial(\Lambda\breve{\kappa}+\hat{\lambda}\hat{\kappa}+\breve{\lambda}K)}{\partial l}+c_\lambda\frac{\partial \breve{\lambda}}{\partial l}+\left[\left(\breve{x}_b\frac{\partial \mathbf{\Sigma}}{\partial x}+\breve{y}_b\frac{\partial \mathbf{\Sigma}}{\partial y}+\frac{(\hat{x}_b)^2}{2}\frac{\partial^2 \mathbf{\Sigma}}{\partial x^2}\right)\mathbf{N}\right]\cdot\mathbf{T}$$
$$+\left[\left(\frac{(\hat{y}_b)^2}{2}\frac{\partial^2 \mathbf{\Sigma}}{\partial y^2}+\frac{\hat{x}_b\hat{y}_b}{2}\frac{\partial^2 \mathbf{\Sigma}}{\partial x^2}+\hat{x}_b\frac{\partial \hat{\boldsymbol{\sigma}}}{\partial x}+\hat{y}_b\frac{\partial \hat{\boldsymbol{\sigma}}}{\partial y}\right)\mathbf{N}\right]\cdot\mathbf{T}+(\breve{\boldsymbol{\sigma}}\mathbf{N})\cdot\mathbf{T},$$
$$(0\le l\le L_0), \quad (4.2.42)$$

$$\frac{\rho_m}{\Lambda}\left(\frac{\partial X_b}{\partial l}\frac{\partial^2 \breve{y}_b}{\partial t^2}-\frac{\partial Y_b}{\partial l}\frac{\partial^2 \breve{x}_b}{\partial t^2}+\frac{\partial \hat{x}_b}{\partial l}\frac{\partial^2 \hat{y}_b}{\partial t^2}-\frac{\partial \hat{y}_b}{\partial l}\frac{\partial^2 \hat{x}_b}{\partial t^2}\right)-\frac{\rho_m\hat{\lambda}}{(\Lambda)^2}\left(\frac{\partial X_b}{\partial l}\frac{\partial^2 \hat{y}_b}{\partial t^2}-\frac{\partial Y_b}{\partial l}\frac{\partial^2 \hat{x}_b}{\partial t^2}\right)$$
$$=-c_\kappa\frac{\partial}{\partial l}\left[\frac{1}{\Lambda}\left(K\frac{\partial \breve{\lambda}}{\partial l}+\hat{\kappa}\frac{\partial \hat{\lambda}}{\partial l}+\breve{\kappa}\frac{\partial \Lambda}{\partial l}\right)-\frac{\hat{\lambda}}{\Lambda^2}\left(K\frac{\partial \hat{\lambda}}{\partial l}+\hat{\kappa}\frac{\partial \Lambda}{\partial l}\right)+K\frac{\partial \Lambda}{\partial l}\left(\frac{\hat{\lambda}^2}{\Lambda^3}-\frac{\breve{\lambda}}{\Lambda^2}\right)\right]$$
$$-c_\kappa\frac{\partial^2 \breve{\kappa}}{\partial l^2}+c_\lambda\left[\Lambda K\breve{\lambda}+\left(\Lambda\hat{\kappa}+\hat{\lambda}K\right)\hat{\lambda}+\left(\Lambda\breve{\kappa}+\hat{\lambda}\hat{\kappa}+\breve{\lambda}K\right)(\Lambda-1)\right]$$
$$+\left(\Lambda\breve{\kappa}+\hat{\lambda}\hat{\kappa}+\breve{\lambda}K\right)T+\left[\left(\frac{(\hat{x}_b)^2}{2}\frac{\partial^2 \mathbf{\Sigma}}{\partial x^2}+\frac{(\hat{y}_b)^2}{2}\frac{\partial^2 \mathbf{\Sigma}}{\partial y^2}+\frac{\hat{x}_b\hat{y}_b}{2}\frac{\partial^2 \mathbf{\Sigma}}{\partial x^2}+\hat{x}_b\frac{\partial \hat{\boldsymbol{\sigma}}}{\partial x}\right)\mathbf{N}\right]\cdot\mathbf{N}$$
$$+\left[\left(\hat{y}_b\frac{\partial \hat{\boldsymbol{\sigma}}}{\partial y}\right)\mathbf{N}\right]\cdot\mathbf{N}+\left[\left(\breve{x}_b\frac{\partial \mathbf{\Sigma}}{\partial x}+\breve{y}_b\frac{\partial \mathbf{\Sigma}}{\partial y}\right)\mathbf{N}\right]\cdot\mathbf{N}+(\breve{\boldsymbol{\sigma}}\mathbf{N})\cdot\mathbf{N}-\breve{\lambda}p_e,$$
$$(0\le l\le L_0), \quad (4.2.43)$$

$$\breve{\mathbf{u}}_b=\mathbf{0}, \qquad (l=0,L_0), \quad (4.2.44)$$

$$\frac{\partial \breve{\theta}}{\partial t}=0, \qquad (l=0,L_0). \quad (4.2.45)$$

In deriving the linearised energy budget in later sections, we must integrate over the deformed static configuration for the beam. Hence, here we rewrite the beam energy equation (3.3.32) in the current description (using the arc-length coordinate S), at $O(\varepsilon^2)$ we have

$$
\begin{aligned}
&(\boldsymbol{\Sigma}\mathbf{N})\cdot\breve{\mathbf{u}}_b^{(c)} + (\boldsymbol{\Sigma}\hat{\mathbf{n}})\cdot\hat{\mathbf{u}}_b + (\hat{\boldsymbol{\sigma}}\mathbf{N})\cdot\hat{\mathbf{u}}_b^{(c)} + \left[\left(\hat{x}_b^{(c)}\frac{\partial\boldsymbol{\Sigma}}{\partial x} + \hat{y}_b^{(c)}\frac{\partial\boldsymbol{\Sigma}}{\partial y}\right)\mathbf{N}\right]\cdot\hat{\mathbf{u}}_b^{(c)},\\
=&c_\kappa\left[K^{(c)}\frac{\partial(\Lambda^{(c)}K^{(c)})}{\partial S}\breve{u}_{b1}^{(c)} - \frac{\partial^2(\Lambda^{(c)}K^{(c)})}{\partial S^2}\breve{u}_{b2}^{(c)} + K^{(c)}\frac{\partial\left(\Lambda^{(c)}\hat{\kappa}^{(c)}+\hat{\lambda}^{(c)}K^{(c)}\right)}{\partial S}\hat{u}_{b1}^{(c)}\right]\\
&+c_\kappa\left[\hat{\kappa}^{(c)}\frac{\partial\left(\Lambda^{(c)}K^{(c)}\right)}{\partial S}\hat{u}_{b1}^{(c)} - \frac{\partial^2\left(\Lambda^{(c)}\hat{\kappa}^{(c)}+\hat{\lambda}^{(c)}K^{(c)}\right)}{\partial S^2}\hat{u}_{b2}^{(c)}\right]\\
&+c_\lambda\left[\frac{\partial\Lambda^{(c)}}{\partial S}\breve{u}_{b1}^{(c)} + K^{(c)}\left(\Lambda^{(c)}-1\right)\breve{u}_{b2}^{(c)} + \frac{\partial\hat{\lambda}^{(c)}}{\partial S}\hat{u}_{b1}^{(c)} + K^{(c)}\hat{\lambda}^{(c)}\hat{u}_{b2}^{(c)} + \hat{\kappa}^{(c)}\left(\Lambda^{(c)}-1\right)\hat{u}_{b2}^{(c)}\right]\\
&+T\left(K^{(c)}\breve{u}_{b2}^{(c)} + \hat{\kappa}^{(c)}\hat{u}_{b1}^{(c)}\right) - p_e\breve{u}_{b2}^{(c)}, \qquad (S\in\partial\bar{\Omega}_b). \qquad (4.2.46)
\end{aligned}
$$

4.3 Global stability eigensolver

In this section, we solve the first order problem for the global perturbation (4.2.16-4.2.27). We use the reference (material) description of the linearised beam equations and assume all the first order variables are the wave-like form to obtain the eigen-value problem of the perturbed system, in the form,

$$
\hat{f}(x,y,t) = \bar{\hat{f}}(x,y)e^{\sigma t} + \left(\bar{\hat{f}}(x,y)e^{\sigma t}\right)^*,\ \hat{g}(l,t) = \bar{\hat{g}}(l)e^{\sigma t} + \left(\bar{\hat{g}}(l)e^{\sigma t}\right)^*, \qquad (4.3.1)
$$

here $\hat{f}(x,y,t)$ represents all the first order fluid related variables while $\hat{g}(l,t)$ represents all the first order beam related variables. Here * denotes a complex conjugate and $\sigma = \sigma_r + i\sigma_i \in \mathbb{C}$, where σ_r is the growth rate of disturbance while σ_i is the frequency of disturbance. We must express our beam variables in the material description as time derivatives are taken holding l fixed in our formulation. Hence, when the real part of the growth rate $\sigma_r = 0$, *i.e.* what we called neutrally stable state, the product of two first order variables has a steady (time-independent) component arising from the product of an $e^{\sigma t} = e^{\sigma_r t}e^{i\sigma_i t}$ and an $(e^{\sigma t})^* = e^{\sigma_r t}e^{-i\sigma_i t}$ term, in addition to terms $e^{2\sigma t}$ and $\left(e^{2\sigma t}\right)^*$. For consistency, although not calculated directly in this chapter, the formulation requires the second order (breved) quantities to be expanded according to

$$
\begin{aligned}
&\breve{f}(x,y,t) = \bar{\breve{f}}_1(x,y)e^{2\sigma t} + \bar{\breve{f}}_2(x,y) + \left(\bar{\breve{f}}_1(x,y)e^{(2\sigma t)}\right)^*,\\
&\breve{g}(l,t) = \bar{\breve{g}}_1(l)e^{2\sigma t} + \bar{\breve{g}}_2(l) + \left(\bar{\breve{g}}_1 e^{2\sigma t}\right)^*. \qquad (4.3.2)
\end{aligned}
$$

Substituting (4.3.1) into the first order governing equations (4.2.16-4.2.25) we obtain the following eigenvalue problem for the system,

$$\frac{\partial \bar{\hat{u}}_1}{\partial x} + \frac{\partial \bar{\hat{u}}_2}{\partial y} = 0, \qquad (\mathbf{x} \in \bar{\Omega}), \quad (4.3.3)$$

$$\sigma \bar{\hat{u}}_1 + U_1 \frac{\partial \bar{\hat{u}}_1}{\partial x} + U_2 \frac{\partial \bar{\hat{u}}_1}{\partial y} + \bar{\hat{u}}_1 \frac{\partial U_1}{\partial x} + \bar{\hat{u}}_2 \frac{\partial U_1}{\partial y} = -\frac{\partial \bar{\hat{p}}}{\partial x} + R^{-1}\left(\frac{\partial^2 \bar{\hat{u}}_1}{\partial x^2} + \frac{\partial^2 \bar{\hat{u}}_1}{\partial y^2}\right), \qquad (\mathbf{x} \in \bar{\Omega}), \quad (4.3.4)$$

$$\sigma \bar{\hat{u}}_2 + U_1 \frac{\partial \bar{\hat{u}}_2}{\partial x} + U_2 \frac{\partial \bar{\hat{u}}_2}{\partial y} + \bar{\hat{u}}_1 \frac{\partial U_2}{\partial x} + \bar{\hat{u}}_2 \frac{\partial U_2}{\partial y} = -\frac{\partial \bar{\hat{p}}}{\partial y} + R^{-1}\left(\frac{\partial^2 \bar{\hat{u}}_2}{\partial x^2} + \frac{\partial^2 \bar{\hat{u}}_2}{\partial y^2}\right), \qquad (\mathbf{x} \in \bar{\Omega}), \quad (4.3.5)$$

$$\bar{\hat{u}}_1 = 0,\ \bar{\hat{u}}_2 = 0, \qquad (y = 0;\ \ y = 1, -L_u < x < 0,\ L_0 < x < L_0 + L_d), \quad (4.3.6)$$

$$\bar{\hat{\mathbf{u}}} + \left(\bar{\hat{x}}_b \frac{\partial \mathbf{U}}{\partial x} + \bar{\hat{y}}_b \frac{\partial \mathbf{U}}{\partial y}\right) = \sigma \bar{\hat{\mathbf{x}}}_b, \qquad (\mathbf{x} \in \partial \bar{\Omega}_b), \quad (4.3.7)$$

$$\frac{\partial \bar{\hat{x}}_b}{\partial l} = -\Lambda \bar{\hat{\theta}} \sin(\Theta) + \bar{\hat{\lambda}} \cos(\Theta), \qquad (0 \le l \le L_0), \quad (4.3.8)$$

$$\frac{\partial \bar{\hat{y}}_b}{\partial l} = \Lambda \bar{\hat{\theta}} \cos(\Theta) + \bar{\hat{\lambda}} \sin(\Theta), \qquad (0 \le l \le L_0), \quad (4.3.9)$$

$$\frac{\partial \bar{\hat{\theta}}}{\partial l} = \Lambda \bar{\hat{\kappa}} + \bar{\hat{\lambda}} K, \qquad (0 \le l \le L_0), \quad (4.3.10)$$

$$\frac{\rho_m}{\Lambda}\sigma^2 \left(\frac{\partial X_b}{\partial l}\bar{\hat{x}}_b + \frac{\partial Y_b}{\partial l}\bar{\hat{y}}_b\right) = c_\kappa \left(\frac{\partial (\Lambda K)}{\partial l}\bar{\hat{\kappa}} + \frac{\partial (\bar{\hat{\lambda}} K + \Lambda \bar{\hat{\kappa}})}{\partial l} K\right) + c_\lambda \frac{\partial \bar{\hat{\lambda}}}{\partial l} + \left[\left(\bar{\hat{\boldsymbol{\sigma}}} + \bar{\hat{x}}_b \frac{\partial \boldsymbol{\Sigma}}{\partial x} + \bar{\hat{y}}_b \frac{\partial \boldsymbol{\Sigma}}{\partial y}\right)\mathbf{N}\right] \cdot \mathbf{T}, \qquad (0 \le l \le L_0), \quad (4.3.11)$$

$$\frac{\rho_m}{\Lambda}\sigma^2 \left(\frac{\partial X_b}{\partial l}\bar{\hat{y}}_b - \frac{\partial Y_b}{\partial l}\bar{\hat{x}}_b\right) = -c_\kappa \frac{\partial}{\partial l}\left(\Lambda^{-1}\left(K \frac{\partial \bar{\hat{\lambda}}}{\partial l} + \bar{\hat{\kappa}} \frac{\partial \Lambda}{\partial l}\right) - \Lambda^{-2} \bar{\hat{\lambda}} K \frac{\partial \Lambda}{\partial l} + \frac{\partial \bar{\hat{\kappa}}}{\partial l}\right) + c_\lambda \left(\Lambda K \bar{\hat{\lambda}} + (\Lambda \bar{\hat{\kappa}} + \bar{\hat{\lambda}} K)(\Lambda - 1)\right) + \left(\Lambda \bar{\hat{\kappa}} + \bar{\hat{\lambda}} K\right) T + \left[\left(\bar{\hat{\boldsymbol{\sigma}}} + \bar{\hat{x}}_b \frac{\partial \boldsymbol{\Sigma}}{\partial x} + \bar{\hat{y}}_b \frac{\partial \boldsymbol{\Sigma}}{\partial y}\right)\mathbf{N}\right] \cdot \mathbf{N} - \bar{\hat{\lambda}} p_e, \qquad (0 \le l \le L_0), \quad (4.3.12)$$

$$\bar{\hat{\mathbf{u}}}_b = \mathbf{0}, \qquad (l = 0, L_0), \quad (4.3.13)$$

$$\bar{\hat{\theta}} = 0, \qquad (l = 0, L_0). \quad (4.3.14)$$

We solve this linear eigenvalue problem numerically in *Sec*. 4.5.

4.4 Perturbation energy budgets

In the same manner as section 4.2, by substituting the small amplitude expansions (4.1.1) into the fluid energy equation (3.5.2) in chapter 3, we can obtain the perturbed fluid energy equation.

At $O(1)$, after rearrangement we obtain,

$$\frac{1}{2}\nabla\cdot\left(\left(U_1^2+U_2^2\right)\mathbf{U}\right)+\nabla\cdot(P\mathbf{U})-R^{-1}\left[U_1\nabla^2U_1+U_2\nabla^2U_2+\mathbf{U}\cdot\left(\nabla\cdot\left(\nabla^{\mathrm{T}}\mathbf{U}\right)\right)\right]=0,$$
$$(\mathbf{x}\in\bar{\Omega}). \quad (4.4.1)$$

This can be rearranged into the form (3.6.1-3.6.4) presented in *Sec*. 3.6.
After rearrangement, at $O(\varepsilon)$ we have,

$$(U_1\hat{u}_1+U_2\hat{u}_2)_t+\left[\frac{1}{2}\nabla\cdot\left(\left(U_1^2+U_2^2\right)\hat{\mathbf{u}}\right)+\nabla\cdot\left((U_1\hat{u}_1+U_2\hat{u}_2)\mathbf{U}\right)\right]+\nabla\cdot(P\hat{\mathbf{u}}+\hat{p}\mathbf{U})$$
$$-R^{-1}\left[U_1\nabla^2\hat{u}_1+U_2\nabla^2\hat{u}_2+\hat{u}_1\nabla^2U_1+\hat{u}_2\nabla^2U_2+\mathbf{U}\cdot\left(\nabla\cdot\left(\nabla^{\mathrm{T}}\hat{\mathbf{u}}\right)\right)+\hat{\mathbf{u}}\cdot\left(\nabla\cdot\left(\nabla^{\mathrm{T}}\mathbf{U}\right)\right)\right]=0,$$
$$(\mathbf{x}\in\bar{\Omega}). \quad (4.4.2)$$

The fluid energy equation (3.5.2) at $O(\varepsilon^2)$ becomes,

$$\hat{u}_1\hat{u}_2\frac{\partial U_1}{\partial y}+\hat{u}_2^2\frac{\partial V_1}{\partial y}+\hat{u}_1^2\frac{\partial U_1}{\partial x}+\hat{u}_1\hat{u}_2\frac{\partial U_2}{\partial x}+\hat{u}_1\frac{\partial\hat{u}_1}{\partial t}+\hat{u}_2\frac{\partial\hat{u}_2}{\partial t}+\hat{u}_2\frac{\partial\hat{p}}{\partial y}+\hat{u}_1U_2\frac{\partial\hat{u}_1}{\partial y}$$
$$+U_1\hat{u}_2\frac{\partial\hat{u}_1}{\partial y}+2U_2\hat{u}_2\frac{\partial\hat{u}_2}{\partial y}+\hat{u}_1\frac{\partial\hat{p}}{\partial x}+2U_1\hat{u}_1\frac{\partial\hat{u}_1}{\partial x}+\hat{u}_1U_2\frac{\partial\hat{u}_1}{\partial x}+U_1\hat{u}_2\frac{\partial\hat{u}_2}{\partial x}$$
$$-R^{-1}\hat{u}_1\left(\frac{\partial^2\hat{u}_1}{\partial x^2}+\frac{\partial^2\hat{u}_1}{\partial y^2}\right)-R^{-1}\hat{u}_2\left(\frac{\partial^2\hat{u}_2}{\partial x^2}+\frac{\partial^2\hat{u}_2}{\partial y^2}\right)+U_1\frac{\partial\breve{u}_1}{\partial t}+U_2\frac{\partial\breve{u}_2}{\partial t}+2\breve{u}_1U_1\frac{\partial U_1}{\partial x}$$
$$+\breve{u}_1U_2\frac{\partial U_1}{\partial y}+\breve{u}_1U_2\frac{\partial U_2}{\partial x}+2\breve{u}_2U_2\frac{\partial U_2}{\partial y}+\breve{u}_2U_1\frac{\partial U_1}{\partial y}+\breve{u}_2U_1\frac{\partial U_2}{\partial x}+U_1U_2\frac{\partial\breve{u}_1}{\partial y}+U_2^2\frac{\partial\breve{u}_2}{\partial y}$$
$$+U_1^2\frac{\partial\breve{u}_1}{\partial x}+U_1U_2\frac{\partial\breve{u}_2}{\partial x}+\breve{u}_1\frac{\partial P}{\partial x}+\breve{u}_2\frac{\partial P}{\partial y}+U_2\frac{\partial\breve{p}}{\partial y}+U_1\frac{\partial\breve{p}}{\partial x}-R^{-1}\breve{u}_1\left(\frac{\partial^2U_1}{\partial x^2}+\frac{\partial^2U_1}{\partial y^2}\right)$$
$$-R^{-1}\breve{u}_2\left(\frac{\partial^2U_2}{\partial x^2}+\frac{\partial^2U_2}{\partial y^2}\right)-R^{-1}U_1\left(\frac{\partial^2\breve{u}_1}{\partial x^2}+\frac{\partial^2\breve{u}_1}{\partial y^2}\right)-R^{-1}U_2\left(\frac{\partial^2\breve{u}_2}{\partial x^2}+\frac{\partial^2\breve{u}_2}{\partial y^2}\right)=0,$$
$$(\mathbf{x}\in\bar{\Omega}). \quad (4.4.3)$$

This equation admits a distinction between terms at $O(\varepsilon^2)$ which are linear in breved variables and others which occur as the product of two hatted variables. We express (4.4.3) as,

$$\hat{\varepsilon}+\breve{\varepsilon}=0, \quad (4.4.4)$$

where,

$$\hat{\varepsilon}=\hat{u}_1\hat{u}_2\frac{\partial U_1}{\partial y}+\hat{u}_2^2\frac{\partial U_2}{\partial y}+\hat{u}_1^2\frac{\partial U_1}{\partial x}+\hat{u}_1\hat{u}_2\frac{\partial U_2}{\partial x}+\hat{u}_1\frac{\partial\hat{u}_1}{\partial t}+\hat{u}_2\frac{\partial\hat{u}_2}{\partial t}+\hat{u}_2\frac{\partial\hat{p}}{\partial y}+\hat{u}_1U_2\frac{\partial\hat{u}_1}{\partial y}$$
$$+U_1\hat{u}_2\frac{\partial\hat{u}_1}{\partial y}+2U_2\hat{u}_2\frac{\partial\hat{u}_2}{\partial y}+\hat{u}_1\frac{\partial\hat{p}}{\partial x}+2U_1\hat{u}_1\frac{\partial\hat{u}_1}{\partial x}+\hat{u}_1U_2\frac{\partial\hat{u}_1}{\partial x}+U_1\hat{u}_2\frac{\partial\hat{u}_2}{\partial x}$$

$$
\begin{aligned}
&- R^{-1}\hat{u}_1\left(\frac{\partial^2\hat{u}_1}{\partial x^2}+\frac{\partial^2\hat{u}_1}{\partial y^2}\right) - R^{-1}\hat{u}_2\left(\frac{\partial^2\hat{u}_2}{\partial x^2}+\frac{\partial^2\hat{u}_2}{\partial y^2}\right) + U_1\frac{\partial\breve{u}_1}{\partial t} + V\frac{\partial\breve{u}_2}{\partial t} \\
&+ 2\breve{u}_1U_1\frac{\partial U_1}{\partial x} + \breve{u}_1U_2\frac{\partial U_1}{\partial y}, \qquad (\mathbf{x}\in\bar{\Omega}), \quad (4.4.5)\\
\breve{\varepsilon} =& U_1\frac{\partial\breve{u}_1}{\partial t} + U_2\frac{\partial\breve{u}_2}{\partial t} + 2\breve{u}_1U_1\frac{\partial U_1}{\partial x} + \breve{u}_1U_2\frac{\partial U_1}{\partial y} + \breve{u}_1U_2\frac{\partial U_2}{\partial x} + 2\breve{u}_2U_2\frac{\partial U_2}{\partial y} + \breve{u}_2U_1\frac{\partial U_1}{\partial y} \\
&+ \breve{u}_2U_1\frac{\partial U_2}{\partial x} + U_1U_2\frac{\partial\breve{u}_1}{\partial y} + U_2^2\frac{\partial\breve{u}_2}{\partial y} + U_1^2\frac{\partial\breve{u}_1}{\partial x} + U_1U_2\frac{\partial\breve{u}_2}{\partial x} + \breve{u}_1\frac{\partial P}{\partial x} + \breve{u}_2\frac{\partial P}{\partial y} + U_2\frac{\partial\breve{p}}{\partial y} \\
&+ U_1\frac{\partial\breve{p}}{\partial x} - R^{-1}\breve{u}_1\left(\frac{\partial^2U_1}{\partial x^2}+\frac{\partial^2U_1}{\partial y^2}\right) - R^{-1}\breve{u}_2\left(\frac{\partial^2U_2}{\partial x^2}+\frac{\partial^2U_2}{\partial y^2}\right) \\
&- R^{-1}U_1\left(\frac{\partial^2\breve{u}_1}{\partial x^2}+\frac{\partial^2\breve{u}_1}{\partial y^2}\right) - R^{-1}U_2\left(\frac{\partial^2\breve{u}_2}{\partial x^2}+\frac{\partial^2\breve{u}_2}{\partial y^2}\right), \qquad (\mathbf{x}\in\bar{\Omega}). \quad (4.4.6)
\end{aligned}
$$

We now manipulate $\hat{\varepsilon}$ and $\breve{\varepsilon}$ in turn.
We add the identically zero term $R^{-1}\hat{\mathbf{u}}\cdot\left(\nabla\cdot\left(\nabla\hat{\mathbf{u}}^{\mathrm{T}}\right)\right)=0$ to $\hat{\varepsilon}$ to enable us to rewrite the perturbed dissipation. We then rearrange $\hat{\varepsilon}$ to obtain,

$$
\begin{aligned}
\hat{\varepsilon} =& \frac{1}{2}\frac{\partial\left(\hat{u}_1^2+\hat{u}_2^2\right)}{\partial t} + \left(\frac{1}{2}\nabla\cdot\left(\left(\hat{u}_1^2+\hat{u}_2^2\right)\mathbf{U}\right) + \nabla\cdot\left(\left(U_1\hat{u}_1+U_2\hat{u}_2\right)\hat{\mathbf{u}}\right)\right) + \nabla\cdot\left(\hat{p}\hat{\mathbf{u}}\right) \\
&- R^{-1}\left(\hat{u}_1\nabla^2\hat{u}_1 + \hat{u}_2\nabla^2\hat{u}_2 + \hat{\mathbf{u}}\cdot\left(\nabla\cdot\left(\nabla\hat{\mathbf{u}}^{\mathrm{T}}\right)\right)\right), \qquad (\mathbf{x}\in\bar{\Omega}). \quad (4.4.7)
\end{aligned}
$$

Rewriting the viscous term into tensor form we have,

$$
\begin{aligned}
\hat{\varepsilon} =& \frac{1}{2}\frac{\partial\left(\hat{u}_1^2+\hat{u}_2^2\right)}{\partial t} + \nabla\cdot\left(\frac{1}{2}\left(\hat{u}_1^2+\hat{u}_2^2\right)\mathbf{U} + \left(U_1\hat{u}_1+U_2\hat{u}_2\right)\hat{\mathbf{u}}\right) + \nabla\cdot\left(\hat{p}\hat{\mathbf{u}}\right) \\
&- R^{-1}\left(\nabla\cdot\left(\nabla\hat{\mathbf{u}}+\nabla^{\mathrm{T}}\hat{\mathbf{u}}\right)\right)\cdot\hat{\mathbf{u}}, \qquad (\mathbf{x}\in\bar{\Omega}). \quad (4.4.8)
\end{aligned}
$$

Manipulating $\breve{\varepsilon}$, we have,

$$
\begin{aligned}
\breve{\varepsilon} =& U_1\left(\frac{\partial\breve{u}_1}{\partial t} + U_1\frac{\partial\breve{u}_1}{\partial x} + U_2\frac{\partial\breve{u}_1}{\partial y} + \breve{u}_1\frac{\partial U_1}{\partial x} + \breve{u}_2\frac{\partial U_1}{\partial y} + \frac{\partial\breve{p}}{\partial x} - R^{-1}\nabla^2\breve{u}_1\right) \\
&+ U_2\left(\frac{\partial\breve{u}_2}{\partial t} + U_1\frac{\partial\breve{u}_2}{\partial x} + U_2\frac{\partial\breve{u}_2}{\partial y} + \breve{u}_1\frac{\partial U_2}{\partial x} + \breve{u}_2\frac{\partial U_2}{\partial y} + \frac{\partial\breve{p}}{\partial y} - R^{-1}\nabla^2\breve{u}_2\right) \\
&+ \breve{u}_1\left(U_1\frac{\partial U_1}{\partial x} + U_2\frac{\partial U_1}{\partial y} + \frac{\partial P}{\partial x} - R^{-1}\nabla U_1\right) \\
&+ \breve{u}_2\left(U_1\frac{\partial U_2}{\partial x} + U_2\frac{\partial U_2}{\partial y} + \frac{\partial P}{\partial y} - R^{-1}\nabla U_2\right), \qquad (\mathbf{x}\in\bar{\Omega}); \quad (4.4.9)
\end{aligned}
$$

the last two terms in (4.4.9) disappear due to the zero-order fluid governing equations (4.2.6, 4.2.7), while substituting the second order fluid governing equations (4.2.38, 4.2.39) into the

remainder we obtain,

$$\check{\varepsilon} = -U_1\left(\hat{u}_1\frac{\partial\hat{u}_1}{\partial x}+\hat{u}_2\frac{\partial\hat{u}_1}{\partial y}\right)-U_2\left(\hat{u}_1\frac{\partial\hat{u}_2}{\partial x}+\hat{u}_2\frac{\partial\hat{u}_2}{\partial y}\right), \qquad (\mathbf{x}\in\bar{\Omega}). \quad (4.4.10)$$

Substituting $\hat{\varepsilon}$ and $\check{\varepsilon}$ back into the full fluid energy equation at $O(\varepsilon^2)$ we obtain,

$$\begin{aligned}&-U_1\left(\hat{u}_1\frac{\partial\hat{u}_1}{\partial x}+\hat{u}_2\frac{\partial\hat{u}_1}{\partial y}\right)-U_2\left(\hat{u}_1\frac{\partial\hat{u}_2}{\partial x}+\hat{u}_2\frac{\partial\hat{u}_2}{\partial y}\right)+\frac{1}{2}\frac{\partial\left(\hat{u}_1^2+\hat{u}_2^2\right)}{\partial t}\\&+\nabla\cdot\left(\frac{1}{2}\left(\hat{u}_1^2+\hat{u}_2^2\right)\mathbf{U}+\left(U_1\hat{u}_1+U_2\hat{u}_2\right)\hat{\mathbf{u}}\right)+\nabla\cdot\left(\hat{p}\hat{\mathbf{u}}\right)-R^{-1}\left(\nabla\cdot\left(\nabla\hat{\mathbf{u}}+\nabla^{\mathrm{T}}\hat{\mathbf{u}}\right)\right)\cdot\hat{\mathbf{u}}=0,\\&\qquad\qquad(\mathbf{x}\in\bar{\Omega}). \quad (4.4.11)\end{aligned}$$

After integration across the steady domain $\bar{\Omega}$, the fluid energy equation (3.5.2) at $O(\varepsilon^2)$ becomes,

$$\begin{aligned}&\underbrace{\int_{\bar{\Omega}}\frac{1}{2}\frac{\partial\left(\hat{u}_1^2+\hat{u}_2^2\right)}{\partial t}\,\mathrm{d}A}_{I}+\underbrace{\int_{\bar{\Omega}}\nabla\cdot\left(\frac{1}{2}\left(\hat{u}_1^2+\hat{u}_2^2\right)\mathbf{U}+\left(U_1\hat{u}_1+U_2\hat{u}_2\right)\hat{\mathbf{u}}\right)\mathrm{d}A}_{II}+\underbrace{\int_{\bar{\Omega}}\nabla\cdot\left(\hat{p}\hat{\mathbf{u}}\right)\mathrm{d}A}_{III}\\&\underbrace{-R^{-1}\int_{\bar{\Omega}}\left[\left(\nabla\cdot\left(\nabla\hat{\mathbf{u}}+\nabla^{\mathrm{T}}\hat{\mathbf{u}}\right)\right)\cdot\hat{\mathbf{u}}\right]\mathrm{d}A}_{IV}\\&\underbrace{-\int_{\bar{\Omega}}\left[U_1\left(\hat{u}_1\frac{\partial\hat{u}_1}{\partial x}+\hat{u}_2\frac{\partial\hat{u}_1}{\partial y}\right)+U_1\left(\hat{u}_1\frac{\partial\hat{u}_2}{\partial x}+\hat{u}_2\frac{\partial\hat{u}_2}{\partial y}\right)\right]\mathrm{d}A}_{\hat{S}_f}=0. \qquad (4.4.12)\end{aligned}$$

We label these terms $I-IV$ and consider each in turn. We denote the last term as $\hat{S}_f$, the work denoting non-linear Reynolds stresses, which arises from the decomposition (4.4.10). A similar idea was presented in this context by Stewart *et al* [66].

For I, we take the time derivative outside the integral directly as we are integrating based on the static domain (*i.e.* the domain is independent of time),

$$I=\underbrace{\frac{\partial}{\partial t}\int_{\bar{\Omega}}\frac{1}{2}\left(\hat{u}_1^2+\hat{u}_2^2\right)\mathrm{d}A}_{\hat{K}_f}. \qquad (4.4.13)$$

We denote above term as $\hat{K}_f$, the rate of working of perturbation kinetic energy.

For II, we apply the divergence theorem to obtain

$$II=\int_{\partial\bar{\Omega}_u}\left[-\left(\frac{1}{2}\left(\hat{u}_1^2+\hat{u}_2^2\right)\mathbf{U}+\left(U_1\hat{u}_1+U_2\hat{u}_2\right)\hat{\mathbf{u}}\right)\cdot\mathbf{g}_1\right]\mathrm{d}S$$

$$
\begin{aligned}
&+\int_{\partial\bar{\Omega}_d}\left[\left(\frac{1}{2}\left(\hat{u}_1^2+\hat{u}_2^2\right)\mathbf{U}+\left(U_1\hat{u}_1+U_2\hat{u}_2\right)\hat{\mathbf{u}}\right)\cdot\mathbf{g}_1\right]\mathrm{d}S\\
&+\int_{\partial\bar{\Omega}_b}\left[\left(\frac{1}{2}\left(\hat{u}_1^2+\hat{u}_2^2\right)\mathbf{U}+\left(U_1\hat{u}_1+U_2\hat{u}_2\right)\hat{\mathbf{u}}\right)\cdot\mathbf{N}\right]\mathrm{d}S,\\
=&\left[\int_0^1\left(\frac{1}{2}\left(\hat{u}_1^2+\hat{u}_2^2\right)U_1+\left(U_1\hat{u}_1+U_2\hat{u}_2\right)\hat{u}_1\right)\mathrm{d}y\right]_{x=-L_u}^{x=L_0+L_d}\\
&+\int_{\partial\bar{\Omega}_b}\left[\left(\frac{1}{2}\left(\hat{u}_1^2+\hat{u}_2^2\right)\mathbf{U}+\left(\mathbf{U}\cdot\hat{\mathbf{u}}\right)\hat{\mathbf{u}}\right)\cdot\mathbf{N}\right]\mathrm{d}S.
\end{aligned}
\tag{4.4.14}
$$

The second term in (4.4.14) cancels as $\mathbf{U}$ is zero on $\partial\bar{\Omega}_b$ due to the no-slip condition (4.2.9), so we have

$$
II=\underbrace{\left[\int_0^1\left(\frac{1}{2}\left(\hat{u}_1^2+\hat{u}_2^2\right)U_1+\left(U_1\hat{u}_1+U_2\hat{u}_2\right)\hat{u}_1\right)\mathrm{d}y\right]_{x=-L_u}^{x=L_0+L_d}}_{\hat{F}_f}. \tag{4.4.15}
$$

The above term is denoted as $\hat{F}_f$, the net perturbation kinetic flux extracted from the mean flow. For III, we again use the divergence theorem to obtain

$$
\begin{aligned}
III=&\int_{\partial\bar{\Omega}_u}\left[-\left(\left(\hat{p}\hat{\mathbf{u}}\right)\cdot\mathbf{g}_1\right)\right]\mathrm{d}S+\int_{\partial\bar{\Omega}_d}\left[\left(\hat{p}\hat{\mathbf{u}}\right)\cdot\mathbf{g}_1\right]\mathrm{d}S+\int_{\partial\bar{\Omega}_b}\left[\left(\hat{p}\hat{\mathbf{u}}\right)\cdot\mathbf{N}\right]\mathrm{d}S,\\
=&\underbrace{\left[\int_0^1\left(-\hat{p}\hat{u}_1\right)\mathrm{d}y\right]_{x=-L_u}^{x=L_0+L_d}}_{\hat{P}_f}+\int_{\partial\bar{\Omega}_b}\left[\left(\hat{p}\hat{\mathbf{u}}\right)\cdot\mathbf{N}\right]\mathrm{d}S.
\end{aligned}
\tag{4.4.16}
$$

We denote the first term as $\hat{P}_f$, the rate of working of the perturbation pressure force at the channel ends. The remaining term is utilized below.

For IV, we first divide it into two portions (labeled B_1+B_2 as follows) and then consider each in turn

$$
IV=\underbrace{R^{-1}\int_{\bar{\Omega}}\left[\left(\nabla\cdot\left(\nabla\hat{\mathbf{u}}\right)\right)\cdot\hat{\mathbf{u}}\right]\mathrm{d}A}_{B_1}+\underbrace{R^{-1}\int_{\bar{\Omega}}\left[\left(\nabla\cdot\left(\nabla^{\mathrm{T}}\hat{\mathbf{u}}\right)\right)\cdot\hat{\mathbf{u}}\right]\mathrm{d}A}_{B_2}. \tag{4.4.17}
$$

For B_1, we apply the identity $(\nabla\cdot\mathbf{A})\cdot\mathbf{u}=\nabla\cdot\left(\mathbf{A}^{\mathrm{T}}\mathbf{u}\right)-\mathrm{Tr}\left(\mathbf{A}^{\mathrm{T}}\nabla\mathbf{u}\right)$ (here $\mathbf{A}$ is a 2×2 matrix to obtain,

$$
B_1=R^{-1}\int_{\bar{\Omega}}\nabla\cdot\left(\left(\nabla\hat{\mathbf{u}}^{\mathrm{T}}\right)\hat{\mathbf{u}}\right)\mathrm{d}A-R^{-1}\int_{\bar{\Omega}}\mathrm{Tr}\left(\left(\nabla\hat{\mathbf{u}}\right)^{\mathrm{T}}\nabla\hat{\mathbf{u}}\right)\mathrm{d}A; \tag{4.4.18}
$$

applying the divergence theorem to the first term we obtain,

$$
B_1=R^{-1}\int_{\partial\bar{\Omega}_u}\left[-\left(\left(\nabla\hat{\mathbf{u}}\right)^{\mathrm{T}}\hat{\mathbf{u}}\right)\cdot\mathbf{g}_1\right]\mathrm{d}S+R^{-1}\int_{\partial\bar{\Omega}_d}\left[\left(\left(\nabla\hat{\mathbf{u}}\right)^{\mathrm{T}}\hat{\mathbf{u}}\right)\cdot\mathbf{g}_1\right]\mathrm{d}S
$$

$$
\begin{aligned}
&+R^{-1}\int_{\partial\bar{\Omega}_b}\left[\left((\nabla\hat{\mathbf{u}})^{\mathrm{T}}\hat{\mathbf{u}}\right)\cdot\mathbf{N}\right]\mathrm{d}S-R^{-1}\int_{\bar{\Omega}}\mathrm{Tr}\left((\nabla\hat{\mathbf{u}})^{\mathrm{T}}\nabla\hat{\mathbf{u}}\right)\mathrm{d}A,\\
&=\left[R^{-1}\int_0^1\left(\hat{u}_1\frac{\partial\hat{u}_1}{\partial x}+\hat{u}_2\frac{\partial\hat{u}_2}{\partial x}\right)\mathrm{d}y\right]_{x=-L_u}^{x=L_0+L_d}+R^{-1}\int_{\partial\bar{\Omega}_b}\left[\left((\nabla\hat{\mathbf{u}})^{\mathrm{T}}\hat{\mathbf{u}}\right)\cdot\mathbf{N}\right]\mathrm{d}S\\
&-R^{-1}\int_{\bar{\Omega}}\mathrm{Tr}\left((\nabla\hat{\mathbf{u}})^{\mathrm{T}}\nabla\hat{\mathbf{u}}\right)\mathrm{d}A. \qquad (4.4.19)
\end{aligned}
$$

The first term in (4.4.19) cancels since we assume parallel flow at the inlet and outlet boundaries and we write the last two terms in vector form. Therefore, we have,

$$
B_1=R^{-1}\int_{\partial\bar{\Omega}_b}\left[\left(\left(\nabla\hat{\mathbf{u}}^{\mathrm{T}}\right)\hat{\mathbf{u}}\right)\cdot\mathbf{N}\right]\mathrm{d}S-R^{-1}\int_{\bar{\Omega}}\mathrm{Tr}\left((\nabla\hat{\mathbf{u}})^{\mathrm{T}}(\nabla\hat{\mathbf{u}})\right)\mathrm{d}A. \qquad (4.4.20)
$$

Similar to B_1, we again apply the identity $\left(\nabla\cdot\mathbf{A}^{\mathrm{T}}\right)\cdot\mathbf{u}=\nabla\cdot(\mathbf{A}\mathbf{u})-\mathrm{Tr}\left(\mathbf{A}\nabla\mathbf{u}\right)$ to obtain,

$$
B_2=R^{-1}\int_{\bar{\Omega}}\nabla\cdot\left((\nabla\hat{\mathbf{u}})\hat{\mathbf{u}}\right)\mathrm{d}A-R^{-1}\int_{\bar{\Omega}}\mathrm{Tr}\left((\nabla\hat{\mathbf{u}})(\nabla\hat{\mathbf{u}})\right)\mathrm{d}A. \qquad (4.4.21)
$$

We then apply the divergence theorem to the first term to obtain,

$$
\begin{aligned}
B_2=&R^{-1}\int_{\partial\bar{\Omega}_u}-\left[((\nabla\hat{\mathbf{u}})\hat{\mathbf{u}})\cdot\mathbf{g}_1\right]\mathrm{d}S+R^{-1}\int_{\partial\bar{\Omega}_d}\left[\left((\nabla\hat{\mathbf{u}})\hat{\mathbf{u}}\right)\cdot\mathbf{g}_1\right]\mathrm{d}S\\
&+R^{-1}\int_{\partial\bar{\Omega}_b}\left[\left((\nabla\hat{\mathbf{u}})\hat{\mathbf{u}}\right)\cdot\mathbf{N}\right]\mathrm{d}S-R^{-1}\int_{\bar{\Omega}}\mathrm{Tr}\left((\nabla\hat{\mathbf{u}})(\nabla\hat{\mathbf{u}})\right)\mathrm{d}A, \qquad (4.4.22)
\end{aligned}
$$

where the first two terms vanish as we assume the inlet and outlet flow are parallel to the rigid wall, so we have,

$$
B_2=R^{-1}\int_{\partial\bar{\Omega}_b}\left[\left((\nabla\hat{\mathbf{u}})\hat{\mathbf{u}}\right)\cdot\mathbf{N}\right]\mathrm{d}S-R^{-1}\int_{\bar{\Omega}}\mathrm{Tr}\left((\nabla\hat{\mathbf{u}})(\nabla\hat{\mathbf{u}})\right)\mathrm{d}A. \qquad (4.4.23)
$$

We obtain term IV when we compute the sum of B_1+B_2, in the form

$$
IV=B_1+B_2=R^{-1}\int_{\partial\bar{\Omega}_b}\left[\left((\nabla\hat{\mathbf{u}}+\nabla\hat{\mathbf{u}}^{\mathrm{T}})\hat{\mathbf{u}}\right)\cdot\mathbf{N}\right]\mathrm{d}S-\underbrace{R^{-1}\int_{\bar{\Omega}}\mathrm{Tr}\left(\left(\nabla\hat{\mathbf{u}}^{\mathrm{T}}+\nabla\hat{\mathbf{u}}\right)\nabla\hat{\mathbf{u}}\right)\mathrm{d}A}_{\hat{D}_f}. \qquad (4.4.24)
$$

We denote the second term in (4.4.24) as $\hat{D}_f$, the energy loss due to viscous dissipation in the perturbation.

We then gather the remaining terms (all evaluated on $\partial\bar{\Omega}_b$) in II and IV to obtain $\hat{E}_f$; after rearrangement we have,

$$
\hat{E}_f=\int_{\partial\bar{\Omega}_b}\left(-\hat{p}\hat{\mathbf{u}}\cdot\mathbf{N}+R^{-1}\left(\left(\nabla\hat{\mathbf{u}}^{\mathrm{T}}+\nabla\hat{\mathbf{u}}\right)\hat{\mathbf{u}}\right)\cdot\mathbf{N}\right)\mathrm{d}S
$$

$$= \int_{\partial\bar{\Omega}_b} \left[\left(\left(-p\mathbf{I} + R^{-1}\left(\nabla\hat{\mathbf{u}}^{\mathrm{T}} + \nabla\hat{\mathbf{u}}\right)\right)\hat{\mathbf{u}} \right) \cdot \mathbf{N} \right] \mathrm{d}S. \tag{4.4.25}$$

We use the linearised expression for the fluid stress tensor $\hat{\boldsymbol{\sigma}}$ (detail in *Sec*. *A*.5) to obtain,

$$\hat{E}_f = \int_{\partial\bar{\Omega}_b} \left[(\hat{\boldsymbol{\sigma}}\hat{\mathbf{u}}) \cdot \mathbf{N} \right] \mathrm{d}S. \tag{4.4.26}$$

Gathering all the terms in (4.4.12), we obtain the perturbation fluid energy budget at $O(\varepsilon^2)$ as,

$$\hat{K}_f + \hat{F}_f - \hat{P}_f - \hat{E}_f + \hat{D}_f - \hat{S}_f = 0, \tag{4.4.27}$$

where,

$$\hat{K}_f = \frac{\partial}{\partial t} \int_{\bar{\Omega}} \frac{1}{2} \left(\hat{u}_1^2 + \hat{u}_2^2 \right) \mathrm{d}A, \tag{4.4.28}$$

$$\hat{F}_f = \left[\int_0^1 \frac{1}{2} (\hat{u}_1^2 + \hat{u}_2^2) U_1 + (\hat{u}_1 U_1 + \hat{u}_2 U_2) \hat{u}_1 \, \mathrm{d}y \right]_{x=-L_u}^{x=L_0+L_d}, \tag{4.4.29}$$

$$\hat{P}_f = \left[\int_0^1 (-\hat{p}\hat{u}_1) \, \mathrm{d}y \right]_{x=-L_u}^{x=L_0+L_d}, \tag{4.4.30}$$

$$\hat{E}_f = \int_{\partial\bar{\Omega}_b} \left[(\hat{\boldsymbol{\sigma}}\hat{\mathbf{u}}) \cdot \mathbf{N} \right] \mathrm{d}S, \tag{4.4.31}$$

$$\hat{D}_f = R^{-1} \int_{\bar{\Omega}} \mathrm{Tr}\left(\left(\nabla\hat{\mathbf{u}}^{\mathrm{T}} + \nabla\hat{\mathbf{u}} \right) \nabla\hat{\mathbf{u}} \right) \mathrm{d}A, \tag{4.4.32}$$

$$\hat{S}_f = \int_{\bar{\Omega}} \left[U_1 \left(\hat{u}_1 \frac{\partial \hat{u}_1}{\partial x} + \hat{u}_2 \frac{\partial \hat{u}_1}{\partial y} \right) + U_2 \left(\hat{u}_1 \frac{\partial \hat{u}_2}{\partial x} + \hat{u}_2 \frac{\partial \hat{u}_2}{\partial y} \right) \right] \mathrm{d}A. \tag{4.4.33}$$

Here $\hat{K}_f$ is the rate of working of perturbation kinetic energy, $\hat{F}_f$ is the net perturbation kinetic energy flux extracted from the main flow, $\hat{P}_f$ is the rate of working of the perturbed pressure force at the channel ends, $\hat{E}_f$ is the rate of working of perturbation fluid stresses on the beam, $\hat{D}_f$ is the energy loss due to viscous dissipation in the perturbation, and $\hat{S}_f$ is the work done by non-linear Reynolds stresses. These terms are all analogous to fully non-linear energy budget (3.5.11-3.5.16) except for the rate of working of non-linear Reynolds stress.
The perturbation energy loss due to viscous dissipation $\hat{D}_f$ is non-negative, since it can be manipulated into the form,

$$\hat{D}_f = R^{-1} \int_{\bar{\Omega}} \left[2 \left(\frac{\partial \hat{u}_1}{\partial x} \right)^2 + 2 \left(\frac{\partial \hat{u}_2}{\partial y} \right)^2 + \left(\frac{\partial \hat{u}_1}{\partial y} + \frac{\partial \hat{u}_2}{\partial x} \right)^2 \right] \mathrm{d}A. \tag{4.4.34}$$

Similar to the fully non-linear energy budget, we reverse the position of $\hat{\mathbf{u}}$ and $\mathbf{N}$ since $\hat{\boldsymbol{\sigma}} = \hat{\boldsymbol{\sigma}}^{\mathrm{T}}$

(detailed derivation see appendix $A.5$) to obtain,

$$\hat{E}_f = \int_{\partial\bar{\Omega}_b} [(\hat{\boldsymbol{\sigma}}\mathbf{N})\cdot\hat{\mathbf{u}}]\,\mathrm{d}S,$$

now we apply the boundary condition (4.2.20) on the steady beam to obtain,

$$\hat{E}_f = \int_{\partial\bar{\Omega}_b} \left[(\hat{\boldsymbol{\sigma}}\mathbf{N})\cdot\hat{\mathbf{u}}_b^{(c)}\right]\mathrm{d}S - \int_{\partial\bar{\Omega}_b} (\hat{\boldsymbol{\sigma}}\mathbf{N})\cdot\left(\hat{x}_b^{(c)}\frac{\partial\mathbf{U}}{\partial x} + \hat{y}_b^{(c)}\frac{\partial\mathbf{U}}{\partial y}\right)\mathrm{d}S. \tag{4.4.35}$$

We then substitute (4.2.46) into $\hat{E}_f$ (4.4.35) to obtain,

$$\begin{aligned}
\hat{E}_f = &\underbrace{\int_{\partial\bar{\Omega}_b} c_\kappa\left(K^{(c)}\frac{\Lambda^{(c)}K^{(c)}}{\partial S}\breve{u}_{b1}^{(c)} - \frac{\partial^2(\Lambda^{(c)}K^{(c)})}{\partial S^2}\breve{u}_{b2}^{(c)}\right)\mathrm{d}S}_{I}\\
&+\underbrace{\int_{\partial\bar{\Omega}_b} c_\kappa\left(K^{(c)}\frac{\partial(\Lambda^{(c)}\hat{\boldsymbol{\kappa}}^{(c)}+\hat{\boldsymbol{\lambda}}^{(c)}K^{(c)})}{\partial S}\hat{u}_{b1}^{(c)} + \hat{\boldsymbol{\kappa}}^{(c)}\frac{\partial(\Lambda^{(c)}K^{(c)})}{\partial S}\hat{u}_{b1}^{(c)}\right)}_{IIa}\\
&+\underbrace{\int_{\partial\bar{\Omega}_b} c_\kappa\left(-\frac{\partial^2(\Lambda^{(c)}\hat{\boldsymbol{\kappa}}^{(c)}+\hat{\boldsymbol{\lambda}}^{(c)}K^{(c)})}{\partial S^2}\hat{u}_{b2}^{(c)}\right)\mathrm{d}S}_{IIb}\\
&+\underbrace{\int_{\partial\bar{\Omega}_b} c_\lambda\left(\frac{\partial\Lambda^{(c)}}{\partial S}\breve{u}_{b1}^{(c)} + K^{(c)}(\Lambda^{(c)}-1)\breve{u}_{b2}^{(c)}\right)\mathrm{d}S}_{III}\\
&+\underbrace{\int_{\partial\bar{\Omega}_b} c_\lambda\left(\frac{\partial\hat{\boldsymbol{\lambda}}^{(c)}}{\partial S}\hat{u}_{b1}^{(c)} + K^{(c)}\hat{\boldsymbol{\lambda}}^{(c)}\hat{u}_{b2}^{(c)} + \hat{\boldsymbol{\kappa}}^{(c)}(\Lambda^{(c)}-1)\hat{u}_{b2}^{(c)}\right)\mathrm{d}S}_{IV}\\
&+\underbrace{\int_{\partial\bar{\Omega}_b} T\left(K^{(c)}\breve{u}_{b2}^{(c)} + \hat{\boldsymbol{\kappa}}^{(c)}\hat{u}_{b2}^{(c)}\right)\mathrm{d}S}_{V} - \underbrace{\int_{\partial\bar{\Omega}_b}\left(p_e\breve{u}_{b2}\right)\mathrm{d}S}_{VI}\\
&-\underbrace{\int_{\partial\bar{\Omega}_b}\left[(\boldsymbol{\Sigma}\mathbf{N})\cdot\breve{\mathbf{u}}_b^{(c)} + (\boldsymbol{\Sigma}\hat{\mathbf{n}})\cdot\hat{\mathbf{u}}_b + \left(\left(\hat{x}_b^{(c)}\frac{\partial\boldsymbol{\Sigma}}{\partial x} + \hat{y}_b^{(c)}\frac{\partial\boldsymbol{\Sigma}}{\partial y}\right)\mathbf{N}\right)\cdot\hat{\mathbf{u}}_b^{(c)}\right]\mathrm{d}S}_{VII}\\
&-\underbrace{\int_{\partial\bar{\Omega}_b}(\hat{\boldsymbol{\sigma}}\mathbf{N})\cdot\left(\hat{x}_b^{(c)}\frac{\partial\mathbf{U}}{\partial x} + \hat{y}_b^{(c)}\frac{\partial\mathbf{U}}{\partial y}\right)\mathrm{d}S}_{VIII},
\end{aligned} \tag{4.4.36}$$

we label these terms $I-VIII$ (as underbraces below) and consider each in turn.

For terms $I-V$, we need to use the following linearised identities (note the third and sixth

identities are expressed in reference (material) description),

$$\frac{\partial \hat{u}_{b1}^{(c)}}{\partial S} = \Lambda^{-1}\frac{\partial \hat{\lambda}^{(c)}}{\partial t} + K^{(c)}\hat{u}_{b2}^{(c)}, \qquad (S \in \partial\bar{\Omega}_b), \quad (4.4.37)$$

$$\frac{\partial \hat{u}_{b2}^{(c)}}{\partial S} = \frac{\partial \hat{\theta}^{(c)}}{\partial t} - K^{(c)}\hat{u}_{b1}^{(c)}, \qquad (S \in \partial\bar{\Omega}_b), \quad (4.4.38)$$

$$\frac{\partial \hat{\theta}}{\partial l} = \Lambda\hat{\kappa} + K\hat{\lambda}, \qquad (0 \le l \le L_0). \quad (4.4.39)$$

$$\frac{\partial \breve{u}_{b1}^{(c)}}{\partial S} = \frac{1}{\Lambda^{(c)}}\frac{\partial \breve{\lambda}^{(c)}}{\partial t} - \frac{\hat{\lambda}^{(c)}}{\left(\Lambda^{(c)}\right)^2}\frac{\partial \hat{\lambda}^{(c)}}{\partial t} + K^{(c)}\breve{u}_{b2}^{(c)} + \hat{\kappa}^{(c)}\hat{u}_{b2}^{(c)}, \qquad (S \in \partial\bar{\Omega}_b), \quad (4.4.40)$$

$$\frac{\partial \breve{u}_{b2}^{(c)}}{\partial S} = \frac{\partial \breve{\theta}^{(c)}}{\partial t} - K^{(c)}\breve{u}_{b1}^{(c)} - \hat{\kappa}^{(c)}\hat{u}_{b1}^{(c)}, \qquad (S \in \partial\bar{\Omega}_b), \quad (4.4.41)$$

$$\frac{\partial \breve{\theta}}{\partial l} = \Lambda\breve{\kappa} + \hat{\lambda}\,\hat{\kappa} + \breve{\lambda}K, \qquad (0 \le l \le L_0). \quad (4.4.42)$$

detailed derivation of linearization of these identities see appendix A.6.
For I, we use integration by parts to obtain,

$$\begin{aligned} I = &\int_{\partial\bar{\Omega}_b} c_\kappa^{(c)}\left(K^{(c)}\frac{\partial(\Lambda^{(c)}K^{(c)})}{\partial S}\breve{u}_{b1}^{(c)}\right)\mathrm{d}S - c_\kappa\left[\frac{\partial(\Lambda^{(c)}K^{(c)})}{\partial S}\breve{u}_{b2}^{(c)}\right]_0^{S_0} \\ &+ \int_{\partial\bar{\Omega}_b} c_\kappa\left(\frac{\partial(\Lambda^{(c)}K^{(c)})}{\partial S}\frac{\partial \breve{u}_{b2}^{(c)}}{\partial S}\right)\mathrm{d}S, \end{aligned}$$

where $S = 0$ and $S = S_0$ are two end points of the steady beam (*i.e.* $S(L_0) = S_0$). The second term then vanish as due to the boundary condition (4.2.44). Using (4.4.41) for the last term we have,

$$\begin{aligned} I = &\int_{\partial\bar{\Omega}_b} c_\kappa\frac{\partial(\Lambda^{(c)}K^{(c)})}{\partial S}\left(\frac{\partial \breve{\theta}^{(c)}}{\partial t} - (K^{(c)}\breve{u}_{b1}^{(c)} + \hat{\kappa}^{(c)}\hat{u}_{b1}^{(c)})\right)\mathrm{d}S \\ &+ \int_{\partial\bar{\Omega}_b} c_\kappa\left(K^{(c)}\frac{\partial(\Lambda^{(c)}K^{(c)})}{\partial S}\breve{u}_{b1}^{(c)}\right)\mathrm{d}S, \\ = &\int_{\partial\bar{\Omega}_b} c_\kappa\left(\frac{\partial(\Lambda^{(c)}K^{(c)})}{\partial S}\frac{\partial \breve{\theta}^{(c)}}{\partial t}\right)\mathrm{d}S - \int_{\partial\bar{\Omega}_b} c_\kappa\left[\frac{\partial(\Lambda^{(c)}K^{(c)})}{\partial S}(\hat{\kappa}^{(c)}\hat{u}_{b1}^{(c)})\right]\mathrm{d}S, \\ = &c_\kappa\left[(\Lambda^{(c)}K^{(c)})\frac{\partial \breve{\theta}^{(c)}}{\partial t}\right]_0^{S_0} - \int_{\partial\bar{\Omega}_b}\left[c_\kappa(\Lambda^{(c)}K^{(c)})\frac{\partial}{\partial S}\left(\frac{\partial \breve{\theta}^{(c)}}{\partial t}\right)\right]\mathrm{d}S \\ &- \int_{\partial\bar{\Omega}_b} c_\kappa\left[\frac{\partial(\Lambda^{(c)}K^{(c)})}{\partial S}(\hat{\kappa}^{(c)}\hat{u}_{b1}^{(c)})\right]\mathrm{d}S. \end{aligned}$$

The first term then disappears due to identity (4.2.45). We then pull-back the second term to the

reference (material) description to obtain,

$$
\begin{aligned}
I &= -\int_0^{L_0}\left[c_\kappa(\Lambda K)\frac{\partial}{\partial l}\left(\frac{\partial \breve{\theta}}{\partial t}\right)\right]\mathrm{d}l - \int_{\partial\bar{\Omega}_b} c_\kappa\left(\frac{\partial(\Lambda^{(c)}K^{(c)})}{\partial S}(\hat{\kappa}^{(c)}\hat{u}_{b1}^{(c)})\right)\mathrm{d}S,\\
&= -\int_0^{L_0}\left[c_\kappa(\Lambda K)\frac{\partial}{\partial t}\left(\frac{\partial \breve{\theta}}{\partial l}\right)\right]\mathrm{d}l - \int_{\partial\bar{\Omega}_b} c_\kappa\left(\frac{\partial(\Lambda^{(c)}K^{(c)})}{\partial S}(\hat{\kappa}^{(c)}\hat{u}_{b1}^{(c)})\right)\mathrm{d}S.
\end{aligned}
$$

We apply identity (4.4.42) to the first term to obtain,

$$
\begin{aligned}
I &= -\int_0^{L_0}\left[c_\kappa(\Lambda K)\frac{\partial}{\partial t}\left(\Lambda\breve{\kappa}+\breve{\lambda}K+\hat{\lambda}\hat{\kappa}\right)\right]\mathrm{d}l - \int_{\partial\bar{\Omega}_b} c_\kappa\left(\frac{\partial(\Lambda^{(c)}K^{(c)})}{\partial S}(\hat{\kappa}^{(c)}\hat{u}_{b1}^{(c)})\right)\mathrm{d}S,\\
&= -\frac{\partial}{\partial t}\int_0^{L_0}\left[c_\kappa(\Lambda K)\left(\Lambda\breve{\kappa}+\breve{\lambda}K+\hat{\lambda}\hat{\kappa}\right)\right]\mathrm{d}l - \int_{\partial\bar{\Omega}_b} c_\kappa\left(\frac{\partial(\Lambda^{(c)}K^{(c)})}{\partial S}(\hat{\kappa}^{(c)}\hat{u}_{b1}^{(c)})\right)\mathrm{d}S,
\end{aligned}
\tag{4.4.43}
$$

where we have taken the time derivative outside the integral as Λ, K are independent of time. In this final form, the first term is a complete time derivative (in the material description) and the second term will be canceled below.
Similarly, for II applying integration by two parts, we have,

$$
\begin{aligned}
II = &\int_{\partial\bar{\Omega}_b} c_\kappa\left(K^{(c)}\frac{\partial(\Lambda^{(c)}\hat{\kappa}^{(c)}+\hat{\lambda}^{(c)}K^{(c)})}{\partial S}\hat{u}_{b1}^{(c)} + \hat{\kappa}^{(c)}\frac{\partial(\Lambda^{(c)}K^{(c)})}{\partial S}\hat{u}_{b1}^{(c)}\right)\mathrm{d}S\\
&- c_\kappa\left[\frac{\partial(\Lambda^{(c)}\hat{\kappa}^{(c)}+\hat{\lambda}^{(c)}K^{(c)})}{\partial S}\hat{u}_{b1}^{(c)}\right]_0^{S_0} + \int_{\partial\bar{\Omega}_b}\left[c_\kappa\frac{\partial(\Lambda^{(c)}\hat{\kappa}^{(c)}+\hat{\lambda}^{(c)}K^{(c)})}{\partial S}\frac{\partial\hat{u}_{b2}^{(c)}}{\partial S}\right]\mathrm{d}S,
\end{aligned}
$$

the second term cancels due to the boundary condition (4.2.26). Applying identity (4.4.38) to the the final term, we obtain,

$$
\begin{aligned}
II = &\int_{\partial\bar{\Omega}_b} c_\kappa\left(K^{(c)}\frac{\partial(\Lambda^{(c)}\hat{\kappa}^{(c)}+\hat{\lambda}^{(c)}K^{(c)})}{\partial S}\hat{u}_{b1}^{(c)} + \hat{\kappa}^{(c)}\frac{\partial(\Lambda^{(c)}K^{(c)})}{\partial S}\hat{u}_{b1}^{(c)}\right)\mathrm{d}S\\
&+ \int_{\partial\bar{\Omega}_b} c_\kappa\frac{\partial(\Lambda^{(c)}\hat{\kappa}^{(c)}+\hat{\lambda}^{(c)}K^{(c)})}{\partial S}\left(\frac{\partial\hat{\theta}^{(c)}}{\partial t} - K^{(c)}\hat{u}_{b1}^{(c)}\right)\mathrm{d}S,\\
= &\int_{\partial\bar{\Omega}_b} c_\kappa\left(\hat{\kappa}^{(c)}\frac{\partial(\Lambda^{(c)}K^{(c)})}{\partial S}\hat{u}_{b1}^{(c)}\right)\mathrm{d}S + \int_{\partial\bar{\Omega}_b} c_\kappa\left(\frac{\partial(\Lambda^{(c)}\hat{\kappa}^{(c)}+\hat{\lambda}^{(c)}K^{(c)})}{\partial S}\frac{\partial\hat{\theta}^{(c)}}{\partial t}\right)\mathrm{d}S,\\
= &\int_{\partial\bar{\Omega}_b} c_\kappa\left(\hat{\kappa}^{(c)}\frac{\partial(\Lambda^{(c)}K^{(c)})}{\partial S}\hat{u}_{b1}^{(c)}\right)\mathrm{d}S + c_\kappa\left[\left(\Lambda^{(c)}\hat{\kappa}^{(c)}+\hat{\lambda}^{(c)}K^{(c)}\right)\frac{\partial\hat{\theta}^{(c)}}{\partial t}\right]_0^{S_0}\\
&- \int_{\partial\bar{\Omega}_b} c_\kappa\left(\Lambda^{(c)}\hat{\kappa}^{(c)}+\hat{\lambda}^{(c)}K^{(c)}\right)\frac{\partial}{\partial S}\left(\frac{\partial\hat{\theta}^{(c)}}{\partial t}\right)\mathrm{d}S.
\end{aligned}
$$

The second term disappears due to the boundary condition (4.2.27). We again pull-back the third term to the reference (material) description to obtain,

$$\begin{aligned} II &= \int_{\partial\bar{\Omega}_b} c_\kappa \left(\hat{\kappa}^{(c)} \frac{\partial(\Lambda^{(c)} K^{(c)})}{\partial S} \hat{u}_{b1}^{(c)} \right) \mathrm{d}S - \int_0^{L_0} c_\kappa \left(\Lambda\hat{\kappa} + \hat{\lambda} K \right) \frac{\partial}{\partial l} \left(\frac{\partial \hat{\theta}}{\partial t} \right) \mathrm{d}l, \\ &= -\int_0^{L_0} c_\kappa \left(\Lambda\hat{\kappa} + \hat{\lambda} K \right) \frac{\partial}{\partial t} \left(\frac{\partial \hat{\theta}}{\partial l} \right) \mathrm{d}l + \int_{\partial\bar{\Omega}_b} c_\kappa \left(\hat{\kappa}^{(c)} \frac{\partial(\Lambda^{(c)} K^{(c)})}{\partial S} \hat{u}_{b1}^{(c)} \right) \mathrm{d}S. \end{aligned}$$

We then apply (4.4.39) to the first term to obtain,

$$\begin{aligned} II &= -\int_0^{L_0} c_\kappa \left(\Lambda\hat{\kappa} + \hat{\lambda} K \right) \frac{\partial}{\partial t} \left(\Lambda\hat{\kappa} + \hat{\lambda} K \right) \mathrm{d}l + \int_{\partial\bar{\Omega}_b} c_\kappa \left(\hat{\kappa}^{(c)} \frac{\partial(\Lambda^{(c)} K^{(c)})}{\partial S} \hat{u}_{b1}^{(c)} \right) \mathrm{d}S, \\ &= -\frac{\partial}{\partial t} \int_0^{L_0} \frac{c_\kappa}{2} \left(\Lambda\hat{\kappa} + \hat{\lambda} K \right)^2 \mathrm{d}l + \int_{\partial\bar{\Omega}_b} c_\kappa \left(\hat{\kappa}^{(c)} \frac{\partial(\Lambda^{(c)} K^{(c)})}{\partial S} \hat{u}_{b1}^{(c)} \right) \mathrm{d}S. \end{aligned} \tag{4.4.44}$$

The final terms in I and II cancel each other when we compute their sum $(I+II)$; after rearrangement we have,

$$(I+II) = -\underbrace{\frac{\partial}{\partial t} \int_0^{L_0} c_\kappa \Lambda K \left(\Lambda\breve{\kappa} + \breve{\lambda} K \right) \mathrm{d}l}_{\breve{U}_\kappa} - \underbrace{\frac{\partial}{\partial t} \int_0^{L_0} c_\kappa \left((\Lambda K) \left(\hat{\lambda}\hat{\kappa} \right) + \frac{1}{2} \left(\Lambda\hat{\kappa} + \hat{\lambda} K \right)^2 \right) \mathrm{d}l}_{\hat{U}_\kappa}. \tag{4.4.45}$$

We denote the above terms as $\breve{U}_\kappa$, the rate of working of bending stresses that contains the second order variables and $\hat{U}_\kappa$, the rate of working of bending stresses that contains the first order variables.

Similarly, for III, we use integration by parts to obtain,

$$III = c_\lambda \left[\Lambda^{(c)} \breve{u}_{b1}^{(c)} \right]_0^{S_0} - c_\lambda \int_{\partial\bar{\Omega}_b} \left(\Lambda^{(c)} \frac{\partial \breve{u}_{b1}^{(c)}}{\partial S} \right) \mathrm{d}S + c_\lambda \int_{\partial\bar{\Omega}_b} \left(K^{(c)} \left(\Lambda^{(c)} - 1 \right) \breve{u}_{b2}^{(c)} \right) \mathrm{d}S;$$

the first term disappears due to the boundary condition (4.2.44) and we substitute (4.4.40) to the second term to obtain,

$$\begin{aligned} III =& -c_\lambda \int_{\partial\bar{\Omega}_b} \Lambda^{(c)} \left(\frac{1}{\Lambda^{(c)}} \frac{\partial \breve{\lambda}^{(c)}}{\partial t} - \frac{\hat{\lambda}^{(c)}}{\left(\Lambda^{(c)}\right)^2} \frac{\partial \hat{\lambda}^{(c)}}{\partial t} + K^{(c)} \breve{u}_{b2}^{(c)} + \hat{\kappa}^{(c)} \hat{u}_{b2}^{(c)} \right) \mathrm{d}S \\ &+ c_\lambda \int_{\partial\bar{\Omega}_b} \left(K^{(c)} \left(\Lambda^{(c)} - 1 \right) \breve{u}_{b2}^{(c)} \right) \mathrm{d}S, \\ =& c_\lambda \int_{\partial\bar{\Omega}_b} \left(\frac{1}{\Lambda^{(c)}} \hat{\lambda}^{(c)} \frac{\partial \hat{\lambda}^{(c)}}{\partial t} - \Lambda^{(c)} \hat{\kappa}^{(c)} \hat{u}_{b2}^{(c)} \right) \mathrm{d}S - c_\lambda \int_{\partial\bar{\Omega}_b} \left(\frac{\partial \breve{\lambda}^{(c)}}{\partial t} + K^{(c)} \breve{u}_{b2}^{(c)} \right) \mathrm{d}S. \end{aligned} \tag{4.4.46}$$

For IV, we use integration by parts to obtain,

$$\begin{aligned} IV =& c_\lambda \left[\hat{\lambda}^{(c)}\hat{u}_{b1}^{(c)}\right]_0^{S_0} - c_\lambda \int_{\partial\bar{\Omega}_b} \left(\hat{\lambda}^{(c)}\frac{\partial \hat{u}_{b1}^{(c)}}{\partial S}\right) \mathrm{d}S \\ &+ c_\lambda \int_{\partial\bar{\Omega}_b} \left(K^{(c)}\hat{\lambda}^{(c)}\hat{u}_{b2}^{(c)} + \hat{\kappa}^{(c)}(\Lambda^{(c)}-1)\hat{u}_{b2}^{(c)}\right) \mathrm{d}S; \end{aligned}$$

the first term cancels because of the boundary condition (4.2.26). We then apply identity (4.4.37) to the second term to obtain,

$$\begin{aligned} IV =& c_\lambda \int_{\partial\bar{\Omega}_b} \left(K^{(c)}\hat{\lambda}^{(c)}\hat{u}_{b2}^{(c)} + \hat{\kappa}^{(c)}(\Lambda^{(c)}-1)\hat{u}_{b2}^{(c)}\right) \mathrm{d}S \\ &- c_\lambda \int_{\partial\bar{\Omega}_b} \hat{\lambda}^{(c)} \left(\frac{1}{\Lambda^{(c)}}\frac{\partial \hat{\lambda}^{(c)}}{\partial t} + K^{(c)}\hat{u}_{b2}^{(c)}\right) \mathrm{d}S, \\ =& - c_\lambda \int_{\partial\bar{\Omega}_b} \left[\frac{\hat{\lambda}^{(c)}}{\Lambda^{(c)}}\frac{\partial \hat{\lambda}^{(c)}}{\partial t} - \hat{\kappa}^{(c)}\Lambda^{(c)}\hat{u}_{b2}^{(c)}\right] \mathrm{d}S - c_\lambda \int_{\partial\bar{\Omega}_b} \left(\hat{\kappa}^{(c)}\hat{u}_{b2}^{(c)}\right) \mathrm{d}S. \end{aligned} \tag{4.4.47}$$

The first term in III and IV cancels when we compute their sum $(III+IV)$. After rearrangement, we have

$$(III+IV) = -c_\lambda \int_{\partial\bar{\Omega}_b} \left(\kappa^{(c)}\breve{u}_{b2}^{(c)} + \hat{\kappa}^{(c)}\hat{u}_{b2}^{(c)}\right) \mathrm{d}S - c_\lambda \int_{\partial\bar{\Omega}_b} \frac{\partial \breve{\lambda}^{(c)}}{\partial t} \mathrm{d}S.$$

We apply identity (4.4.40) to the first term to obtain,

$$\begin{aligned} (III+IV) &= -c_\lambda \int_{\partial\bar{\Omega}_b} \left[\frac{\partial \breve{u}_{b1}^{(c)}}{\partial S} + \Lambda^{-2}\hat{\lambda}^{(c)}\frac{\partial \hat{\lambda}^{(c)}}{\partial t} - \frac{1}{\Lambda^{(c)}}\frac{\partial \breve{\lambda}^{(c)}}{\partial t}\right] \mathrm{d}S - c_\lambda \int_{\partial\bar{\Omega}_b} \frac{\partial \breve{\lambda}^{(c)}}{\partial t} \mathrm{d}S, \\ &= -c_\lambda \left[\breve{u}_{b1}^{(c)}\right]_0^{S_0} + c_\lambda \int_{\partial\bar{\Omega}_b} \left[-\frac{\hat{\lambda}^{(c)}}{\left(\Lambda^{(c)}\right)^2}\frac{\partial \hat{\lambda}^{(c)}}{\partial t} + \frac{1}{\Lambda^{(c)}}\frac{\partial \breve{\lambda}^{(c)}}{\partial t} - \frac{\partial \breve{\lambda}^{(c)}}{\partial t}\right] \mathrm{d}S. \end{aligned}$$

The first term cancels due to the boundary condition (4.2.44). We then pull-back the remaining term to the reference (material) description to obtain,

$$\begin{aligned} (III+IV) &= c_\lambda \int_0^{L_0} \left[-\Lambda^{-1}\hat{\lambda}\frac{\partial \hat{\lambda}}{\partial t} + (\Lambda-1)\frac{\partial \breve{\lambda}}{\partial t}\right] \mathrm{d}l, \\ &= -\frac{\partial}{\partial t}\int_0^{L_0} c_\lambda \left[\breve{\lambda}(\Lambda-1)\right] \mathrm{d}l - \frac{\partial}{\partial t}\int_0^{L_0} c_\lambda \left(\frac{1}{2}\Lambda^{-1}\hat{\lambda}^2\right) \mathrm{d}l. \end{aligned} \tag{4.4.48}$$

This is a complete time derivative in the material description.
For V, we apply identity (4.4.40) to obtain,

$$
\begin{aligned}
V &= \int_{\partial\bar{\Omega}_b} T\left[\frac{\partial \breve{u}_{b1}^{(c)}}{\partial S} + \frac{\hat{\lambda}^{(c)}}{\left(\Lambda^{(c)}\right)^2}\frac{\partial \hat{\lambda}^{(c)}}{\partial t} - \frac{1}{\Lambda^{(c)}}\frac{\partial \breve{\lambda}^{(c)}}{\partial t}\right] \mathrm{d}S, \\
&= -T\left[\breve{u}_{b1}^{(c)}\right]_0^{S_0} + \int_{\partial\bar{\Omega}_b} T\left[\frac{\hat{\lambda}^{(c)}}{\left(\Lambda^{(c)}\right)^2}\frac{\partial \hat{\lambda}^{(c)}}{\partial t} - \frac{1}{\Lambda^{(c)}}\frac{\partial \breve{\lambda}^{(c)}}{\partial t}\right] \mathrm{d}S,
\end{aligned}
$$

the first term disappears because of the boundary condition (4.2.44). We rewrite the remaining terms in the reference (material) description to obtain,

$$
V = -\frac{\partial}{\partial t}\int_0^{L_0}\left(T\breve{\lambda}\right)\mathrm{d}l + \frac{\partial}{\partial t}\int_0^{L_0} T\left(\frac{1}{2}\Lambda^{-1}\hat{\lambda}^2\right)\mathrm{d}l. \tag{4.4.49}
$$

We group terms for $-(III+IV+V)$ in the form,

$$
(III+IV+V) = -\underbrace{\frac{\partial}{\partial t}\int_0^{L_0}\left[c_\lambda\breve{\lambda}(\Lambda-1)+T\breve{\lambda}\right]\mathrm{d}l}_{\breve{U}_\lambda} - \underbrace{\frac{\partial}{\partial t}\int_0^{L_0}\left[\frac{1}{2}(c_\lambda - T)\Lambda^{-1}\hat{\lambda}^2\right]\mathrm{d}l}_{\hat{U}_\lambda}. \tag{4.4.50}
$$

We denote the above terms as $\breve{U}_\lambda$, the rate of working of extensional stresses that contains second order variables and $\hat{U}_\lambda$, the rate of working of extensional stresses that contains first order variables.

For VI, we change back to reference (material) description and apply $\breve{\mathbf{u}}_b = \partial\breve{\mathbf{x}}_b/\partial t$, we have,

$$
VI = \int_0^{L_0} p_e\Big(\frac{\partial\breve{\mathbf{x}}_b}{\partial t}\cdot\mathbf{N} + \hat{\mathbf{u}}_b\cdot\hat{\mathbf{n}}\Big)\Lambda\,\mathrm{d}l = \underbrace{\frac{\partial}{\partial t}\int_0^{L_0} p_e\Big(\breve{\mathbf{x}}_b\cdot\mathbf{N}\Big)\Lambda\,\mathrm{d}l}_{\breve{P}_e} + \underbrace{\int_0^{L_0} p_e\,(\hat{\mathbf{u}}_b\cdot\hat{\mathbf{n}})\,\Lambda\,\mathrm{d}l}_{\hat{P}_e}. \tag{4.4.51}
$$

We denote the two terms above as the rate of working of external pressure which contain the second order variables, $\breve{P}_e$, and the work done by external pressure that contains the first order variables, $\hat{P}_e$, respectively.

Similarly, for VII we change to reference (material) description and apply $\breve{\mathbf{u}}_b = \partial\breve{\mathbf{x}}_b/\partial t$ to obtain,

$$
\begin{aligned}
VII &= \int_0^{L_0}\left[(\boldsymbol{\Sigma}\mathbf{N})\cdot\frac{\partial\breve{\mathbf{x}}_b}{\partial t}\right]\Lambda\,\mathrm{d}l + \int_0^{L_0}\left[(\boldsymbol{\Sigma}\hat{\mathbf{n}})\cdot\hat{\mathbf{u}}_b + \left(\left(\hat{x}_b\frac{\partial\boldsymbol{\Sigma}}{\partial x} + \hat{y}_b\frac{\partial\boldsymbol{\Sigma}}{\partial y}\right)\mathbf{N}\right)\cdot\hat{\mathbf{u}}_b\right]\Lambda\,\mathrm{d}l, \\
&= \underbrace{\frac{\partial}{\partial t}\int_0^{L_0}\left[(\boldsymbol{\Sigma}\mathbf{N})\cdot\breve{\mathbf{x}}_b\right]\Lambda\,\mathrm{d}l}_{\breve{S}_b} + \underbrace{\int_0^{L_0}\left[(\boldsymbol{\Sigma}\hat{\mathbf{n}})\cdot\hat{\mathbf{u}}_b + \left(\left(\hat{x}_b\frac{\partial\boldsymbol{\Sigma}}{\partial x} + \hat{y}_b\frac{\partial\boldsymbol{\Sigma}}{\partial y}\right)\mathbf{N}\right)\cdot\hat{\mathbf{u}}_b\right]\Lambda\,\mathrm{d}l}_{\hat{S}_b}.
\end{aligned} \tag{4.4.52}
$$

We denote the above terms as $\check{S}_b$, the rate of working of fluid stress tensor on the wall that contains the second order variables and $\hat{S}_b$, the rate of working of the fluid stress tensor on the wall that contains first order variables.
We pull-back *VIII* to the reference (material) description. Since we can describe the shape of the deformed beam in the static state using Cartesian coordinates, where $\mathrm{d}x = \Lambda\cos(\Theta)\mathrm{d}l$, $\mathrm{d}y = \Lambda\sin(\Theta)\mathrm{d}l$; substituting these into *VIII* we obtain,

$$VIII = \int_0^{L_0}\left[\frac{\hat{x}_b}{\cos(\Theta)}(\hat{\boldsymbol{\sigma}}\mathbf{N})\cdot\frac{\partial\mathbf{U}}{\partial l}\right]\mathrm{d}l + \int_0^{L_0}\left[\frac{\hat{y}_b}{\sin(\Theta)}(\hat{\boldsymbol{\sigma}}\mathbf{N})\cdot\frac{\partial\mathbf{U}}{\partial l}\right]\mathrm{d}l.$$

We apply integration by parts to obtain,

$$\begin{aligned} VIII = &\left[\left(\frac{\hat{x}_b}{\cos(\Theta)}+\frac{\hat{y}_b}{\sin(\Theta)}\right)\left(\hat{\boldsymbol{\Sigma}}\mathbf{N}\right)\cdot\mathbf{U}\right]_0^{L_0} \\ &-\int_0^{L_0}\left[\frac{\partial}{\partial l}\left(\left(\frac{\hat{x}_b}{\cos(\Theta)}+\frac{\hat{y}_b}{\sin(\Theta)}\right)\left(\hat{\boldsymbol{\Sigma}}\mathbf{N}\right)\right)\cdot\mathbf{U}\right]\mathrm{d}l = 0, \end{aligned} \tag{4.4.53}$$

where we apply $\mathbf{U} = \mathbf{U}_b = 0$ on the static beam.
In total, we substitute $I - VIII$ into $\hat{E}_f$ in equation (4.4.36) to obtain,

$$\hat{E}_f = -\hat{U}_\kappa - \hat{U}_\lambda - \hat{P}_e - \hat{S}_b - \check{U}_\kappa - \check{U}_\lambda - \check{P}_e - \check{S}_b, \tag{4.4.54}$$

where,

$$\hat{U}_\kappa = \frac{\partial}{\partial t}\int_0^{L_0} c_\kappa\left[(\Lambda K)\left(\hat{\lambda}\hat{\kappa}\right)+\frac{1}{2}\left(\Lambda\hat{\kappa}+\hat{\lambda}K\right)^2\right]\mathrm{d}l, \tag{4.4.55}$$

$$\hat{U}_\lambda = \frac{\partial}{\partial t}\int_0^{L_0}\left[\frac{1}{2}(c_\lambda - T)\Lambda^{-1}\hat{\lambda}^2\right]\mathrm{d}l, \tag{4.4.56}$$

$$\hat{P}_e = \int_0^{L_0} p_e\,(\hat{\mathbf{u}}_b\cdot\hat{\mathbf{n}})\Lambda\,\mathrm{d}l, \tag{4.4.57}$$

$$\hat{S}_b = \int_0^{L_0}\left[(\boldsymbol{\Sigma}\hat{\mathbf{n}})\cdot\hat{\mathbf{u}}_b + \left(\left(\hat{x}_b\frac{\partial\boldsymbol{\Sigma}}{\partial x}+\hat{y}_b\frac{\partial\boldsymbol{\Sigma}}{\partial y}\right)\mathbf{N}\right)\cdot\hat{\mathbf{u}}_b\right]\Lambda\,\mathrm{d}l, \tag{4.4.58}$$

$$\check{U}_\kappa = \frac{\partial}{\partial t}\int_0^{L_0} c_\kappa(\Lambda K)\left(\Lambda\check{\kappa}+\check{\lambda}K\right)\mathrm{d}l, \tag{4.4.59}$$

$$\check{U}_\lambda = \frac{\partial}{\partial t}\int_0^{L_0}\left[c_\lambda\check{\lambda}(\Lambda-1)+T\check{\lambda}\right]\mathrm{d}l, \tag{4.4.60}$$

$$\check{P}_e = \frac{\partial}{\partial t}\int_0^{L_0} p_e\left(\check{\mathbf{x}}_b\cdot\mathbf{N}\right)\Lambda\,\mathrm{d}l, \tag{4.4.61}$$

$$\check{S}_b = \frac{\partial}{\partial t}\int_0^{L_0}\left[(\boldsymbol{\Sigma}\mathbf{N})\cdot\check{\mathbf{x}}_b\right]\Lambda\,\mathrm{d}l. \tag{4.4.62}$$

Here $\hat{U}_\kappa$ and $\check{U}_\kappa$ are the rate of working of bending stresses that contain the first order and second order variables respectively, $\hat{U}_\lambda$ and $\check{U}_\lambda$ are the rate of working of extensional stresses

that contain first order and second order variables respectively, $\hat{P}_e$ and $\breve{P}_e$ are the rate of working of external pressure that contain first and second order variables respectively while $\hat{S}_b$ and $\breve{S}_b$ are the work done by fluid stress that contain first order and second order variables respectively. Note that $\hat{U}_\kappa$, $\hat{U}_\lambda$, $\breve{P}_e$, $\breve{U}_\lambda$, $\breve{U}_\kappa$ and $\breve{S}_b$ will disappear upon integrating over a period of oscillation. We substitute (4.4.54) into the fluid energy budget to obtain the energy budget of the system and consider it over a period of oscillation. At $O(\varepsilon^2)$, we obtain the average energy budget (denoted by overline) for the linearised system in the form,

$$\bar{\hat{F}}_f - \bar{\hat{P}}_f + \bar{\hat{D}}_f - \bar{\hat{S}}_f + \bar{\hat{S}}_b + \bar{\hat{P}}_e = \bar{\hat{T}} = 0, \tag{4.4.63}$$

where,

$$\bar{\hat{F}}_f = \left[\int_0^1 \frac{1}{2}(\bar{\hat{u}}_1{}^2 + \bar{\hat{u}}_2{}^2)U_1 + (\bar{\hat{u}}_1 U_1 + \bar{\hat{u}}_2 U_2)\bar{\hat{u}}_1 \,\mathrm{d}y\right]_{x=-L_u}^{x=L_0+L_d}, \tag{4.4.64}$$

$$\hat{P}_f = \left[\int_0^1 \left(-\bar{\hat{p}}\bar{\hat{u}}_1\right) \mathrm{d}y\right]_{x=-L_u}^{x=L_0+L_d}, \tag{4.4.65}$$

$$\bar{\hat{D}}_f = R^{-1}\int_{\bar{\Omega}} \left[2\left(\frac{\partial \bar{\hat{u}}_1}{\partial x}\right)^2 + 2\left(\frac{\partial \bar{\hat{u}}_2}{\partial y}\right)^2 + \left(\frac{\partial \bar{\hat{u}}_1}{\partial y} + \frac{\partial \bar{\hat{u}}_2}{\partial x}\right)^2\right] \mathrm{d}A, \tag{4.4.66}$$

$$\bar{\hat{S}}_f = \int_{\bar{\Omega}} \left[U_1\left(\bar{\hat{u}}_1\frac{\partial \bar{\hat{u}}_1}{\partial x} + \bar{\hat{u}}_2\frac{\partial \bar{\hat{u}}_1}{\partial y}\right) + U_2\left(\bar{\hat{u}}_1\frac{\partial \bar{\hat{u}}_2}{\partial x} + \bar{\hat{u}}_2\frac{\partial \bar{\hat{u}}_2}{\partial y}\right)\right] \mathrm{d}A, \tag{4.4.67}$$

$$\bar{\hat{S}}_b = \int_0^{L_0} \left[\left(\boldsymbol{\Sigma}\bar{\hat{\mathbf{n}}}\right)\cdot\bar{\hat{\mathbf{u}}}_b + \left(\left(\bar{\hat{x}}_b\frac{\partial \boldsymbol{\Sigma}}{\partial x} + \bar{\hat{y}}_b\frac{\partial \boldsymbol{\Sigma}}{\partial y}\right)\mathbf{N}\right)\cdot\bar{\hat{\mathbf{u}}}_b\right] \Lambda \,\mathrm{d}l, \tag{4.4.68}$$

$$\bar{\hat{P}}_e = \int_0^{L_0} p_e\left(\bar{\hat{\mathbf{u}}}_b\cdot\bar{\hat{\mathbf{n}}}\right)\Lambda \,\mathrm{d}l. \tag{4.4.69}$$

4.5 Numerical method

In this section, we give a detailed explanation of the numerical methods we adopt to solve for the eigenvalue problem and construct the discretized form of the corresponding energy budget on each element.

4.5.1 Numerical methods for eigenvalue problem

We linearise the global vector of unknowns in the form $\mathbf{U}' = \bar{\mathbf{U}}' + \varepsilon\hat{\mathbf{U}}'$, where $\bar{\mathbf{U}}'$ denotes the steady variable vector, $\hat{\mathbf{U}}'$ denotes for the first order variable vector. We then substitute it into the system's discretized matrix equation (3.7.12) to obtain

$$\mathbf{M}\left(\bar{\mathbf{U}}' + \varepsilon\hat{\mathbf{U}}'\right)\frac{\mathrm{d}\left(\bar{\mathbf{U}}' + \varepsilon\hat{\mathbf{U}}'\right)}{\mathrm{d}t} + \mathbf{K}\left(\bar{\mathbf{U}}' + \varepsilon\hat{\mathbf{U}}'\right)\left(\bar{\mathbf{U}}' + \varepsilon\hat{\mathbf{U}}'\right) = \mathbf{R}\left(\bar{\mathbf{U}}', \hat{\mathbf{U}}'\right) = 0. \tag{4.5.1}$$

Using a Taylor expansion for $\mathbf{M}\left(\bar{\mathbf{U}}' + \varepsilon\hat{\mathbf{U}}'\right)$ and $\mathbf{K}\left(\bar{\mathbf{U}}' + \varepsilon\hat{\mathbf{U}}'\right)$ we have,

$$\mathbf{M}\left(\bar{\mathbf{U}}' + \varepsilon\hat{\mathbf{U}}'\right) = \mathbf{M}\left(\bar{\mathbf{U}}'\right) + \varepsilon\frac{\partial\mathbf{M}\left(\bar{\mathbf{U}}'\right)}{\partial\bar{\mathbf{U}}'}\hat{\mathbf{U}}' + O(\varepsilon^2), \tag{4.5.2}$$

$$\mathbf{K}\left(\bar{\mathbf{U}}' + \varepsilon\hat{\mathbf{U}}'\right) = \mathbf{K}\left(\bar{\mathbf{U}}'\right) + \varepsilon\frac{\partial\mathbf{K}\left(\bar{\mathbf{U}}'\right)}{\partial\bar{\mathbf{U}}'}\hat{\mathbf{U}}' + O(\varepsilon^2). \tag{4.5.3}$$

Substituting (4.5.2) and (4.5.3) into equation (4.5.1), at $O(\varepsilon)$ we have,

$$\mathbf{M}\left(\bar{\mathbf{U}}'\right)\frac{\mathrm{d}\hat{\mathbf{U}}'}{\mathrm{d}t} + \left(\mathbf{K}\left(\bar{\mathbf{U}}'\right) + \frac{\partial\mathbf{K}\left(\bar{\mathbf{U}}'\right)}{\partial\bar{\mathbf{U}}'}\bar{\mathbf{U}}'\right)\hat{\mathbf{U}}' = \mathbf{0}. \tag{4.5.4}$$

We assume the first order vector $\hat{\mathbf{U}}'$ has the wave-like form $\hat{\mathbf{U}}' = e^{\sigma t}\tilde{\mathbf{U}}'$, where $\sigma = \sigma_r + i\sigma_i$ ($\sigma_r, \sigma_i \in \mathbb{R}$). Substituting the wavelike form into equation (4.5.4), we obtain a general eigenvalue problem

$$\sigma\mathbf{A}\tilde{\mathbf{U}}' = \mathbf{B}\tilde{\mathbf{U}}', \tag{4.5.5}$$

where

$$\mathbf{A} = \mathbf{M}\left(\bar{\mathbf{U}}'\right), \quad \mathbf{B} = \left(-\mathbf{K}\left(\bar{\mathbf{U}}'\right) - \frac{\partial\mathbf{K}\left(\bar{\mathbf{U}}'\right)}{\partial\bar{\mathbf{U}}'}\bar{\mathbf{U}}'\right). \tag{4.5.6}$$

The scalar σ and vector $\tilde{\mathbf{U}}'$ are eigenvalue and eigenfunction of this eigenvalue problem respectively. We solve the above eigenvalue problem using the Arnoldi-frontal method, which employs a frontal method during an Arnoldi iteration scheme. This has the advantage that it does not need to form the large matrices **A** and **B** in equation (4.5.5) (details see Hao *et al*. [25], Arnoldi [1]).

4.5.2 Numerical methods for linearised energy budget

Using the eigenfunction calculated from the eigensolver (4.5.5), we can compute the average energy budget of the linearised system over one period of time at $O(\varepsilon^2)$.

We substitute the shape functions (3.7.6) into the second order energy budget to obtain its discretized form on each element.

Similar to the discretization of fully nonlinear energy budget in chapter 3, we substitute the discretized variables (4.1.1) into $\bar{\hat{D}}_f$, the expansion of the viscous dissipation energy budget at

second order over one period of oscillation takes the form

$$\begin{aligned}\bar{\hat{D}}_f =& \sum_{\Delta_a}\left(R^{-1}\sum_{l=1}^{l=6}\sum_{i=1}^{i=6}\sum_{j=1}^{j=6}\sum_{k=1}^{k=6}(2\hat{u}_{1l}\hat{u}_{1i}+\hat{u}_{2l}\hat{u}_{2i})\,y_j y_k\int\int A_{lk}A_{ij}|\mathbf{J}|^{-2}\,\mathrm{d}x\mathrm{d}y\right)\\ &+\sum_{\Delta_a}\left(R^{-1}\sum_{l=1}^{l=6}\sum_{i=1}^{i=6}\sum_{j=1}^{j=6}\sum_{k=1}^{k=6}(\hat{u}_{1l}\hat{u}_{1i}+2\hat{u}_{2l}\hat{u}_{2i})\,x_j x_k\int\int A_{lk}A_{ij}|\mathbf{J}|^{-2}\,\mathrm{d}x\mathrm{d}y\right)\\ &-\sum_{\Delta_a}\left(R^{-1}\sum_{l=1}^{l=6}\sum_{i=1}^{i=6}\sum_{j=1}^{j=6}\sum_{k=1}^{k=6}2\hat{u}_{1l}\hat{u}_{2i}y_j x_k\int\int A_{lk}A_{ij}|\mathbf{J}|^{-2}\,\mathrm{d}x\mathrm{d}y\right).\end{aligned}\tag{4.5.7}$$

The double integration $\int\int \mathrm{d}x\mathrm{d}y$ is taken over each triangular element Δ_a. We then sum up these integrations over the whole domain.

Similarly, the expansion of the work done by non-linear Reynolds stresses over one period of oscillation $\bar{\hat{S}}_f$ can be written as,

$$\begin{aligned}\bar{\hat{S}}_f =& \sum_{\Delta_a}\left(\sum_{l=1}^{l=6}\sum_{i=1}^{i=6}\sum_{j=1}^{j=6}\sum_{k=1}^{k=6}\left(\hat{u}_{1l}\hat{u}_{1i}U_{1j}+\hat{u}_{1l}\hat{u}_{2i}U_{2j}\right)y_k\int\int N_l A_{ik}N_j|\mathbf{J}|^{-1}\,\mathrm{d}x\mathrm{d}y\right)\\ &-\sum_{\Delta_a}\left(\sum_{l=1}^{l=6}\sum_{i=1}^{i=6}\sum_{j=1}^{j=6}\sum_{k=1}^{k=6}\left(\hat{u}_{2l}\hat{u}_{1i}U_{1j}+\hat{u}_{2l}\hat{u}_{2i}U_{2j}\right)x_k\int\int N_l A_{ik}N_j|\mathbf{J}|^{-1}\,\mathrm{d}x\mathrm{d}y\right).\end{aligned}\tag{4.5.8}$$

The discretized form of the net perturbation kinetic energy flux extracted from the mean flow over one period of oscillation $\bar{\hat{F}}_f$ takes the form,

$$\bar{\hat{F}}_f = \sum_{I_r}\left(\sum_{l=1}^{l=6}\sum_{i=1}^{i=6}\sum_{j=1}^{j=6}\frac{1}{2}\left(3\hat{u}_{1l}\hat{u}_{1i}U_{1j}+\hat{u}_{2l}\hat{u}_{2i}U_{1j}+2\hat{u}_{1l}\hat{u}_{2i}U_{2j}\right)\int N_l N_i N_j\,\mathrm{d}y\right).\tag{4.5.9}$$

This is similar to the discretization of fully nonlinear energy budget, where $\int \mathrm{d}y$ is the integration evaluated along each three-node element of the inlet and outlet boundaries and then sum up these integrations.

The expansion of the work done by perturbation pressure over one period of oscillation $\bar{\hat{P}}_f$ can be written as,

$$\bar{\hat{P}}_f = \sum_{I_r}\left(\sum_{l=1}^{l=6}\sum_{i=1}^{i=6}-\hat{u}_{1l}\hat{p}_i\int N_l N_i\,\mathrm{d}y\right).\tag{4.5.10}$$

For $\bar{\hat{S}}_b$, we can first simplify the energy budget $\bar{\hat{S}}_b$ by applying integration by parts. We denote the two terms of $\bar{\hat{S}}_b$ in *I* and *II*. To simplify the average $\bar{\hat{S}}_b$ over one period, we can rearrange it

as,

$$\bar{\hat{S}}_b = \underbrace{\int_0^{L_0} \Lambda\left(\boldsymbol{\Sigma}\bar{\hat{\mathbf{n}}}\right)\cdot\bar{\hat{\mathbf{u}}}_b\,\mathrm{d}l}_{I} + \underbrace{\int_0^{L_0}\Lambda\left[\left(\bar{\hat{x}}_b\frac{\partial\boldsymbol{\Sigma}}{\partial x}+\bar{\hat{y}}_b\frac{\partial\boldsymbol{\Sigma}}{\partial y}\right)\mathbf{N}\right]\cdot\bar{\hat{\mathbf{u}}}_b\,\mathrm{d}l}_{II}. \tag{4.5.11}$$

We substitute the expression of the static fluid stress tensor $\boldsymbol{\Sigma}$ (see appendix A.5), the first order normal vector $\bar{\hat{\mathbf{n}}} = -\hat{\theta}\cos(\Theta)\mathbf{g}_1 - \hat{\theta}\sin(\Theta)\mathbf{g}_2$ into I, and apply the first order velocity boundary condition (4.2.20) to obtain,

$$\begin{aligned} I = &\int_0^{L_0}\bar{\hat{\theta}}P\Lambda\left(\bar{\hat{u}}_1\cos(\Theta)+\bar{\hat{u}}_2\sin(\Theta)\right)\mathrm{d}l - R^{-1}\int_0^{L_0}\left(2\bar{\hat{\theta}}\bar{\hat{u}}_1+\bar{\hat{\theta}}\bar{\hat{u}}_1+\bar{\hat{\theta}}\bar{\hat{u}}_2\cot(\Theta)\right)\frac{\partial U_1}{\partial l}\,\mathrm{d}l \\ &- R^{-1}\int_0^{L_0}\left(2\bar{\hat{\theta}}\bar{\hat{u}}_2+\bar{\hat{\theta}}\bar{\hat{u}}_2+\bar{\hat{\theta}}\bar{\hat{u}}_1\tan(\Theta)\right)\frac{\partial U_2}{\partial l}\,\mathrm{d}l. \end{aligned}$$

We use integration by parts for the final two terms to obtain,

$$\begin{aligned} I = &\int_0^{L_0}\bar{\hat{\theta}}P\Lambda\left(\bar{\hat{u}}_1\cos(\Theta)+\bar{\hat{u}}_2\sin(\Theta)\right)\mathrm{d}l - R^{-1}\left[\left(2\bar{\hat{\theta}}\bar{\hat{u}}_1+\bar{\hat{\theta}}\bar{\hat{u}}_1+\bar{\hat{\theta}}\bar{\hat{u}}_2\cot(\Theta)\right)U_1\right]_0^{L_0} \\ &+R^{-1}\int_0^{L_0}\frac{\partial}{\partial l}\left(\bar{\hat{u}}_1\cos(\Theta)+\bar{\hat{u}}_2\sin(\Theta)\right)U_1\,\mathrm{d}l - R^{-1}\left[\left(2\bar{\hat{\theta}}\bar{\hat{u}}_2+\bar{\hat{\theta}}\bar{\hat{u}}_2+\bar{\hat{\theta}}\bar{\hat{u}}_1\tan(\Theta)\right)U_2\right]_0^{L_0} \\ &+R^{-1}\int_0^{L_0}\frac{\partial}{\partial l}\left(2\bar{\hat{\theta}}\bar{\hat{u}}_2+\bar{\hat{\theta}}\bar{\hat{u}}_2+\bar{\hat{\theta}}\bar{\hat{u}}_1\tan(\Theta)\right)U_2\,\mathrm{d}l, \\ = &\int_0^{L_0}\bar{\hat{\theta}}P\Lambda\left(\bar{\hat{u}}_1\cos(\Theta)+\bar{\hat{u}}_2\sin(\Theta)\right)\mathrm{d}l; \end{aligned}$$

here we apply the static velocity boundary condition (4.2.9) on the static elastic beam.
We substitute the expression of the static fluid stress tensor $\boldsymbol{\Sigma}$ (see appendix A.5), the static normal vector $\mathbf{N} = -\sin(\Theta)\mathbf{g}_1 + \cos(\Theta)\mathbf{g}_2$ into II, and use $\hat{\mathbf{u}}_b = \partial\hat{\mathbf{x}}_b/\partial t$, to obtain

$$\begin{aligned} II = &\frac{\partial}{\partial t}\int_0^{L_0}\left[\frac{\bar{\hat{x}}_b^2}{2}\frac{\partial P}{\partial x} - \frac{\bar{\hat{y}}_b^2}{2R}\left(\frac{\partial^2 U_1}{\partial y^2}+\frac{\partial^2 U_2}{\partial x^2}+2\frac{\partial^2 U_2}{\partial y^2}\right) - \frac{\bar{\hat{x}}_b\bar{\hat{y}}_b}{R}\left(\frac{\partial^2 U_1}{\partial x\partial y}+\frac{\partial^2 U_2}{\partial x^2}\right)\right]\sin(\Theta)\,\mathrm{d}l \\ &-\frac{\partial}{\partial t}\int_0^{L_0}\left[\bar{\hat{x}}_b\bar{\hat{y}}_b\frac{\partial P}{\partial x}+\frac{\bar{\hat{y}}_b^2}{2}\frac{\partial P}{\partial y} - \frac{\bar{\hat{x}}_b^2}{2R}\left(\frac{\partial^2 U_1}{\partial x\partial y}+\frac{\partial^2 U_2}{\partial x^2}\right) - \frac{\bar{\hat{y}}_b^2}{R}\frac{\partial^2 U_2}{\partial y^2}\right]\cos(\Theta)\,\mathrm{d}l \\ &+\frac{\partial}{\partial t}\int_0^{L_0}\left[\frac{\bar{\hat{x}}_b\bar{\hat{y}}_b}{R}\left(\frac{\partial^2 U_2}{\partial x\partial y}+\frac{\partial^2 U_2}{\partial y^2}\right)\right]\cos(\Theta)\,\mathrm{d}l \\ &+\int_0^{L_0}\bar{\hat{y}}_b\frac{\bar{\hat{x}}_b}{\partial t}\left[\frac{\partial P}{\partial x}\cos(\Theta)+\frac{\partial P}{\partial y}\sin(\Theta) - \frac{1}{R}\left(\frac{\partial^2 U_1}{\partial x\partial y}\sin(\Theta)+\frac{\partial^2 U_2}{\partial x\partial y}\cos(\Theta)\right)\right]\mathrm{d}l \\ &+\int_0^{L_0}\bar{\hat{y}}_b\frac{\bar{\hat{x}}_b}{\partial t}\left[\left(R^{-1}\frac{\partial^2 U_1}{\partial y^2}\right)\cos(\Theta)+\left(R^{-1}\frac{\partial^2 U_2}{\partial x^2}\right)\sin(\Theta)\right]\mathrm{d}l. \end{aligned}$$

The first three terms vanish over one period of oscillation. We substitute the steady fluid equation (4.2.6,4.2.7) into the final term to obtain,

$$
\begin{aligned}
II =& \frac{\partial}{\partial t}\int_0^{L_0}\left[\frac{\bar{x}_b^2}{2}\frac{\partial P}{\partial x}-\frac{\bar{y}_b^2}{2R}\left(\frac{\partial^2 U_1}{\partial y^2}+\frac{\partial^2 U_2}{\partial x^2}+2\frac{\partial^2 U_2}{\partial y^2}\right)-\frac{\bar{x}_b\bar{y}_b}{R}\left(\frac{\partial^2 U_1}{\partial x\partial y}+\frac{\partial^2 U_2}{\partial x^2}\right)\right]\sin(\Theta)\,\mathrm{d}l\\
&-\frac{\partial}{\partial t}\int_0^{L_0}\left[\bar{x}_b\bar{y}_b\frac{\partial P}{\partial x}+\frac{\bar{y}_b^2}{2}\frac{\partial P}{\partial y}-\frac{\bar{x}_b^2}{2R}\left(\frac{\partial^2 U_1}{\partial x\partial y}+\frac{\partial^2 U_2}{\partial x^2}\right)-\frac{\bar{y}_b^2}{R}\frac{\partial^2 U_2}{\partial y^2}\right]\cos(\Theta)\,\mathrm{d}l\\
&+\frac{\partial}{\partial t}\int_0^{L_0}\left[\frac{\bar{x}_b\bar{y}_b}{R}\left(\frac{\partial^2 U_2}{\partial x\partial y}+\frac{\partial^2 U_2}{\partial y^2}\right)\right]\cos(\Theta)\,\mathrm{d}l\\
&+\int_0^{L_0}\bar{y}_b\frac{\partial\bar{x}_b}{\partial t}\left[2\frac{\partial P}{\partial x}\cos(\Theta)+2\frac{\partial P}{\partial y}\sin(\Theta)\right]\mathrm{d}l\\
&+\int_0^{L_0}\bar{y}_b\frac{\partial\bar{x}_b}{\partial t}\left[\left(U_1\frac{\partial U_1}{\partial x}+U_2\frac{\partial U_1}{\partial y}\right)\cos(\Theta)+\left(U_1\frac{\partial U_2}{\partial x}+U_2\frac{\partial U_2}{\partial y}\right)\sin(\Theta)\right]\mathrm{d}l\\
&-\int_0^{L_0}\bar{y}_b\frac{\partial\bar{x}_b}{\partial t}\left[\frac{1}{R}\frac{\partial}{\partial x}\left(\frac{\partial U_1}{\partial x}+\frac{\partial U_2}{\partial y}\right)+\frac{1}{R}\frac{\partial}{\partial y}\left(\frac{\partial U_1}{\partial x}+\frac{\partial U_2}{\partial y}\right)\right]\mathrm{d}l. \qquad (4.5.12)
\end{aligned}
$$

Substituting the incompressible condition at static state (4.2.5) and again applying $\mathrm{d}x=\Lambda\cos(\Theta)\mathrm{d}l$, $\mathrm{d}y=\Lambda\sin(\Theta)\mathrm{d}l$ into the above terms, we obtain

$$
\begin{aligned}
II =& \frac{\partial}{\partial t}\int_0^{L_0}\left[\frac{\bar{x}_b^2}{2}\frac{\partial P}{\partial x}-\frac{\bar{y}_b^2}{2R}\left(\frac{\partial^2 U_1}{\partial y^2}+\frac{\partial^2 U_2}{\partial x^2}+2\frac{\partial^2 U_2}{\partial y^2}\right)-\frac{\bar{x}_b\bar{y}_b}{R}\left(\frac{\partial^2 U_1}{\partial x\partial y}+\frac{\partial^2 U_2}{\partial x^2}\right)\right]\sin(\Theta)\,\mathrm{d}l\\
&-\frac{\partial}{\partial t}\int_0^{L_0}\left[\bar{x}_b\bar{y}_b\frac{\partial P}{\partial x}+\frac{\bar{y}_b^2}{2}\frac{\partial P}{\partial y}-\frac{\bar{x}_b^2}{2R}\left(\frac{\partial^2 U_1}{\partial x\partial y}+\frac{\partial^2 U_2}{\partial x^2}\right)-\frac{\bar{y}_b^2}{R}\frac{\partial^2 U_2}{\partial y^2}\right]\cos(\Theta)\,\mathrm{d}l\\
&+\frac{\partial}{\partial t}\int_0^{L_0}\left[\frac{\bar{x}_b\bar{y}_b}{R}\left(\frac{\partial^2 U_2}{\partial x\partial y}+\frac{\partial^2 U_2}{\partial y^2}\right)\right]\cos(\Theta)\,\mathrm{d}l+\int_0^{L_0}4\bar{y}_b\frac{\partial\bar{x}_b}{\partial t}\frac{\partial P}{\partial l}\,\mathrm{d}l\\
&+\int_0^{L_0}\left[\bar{y}_b\frac{\partial\bar{x}_b}{\partial t}\left(U_1+U_2\cot(\Theta)\right)\frac{\partial U_1}{\partial l}+\bar{y}_b\frac{\partial\bar{x}_b}{\partial t}\left(U_1\tan(\Theta)+U_2\right)\frac{\partial U_2}{\partial l}\right]\mathrm{d}l.
\end{aligned}
$$

We use integration by parts for the final term to obtain,

$$
\begin{aligned}
II =& \frac{\partial}{\partial t}\int_0^{L_0}\left[\frac{\bar{x}_b^2}{2}\frac{\partial P}{\partial x}-\frac{\bar{y}_b^2}{2R}\left(\frac{\partial^2 U_1}{\partial y^2}+\frac{\partial^2 U_2}{\partial x^2}+2\frac{\partial^2 U_2}{\partial y^2}\right)-\frac{\bar{x}_b\bar{y}_b}{R}\left(\frac{\partial^2 U_1}{\partial x\partial y}+\frac{\partial^2 U_2}{\partial x^2}\right)\right]\sin(\Theta)\,\mathrm{d}l\\
&-\frac{\partial}{\partial t}\int_0^{L_0}\left[\bar{x}_b\bar{y}_b\frac{\partial P}{\partial x}+\frac{\bar{y}_b^2}{2}\frac{\partial P}{\partial y}-\frac{\bar{x}_b^2}{2R}\left(\frac{\partial^2 U_1}{\partial x\partial y}+\frac{\partial^2 U_2}{\partial x^2}\right)-\frac{\bar{y}_b^2}{R}\frac{\partial^2 U_2}{\partial y^2}\right]\cos(\Theta)\,\mathrm{d}l\\
&+\frac{\partial}{\partial t}\int_0^{L_0}\left[\frac{\bar{x}_b\bar{y}_b}{R}\left(\frac{\partial^2 U_2}{\partial x\partial y}+\frac{\partial^2 U_2}{\partial y^2}\right)\right]\cos(\Theta)\,\mathrm{d}l\\
&+\int_0^{L_0}4\bar{y}_b\frac{\partial\bar{x}_b}{\partial t}\frac{\partial P}{\partial l}\,\mathrm{d}l+\left[\bar{y}_b\frac{\partial\bar{x}_b}{\partial t}\left(U_1+U_2\cot(\Theta)\right)U_1+\bar{y}_b\frac{\partial\bar{x}_b}{\partial t}\left(U_1\tan(\Theta)+U_2\right)U_2\right]_0^{L_0}\\
&-\int_0^{L_0}\left[\frac{\partial}{\partial l}\left(\bar{y}_b\frac{\partial x_b}{\partial t}\left(U_1+U_2\cot(\Theta)\right)\right)U_1+\frac{\partial}{\partial l}\left(\bar{y}_b\frac{\partial\bar{x}_b}{\partial t}\left(U_1\tan(\Theta)+U_2\right)\right)U_2\right]\mathrm{d}l,\\
=& \frac{\partial}{\partial t}\int_0^{L_0}\left[\frac{\bar{x}_b^2}{2}\frac{\partial P}{\partial x}-\frac{\bar{y}_b^2}{2R}\left(\frac{\partial^2 U_1}{\partial y^2}+\frac{\partial^2 U_2}{\partial x^2}+2\frac{\partial^2 U_2}{\partial y^2}\right)-\frac{\bar{x}_b\bar{y}_b}{R}\left(\frac{\partial^2 U_1}{\partial x\partial y}+\frac{\partial^2 U_2}{\partial x^2}\right)\right]\sin(\Theta)\,\mathrm{d}l
\end{aligned}
$$

$$-\frac{\partial}{\partial t}\int_0^{L_0}\left[\bar{\hat{x}}_b\bar{\hat{y}}_b\frac{\partial P}{\partial x}+\frac{\bar{\hat{y}}_b^2}{2}\frac{\partial P}{\partial y}-\frac{\bar{\hat{x}}_b^2}{2R}\left(\frac{\partial^2 U_1}{\partial x\partial y}+\frac{\partial^2 U_2}{\partial x^2}\right)-\frac{\bar{\hat{y}}_b^2}{R}\frac{\partial^2 U_2}{\partial y^2}\right]\cos(\Theta)\,\mathrm{d}l$$
$$+\frac{\partial}{\partial t}\int_0^{L_0}\left[\frac{\bar{\hat{x}}_b\bar{\hat{y}}_b}{R}\left(\frac{\partial^2 U_2}{\partial x\partial y}+\frac{\partial^2 U_2}{\partial y^2}\right)\right]\cos(\Theta)\,\mathrm{d}l+\int_0^{L_0}4\bar{\hat{y}}_b\frac{\partial\bar{\hat{x}}_b}{\partial t}\frac{\partial P}{\partial l}\,\mathrm{d}l,$$

here we apply the static velocity boundary condition (4.2.9) on the static elastic beam.
In total, grouping I and II, we simplify $\bar{\hat{S}}_b$ over one period of oscillation to obtain,

$$\bar{\hat{S}}_b=\int_0^{L_0}\bar{\hat{\theta}}P\Lambda\left(\bar{\hat{u}}_1\cos(\Theta)+\bar{\hat{u}}_2\sin(\Theta)\right)\,\mathrm{d}l+\int_0^{L_0}4\bar{\hat{y}}_b\frac{\partial\bar{\hat{x}}_b}{\partial t}\frac{\partial P}{\partial l}\,\mathrm{d}l. \tag{4.5.13}$$

Thus, the discretized form of the simplified $\bar{\hat{S}}_b$ can be written as,

$$\bar{\hat{S}}_b=\sum_{I_e}\left(\sum_{l=1}^{l=3}\sum_{i=1}^{i=3}\sum_{j=1}^{j=3}\sum_{k=1}^{k=6}\left[\hat{\theta}_l P_i\Lambda_j\hat{u}_{1k}\int N_lN_iN_jN_k\cos(\Theta)\,\mathrm{d}l+\hat{\theta}_l P_i\Lambda_j\hat{u}_{2k}\int N_lN_iN_jN_k\sin(\Theta)\,\mathrm{d}l\right]\right)$$
$$+\sum_{I_e}\left(\sum_{l=1}^{l=3}\sum_{i=1}^{i=6}\sum_{j=1}^{j=3}4\hat{y}_{bl}\hat{u}_{1i}P_j\int N_lN_i\frac{\mathrm{d}N_j}{\mathrm{d}l}\,\mathrm{d}l\right) \tag{4.5.14}$$

where $\int \mathrm{d}l$ is the integration evaluated along each three-node element (I_e) of the elastic beam; we then sum up these integrations.
We apply $\hat{\mathbf{n}}=-\hat{\theta}\cos(\Theta)\mathbf{g}_1-\hat{\theta}\sin(\Theta)\mathbf{g}_2$ for the work done by the external pressure over one period of oscillation, the expansion of $\bar{\hat{P}}_e$ takes the form,

$$\bar{\hat{P}}_e=\sum_{I_e}\left(\sum_{l=1}^{l=3}\sum_{i=1}^{i=3}\sum_{j=1}^{j=6}\left[-p_e\Lambda_l\hat{\theta}_i\hat{u}_{1j}\int N_lN_iN_j\cos(\Theta)\,\mathrm{d}l-p_e\Lambda_l\hat{\theta}_i\hat{u}_{2j}\int N_lN_iN_j\sin(\Theta)\,\mathrm{d}l\right]\right). \tag{4.5.15}$$

4.6 Numerical results

In this section, we give numerical results for the eigenvalue problem (4.5.5) for the flow-driven system (*i.e.* the flux on inlet boundary is fixed). The growth rate σ_r and frequency σ_i of the most unstable eigenfunction are computed as functions of Reynolds number for several extensional stiffnesses (see figure 4.1). We then construct the neutral stability curve in the parameter space spanned by Reynolds number and extensional stiffness (R, c_λ). We elucidate the difference between the results of Hao *et al*. [25] (as well as Luo *et al*. [48]) and our model since we have modified the beam Kirchhoff law (equation 3.3.12). Finally, we illustrate the numerical results of the second order energy budget at several points on the neutral stability curve.

4.6.1 Numerical results for eigenvalue problem

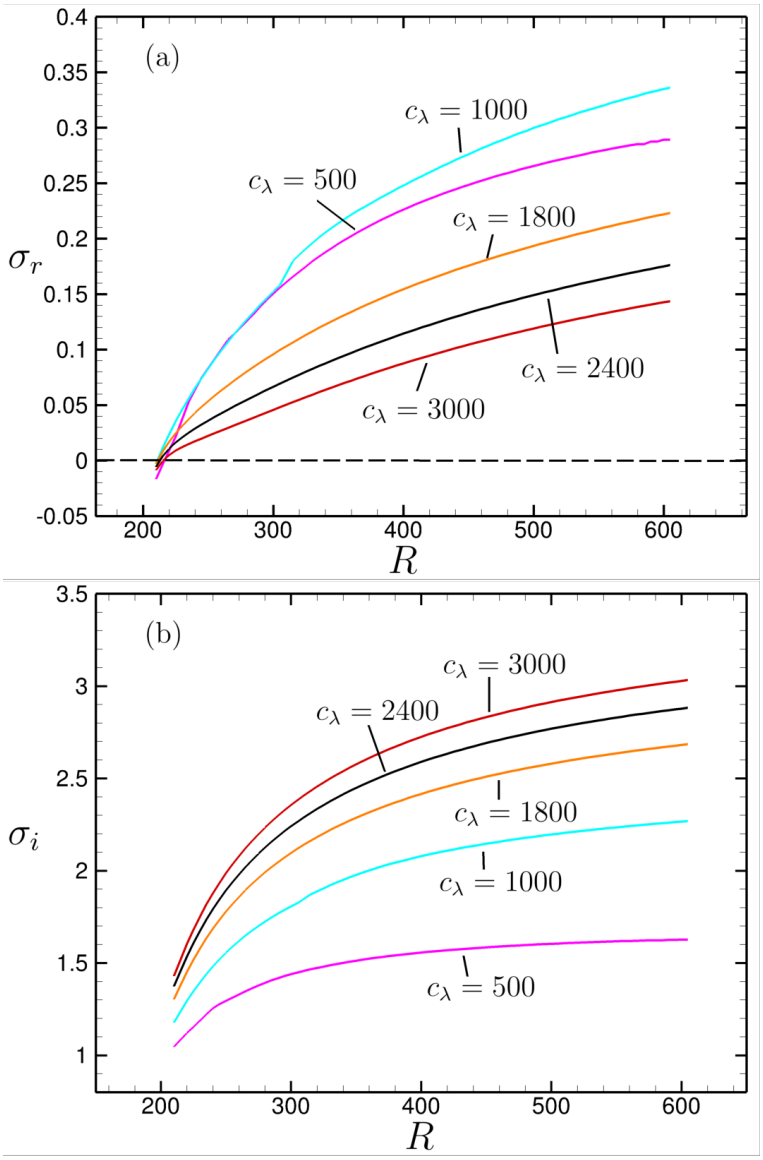

Figure 4.1: (a) Maximal growth rate σ_r against Reynolds number R for $c_\lambda = 500, 1000, 1800, 2400, 3000$; (b) Corresponding frequency σ_i against Reynolds number R.

The system is stable when the real part of σ (*i.e.* σ_r) is negative (see equation 4.3.1 in *Sec.* 4.3), while the system is unstable when the real part of σ (*i.e.* σ_r) is positive. We say the system is neutrally stable when $\sigma_r = 0$.

The maximal growth rate σ_r and corresponding frequency σ_i are plotted against the Reynolds number R for various c_λ (see figure 4.1). We observe that the maximal growth rate increases as the Reynolds number increases for all selected extensional stiffness c_λ. The growth rate σ_r is negative (*i.e.* the system is stable) for low R, eventually crossing zero (*i.e.* the system is neutrally stable) and reach positive values for large R (*i.e.* the system is unstable).

The corresponding frequency of oscillation is plotted in figure 4.1 (b). The oscillation frequency

σ_i increases as R increases. We note that those frequencies become greater as the extensional stiffness increases, since the elastic wall will oscillate at a higher frequency for a stiffer wall. This is similar to that found in Luo *et al*. [48] and Jensen & Heil [42].

4.6.2 Neutrally stable curve

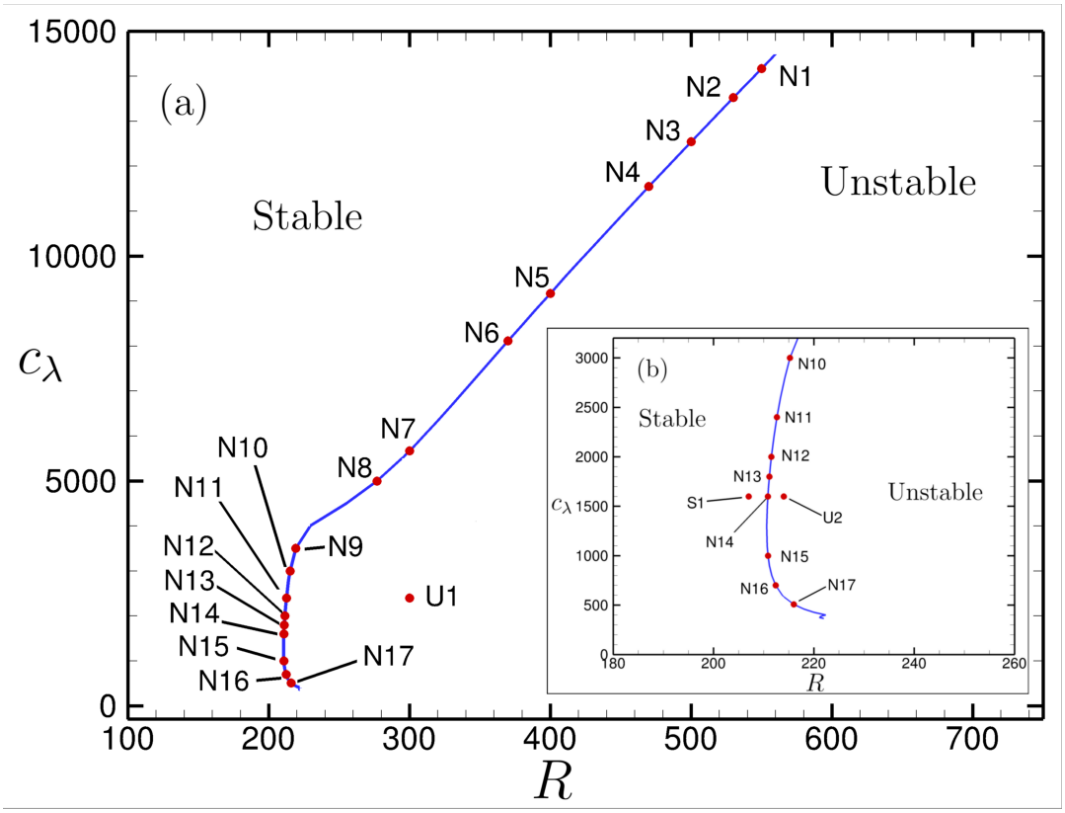

Figure 4.2: (a) Neutral stability curve in parameter space spanned by (R, c_λ); (b) Zoom in of neutral stability curve.

We use a bisection method to isolate the neutral stability curve when $\sigma_r = 0$ and plot in the parameter space spanned by (R, c_λ), shown in figure 4.2. The system is stable on the left side of the neutral stability curve and unstable on the right side of the neutral stability curve in figure 4.2. The value of c_λ on the neutral stability curve grows linearly with Reynolds number for $c_\lambda \geq 4000$. This is similar to observation of Stewart [65], where for his fluid-membrane model the critical Reynolds number along the neutral curve grows proportional to membrane tension as tension becomes large.

For $c_\lambda < 500$, the netrally stable curve shows a small cascade structure. Details of neutral points are listed in table 4.1.

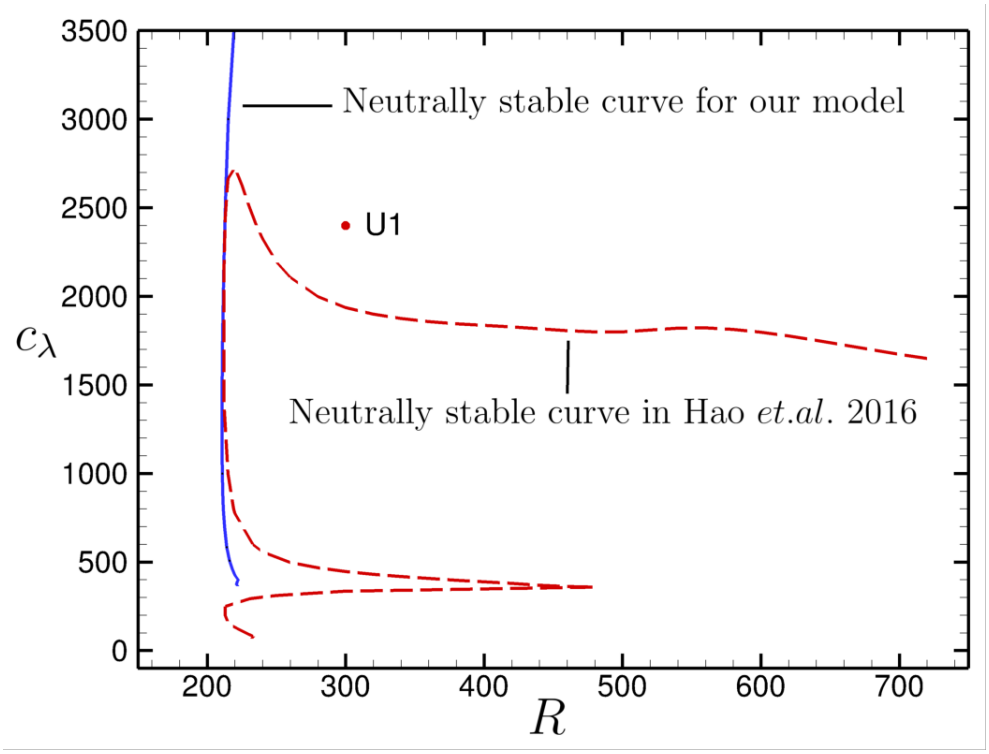

Figure 4.3: Neutrally stable curves for the model used in this thesis and in Hao *et al*. [25].

Hao *et*. *al*. [25] (as well as Luo *et al*. [48]) demonstrated a cascade stability structure in (R, c_λ) space while their system is stable for all Reynolds number when $c_\lambda > 2600$. Whereas, we note that our system can be unstable for $c_\lambda > 2600$ (shown in figure 4.3). Taking point U1 ($R = 300$, $c_\lambda = 2400$) as an example point, U1 is unstable for our system while stable for the Hao system (see figure 4.3). Here we also display the time evolution of mid-point pressure (p_{mid}) and minimal channel width (y_{min}) for point U1 using unsteady numerical stimulation elucidated in chapter 3 (shown in figure 4.5).

Also our neutral stability curve is a mixture of mode-2 and mode-3 neutral points, and neither do we find mode-4 neutral stable points for this parameter range. Whereas, the neutral stability curve in Hao *et*. *al*. 2016 (as well as Luo *et*. *al*. 2008) is consist of mode-2, mode-3 and mode-4 branches. We suggest that the different behavior of the two systems is caused by the new Kirchhoff law we employed for our model, though this will need further verification.

Figure 4.4 plots the first order beam shape, the time evolution of first order mid-point location and the amplitude of the beam calculated from the eigenvalue problem, for three different neutral stable points N13, N15 and N16. The first order beam shape are evaluated at three different time, $t_p = 2\pi/\sigma_i$ denotes the peroid of each oscillation.

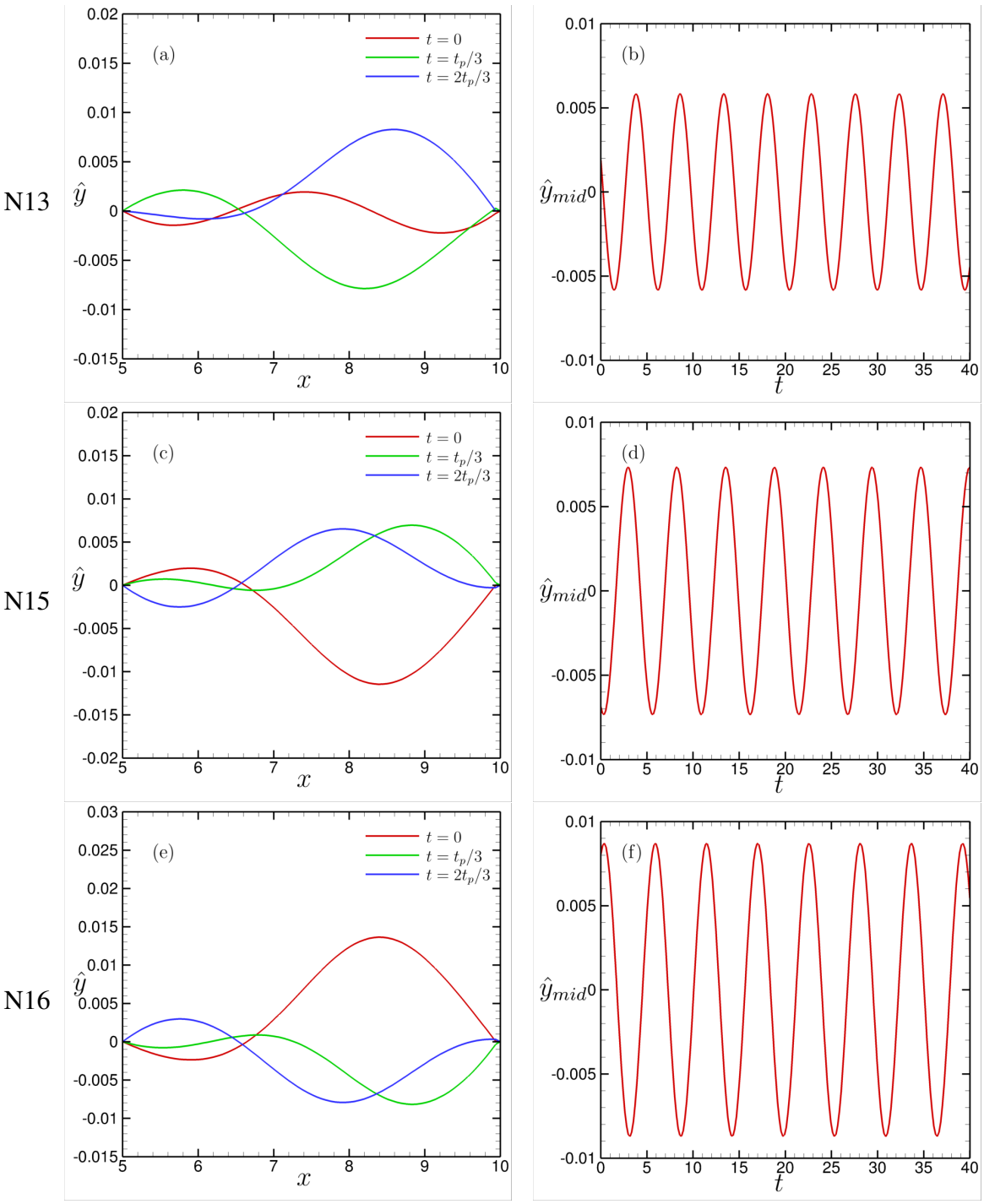

Figure 4.4: (a), (b): The linearised beam shape at different time; the time evolution mid-point position $\hat{y}_{mid}$ on the beam, on neutral point N13; (c), (d):The linearised beam shape at different time; the time evolution mid-point position $\hat{y}_{mid}$ on the beam, on neutral point N15; (e), (f): The linearised beam shape at different time; the time evolution mid-point position $\hat{y}_{mid}$ on the beam, on neutral point N16;

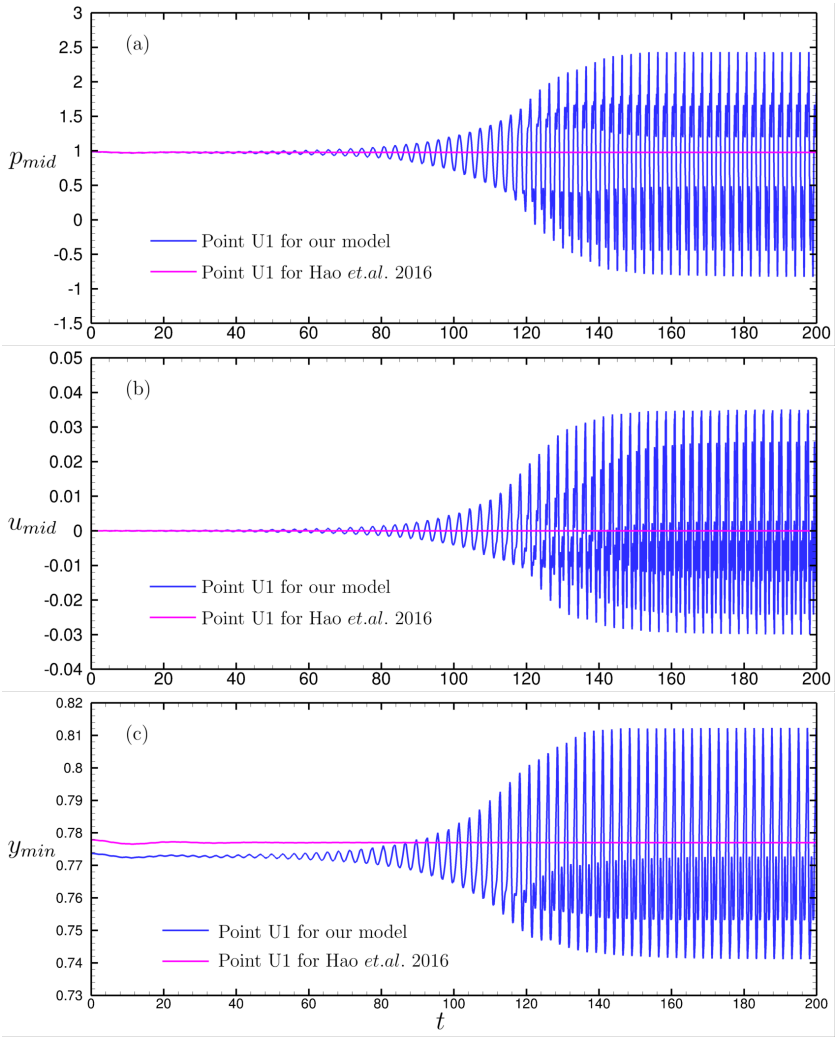

Figure 4.5: (a) The time evolution of mid-point pressure p_{mid} for point U1;(b) The time evolution of mid-point velocity u_{mid} for point U1 (c) The time evolution of minimal channel width y_{min} for point U1.

Table 4.1 listed the points labeled on neutral curve (shown in figure 4.2). The corresponding Reynolds number, extensional stiffness, growth rate, oscillation frequency and instability mode are also listed in this table. The point S1 ($R = 207, c_\lambda = 1600$) listed in table 4.1 is a stable point (*i.e.* corresponding $\sigma_i < 0$), while the point U2 ($R = 214, c_\lambda = 1600$) is a unstable point (*i.e.* corresponding $\sigma_i > 0$). The neutral points This is consistent with our predictions using unsteady numerical stimulation (see chapter 3, see figure 3.10 and 3.11).

Point	R	c_λ	σ_r	σ_i	mode
N1	550	14171.875	-5.4717020E-07	4.088722	mode-2
N2	530	13523.925	-4.9766690E-07	4.020952	mode-2
N3	500	12543.457	5.8052460E-07	3.911252	mode-2
N4	470	11551.757	-5.8001090E-07	3.790225	mode-2
N5	400	9171.8750	4.7121650E-07	3.447506	mode-3
N6	370	8116.215	7.8881270E-07	3.264403	mode-2
N7	300	5669.433	9.4262750E-07	2.705644	mode-2
N8	277.066	5000	1.1594730E-07	2.473291	mode-3
N9	219.195	3500	9.4714320E-07	1.637742	mode-2
N10	215.233	3000	2.1043500E-07	1.522616	mode-2
N11	212.636	2400	-3.5048560E-08	1.417463	mode-2
N12	211.535	2000	-5.9519050E-07	1.353594	mode-3
N13	211.129	1800	-3.9422960E-08	1.321926	mode-3
N14	210.825	1600	3.6688973E-06	1.289915	mode-2
N15	210.853	1000	-4.8466350E-07	1.187952	mode-2
N16	212.382	700	-2.0064561E-07	1.131888	mode-2
N17	216	507.519	8.8535530E-07	1.095395	mode-3
S1	207	1600	-1.1072994E-02	1.2342519	mode-2
U1	300	2400	6.6514461E-02	2.2400386	mode-3
U2	214	1600	7.5386082E-03	1.3363302	mode-2

Table 4.1: Neutrally stable points labeled in figure 4.2.

We denote the eigenmode as mode-i when the oscillation to the elastic wall contains i half wavelengths (*e.g.* Jensen [39]), *e.g.* mode-2 is consists of two humps, while mode-3 consists of three humps. Figure 4.6 demonstrates the elastic oscillation wall shape for point N14, a mode-2 neutrally stable point (*i.e.* contains 2 half wavelength) and point N-13, a mode-3 neutrally stable point (*i.e.* contains 3 half wavelengths).

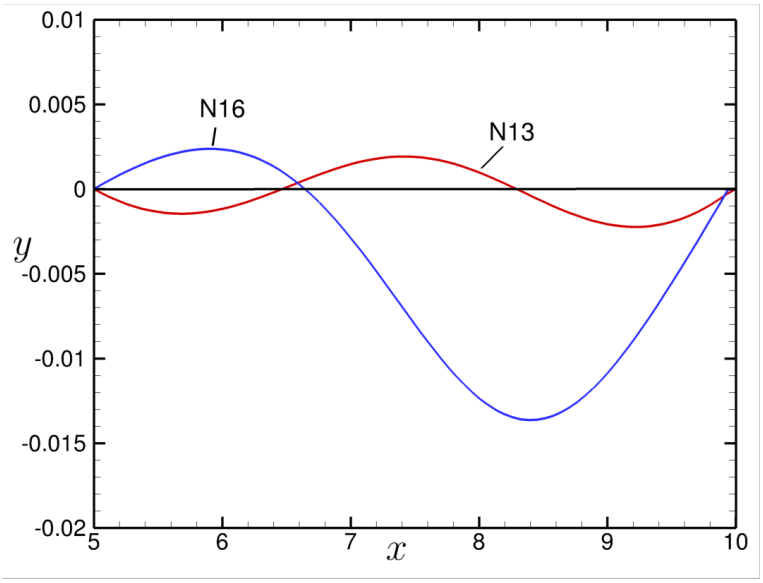

Figure 4.6: The elastic oscillation beam shape for neutral points N13 and N16.

4.6.3 Energy budget of eigenvalue problem

R	c_λ	$\bar{\tilde{D}}_f$	$\bar{\tilde{S}}_f$	$\bar{\tilde{F}}_f$	$\bar{\tilde{P}}_f$	$\bar{\tilde{S}}_b$	$\bar{\tilde{P}}_e$	$\bar{\tilde{T}}/\bar{\tilde{D}}_f$
210.853	1000	3.26E-04	1.40E-04	6.63E-08	5.85E-09	-1.83E-04	1.19E-05	-2.76%
210.713	1500	2.09E-04	8.73E-05	3.88E-08	3.48E-09	-1.02E-04	8.32E-06	5.01%
210.825	1600	1.95E-04	8.11E-05	3.58E-08	3.21E-09	-9.42E-05	7.93E-06	6.15%
211.129	1800	1.77E-04	7.81E-05	3.09E-08	2.79E-09	-7.60E-05	6.91E-06	9.13%
219.195	3500	1.12E-04	3.91E-05	1.65E-08	1.54E-09	-3.86E-05	7.32E-06	24.3%

Table 4.2: The average second order energy budget on neutral points.

Using the numerical solution of eigenvalue problem, we can compute the average second order energy budget over one period of oscillation on neutrally stable points, shown in table 4.2. The second order dissipation energy budget $\bar{\tilde{D}}_f$ is positive-definite, which is consistent with the theoretical derivation (see equation (4.4.66)). The linearised system energy is mainly balanced by the perturbation energy loss due to viscous dissipation $\bar{\tilde{D}}_f$, the work done by non-linear Reynolds stresses $\bar{\tilde{S}}_f$ and the rate of working of perturbation fluid stress tensor on the elastic wall $\bar{\tilde{S}}_b$. We scale the total second order energy budget $\bar{\tilde{T}} = \bar{\tilde{F}}_f - \bar{\tilde{P}}_f + \bar{\tilde{D}}_f - \bar{\tilde{S}}_f + \bar{\tilde{S}}_b - \bar{\tilde{P}}_e$ in equation (4.4.63) (*i.e.* the numerical error) with $\bar{\tilde{D}}_f$. The error are acceptable for neutral points with low extensional stiffness ($c_\lambda = 1000, 1600, 1800$). However, for higher extensional stiffness the total error is quit large ($c_\lambda = 3500$).

4.7 Discussion

In this chapter we revisited the model for flow in a finite-length flexible-walled channel presented in chapter 3. However, in this case we assumed small amplitude perturbations from the static beam and expanded the variables to second order in amplitude. We then substituted these linearised variables into the system governing equations to obtain the corresponding governing equations at each order. We assumed a temporal wave-like form for all the first order variables and substituted into the first order governing equations (4.2.16-4.2.27) to obtain the eigenvalue problem of the system.

This eigenvalue problem was solved numerically using a numerical method similar to the fully non-linear problem.

We constructed numerical results for the eigenvalue problems. In particular, using a bisection method, we found the neutrally stable curve in parameter space spanned by Reynolds number and extensional stiffness (figure 4.2). The stability behavior of our model is consistent with Hao *et al*. [25] (as well as Luo *et al*. [48]) for extensional stiffness in the range $1000 - 2500$. However, for higher extensional stiffness, the stability properties are different. We presume this difference appears because we adopted a different Kirchhoff law in our model. The growth rate and frequency of the instability for several points in the parameter space were calculated (table 4.1). For example the growth rate of point $R = 207, c_\lambda = 1600, p_e = 1.95$ is negative while the growth rate of point $R = 214, c_\lambda = 1600, p_e = 1.95$ is positive, consistent with the observation of fully nonlinear system in chapter 3. We also calculated the second order energy budget time-averaged over one period of oscillation at neutrally stable points. However, for high extensional stiffness (*i.e.* $c_\lambda = 3500$) the error (*i.e.* the total energy in the system) is not yet sufficiently small. Developing methods to reduce this error is an on-going area of future work. We anticipate that once the error is within acceptable limits, the perturbation energy budget may provide a useful tool to distinguish the various modes of oscillation.

Chapter 5

Discussion and future work

In this thesis we have mainly discussed two models: a fluid-membrane model in an infinitely long channel and a fluid-beam model in a finite channel. We analysed the energy budget of both the fully nonlinear system and the linearised system for these two models. In each case the energy budget was derived in a way where the work done by the viscous forces was divided into two parts. One part of this work was contributed to the rate of working of fluid stress on the elastic wall while the other part was the dissipation energy in the bulk (which was positive definite as expected). Our aim was to then use this energy budget to distinguish the different modes which occur.

In chapter 2 we considered a fluid-membrane model where the effects of wall inertia, damping and viscous stresses acting on the membrane were taken into consideration. Three different modes of instability, *i.e*. Tollmien-Schlichting waves (TS), traveling-wave flutter (TWF) and static divergence (SD), were identified (see figure 2.2, 2.3 and 2.5). The classification of these modes of instability was verified by wall damping: TS waves and SD waves were class A (destabilised by wall damping) and TWF was class B (stabilised by wall damping) (see figure 2.6, 2.7 and 2.8). These were consistent with the observations of Davies & Carpenter [22]. We aimed to use the overall energy budget of the system to distinguish the different modes of instability (*i.e*. class A,B and C from Benjamin [3]). However, we found that the 'activation energy' (Landahl [45] and Cairns [17]) used to classify the instability mode is not equivalent to the work done by the fluid on the wall in our energy budget.

In future work we will compute the 'wave energy' discussed by Cairns [17] to connect the 'activation energy' (Landahl [45], Cairns [17]) with the Reynolds-Orr style energy discussed in chapter 2. We will also use the scalings identified in the numerical results as the mass of the wall becomes large to produce simplified (asymptotic) models of the system.

In chapter 3 and chapter 4 we employed a new beam law for the fluid-beam system compared with Luo *et al*. [48]. Both a fully nonlinear system (chapter 3) and a linearised system (chapter 4) were considered. Three possible static beam shapes were illustrated (see figure 3.7). The sta-

bility of these static shapes was analysed using the eigenvalue problem and the fully nonlinear simulation (see figure 3.10, 3.11 and points S1, N2 in table 4.1) and the predictions of both methods compared well. Large amplitude vorticity waves were observed in the plots of streamlines at different time instant in the downstream rigid section (in figure 3.13), which was previously observed by Luo *et al*. [48]. The neutral curve in the parameter space spanned by wall extensional stiffness and Reynolds number was traced, and both mode-2 and mode-3 neutral points were identified (see figure 4.2). The neutral curve for large extensional stiffness grew linearly with Reynolds number, which was consistent with the observation of Stewart [65]. The neutral curve of our model agreed with that of Luo *et al*. [48] when the wall extensional stiffness was in the range of $1000 - 2500$ (see figure 4.3) although they diverged strongly for larger stiffnesses. The energy budget of both fully nonlinear system and the linearised system were calculated. The derivations elucidated that the average energy budget over one period of oscillation for the fully nonlinear system exhibited a balance between the average of the net kinetic energy flux, the excess rate of working of pressure forces at the upstream end and the excess energy loss due to viscosity over one period (*i.e*. excess from the corresponding static state). This agreed with the computational results (see table 3.3). The energy budget of the linearised system was also calculated on neutral points (see table 4.2). For large extensional stiffness, the average of the total energy budget over one period (*i.e*. the error) was too large to be convinced about the validity of the results. We will continue working on the energy budget of the linearised system to get better agreement.

The numerical results has been calculated for a flux-driven problem (*i.e*. fixed inlet flux). For future work we will analyse the behavior of the pressure-driven problem (*i.e*. fixed pressure on inlet channel boundary) for the fluid-beam model used. We will test the energy partition for the pressure-driven problem identified by Jensen & Heil [42], who shared that two-thirds of the kinetic energy flux extracted from the mean flow was lost to dissipation energy for neutrally stable oscillations. This will require a much denser mesh to resolve the narrow Stokes layers on the channel walls.

Appendix A

Supplementary derivations for the fluid-beam model

In this appendix we give some detailed explanation of equations used in beam-fluid model.

A.1 Derivation of the beam governing equations

From the first beam momentum equation (3.3.5), rearranging it we obtain,

$$\frac{\partial}{\partial t}\left(\frac{\partial \mathbf{x}_b}{\partial t}\rho_m \partial l\right) = \partial \mathbf{F} + \mathbf{q}\partial s, \tag{A.1.1}$$

we divide both sides with ∂l ($\lambda = \partial l/\partial s$) to obtain,

$$\frac{\rho_m}{\lambda}\frac{\partial^2 \mathbf{x}_b}{\partial t^2} - \frac{\partial \mathbf{F}}{\partial l} - \lambda \mathbf{q} = 0. \tag{A.1.2}$$

We now rewrite the left hand side of (A.1.2) into the tangent and normal directions of beam by substituting (3.2.10) in *Sec*. 3.2 to obtain,

$$\begin{aligned}\frac{\rho_m}{\lambda}\left(\frac{\partial^2 x_b}{\partial t^2}\mathbf{g}_1 + \frac{\partial^2 y_b}{\partial t^2}\mathbf{g}_2\right) =& \frac{\rho_m}{\lambda}\left[\left(\frac{\partial x_b}{\partial l}\frac{\partial^2 x_b}{\partial t^2} + \frac{\partial y_b}{\partial l}\frac{\partial^2 y_b}{\partial t^2}\right)\mathbf{e}_1\right] \\ &+ \frac{\rho_m}{\lambda}\left[\left(\frac{\partial x_b}{\partial l}\frac{\partial^2 y_b}{\partial t^2} - \frac{\partial y_b}{\partial l}\frac{\partial^2 x_b}{\partial t^2}\right)\mathbf{e}_2\right].\end{aligned} \tag{A.1.3}$$

Firstly, we apply the Frenet Formulae ([55]) for the derivation of right hand of (A.1.2),

$$\frac{\partial \mathbf{e}_1}{\partial s} = \kappa \mathbf{e}_2, \quad \frac{\partial \mathbf{e}_2}{\partial s} = -\kappa \mathbf{e}_1 + \tau \mathbf{e}_3, \tag{A.1.4}$$

where κ and τ are the curvature and torsion of the curve. In our problem the torsion $\tau = 0$ for plane curve, so we have,

$$\frac{\partial \mathbf{e}_1}{\partial l} = \frac{\partial \mathbf{e}_1}{\partial s}\frac{\partial s}{\partial l} = \lambda\kappa\mathbf{e}_2, \quad \frac{\partial \mathbf{e}_2}{\partial l} = \frac{\partial \mathbf{e}_2}{\partial s}\frac{\partial s}{\partial l} = -\lambda\kappa\mathbf{e}_1. \tag{A.1.5}$$

We rewrite the right hand side of (A.1.2) with tangent and normal vectors of the beam $(\mathbf{e}_1, \mathbf{e}_2)$ and substitute (A.1.5) to obtain,

$$\begin{aligned}&\frac{\partial F_1}{\partial l}\mathbf{e}_1 + \frac{\partial F_2}{\partial l}\mathbf{e}_2 + F_1\frac{\partial \mathbf{e}_1}{\partial l} + F_2\frac{\partial \mathbf{e}_2}{\partial l} + (q_1\mathbf{e}_1 + q_2\mathbf{e}_2)\\ &= \left(\frac{\partial F_1}{\partial l} - \lambda\kappa F_2 + \lambda q_1\right)\mathbf{e}_1 + \left(\frac{\partial F_2}{\partial l} + \lambda\kappa F_1 + \lambda q_2\right)\mathbf{e}_2.\end{aligned} \tag{A.1.6}$$

By grouping the terms in the $\mathbf{e}_1$ and $\mathbf{e}_2$ directions from (A.1.2) we obtain,

$$\frac{\rho_m}{\lambda}\left(\frac{\partial x_b}{\partial l}\frac{\partial^2 x_b}{\partial t^2} + \frac{\partial y_b}{\partial l}\frac{\partial^2 y_b}{\partial t^2}\right) = \frac{\partial F_1}{\partial l} - \lambda\kappa F_2 + \lambda q_1, \tag{A.1.7}$$

$$\frac{\rho_m}{\lambda}\left(\frac{\partial x_b}{\partial l}\frac{\partial^2 y_b}{\partial t^2} - \frac{\partial y_b}{\partial l}\frac{\partial^2 x_b}{\partial t^2}\right) = \frac{\partial F_2}{\partial l} + \lambda\kappa F_1 + \lambda q_2. \tag{A.1.8}$$

Simplifying equation (3.3.6) we obtain

$$\frac{\partial}{\partial t}\left(\rho_m\mathbf{x}_b \times \frac{\partial \mathbf{x}_b}{\partial t}\right) = \frac{\partial \mathbf{M}}{\partial l} + \lambda\mathbf{x}_b \times \mathbf{q} + \frac{\partial \mathbf{x}_b}{\partial l} \times \mathbf{F} + \mathbf{x}_b \times \frac{\partial \mathbf{F}}{\partial l} + \frac{\partial \mathbf{x}_b \times \partial \mathbf{F}}{\partial l}. \tag{A.1.9}$$

Rearranging above equation (A.1.9) to obtain

$$\mathbf{x}_b \times \left(\frac{\partial}{\partial t}\left(\rho_m\frac{\partial \mathbf{x}_b}{\partial t}\right) - \lambda\mathbf{q} - \frac{\partial \mathbf{F}}{\partial l}\right) = \frac{\partial \mathbf{M}}{\partial l} + \frac{\partial \mathbf{x}_b}{\partial l} \times \mathbf{F} + \frac{\partial \mathbf{x}_b \times \partial \mathbf{F}}{\partial l}, \tag{A.1.10}$$

the left hand side of equation (A.1.10) equal to zero after applying equation (A.1.2), therefore we have

$$\underbrace{\frac{\partial \mathbf{M}}{\partial l}}_{I} + \underbrace{\frac{\partial \mathbf{x}_b}{\partial l} \times \mathbf{F}}_{II} + \underbrace{\frac{\partial \mathbf{x}_b \times \partial \mathbf{F}}{\partial l}}_{III} = 0, \tag{A.1.11}$$

we label above term as I, II and III and consider these in turn.
For I, by applying $\mathbf{M} = M\mathbf{e}_3$ we have,

$$I = \frac{\partial (M\mathbf{e}_3)}{\partial s} = \frac{\partial M}{\partial s}\mathbf{e}_3. \tag{A.1.12}$$

We apply (3.2.6) to write terms in the tangent and normal directions to the elastic beam and neglect the higher order terms (*i.e.* the product of two or more than two incremental terms) for II and III in the following derivation.

For II we have,

$$\begin{aligned}
II =& \frac{\partial}{\partial l}\left[\frac{1}{\lambda}\left(x_b\frac{\partial x_b}{\partial l}+y_b\frac{\partial y_b}{\partial l}\right)\mathbf{e}_1+\frac{1}{\lambda}\left(y_b\frac{\partial x_b}{\partial l}-x_b\frac{\partial y_b}{\partial l}\right)\mathbf{e}_2\right]\times\mathbf{F}\\
=& -\frac{1}{\lambda^2}\frac{\partial\lambda}{\partial l}\left[\left(x_b\frac{\partial x_b}{\partial l}+y_b\frac{\partial y_b}{\partial l}\right)\mathbf{e}_1+\left(y_b\frac{\partial x_b}{\partial l}-x_b\frac{\partial y_b}{\partial l}\right)\mathbf{e}_2\right]\times\mathbf{F}\\
&+\frac{1}{\lambda}\left[\left(\frac{\partial x_b}{\partial l}\right)^2+\left(\frac{\partial y_b}{\partial l}\right)^2+x_b\frac{\partial^2 x_b}{\partial l^2}+y_b\frac{\partial^2 y_b}{\partial l^2}\right]\mathbf{e}_1\times\mathbf{F}\\
&-\kappa\left(\frac{\partial x_b}{\partial l}y_b-\frac{\partial y_b}{\partial l}\right)\mathbf{e}_1\times\mathbf{F}+\left(\frac{\partial^2 x_b}{\partial l^2}y_b-\frac{\partial^2 y_b}{\partial l^2}x_b\right)\mathbf{e}_2\times\mathbf{F}\\
&+\kappa\left(x_b\frac{\partial x_b}{\partial l}+y_b\frac{\partial y_b}{\partial l}\right)\mathbf{e}_2\times\mathbf{F},\\
\approx&\lambda F_2\mathbf{e}_3,
\end{aligned}\tag{A.1.13}$$

Similarly, for III we have,

$$\begin{aligned}
III =& \partial\left[\frac{1}{\lambda}\left(x_b\frac{\partial x_b}{\partial l}+y_b\frac{\partial y_b}{\partial l}\right)\mathbf{e}_1+\frac{1}{\lambda}\left(x_b\frac{\partial y_b}{\partial s}-y_b\frac{\partial x_b}{\partial s}\right)\mathbf{e}_2\right]\\
&\times\left(\frac{\partial F_1}{\partial l}\mathbf{e}_1+F_1\frac{\partial\mathbf{e}_1}{\partial l}+\frac{\partial F_2}{\partial l}\mathbf{e}_2+F_2\frac{\partial\mathbf{e}_2}{\partial l}\right)\\
=&\left[\partial\left(\frac{1}{\lambda}\left(x_b\frac{\partial x_b}{\partial l}+y_b\frac{\partial y_b}{\partial l}\right)\right)\mathbf{e}_1+\frac{1}{\lambda}\left(x_b\frac{\partial x_b}{\partial l}+y_b\frac{\partial y_b}{\partial l}\right)\partial\mathbf{e}_1\right]\\
&\times\left(\frac{\partial F_1}{\partial l}\mathbf{e}_1+F_1\lambda\kappa\mathbf{e}_2+\frac{\partial F_2}{\partial l}\mathbf{e}_2-\lambda\kappa F_2\mathbf{e}_1\right)\\
&+\left[\partial\left(\frac{1}{\lambda}\left(y_b\frac{\partial x_b}{\partial l}-x_b\frac{\partial y_b}{\partial l}\right)\right)\mathbf{e}_2+\frac{1}{\lambda}\left(y_b\frac{\partial x_b}{\partial l}-x_b\frac{\partial y_b}{\partial l}\right)\partial\mathbf{e}_2\right]\\
&\times\left(\frac{\partial F_1}{\partial l}\mathbf{e}_1+F_1\lambda\kappa\mathbf{e}_2+\frac{\partial F_2}{\partial l}\mathbf{e}_2-\lambda\kappa F_2\mathbf{e}_1\right)\approx 0.
\end{aligned}\tag{A.1.14}$$

Therefore, (3.3.6) becomes,

$$\frac{\partial M}{\partial l}+\lambda F_2=0.$$

In total, from the beam momentum equations (3.3.5, 3.3.6), we obtain the beam governing equations,

$$\frac{\rho_m}{\lambda}\left(\frac{\partial x_b}{\partial l}\frac{\partial^2 x_b}{\partial t^2}+\frac{\partial y_b}{\partial l}\frac{\partial^2 y_b}{\partial t^2}\right)=\frac{\partial F_1}{\partial l}-\lambda\kappa F_2+\lambda q_1,\tag{A.1.15}$$

$$\frac{\rho_m}{\lambda}\left(\frac{\partial x_b}{\partial l}\frac{\partial^2 y_b}{\partial t^2}-\frac{\partial y_b}{\partial l}\frac{\partial^2 x_b}{\partial t^2}\right)=\frac{\partial F_2}{\partial l}+\lambda\kappa F_1+\lambda q_2,\tag{A.1.16}$$

$$\frac{\partial M}{\partial l}+\lambda F_2=0.\tag{A.1.17}$$

We rewrite the above equations using the material (reference) description to obtain equations (3.3.7-3.3.9) in *Sec*. 3.2,

$$\frac{\rho_m}{\lambda^{(c)}}\left(\frac{\partial x_b^{(c)}}{\partial s}\frac{\partial^2 x_b^{(c)}}{\partial t^2}+\frac{\partial y_b^{(c)}}{\partial s}\frac{\partial^2 y_b^{(c)}}{\partial t^2}\right)=\frac{\partial F_1^{(c)}}{\partial s}-\kappa^{(c)}F_2^{(c)}+q_1^{(c)}, \tag{3.3.7}$$

$$\frac{\rho_m}{\lambda^{(c)}}\left(\frac{\partial x_b^{(c)}}{\partial s}\frac{\partial^2 y_b^{(c)}}{\partial t^2}-\frac{\partial y_b^{(c)}}{\partial s}\frac{\partial^2 x_b^{(c)}}{\partial t^2}\right)=\frac{\partial F_2^{(c)}}{\partial s}+\kappa^{(c)}F_1^{(c)}+q_2^{(c)}, \tag{3.3.8}$$

$$\frac{\partial M^{(c)}}{\partial s}+F_2^{(c)}=0. \tag{3.3.9}$$

By using the Kirchhoff law (3.3.12) and equation (3.3.9), we have,

$$\frac{\partial F_1^{(c)}}{\partial s}=EA\frac{\partial \lambda^{(c)}}{\partial s}, \tag{A.1.18}$$

$$F_2^{(c)}=-\frac{\partial M^{(c)}}{\partial s}=-EJ\frac{\partial(\lambda^{(c)}\kappa^{(c)})}{\partial s}, \tag{A.1.19}$$

$$\frac{\partial F_2^{(c)}}{\partial s}=-EJ\frac{\partial^2(\lambda^{(c)}\kappa^{(c)})}{\partial s^2}. \tag{A.1.20}$$

Substituting equations (A.1.18-A.1.20) into beam equations (3.3.7, 3.3.8) we obtain the beam governing equations (3.3.13,3.3.14) in *Sec*. 3.2

$$\frac{\rho_m}{\lambda^{(c)}}\left(\frac{\partial x_b^{(c)}}{\partial s}\frac{\partial^2 x_b^{(c)}}{\partial t^2}+\frac{\partial y_b^{(c)}}{\partial s}\frac{\partial^2 y_b^{(c)}}{\partial t^2}\right)=EJ\kappa^{(c)}\frac{\partial\left(\lambda^{(c)}\kappa^{(c)}\right)}{\partial s}+EA\frac{\partial\lambda^{(c)}}{\partial s}+\sigma_1, \tag{3.3.13}$$

$$\begin{aligned}\frac{\rho_m}{\lambda^{(c)}}\left(\frac{\partial x_b^{(c)}}{\partial s}\frac{\partial^2 y_b^{(c)}}{\partial t^2}-\frac{\partial y_b^{(c)}}{\partial s}\frac{\partial^2 x_b^{(c)}}{\partial t^2}\right)=&-EJ\frac{\partial^2(\lambda^{(c)}\kappa^{(c)})}{\partial s^2}+EA\kappa^{(c)}(\lambda^{(c)}-1),\\ &+\kappa^{(c)}T+\sigma_2-p_e.\end{aligned} \tag{3.3.14}$$

A.2 Derivations of equations (3.3.23), (3.3.24) and (3.3.25) in *Sec*. 3.3.3

We introduce the angle θ shown in Figure 3.2 combined with equation (3.2.3). We have

$$\mathbf{e}_1=\frac{1}{\lambda}\mathbf{x}_b=\frac{1}{\lambda}\frac{\partial x_b}{\partial l}\mathbf{g}_1+\frac{1}{\lambda}\frac{\partial y_b}{\partial l}\mathbf{g}_2=\cos\theta\mathbf{g}_1+\sin\theta\mathbf{g}_2. \tag{A.2.1}$$

From the above formula we obtain that,

$$\frac{\partial x_b}{\partial l}=\lambda\cos\theta,\quad \frac{\partial y_b}{\partial l}=\lambda\sin\theta. \tag{A.2.2}$$

Sustituting (A.2.2) into the expression of curvature κ we have,

$$\begin{aligned}\kappa =& \frac{1}{\lambda^2}\left[\cos\theta\left(\frac{\partial\lambda}{\partial l}\sin\theta+\lambda\frac{\partial\theta}{\partial l}\cos\theta\right)-\sin\theta\left(\frac{\partial\lambda}{\partial l}\cos\theta-\lambda\frac{\partial\theta}{\partial l}\sin\theta\right)\right]\\ =& \frac{1}{\lambda}\frac{\partial\theta}{\partial l};\end{aligned} \tag{A.2.3}$$

rearranging (A.2.3) we obtain

$$\frac{\partial\theta}{\partial l}=\lambda\kappa. \tag{A.2.4}$$

A.3 Derivation of fluid energy equation (3.5.1) in *Sec*. 3.5

In this appendix, we give a detailed derivation of the rearrangement of the fluid energy equation (3.5.1) in *Sec*. 3.5.

First we label (3.5.1) in the four terms I, II, III and IV as follow and consider each in turn,

$$\underbrace{\frac{\partial\mathbf{u}}{\partial t}\cdot\mathbf{u}}_{I}+\underbrace{((\mathbf{u}\cdot\nabla)\mathbf{u})\cdot\mathbf{u}}_{II}=\underbrace{(\nabla\cdot(-p\mathbf{I}))\cdot\mathbf{u}}_{III}+\underbrace{R^{-1}\left(\nabla\cdot\left(\nabla\mathbf{u}+\nabla\mathbf{u}^{\mathrm{T}}\right)\right)\cdot\mathbf{u}}_{IV}. \tag{A.3.1}$$

We rearrange I as,

$$I=\frac{\partial\mathbf{u}}{\partial t}\cdot\mathbf{u}=\frac{1}{2}\frac{\partial\left(\mathbf{u}\cdot\mathbf{u}\right)}{\partial t}. \tag{A.3.2}$$

For II, we first write it into scaler form in the form,

$$\begin{aligned}II =& u_1\left(u_1\frac{\partial u_1}{\partial x}+u_2\frac{\partial u_1}{\partial y}\right)+u_2\left(u_1\frac{\partial u_2}{\partial x}+u_2\frac{\partial u_2}{\partial y}\right),\\ =& \left(u_1^2\frac{\partial u_1}{\partial x}+u_1u_2\frac{\partial u_2}{\partial x}\right)+\left(u_1u_2\frac{\partial u_1}{\partial y}+u_2^2\frac{\partial u_2}{\partial y}\right)=\frac{1}{2}u_1\frac{\partial(u_1^2+u_2^2)}{\partial x}+\frac{1}{2}u_2\frac{\partial(u_1^2+u_2^2)}{\partial y},\\ =& \frac{1}{2}\nabla\left(\mathbf{u}\cdot\mathbf{u}\right)\cdot\mathbf{u},\end{aligned}$$

then we write it back into vector form and apply $(\nabla f)\cdot\mathbf{u}=\nabla\cdot(f\mathbf{u})-f\nabla\cdot\mathbf{u}$ (here f is a scalar function, $\mathbf{u}$ is a vector function) to obtain,

$$II=\frac{1}{2}\nabla\cdot\left((\mathbf{u}\cdot\mathbf{u})\mathbf{u}\right)-\frac{1}{2}(\mathbf{u}\cdot\mathbf{u})\left(\nabla\cdot\mathbf{u}\right), \tag{A.3.3}$$

as the fluid is incompressible ($\nabla\cdot\mathbf{u}=0$) we have,

$$II=\frac{1}{2}\nabla\cdot\left((\mathbf{u}\cdot\mathbf{u})\mathbf{u}\right). \tag{A.3.4}$$

For *III*, by applying the identity $\nabla\cdot(f\boldsymbol{A}) = f(\nabla\cdot\boldsymbol{A}) + \boldsymbol{A}\nabla f$ (here $\boldsymbol{A}$ is a 2×2 matrix) we have,

$$III = -\big(p(\nabla\cdot\boldsymbol{I}) + \boldsymbol{I}\nabla p\big)\cdot\mathbf{u} = -(\nabla p)\cdot\mathbf{u};$$

again we apply $(\nabla f)\cdot\mathbf{u} = \nabla\cdot(f\mathbf{u}) - f\nabla\cdot\mathbf{u}$ and $\nabla\cdot\mathbf{u} = 0$ to obtain,

$$III = -\nabla\cdot(p\mathbf{u}) + p\nabla\cdot\mathbf{u} = -\nabla\cdot(p\mathbf{u}). \tag{A.3.5}$$

For *IV*, using $(\nabla\cdot\boldsymbol{A}^{\mathrm{T}})\cdot\mathbf{u} = \nabla\cdot(\boldsymbol{A}\mathbf{u}) - \mathrm{Tr}(\boldsymbol{A}(\nabla\mathbf{u}))$ (here $\boldsymbol{A}$ is a 2×2 matrix and $\mathbf{u}$ is a 2×1 vector, derived at the end of this section and Tr represent the trace of a matirx, detailed derivation in *Sec*. **??**) we have,

$$IV = R^{-1}\nabla\cdot\Big(\big(\nabla\mathbf{u} + \nabla\mathbf{u}^{\mathrm{T}}\big)\mathbf{u}\Big) - R^{-1}\mathrm{Tr}\Big(\big(\nabla\mathbf{u} + \nabla\mathbf{u}^{\mathrm{T}}\big)(\nabla\mathbf{u})\Big). \tag{A.3.6}$$

Therefore, we obtain the energy eqaution (3.5.2) in *Sec*. 3.5,

$$\begin{aligned}\frac{1}{2}\frac{\partial(\mathbf{u}\cdot\mathbf{u})}{\partial t} + \frac{1}{2}\nabla\cdot((\mathbf{u}\cdot\mathbf{u})\mathbf{u}) = &-\nabla\cdot(p\mathbf{u}) + R^{-1}\left[\nabla\cdot\big((\nabla\mathbf{u} + \nabla\mathbf{u}^{\mathrm{T}})\mathbf{u}\big)\right]\\ &- R^{-1}\left[\mathrm{Tr}\big((\nabla\mathbf{u} + \nabla\mathbf{u}^{\mathrm{T}})\nabla\mathbf{u}\big)\right].\end{aligned} \tag{3.5.2}$$

A.4 Derivations of equations (3.5.20) and (3.5.21)

In this appendix, we derive the equations

$$\frac{\partial u_{b1}^{(c)}}{\partial s} = \left(\lambda^{(c)}\right)^{-1}\frac{\partial\lambda^{(c)}}{\partial t} + \kappa u_{b2}^{(c)}, \tag{3.5.20}$$

$$\frac{\partial u_{b2}^{(c)}}{\partial s} = \frac{\partial\theta^{(c)}}{\partial t} - \kappa u_{b1}^{(c)}, \tag{3.5.21}$$

used during the derivation of beam energy budget in *Sec*. 3.5.
By changing equation (3.5.20) back to the material (reference) description and applying $\partial\mathbf{e}_1/\partial l = \lambda\kappa\mathbf{e}_2$ (A.1.5) we have,

$$\begin{aligned}\frac{\partial u_{b1}^{(c)}}{\partial s} =&\lambda^{-1}\frac{\partial(\mathbf{u}_b\cdot\mathbf{e}_1)}{\partial l} = \lambda^{-1}\left(\frac{\partial}{\partial l}\left(\frac{\partial\mathbf{x}_b}{\partial t}\right)\cdot\mathbf{e}_1 + \mathbf{u}_b\cdot\frac{\partial\mathbf{e}_1}{\partial l}\right),\\ =&\lambda^{-1}\left(\frac{\partial}{\partial t}\left(\frac{\partial\mathbf{x}_b}{\partial l}\right)\cdot\mathbf{e}_1 + \mathbf{u}_b\cdot\lambda\kappa\mathbf{e}_2\right),\end{aligned}$$

we apply $\partial\mathbf{x}_b/\partial l = \lambda\mathbf{e}_1$ (3.2.3) to obtain,

$$\frac{\partial u_{b1}^{(c)}}{\partial s} =\lambda^{-1}\left(\frac{\partial\lambda}{\partial t}\mathbf{e}_1\cdot\mathbf{e}_1 + \lambda\frac{\partial\mathbf{e}_1}{\partial t}\cdot\mathbf{e}_1 + \lambda\kappa u_{b2}\right),$$

since $(\partial \mathbf{e}_1/\partial t)\cdot\mathbf{e}_1 = 1/2(\partial(\mathbf{e}_1\cdot\mathbf{e}_1)/\partial t) = 0$ and use spatial (current) description we have,

$$\frac{\partial u_{b1}^{(c)}}{\partial s} = \frac{1}{\lambda^{(c)}}\frac{\partial \lambda^{(c)}}{\partial t} + \kappa^{(c)} u_{b2}^{(c)}. \tag{A.4.1}$$

Similarly, for (3.5.21) we change it back to material (reference) description and apply $\partial \mathbf{x}_b/\partial l = \lambda \mathbf{e}_1$ (3.2.3), $\partial \mathbf{e}_2/\partial l = -\lambda\kappa\mathbf{e}_1$ (A.1.5) to obtain,

$$\begin{aligned}\frac{\partial u_{b2}^{(c)}}{\partial s} &= \lambda^{-1}\left(\frac{\partial}{\partial l}(\mathbf{u}_b\cdot\mathbf{e}_2)\right) = \lambda^{-1}\left(\frac{\partial}{\partial l}\left(\frac{\partial \mathbf{x}_b}{\partial t}\right)\cdot\mathbf{e}_2 + \mathbf{u}_b\frac{\partial \mathbf{e}_2}{\partial l}\right),\\ &= \lambda^{-1}\left(\frac{\partial}{\partial t}(\lambda\mathbf{e}_1)\cdot\mathbf{e}_2 - \lambda\kappa u_{b1}\right) = \lambda^{-1}\left(\frac{\partial\lambda}{\partial t}\mathbf{e}_1\cdot\mathbf{e}_2 + \lambda\frac{\partial \mathbf{e}_1}{\partial t}\cdot\mathbf{e}_2 - \lambda\kappa u_{b1}\right),\\ &= \frac{\partial \mathbf{e}_1}{\partial t}\cdot\mathbf{e}_2 - \kappa u_{b1}.\end{aligned} \tag{A.4.2}$$

Now we need to derive $(\partial\mathbf{e}_1/\partial t)\cdot\mathbf{e}_2 = \partial\theta/\partial t$. On one hand we have,

$$\frac{\partial}{\partial l}\left(\frac{\partial \mathbf{e}_1}{\partial t}\cdot\mathbf{e}_2\right) = \frac{\partial}{\partial l}\left(\frac{\partial \mathbf{e}_1}{\partial t}\right)\cdot\mathbf{e}_2 + \frac{\partial \mathbf{e}_1}{\partial t}\cdot\frac{\partial \mathbf{e}_2}{\partial l} = \frac{\partial}{\partial t}\left(\frac{\partial \mathbf{e}_1}{\partial l}\right)\cdot\mathbf{e}_2 + \frac{\partial \mathbf{e}_1}{\partial t}\cdot\frac{\partial \mathbf{e}_2}{\partial l},$$

by applying (A.1.5), we have

$$\begin{aligned}\frac{\partial}{\partial l}\left(\frac{\partial \mathbf{e}_1}{\partial t}\cdot\mathbf{e}_2\right) &= \frac{\partial(\lambda\kappa\mathbf{e}_2)}{\partial t}\cdot\mathbf{e}_2 + \frac{\partial \mathbf{e}_1}{\partial t}\cdot(-\lambda\kappa\mathbf{e}_1) = \frac{\partial(\lambda\kappa\mathbf{e}_2)}{\partial t}\cdot\mathbf{e}_2 - \lambda\kappa\frac{\partial \mathbf{e}_1}{\partial t}\cdot\mathbf{e}_1,\\ &= \frac{\partial(\lambda\kappa\mathbf{e}_2)}{\partial t}\cdot\mathbf{e}_2.\end{aligned}$$

On the other hand by applying $\partial\theta/\partial l = \lambda\kappa$ (3.5.22) and $\mathbf{e}_2\cdot(\partial\mathbf{e}_2/\partial t) = 1/2(\partial(\mathbf{e}_2\cdot\mathbf{e}_2)/\partial t) = 0$ we have,

$$\frac{\partial}{\partial l}\left(\frac{\partial\theta}{\partial t}\right) = \frac{\partial}{\partial t}\left(\frac{\partial\theta}{\partial l}\right) = \frac{\partial(\lambda\kappa)}{\partial t} = \frac{\partial(\lambda\kappa\mathbf{e}_2\cdot\mathbf{e}_2)}{\partial t} = \frac{\partial(\lambda\kappa\mathbf{e}_2)}{\partial t}\cdot\mathbf{e}_2 + \lambda\kappa\left(\mathbf{e}_2\cdot\frac{\partial \mathbf{e}_2}{\partial t}\right)$$

$$= \frac{\partial(\lambda\kappa\mathbf{e}_2)}{\partial t}\cdot\mathbf{e}_2.$$

Hence, we have

$$\frac{\partial}{\partial l}\left(\frac{\partial \mathbf{e}_1}{\partial t}\cdot\mathbf{e}_2\right) = \frac{\partial}{\partial l}\left(\frac{\partial\theta}{\partial t}\right),$$

which gives us that,

$$\frac{\partial \mathbf{e}_1}{\partial t}\cdot\mathbf{e}_2 = \frac{\partial\theta}{\partial t}. \tag{A.4.3}$$

Substituting (A.4.3) into the first term in (A.4.2) and using the spatial (current) description we have,

$$\frac{\partial u_{b2}^{(c)}}{\partial s} = \frac{\partial \theta^{(c)}}{\partial t} - \kappa^{(c)} u_b^{(c)}. \tag{A.4.4}$$

A.5 Linearise the fluid stress tensor $\boldsymbol{\sigma}$

The fluid stress tensor can be expressed as,

$$\boldsymbol{\sigma} = -p\boldsymbol{I} + R^{-1}\big(\nabla\mathbf{u} + (\nabla\mathbf{u})^{\mathrm{T}}\big). \tag{A.5.1}$$

For the right hand side of (A.5.1), we linearised the velocity and pressure based on the steady beam (4.1.1) using Taylor expansion to obtain,

$$\begin{aligned}
&\Big(-p\boldsymbol{I} + R^{-1}\left(\nabla\mathbf{u} + \nabla\mathbf{u}^{\mathrm{T}}\right)\Big)\Big|_{(x_b,y_b)} = \Big(-P\mathbf{I} + R^{-1}\left(\nabla\mathbf{U} + \nabla\mathbf{U}^{\mathrm{T}}\right)\Big)\Big|_{(X_b,Y_b)} \\
&+\varepsilon\left(\hat{x}_b\frac{\partial}{\partial x}\big(-P\mathbf{I} + R^{-1}(\nabla\mathbf{U} + \nabla\mathbf{U}^{\mathrm{T}})\big) + \hat{y}_b\frac{\partial}{\partial y}\big(-P\mathbf{I} + R^{-1}(\nabla\mathbf{U} + \nabla\mathbf{U}^{\mathrm{T}})\big)\right)\Big|_{(X_b,Y_b)} \\
&+\varepsilon\Big(-\hat{p}\mathbf{I} + R^{-1}(\nabla\hat{\mathbf{u}} + \nabla\hat{\mathbf{u}}^{\mathrm{T}})\Big)\Big|_{(X_b,Y_b)} + \varepsilon^2\Big(\check{x}_b\frac{\partial}{\partial x}\big(-P\mathbf{I} + R^{-1}(\nabla\mathbf{U} + \nabla\mathbf{U}^{\mathrm{T}})\big)\Big)\Big|_{(X_b,Y_b)} \\
&+\varepsilon^2\Big(\check{y}_b\frac{\partial}{\partial y}\big(-P\mathbf{I} + R^{-1}(\nabla\mathbf{U} + \nabla\mathbf{U}^{\mathrm{T}})\big) + \frac{\hat{x}_b^2}{2}\frac{\partial^2}{\partial x^2}\big(-P\mathbf{I} + R^{-1}(\nabla\mathbf{U} + \nabla\mathbf{U}^{\mathrm{T}})\big)\Big)\Big|_{(X_b,Y_b)}
\end{aligned}$$

$$\begin{aligned}
&+\varepsilon^2\Big(\frac{\hat{y}_b^2}{2}\frac{\partial^2}{\partial y^2}\big(-P\mathbf{I} + R^{-1}(\nabla\mathbf{U} + \nabla\mathbf{U}^{\mathrm{T}})\big) + \frac{\hat{x}_b\hat{y}_b}{2}\frac{\partial^2}{\partial x\partial y}\big(-P\mathbf{I} + R^{-1}(\nabla\mathbf{U} + \nabla\mathbf{U}^{\mathrm{T}})\big)\Big)\Big|_{(X_b,Y_b)} \\
&+\varepsilon^2\Big(\hat{x}_b\frac{\partial}{\partial x}\big(-\hat{p}\mathbf{I} + R^{-1}(\nabla\hat{\mathbf{u}} + \nabla\hat{\mathbf{u}}^{\mathrm{T}})\big) + \hat{y}_b\frac{\partial}{\partial y}\big(-\hat{p}\mathbf{I} + R^{-1}(\nabla\hat{\mathbf{u}} + \nabla\hat{\mathbf{u}}^{\mathrm{T}})\big)\Big)\Big|_{(X_b,Y_b)} \\
&+\varepsilon^2\Big(-\check{p}\mathbf{I} + R^{-1}(\nabla\check{\mathbf{u}} + \nabla\check{\mathbf{u}}^{\mathrm{T}})\Big)\Big|_{(X_b,Y_b)}.
\end{aligned} \tag{A.5.2}$$

For the left hand side of (A.5.1), we linearise based on the steady beam using Taylor expansions, where we have

$$\begin{aligned}
\boldsymbol{\sigma}\big|_{(x_b,y_b)} =& \boldsymbol{\Sigma}\big|_{(X_b,Y_b)} + \varepsilon\left(\hat{x}_b\frac{\partial\boldsymbol{\Sigma}}{\partial x} + \hat{y}_b\frac{\partial\boldsymbol{\Sigma}}{\partial y} + \hat{\boldsymbol{\sigma}}\right)\Big|_{(X_b,Y_b)} \\
&+\varepsilon^2\left(\check{x}_b\frac{\partial\boldsymbol{\Sigma}}{\partial x} + \check{y}_b\frac{\partial\boldsymbol{\Sigma}}{\partial y} + \frac{\hat{x}_b^2}{2}\frac{\partial^2\boldsymbol{\Sigma}}{\partial x^2} + \frac{\hat{y}_b^2}{2}\frac{\partial^2\boldsymbol{\Sigma}}{\partial y^2} + \frac{\hat{x}_b\hat{y}_b}{2}\frac{\partial^2\boldsymbol{\Sigma}}{\partial x\partial y}\right)\Big|_{(X_b,Y_b)} \\
&+\varepsilon^2\left(\hat{x}_b\frac{\partial\hat{\boldsymbol{\sigma}}}{\partial x} + \hat{y}_b\frac{\partial\hat{\boldsymbol{\sigma}}}{\partial y} + \check{\boldsymbol{\sigma}}\right)\Big|_{(X_b,Y_b)}.
\end{aligned} \tag{A.5.3}$$

In total, the fluid stress tensor expression (A.5.1), at $O(1)$ we have,

$$\boldsymbol{\Sigma}\big|_{(X_b,Y_b)} = \Big(-P\mathbf{I} + R^{-1}\left(\nabla\mathbf{U} + \nabla\mathbf{U}^{\mathrm{T}}\right)\Big)\Big|_{(X_b,Y_b)}. \tag{A.5.4}$$

At $O(\varepsilon)$ we have,

$$\begin{aligned}\left(\hat{x}_b\frac{\partial\boldsymbol{\Sigma}}{\partial x} + \hat{y}_b\frac{\partial\boldsymbol{\Sigma}}{\partial y} + \hat{\boldsymbol{\sigma}}\right)\Big|_{(X_b,Y_b)} &= \left(\hat{x}_b\frac{\partial}{\partial x}\big(-P\mathbf{I} + R^{-1}(\nabla\mathbf{U} + \nabla\mathbf{U}^{\mathrm{T}})\big)\right)\Big|_{(X_b,Y_b)} \\ &+ \left(\hat{y}_b\frac{\partial}{\partial y}\big(-P\mathbf{I} + R^{-1}(\nabla\mathbf{U} + \nabla\mathbf{U}^{\mathrm{T}})\big) + -\hat{p}\mathbf{I} + R^{-1}(\nabla\hat{\mathbf{u}} + \nabla\hat{\mathbf{u}}^{\mathrm{T}})\right)\Big|_{(X_b,Y_b)}.\end{aligned} \tag{A.5.5}$$

At $O(\varepsilon^2)$ we have,

$$\begin{aligned}&\left(\check{x}_b\frac{\partial\boldsymbol{\Sigma}}{\partial x} + \check{y}_b\frac{\partial\boldsymbol{\Sigma}}{\partial y} + \frac{\hat{x}_b^2}{2}\frac{\partial^2\boldsymbol{\Sigma}}{\partial x^2} + \frac{\hat{y}_b^2}{2}\frac{\partial^2\boldsymbol{\Sigma}}{\partial y^2} + \frac{\hat{x}_b\hat{y}_b}{2}\frac{\partial^2\boldsymbol{\Sigma}}{\partial x\partial y} + \hat{x}_b\frac{\partial\hat{\boldsymbol{\sigma}}}{\partial x} + \hat{y}_b\frac{\partial\hat{\boldsymbol{\sigma}}}{\partial y} + \check{\boldsymbol{\sigma}}\right)\Big|_{(X_b,Y_b)} \\ =&\Big(\check{x}_b\frac{\partial}{\partial x}\big(-P\mathbf{I} + R^{-1}(\nabla\mathbf{U} + \nabla\mathbf{U}^{\mathrm{T}})\big) + \check{y}_b\frac{\partial}{\partial y}\big(-P\mathbf{I} + R^{-1}(\nabla\mathbf{U} + \nabla\mathbf{U}^{\mathrm{T}})\big)\Big)\Big|_{(X_b,Y_b)} \\ &+ \Big(\frac{\hat{x}_b^2}{2}\frac{\partial^2}{\partial x^2}\big(-P\mathbf{I} + R^{-1}(\nabla\mathbf{U} + \nabla\mathbf{U}^{\mathrm{T}})\big) + \frac{\hat{y}_b^2}{2}\frac{\partial^2}{\partial y^2}\big(-P\mathbf{I} + R^{-1}(\nabla\mathbf{U} + \nabla\mathbf{U}^{\mathrm{T}})\big)\Big)\Big|_{(X_b,Y_b)} \\ &+ \Big(\frac{\hat{x}_b\hat{y}_b}{2}\frac{\partial^2}{\partial x\partial y}\big(-P\mathbf{I} + R^{-1}(\nabla\mathbf{U} + \nabla\mathbf{U}^{\mathrm{T}})\big) + \hat{x}_b\frac{\partial}{\partial x}\big(-\hat{p}\mathbf{I} + R^{-1}(\nabla\hat{\mathbf{u}} + \nabla\hat{\mathbf{u}}^{\mathrm{T}})\big)\Big)\Big|_{(X_b,Y_b)} \\ &+ \Big(\hat{y}_b\frac{\partial}{\partial y}\big(-\hat{p}\mathbf{I} + R^{-1}(\nabla\hat{\mathbf{u}} + \nabla\hat{\mathbf{u}}^{\mathrm{T}})\big) - \check{p}\mathbf{I} + R^{-1}(\nabla\check{\mathbf{u}} + \nabla\check{\mathbf{u}}^{\mathrm{T}})\Big)\Big|_{(X_b,Y_b)}.\end{aligned} \tag{A.5.6}$$

Substituting (A.5.4) into (A.5.5), we obtain

$$\hat{\boldsymbol{\sigma}}\big|_{(X_b,Y_b)} = \Big(-\hat{p}\mathbf{I} + R^{-1}\left(\nabla\hat{\mathbf{u}} + \nabla\hat{\mathbf{u}}^{\mathrm{T}}\right)\Big)\Big|_{(X_b,Y_b)}. \tag{A.5.7}$$

Substituting (A.5.4) and (A.5.7) we have

$$\check{\boldsymbol{\sigma}}\big|_{(X_b,Y_b)} = \Big(-\check{p}\mathbf{I} + R^{-1}\left(\nabla\check{\mathbf{u}} + \nabla\check{\mathbf{u}}^{\mathrm{T}}\right)\Big)\Big|_{(X_b,Y_b)}. \tag{A.5.8}$$

Therefore, we obtain the perturbed fluid stress on the steady beam,

$$\boldsymbol{\Sigma}\big|_{(X_b,Y_b)} = \Big(-P\mathbf{I} + R^{-1}\left(\nabla\mathbf{U} + \nabla\mathbf{U}^{\mathrm{T}}\right)\Big)\Big|_{(X_b,Y_b)} \tag{A.5.9}$$

$$\hat{\boldsymbol{\sigma}}\big|_{(X_b,Y_b)} = \Big(-\hat{p}\mathbf{I} + R^{-1}\left(\nabla\hat{\mathbf{u}} + \nabla\hat{\mathbf{u}}^{\mathrm{T}}\right)\Big)\Big|_{(X_b,Y_b)} \tag{A.5.10}$$

$$\check{\boldsymbol{\sigma}}\big|_{(X_b,Y_b)} = \Big(-\check{p}\mathbf{I} + R^{-1}\left(\nabla\check{\mathbf{u}} + \nabla\check{\mathbf{u}}^{\mathrm{T}}\right)\Big)\Big|_{(X_b,Y_b)}. \tag{A.5.11}$$

A.6 Linearize equations (3.5.20), (3.5.21) and (3.5.22)

Here we linearize two equations

$$\frac{\partial u_{b1}^{(c)}}{\partial s} = \left(\lambda^{(c)}\right)^{-1} \frac{\partial \lambda^{(c)}}{\partial t} + \kappa u_{b2}^{(c)}, \tag{3.5.20}$$

$$\frac{\partial u_{b2}^{(c)}}{\partial s} = \frac{\partial \theta^{(c)}}{\partial t} - \kappa u_{b1}^{(c)}, \tag{3.5.21}$$

$$\frac{\partial \theta}{\partial l} = \lambda \kappa, \tag{3.5.22}$$

used during derivation of the perturbation energy budget in chapter 4. For simplicity, we first write these three equations using the reference (material) description in the form

$$\frac{\partial u_{b1}}{\partial l} = \frac{\partial \lambda}{\partial t} + \lambda \kappa u_{b2}, \tag{A.6.1}$$

$$\frac{\partial u_{b2}}{\partial l} = \lambda \frac{\partial \theta}{\partial t} - \lambda \kappa u_{b1}, \tag{A.6.2}$$

$$\frac{\partial \theta}{\partial l} = \lambda \kappa; \tag{A.6.3}$$

Substituting the linearized variables (4.1.2) into above identities (A.6.1-A.6.3), at $O(\varepsilon)$ we obtain

$$\frac{\partial \hat{u}_{b1}}{\partial l} = \frac{\partial \hat{\lambda}}{\partial t} + \Lambda K \hat{u}_{b2}, \tag{A.6.4}$$

$$\frac{\partial \hat{u}_{b2}}{\partial l} = \Lambda \frac{\partial \hat{\theta}}{\partial t} - \Lambda K \hat{u}_{b1}, \tag{A.6.5}$$

$$\frac{\partial \hat{\theta}}{\partial l} = \Lambda \hat{\kappa} + K \hat{\lambda}, \tag{A.6.6}$$

rewriting above two equations (A.6.4) and (A.6.5) using current (spatial) description, while keeping using the reference description for the equation (A.6.6) we obtain,

$$\frac{\partial \hat{u}_{b1}^{(c)}}{\partial S} = \Lambda^{-1} \frac{\partial \hat{\lambda}^{(c)}}{\partial t} + K^{(c)} \hat{u}_{b2}^{(c)}, \tag{A.6.7}$$

$$\frac{\partial \hat{u}_{b2}^{(c)}}{\partial S} = \frac{\partial \hat{\theta}^{(c)}}{\partial t} - K^{(c)} \hat{u}_{b1}^{(c)}, \tag{A.6.8}$$

$$\frac{\partial \hat{\theta}}{\partial l} = \Lambda \hat{\kappa} + K \hat{\lambda}. \tag{A.6.9}$$

At $O(\varepsilon^2)$, the linearised identities using reference (material) description takes the form

$$\frac{\partial \breve{u}_{b1}}{\partial l} = \frac{\partial \breve{\lambda}}{\partial t} + \Lambda K \breve{u}_{b2} + \left(\hat{\lambda} K + \Lambda \hat{k}\right) \hat{u}_{b2}, \tag{A.6.10}$$

$$\frac{\partial \breve{u}_{b2}}{\partial l} = \left(\Lambda \frac{\partial \breve{\theta}}{\partial t} + \hat{\lambda} \frac{\partial \hat{\theta}}{\partial t}\right) - \Lambda K \breve{u}_{b1} - \left(\hat{\lambda} K + \Lambda \hat{k}\right) \hat{u}_{b1}, \tag{A.6.11}$$

$$\frac{\partial \breve{\theta}}{\partial l} = \Lambda \breve{\kappa} + \hat{\lambda} \hat{\kappa} + \breve{\lambda} K; \tag{A.6.12}$$

rewriting above equations (A.6.10), (A.6.11) using current (spatial) description and keeping using reference description for equation (A.6.12), we have

$$\frac{\partial \breve{u}_{b1}^{(c)}}{\partial S} = \frac{1}{\Lambda^{(c)}} \frac{\partial \breve{\lambda}^{(c)}}{\partial t} - \frac{\hat{\lambda}^{(c)}}{\left(\Lambda^{(c)}\right)^2} \frac{\partial \hat{\lambda}^{(c)}}{\partial t} + K^{(c)} \breve{u}_{b2}^{(c)} + \hat{\kappa}^{(c)} \hat{u}_{b2}^{(c)}, \tag{A.6.13}$$

$$\frac{\partial \breve{u}_{b2}^{(c)}}{\partial S} = \frac{\partial \breve{\theta}^{(c)}}{\partial t} - K^{(c)} \breve{u}_{b1}^{(c)} - \hat{\kappa}^{(c)} \hat{u}_{b1}^{(c)}, \tag{A.6.14}$$

$$\frac{\partial \breve{\theta}}{\partial l} = \Lambda \breve{\kappa} + \hat{\lambda} \hat{\kappa} + \breve{\lambda} K. \tag{A.6.15}$$

Bibliography

[1] Walter Edwin Arnoldi. The principle of minimized iterations in the solution of the matrix eigenvalue problem. *Quarterly of applied mathematics*, 9(1):17–29, 1951.

[2] T Brooke Benjamin. Effects of a flexible boundary on hydrodynamic stability. *Journal of Fluid Mechanics*, 9(4):513–532, 1960.

[3] T Brooke Benjamin. The threefold classification of unstable disturbances in flexible surfaces bounding inviscid flows. *Journal of Fluid Mechanics*, 16(3):436–450, 1963.

[4] CD Bertram. Two models of instability in a thick-walled collapsible tube conveying a flow. *Journal of Biomechanics*, 15(3):223–224, 1982.

[5] CD Bertram. Unstable equilibrium behaviour in collapsible tubes. *Journal of biomechanics*, 19(1):61–69, 1986.

[6] CD Bertram. Experimental studies of collapsible tubes. In *Flow past highly compliant boundaries and in collapsible tubes*, pages 51–65. Springer, 2003.

[7] CD Bertram and RJ Castles. Flow limitation in uniform thick-walled collapsible tubes. *Journal of Fluids and Structures*, 13(3):399–418, 1999.

[8] CD Bertram, G Diaz de Tuesta, and AH Nugent. Laser-doppler measurements of velocities just downstream of a collapsible tube during flow-induced oscillations. *Journal of biomechanical engineering*, 123(5):493–499, 2001.

[9] CD Bertram and AH Nugent. The flow field downstream of an oscillating collapsed tube. *Journal of biomechanical engineering*, 127(1):39–45, 2005.

[10] CD Bertram and TJ Pedley. A mathematical model of unsteady collapsible tube behaviour. *Journal of Biomechanics*, 15(1):39–50, 1982.

[11] CD Bertram, CJ Raymond, and KSA Butcher. Oscillations in a collapsed-tube analog of the brachial artery under a sphygmomanometer cuff. *Journal of biomechanical engineering*, 111(3):185–191, 1989.

[12] CD Bertram, CJ Raymond, and TJ Pedley. Mapping of instabilities for flow through collapsed tubes of differing length. *Journal of Fluids and Structures*, 4(2):125–153, 1990.

[13] CD Bertram, CJ Raymond, and TJ Pedley. Application of nonlinear dynamics concepts to the analysis of self-excited oscillations of a collapsible tube conveying a fluid. *Journal of Fluids and Structures*, 5(4):391–426, 1991.

[14] CD Bertram, NK Truong, and SD Hall. Piv measurements of the flow field just downstream of an oscillating collapsible tube. *Journal of biomechanical engineering*, 130(6):061011, 2008.

[15] CD Bertram and J Tscherry. The onset of flow-rate limitation and flow-induced oscillations in collapsible tubes. *Journal of fluids and structures*, 22(8):1029–1045, 2006.

[16] ZX Cai and XY Luo. A fluid–beam model for flow in a collapsible channel. *Journal of Fluids and Structures*, 17(1):125–146, 2003.

[17] RA Cairns. The role of negative energy waves in some instabilities of parallel flows. *Journal of Fluid Mechanics*, 92(1):1–14, 1979.

[18] Claudio Cancelli and TJ Pedley. A separated-flow model for collapsible-tube oscillations. *Journal of Fluid Mechanics*, 157:375–404, 1985.

[19] Peter W Carpenter and Timothy J Pedley. *Flow Past Highly Compliant Boundaries and in Collapsible Tubes: Proceedings of the IUTAM Symposium held at the University of Warwick, United Kingdom, 26–30 March 2001*, volume 72. Springer Science & Business Media, 2013.

[20] PW Carpenter and AD Garrad. The hydrodynamic stability of flow over kramer-type compliant surfaces. part 1. tollmien-schlichting instabilities. *Journal of Fluid Mechanics*, 155:465–510, 1985.

[21] William A Conrad. Pressure-flow relationships in collapsible tubes. *IEEE Transactions on Biomedical Engineering*, (4):284–295, 1969.

[22] Christopher Davies and Peter W Carpenter. Instabilities in a plane channel flow between compliant walls. *Journal of Fluid Mechanics*, 352:205–243, 1997.

[23] Jean Donea, S Giuliani, and Jean-Pierre Halleux. An arbitrary lagrangian-eulerian finite element method for transient dynamic fluid-structure interactions. *Computer methods in applied mechanics and engineering*, 33(1-3):689–723, 1982.

[24] PG Drazin and JC Crepeau. Introduction to hydrodynamic stability, 2003.

[25] Yujue Hao, Zongxi Cai, Steven Roper, and Xiaoyu Luo. An arnoldi-frontal approach for the stability analysis of flows in a collapsible channel. *International Journal of Applied Mechanics*, 8(06):1650073, 2016.

[26] S Hayashi, T Hayase, and H Kawamura. Numerical analysis for stability and self-excited oscillation in collapsible tube flow. *Journal of biomechanical engineering*, 120(4):468–475, 1998.

[27] Andrew L Hazel and Matthias Heil. Steady finite-reynolds-number flows in three-dimensional collapsible tubes. *Journal of Fluid Mechanics*, 486:79–103, 2003.

[28] M Heil and TJ Pedley. Large axisymmetric deformation of a cylindrical shell conveying a viscous flow. *Journal of Fluids and Structures*, 9(3):237–256, 1995.

[29] M Heil and TJ Pedley. Large post-buckling deformations of cylindrical shells conveying viscous flow. *Journal of Fluids and Structures*, 10(6):565–599, 1996.

[30] Matthias Heil. The stability of cylindrical shells conveying viscous flow. *Journal of Fluids and Structures*, 10(2):173–196, 1996.

[31] Matthias Heil. Stokes flow in collapsible tubes: computation and experiment. *Journal of Fluid Mechanics*, 353:285–312, 1997.

[32] Matthias Heil and Sarah L Waters. Transverse flows in rapidly oscillating elastic cylindrical shells. *Journal of Fluid Mechanics*, 547:185–214, 2006.

[33] Matthias Heil and Sarah L Waters. How rapidly oscillating collapsible tubes extract energy from a viscous mean flow. *Journal of Fluid Mechanics*, 601:199–227, 2008.

[34] Gerhard A Holzapfel. Nonlinear solid mechanics: a continuum approach for engineering science. *Meccanica*, 37(4):489–490, 2002.

[35] L Huang. Reversal of the bernoulli effect and channel flutter. *Journal of fluids and structures*, 12(2):131–151, 1998.

[36] PS Huyakorn, C Taylor, RL Lee, and PM Gresho. A comparison of various mixed-interpolation finite elements in the velocity-pressure formulation of the navier-stokes equations. *Computers & Fluids*, 6(1):25–35, 1978.

[37] T Ikeda and Y Matsuzaki. A one-dimensional unsteady separable and reattachable flow model for collapsible tube-flow analysis. *Journal of biomechanical engineering*, 121(2):153–159, 1999.

[38] Bruce M Irons. A frontal solution program for finite element analysis. *International Journal for Numerical Methods in Engineering*, 2(1):5–32, 1970.

[39] OE Jensen. Instabilities of flow in a collapsed tube. *Journal of Fluid Mechanics*, 220:623–659, 1990.

[40] OE Jensen. Chaotic oscillations in a simple collapsible-tube model. *Journal of biomechanical engineering*, 114(1):55–59, 1992.

[41] OE Jensen and TJ Pedley. The existence of steady flow in a collapsed tube. *Journal of Fluid Mechanics*, 206:339–374, 1989.

[42] Oliver E Jensen and Matthias Heil. High-frequency self-excited oscillations in a collapsible-channel flow. *Journal of Fluid Mechanics*, 481:235–268, 2003.

[43] Adolph I Katz, Yu Chen, and Augusto H Moreno. Flow through a collapsible tube: experimental analysis and mathematical model. *Biophysical Journal*, 9(10):1261, 1969.

[44] V Kumaran. Stability of the viscous flow of a fluid through a flexible tube. *Journal of Fluid Mechanics*, 294:259–281, 1995.

[45] Marten T Landahl. On the stability of a laminar incompressible boundary layer over a flexible surface. *Journal of Fluid Mechanics*, 13(4):609–632, 1962.

[46] HF Liu, XY Luo, and ZX Cai. Stability and energy budget of pressure-driven collapsible channel flows. *Journal of Fluid Mechanics*, 705:348–370, 2012.

[47] TW Lowe and TJ Pedley. Computation of stokes flow in a channel with a collapsible segment. *Journal of Fluids and Structures*, 9(8):885–905, 1995.

[48] XY Luo, ZX Cai, WG Li, and TJ Pedley. The cascade structure of linear instability in collapsible channel flows. *Journal of Fluid Mechanics*, 600:45–76, 2008.

[49] XY Luo and TJ Pedley. A numerical simulation of steady flow in a 2-d collapsible channel. *Journal of Fluids and Structures*, 9(2):149–174, 1995.

[50] XY Luo and TJ Pedley. A numerical simulation of unsteady flow in a two-dimensional collapsible channel. *Journal of Fluid Mechanics*, 314:191–225, 1996.

[51] XY Luo and TJ Pedley. The effects of wall inertia on flow in a two-dimensional collapsible channel. *Journal of Fluid Mechanics*, 363:253–280, 1998.

[52] XY Luo and TJ Pedley. Multiple solutions and flow limitation in collapsible channel flows. *Journal of Fluid Mechanics*, 420:301–324, 2000.

[53] A Marzo, XY Luo, and CD Bertram. Three-dimensional collapse and steady flow in thick-walled flexible tubes. *Journal of Fluids and Structures*, 20(6):817–835, 2005.

[54] Yuji Matsuzaki and Kyozo Fujimura. Reexamination of steady solutions of a collapsible channel conveying fluid. *Journal of biomechanical engineering*, 117(4):492–494, 1995.

[55] Barrett O'neill. *Elementary differential geometry*. Elsevier, 2006.

[56] TJ Pedley. Longitudinal tension variation in collapsible channels: a new mechanism for the breakdown of steady flow. *Journal of biomechanical engineering*, 114(1):60–67, 1992.

[57] TJ Pedley and KD Stephanoff. Flow along a channel with a time-dependent indentation in one wall: the generation of vorticity waves. *Journal of Fluid Mechanics*, 160:337–367, 1985.

[58] Mark Peter Rast. Simultaneous solution of the navier-stokes and elastic membrane equations by a finite element method. *International journal for numerical methods in fluids*, 19(12):1115–1135, 1994.

[59] JW Reyn. Multiple solutions and flow limitation for steady flow through a collapsible tube held open at the ends. *Journal of Fluid Mechanics*, 174:467–493, 1987.

[60] Kenneth J Ruschak. A method for incorporating free boundaries with surface tension in finite element fluid-flow simulators. *International Journal for Numerical Methods in Engineering*, 15(5):639–648, 1980.

[61] Hermann Schlichting. Zur enstehung der turbulenz bei der plattenströmung. *Nachrichten von der Gesellschaft der Wissenschaften zu Göttingen, Mathematisch-Physikalische Klasse*, 1933:181–208, 1933.

[62] Peter J Schmid and Dan S Henningson. *Stability and transition in shear flows*, volume 142. Springer Science & Business Media, 2012.

[63] V Shankar and V Kumaran. Stability of wall modes in fluid flow past a flexible surface. *Physics of fluids*, 14(7):2324–2338, 2002.

[64] Ascher H Shapiro. Steady flow in collapsible tubes. *Journal of Biomechanical Engineering*, 99(3):126–147, 1977.

[65] Peter S Stewart. Instabilities in flexible channel flow with large external pressure. *Journal of Fluid Mechanics*, 825:922–960, 2017.

[66] Peter S Stewart, Matthias Heil, Sarah L Waters, and Oliver E Jensen. Sloshing and slamming oscillations in a collapsible channel flow. *Journal of Fluid Mechanics*, 662:288–319, 2010.

[67] Peter S Stewart, Sarah L Waters, John Billingham, and Oliver E Jensen. Spatially localised growth within global instabilities of flexible channel flows. In *Seventh IUTAM Symposium on Laminar-Turbulent Transition*, pages 397–402. Springer, 2010.

[68] Peter S Stewart, Sarah L Waters, and Oliver E Jensen. Local and global instabilities of flow in a flexible-walled channel. *European Journal of Mechanics-B/Fluids*, 28(4):541–557, 2009.

[69] Peter S Stewart, Sarah L Waters, and Oliver E Jensen. Local instabilities of flow in a flexible channel: asymmetric flutter driven by a weak critical layer. *Physics of Fluids*, 22(3):031902, 2010.

[70] Geoffrey Ingram Taylor. Analysis of the swimming of microscopic organisms. *Proc. R. Soc. Lond. A*, 209(1099):447–461, 1951.

[71] W Tollmien. Über die entstehung der turbulenz. nachr. ges. wiss. göttingen 21–24. *English translation NACA TM*, 609:1931, 1929.

[72] AMIRAM Ur and MICHAEL Gordon. Origin of korotkoff sounds. *American Journal of Physiology-Legacy Content*, 218(2):524–529, 1970.

[73] Robert J Whittaker, Matthias Heil, Jonathan Boyle, Oliver E Jensen, and Sarah L Waters. The energetics of flow through a rapidly oscillating tube. part 2. application to an elliptical tube. *Journal of Fluid Mechanics*, 648:123–153, 2010.

[74] Robert J Whittaker, Sarah L Waters, Oliver E Jensen, Jonathan Boyle, and Matthias Heil. The energetics of flow through a rapidly oscillating tube. part 1. general theory. *Journal of Fluid Mechanics*, 648:83–121, 2010.

[75] Rosemary Wild, TJ Pedley, and DS Riley. Viscous flow in collapsible tubes of slowly varying elliptical cross-section. *Journal of Fluid Mechanics*, 81(2):273–294, 1977.

[76] Feng Xu, John Billingham, and Oliver E Jensen. Divergence-driven oscillations in a flexible-channel flow with fixed upstream flux. *Journal of Fluid Mechanics*, 723:706–733, 2013.

[77] Feng Xu, John Billingham, and Oliver E Jensen. Resonance-driven oscillations in a flexible-channel flow with fixed upstream flux and a long downstream rigid segment. *Journal of Fluid Mechanics*, 746:368–404, 2014.

[78] Sen Zhang, Xiaoyu Luo, and Zongxi Cai. Three-dimensional flows in a hyperelastic vessel under external pressure. *Biomechanics and modeling in mechanobiology*, pages 1–21, 2018.

[79] Olek C Zienkiewicz and Robert L Taylor. *The finite element method for solid and structural mechanics*. Elsevier, 2005.